

LIFETIME MEASUREMENTS AND THE FEASABILITY OF VIBRATIONAL
PHONON CONFIGURATIONS IN DEFORMED RARE-EARTH NUCLEI

A Dissertation

Submitted to the Graduate School
of the University of Notre Dame
in Partial Fulfillment of the Requirements
for the Degree of

Doctor of Philosophy

by
Clark R. Casarella

Ani Aprahamian, Director

Graduate Program in Physics

Notre Dame, Indiana

February 2017

This document is in the public domain.

LIFETIME MEASUREMENTS AND THE FEASABILITY OF VIBRATIONAL
PHONON CONFIGURATIONS IN DEFORMED RARE-EARTH NUCLEI

Abstract

by

Clark R. Casarella

One of the many paradigms of nuclear structure involves the coupling of dynamic quadrupole, octupole & hexadecapole vibrations superimposed on top of a well-deformed ground state. Historically, the nature and feasibility of collective vibrational degrees of freedom in deformed nuclei have garnered significant skepticism and experimental/theoretical interest, yet the entire rare-earth region lacked the completeness and richness of data to fully understand the systematic behavior of these low-lying excitations. Successful interpretation of quadrupole and octupole vibrational phonon states hinges upon measurement of E0 transition strengths, two-nucleon transfer reaction cross sections, and absolute transition probabilities, the latter equating to precision lifetime measurements of excited states. We have measured 29 new lifetimes in ^{160}Gd and 47 new lifetimes in ^{162}Dy below 3.1 MeV excitation energy, including many potentially key vibrational phonon states at the University of Kentucky Accelerator Laboratory using the Doppler Shift Attenuation Method via Inelastic Neutron Scattering (DSAM-INS). This work discusses our experimental observations in terms of the various collective multiphonon configurations in two rare-earth nuclei, ^{160}Gd and ^{162}Dy , with a first-of-its-kind measurement of 2 flavors of the two-phonon quadrupole vibrations, a $K^\pi=0^+$ $\gamma\gamma$ -type and a $K^\pi=4^+$ $\gamma\gamma$ -type in ^{162}Dy . This work is funded by the National Science Foundation (NSF) under grant

Clark R. Casarella

numbers PHY-1068192, PHY-1205412, and PHY-0956310.

DEDICATION

To my father, the late Anthony “Tony” Casarella, for *everything*.

CONTENTS

FIGURES	vi
TABLES	xiii
ACKNOWLEDGMENTS	xv
CHAPTER 1: INTRODUCTION	1
1.1 Deformation in Nuclei	6
1.1.1 Vibrations in Deformed Nuclei	7
1.2 Excited States in Deformed Nuclei	10
1.3 Historical Impetus in Experimental Nuclear Structure	17
1.4 Assessing Nuclear Structure from Decay Radiation	22
1.4.1 Importance of Transition Probabilities	25
1.5 Decay and Structure Systematics in the $150 < A < 180$ Region	28
1.5.1 $K^\pi = 0^+, 2^+$ Systematics in Samarium, Gadolinium, and Dysprosium Nuclei	29
1.5.2 $K^\pi = 0^+, 2^+$ Systematics in Erbium, Ytterbium, and Hafnium Nuclei	33
1.5.3 Negative Parity States in Gadolinium and Dysprosium Nuclei	37
1.5.4 Multiphonon Configurations in Deformed Nuclei	41
CHAPTER 2: EXPERIMENTS AND DATA ACQUISITION	46
2.1 Lifetime Measurements of Excited States	46
2.2 DSAM-INS Formalism	48
2.3 $(n, n'\gamma)$ Experiments at the University of Kentucky	51
2.3.1 Excitation Function Measurements	57
2.3.2 Angular Distribution Measurements	59
2.4 Experimental Campaigns	61
2.4.1 The ^{160}Gd Campaign	62
2.4.2 The ^{162}Dy Campaign	62
CHAPTER 3: DATA ANALYSIS	67
3.1 Calibrations and Corrections	67
3.1.1 Energy Calibrations	67
3.1.2 Nonlinearity Calibrations	73

3.1.3	Efficiency Calibrations	74
3.1.4	Self-Absorption Corrections	75
3.2	Statistical Analysis	77
3.2.1	Fitting Procedures	77
3.2.2	Observable Extraction	79
3.2.2.1	Excitation Functions	79
3.2.2.2	Angular Distributions	82
CHAPTER 4: RESULTS		89
4.1	^{160}Gd Results	90
4.1.1	Lifetimes of 0^+ States	94
4.1.2	Lifetimes of 2_{γ}^+ Band	96
4.1.3	Lifetimes of Negative Parity Bands	97
4.1.4	Lifetimes of Positive Parity Bands	97
4.1.5	Lifetimes of States with No K^π Assignment	99
4.2	^{162}Dy Results	102
4.2.1	Lifetimes of 0^+ States	106
4.2.2	Lifetimes of $K^\pi=2_{\gamma}^+$ and 4^+ Bands	114
4.2.3	Lifetimes of Negative Parity Bands ($K^\pi=2^-$, 0^- , and 2_2^-)	118
4.2.4	Lifetimes of Other Negative Parity Bands ($K^\pi=5^-$, 3^- , 1^- and 3_2^-)	125
4.2.5	Lifetimes of $K^\pi=1^+$ Band and Members of M1 Scissors	133
4.2.6	Lifetimes of States with No K^π Assignment	136
4.2.7	All Decays Observed (Intensities)	140
CHAPTER 5: DISCUSSION AND INTERPRETATION		160
5.1	^{160}Gd Discussion	160
5.1.1	Excited 0^+ States and the $K^\pi=2_{\gamma}^+$ Band	160
5.1.2	Negative Parity States	165
5.1.3	Other Lifetime Measurements in ^{160}Gd	168
5.1.3.1	$K^\pi=4^+$ Band as a Hexadecapole Vibration?	169
5.1.3.2	$K^\pi=1^+$ Band	170
5.1.4	Implications and Further Discussion	172
5.2	^{162}Dy Lifetimes	175
5.2.1	0^+ Excitations Not Observed in $(n,n'\gamma)$	175
5.2.2	A Lack of Strong β Vibrations in ^{162}Dy	179
5.2.3	On the Two-Phonon Characteristics	180
5.2.3.1	2_{γ}^+ Band	180
5.2.3.2	0_2^+ Band $\gamma\gamma$ -Vibration	181
5.2.3.3	$K^\pi=4_{1,2}^+$ Bands at 1535,2181 keV as $\gamma\gamma$ -Vibrations .	182
5.2.3.4	$(2,3,4)^+$ State at 2230 keV	183
5.2.4	Negative Parity States	191
5.2.4.1	$K^\pi=2^-$ Band at 1148 keV	191
5.2.4.2	$K^\pi=0^-$ Band at 1275 keV	191

5.2.4.3	$K^\pi=2_2^-$ Band at 1863 keV	192
5.2.5	Other Negative Parity Bands	197
5.2.5.1	$K^\pi=5^-$ Band	197
5.2.5.2	$K^\pi=3^-$ Band	197
5.2.5.3	$K^\pi=1^-$ Band	198
5.2.5.4	$K^\pi=3_2^-$ Band	198
5.2.6	$K^\pi=1^+$ Band	200
5.2.7	States Above 2.2 MeV Excitation Energy	200
5.2.8	Implications and Further Discussion	205
CHAPTER 6: FINAL REMARKS AND FUTURE OUTLOOK		206
6.1	Impact of Presented Lifetime Measurements	206
6.1.1	^{160}Gd	206
6.1.2	^{162}Dy	207
6.2	What Lies Ahead for Rare-Earth Nuclei?	208
APPENDIX A: ^{160}GD 0^+ STATES		214
APPENDIX B: ^{160}GD NEGATIVE PARITY STATES		221
APPENDIX C: ^{162}DY QUADRUPOLE EXCITATIONS		236
APPENDIX D: ^{162}DY NEGATIVE PARITY STATES		260
BIBLIOGRAPHY		280

FIGURES

1.1 Chart of nuclides showing the varying degrees of deformation ($R_{\frac{4}{2}}$ values for even-even nuclei). Orange colored squares mark a well-deformed ground state, with green representing spherical nuclei.	4
1.2 Measured $B(E2)$ transition probabilities in single-particle units as a function of A , highlighting the region of deformation (as well as heavier actinide region) where strong nuclear rotations exist [20].	5
1.3 Schematic of the β quadrupole vibration about a deformed equilibrium shape.	9
1.4 Schematic of the γ quadrupole vibration about a deformed equilibrium shape.	10
1.5 Schematic level scheme of the single- and double-phonon vibrational (quadrupole and octupole) bands expected in deformed nuclei (color online).	11
1.6 Absolute $B(E2; 2^+_2 \rightarrow 0^+_{gs})$ (in Weisskopf units) measurements for rare-earth nuclei, showing the uniformity of the γ -vibration in a deformed nucleus. The bottom plot shows the energy of the 2^+ bandheads as a function of N , highlighting the smoothly varying energies.	15
1.7 Absolute $B(E2; 0^+_2 \rightarrow 2^+_2)$ (in Weisskopf units) measurements for rare-earth nuclei, showing the scattered experimental data that spans an order of magnitude variance. The bottom plot shows the energy of the 0^+_2 bandheads as a function of N , which shows a slightly more variant energy systematic than the 2^+ bandheads.	16
1.8 Schematic of the Q3D magnetic spectrograph at Münich used for precision $(p,t)/(t,p)$ spectroscopy [57].	18
1.9 Angular distribution data for all 0^+ states in ^{158}Gd observed in the (p,t) reaction in [58]. A DWBA calculation for an $L=2$ transition is shown as a dotted line in the $E=1452$ keV plot to show the unique nature of the $L=0$ transitions (in solid black).	19
1.10 Number of 0^+ states in rare earth isotopes of Sm, Gd, Dy, Er, Yb, and Hf. ^{162}Dy is highlighted with a blue circle.	20

1.11 Systematics for the energies of excited 0^+ states, the first excited 2^+ bandhead, and low-lying ground state band members for even-even Samarium nuclei. Proton and neutron pairing gaps ($2\Delta_\pi$ and $2\Delta_\nu$, respectively) are drawn in green and blue and are calculated from Equations 1.5 and 1.6. Transition arrows represent known experimental B(E2) measurements for 0^+ bandheads and 2^+ bandheads (in W.u. where known).	30
1.12 Systematics for the energies of excited 0^+ states, the first excited 2^+ bandhead, and low-lying ground state band members for even-even Gadolinium nuclei. Proton and neutron pairing gaps ($2\Delta_\pi$ and $2\Delta_\nu$, respectively) are drawn in green and blue and are calculated from Equations 1.5 and 1.6. Transition arrows represent known experimental B(E2) measurements for 0^+ bandheads and 2^+ bandheads (in W.u. where known).	31
1.13 Systematics for the energies of excited 0^+ states, the first excited 2^+ bandhead, and low-lying ground state band members for even-even Dysprosium nuclei. New transition probabilities are presented in ^{162}Dy , with the widths proportional to B(E2) values (in W.u.); also shown are the proton and neutron pairing gap ($2\Delta_\pi$ and $2\Delta_\nu$, respectively) for each isotope.	32
1.14 Systematics for the energies of excited 0^+ states, the first excited 2^+ bandhead, and low-lying ground state band members for even-even Erbium nuclei. Proton and neutron pairing gaps ($2\Delta_\pi$ and $2\Delta_\nu$, respectively) are drawn in green and blue and are calculated from Equations 1.5 and 1.6. Transition arrows represent known experimental B(E2) measurements for 0^+ bandheads and 2^+ bandheads (in W.u. where known).	34
1.15 Systematics for the energies of excited 0^+ states, the first excited 2^+ bandhead, and low-lying ground state band members for even-even Ytterbium nuclei. Proton and neutron pairing gaps ($2\Delta_\pi$ and $2\Delta_\nu$, respectively) are drawn in green and blue and are calculated from Equations 1.5 and 1.6. Transition arrows represent known experimental B(E2) measurements for 0^+ bandheads and 2^+ bandheads (in W.u. where known).	35
1.16 Systematics for the energies of excited 0^+ states, the first excited 2^+ bandhead, and low-lying ground state band members for even-even Hafnium nuclei. Proton and neutron pairing gaps ($2\Delta_\pi$ and $2\Delta_\nu$, respectively) are drawn in green and blue and are calculated from Equations 1.5 and 1.6. Transition arrows represent known experimental B(E2) measurements for 0^+ bandheads and 2^+ bandheads (in W.u. where known).	36

1.17	Systematics for the energies of excited negative parity states, the first excited 2^+ bandhead, and low-lying excited 0^+ states below the pairing gap ($2\Delta_\pi$ and $2\Delta_\nu$) for even-even Gadolinium nuclei.	39
1.18	Systematics for the energies of excited negative parity states, the first excited 2^+ bandhead, and low-lying excited 0^+ states below the pairing gap ($2\Delta_\pi$ and $2\Delta_\nu$) for even-even Dysprosium nuclei. States with a ‘ \oplus ’ marker indicate where a literature lifetime measurement exists.	40
1.19	Summary of all known multiphonon ($\gamma\gamma$, $\beta\gamma$, or $\beta\beta$) configurations in rare-earth nuclei, absolute $B(E2)$ from literature are shown in Weisskopf units to signify collective decays to γ -vibrational and/or potential β -vibrational states.	43
2.1	Techniques available to nuclear physicists to measure lifetimes as short as a few attoseconds (10^{-18} s) to the more long-lived lifetimes on the order of microseconds (10^{-6} s) (Adapted from [66], courtesy of M. K. Smith).	46
2.2	Doppler shift of an $E_\gamma=1902.055$ keV de-excitation from the $\theta_{lab}=40$, 90, and 150 degrees in red, blue, and green, respectively. The vertical lines mark the centroid of each peak of corresponding color.	50
2.3	Sample Experimental Setup at UKAL for γ -singles measurements (Made in M. Caprio’s SciDraw software for Mathematica [19])	54
2.4	Typical TOF spectrum with labeled regions for corresponding γ , neutron, and background events.	56
2.5	Superimposed excitation functions for two gamma rays ($E_\gamma=969$ & 1252 keV) leaving the same level ($E_{lev}=1518$ keV), and a single 1195 keV γ -ray leaving a separate $E_{lev}=1275$ keV level in ^{162}Dy . The different thresholds and shape of the 1195 keV and 969 keV de-excitations imply that these decays are from two different levels, clearly showing their placement in the level scheme.	58
2.6	Angular distributions for two different multipolarity γ -rays in ^{162}Dy , an E2 transition of $E_\gamma=282$ keV (the $6_{gs}^+ \rightarrow 4_{gs}^+$ transition) & an E1 transition of $E_\gamma=334$ keV (a $3^- \rightarrow 2_\gamma^+$ transition), showing distinct, inverted shapes.	61
2.7	Angles used in $^{162}\text{Dy}(n,n'\gamma)$ angular distributions. Angles in black are used in all measurements, while angles in red (137° and 145°) are used for the $E_n=1.6$ MeV measurements and angles in blue are used for both $E_n=2.2$ and 3.1 MeV datasets.	64
3.1	Spectrum from a ^{226}Ra calibration run during the ^{162}Dy experiments. Sampled, higher intensity peaks are labeled by their energy in keV (refer to Table 3.1).	70

3.2	Linear energy calibration, taken from the three $^{162}\text{Dy}(n,n'\gamma)$ angular distributions and single excitation function (ExF in the legend)	72
3.3	Order-5 polynomial nonlinearity correction, taken from the $^{162}\text{Dy}(n,n'\gamma)$ angular distribution with $E_n=3.1$ MeV	74
3.4	Fifth-order relative efficiency curve taken from the $^{162}\text{Dy}(n,n'\gamma)$ angular distribution with $E_n=3.1$ MeV	75
3.5	Multiplicative factor calculated by GAMBIT to correct for the angular dependent γ -ray self-absorption by a finite-size target.	76
3.6	Example of an energy-calibrated spectrum from the ^{162}Dy angular distribution at $E_n=1.6$ MeV and $\theta_{lab}=90^\circ$, outlining typical background levels and miscellaneous γ -ray transitions.	78
3.7	A set of plots from a typical excitation function for a single γ -ray transition, in ‘a’), E_γ vs. E_n , and in ‘b’), the peak area vs E_n . Note the dip in γ -ray energy at 2.6 MeV, and corresponding bump in peak area (shown as a blue ellipse to guide the eye), indicating a second transition of a similar (slightly lower) energy being populated.	80
3.8	Spectra from four bombarding neutron energies ($E_n=1.4$, 1.7, 1.775, and 2.3 MeV datasets) to show the typical increase of statistics for a single peak, a 1647 keV decay from the 1728 keV state in ^{162}Dy . Note the peak area emerge just above the level energy threshold (1.775 MeV neutron dataset), with optimal statistics in the $E_n=2.3$ MeV set.	81
3.9	Calculated Winterbon curves ($F(\tau)$) as a function of τ) for $E_n=1.6$, 2.2, and 3.1 MeV ^{162}Dy angular distributions. Sensitive lifetime ranges from DSAM are shown as vertical black lines, with the corresponding $F(\tau)$ values as horizontal lines.	83
3.10	Example Doppler Shift for a 1149 keV γ -ray populated in the 1.5 MeV $^{160}\text{Gd}(n,n'\gamma)$ experiment. Here, the $F(\tau)$ value of 0.665 ± 0.010 corresponds to a lifetime of 21 ± 1 fs.	84
3.11	Example extraction of multipole mixing fraction (δ) for a $4^+ \rightarrow 4^+$ transition in ^{162}Dy . Top-left plot: angular distribution of the 1308 keV γ ray. Top-right plot: CINDY comparison for a range of initial spins (color online) decaying to the final spin of 4; intersections with the black ellipse mark local/global minima of χ^2 vs δ . Bottom plot: projection of CINDY comparison as χ^2 as a function of δ minimization (note the lowest χ^2 value corresponds to the $\delta \approx 1$ for the cyan-colored $4^+ \rightarrow 4^+$ transition). (color online)	88
4.1	Lifetime inflation of the measured lifetimes for two levels ($E_{lev}=1275$ keV and $E_{lev}=1358$ keV) in ^{162}Dy caused by effects due to a higher bombarding neutron energy and unknown level-feeding from higher-lying states.	90

4.2	Level scheme for all level lifetimes measured in the ^{160}Gd experiments, with confirmed band and spin assignments shown. Previously measured lifetimes are in blue, with newly presented lifetimes in red. Individual levels and bands will be discussed in following sections.	92
4.3	Visual representation of all measured lifetimes with respect to literature values (in blue). Each separate color outlines the specific regimes (<1.5 MeV, $1.5 - 2.0$ MeV, and >2.0 MeV excitation energy) of energies studied in the ^{160}Gd angular distributions.	93
4.4	Singles spectra from the $\theta_{lab}=90^\circ$ and $E_n=2.0$ MeV angular distributions of ^{160}Gd	94
4.5	Level scheme for all level lifetimes measured in the ^{162}Dy experiments, with confirmed band and spin assignments shown. Previously measured lifetimes are in blue, with newly presented lifetimes in red, levels in green constitute an unreliable lifetime measurement from our data, where $F(\tau)<0$ or is consistent with zero.	103
4.6	All measured lifetimes in ^{162}Dy (in femtoseconds) plotted as a function of excitation energy in keV. Data points in red are extracted from the $E_n=1.6$ MeV angular distributions, points in green correspond to lifetimes extracted from the 2.2 MeV angular distributions, and blue points are lifetimes from the 3.1 MeV dataset. (color online)	106
4.7	Singles spectra from the $\theta_{lab}=90^\circ$ and $E_n=2.2$ MeV angular distributions of ^{162}Dy	107
4.8	Angular distributions of $0_i^+ \rightarrow 2_{g.s.}^+$ γ -rays observed in ^{162}Dy , highlighting their isotropic nature (color online).	108
4.9	Doppler energy shifts of $0_i^+ \rightarrow 2_{g.s.}^+$ γ -rays observed in ^{162}Dy (color online).	109
4.10	Lowest-lying negative parity bands in ^{162}Dy with reliable lifetimes measured in our experiments in red, existing literature values in blue, and unreliable lifetimes measured in green (color online).	119
4.11	$E_\gamma=260$ keV γ ray (from the $E_x=1148$ keV level) Doppler shift and excitation functions for decays from the first 2^- band (color online). The vertical black lines highlight our justification for using a slightly higher bombarding neutron energy, for the sake of better statistics, without the potential for contaminant decay channels from other states.	124
4.12	$E_\gamma=912$ & 1010 keV (de-excitations from the $E_x=1974$ keV level) Doppler shifts and excitation functions (color online). The excitation function (in blue) for the 1010 keV γ ray is scaled by a factor of 0.33 to normalize to the branching ratio of the level.	126

4.13 $E_\gamma=937$ & 1220 keV (de-excitations from the $E_x=1485$ keV level) Doppler shifts and overlaid excitation functions (color online). The excitation function (in blue) for the 1220 keV γ ray is scaled by a factor of 0.291.	127
4.14 Excitation functions for the decays leaving the $E_x=1637$ keV state. Note the differing population threshold energies for each γ -ray. (color online)	129
5.1 Non-isotropic decay from the tentative 0^+ state in ^{160}Gd at $E_x=1325$ keV. 162	
5.2 Excitation function measurement from the tentative 0^+ state in ^{160}Gd at $E_x=2236$ keV.	163
5.3 Level scheme showing the calculated $B(E2)$ in W.u. and $B(E1)$ in mW.u. for the confirmed 0^+ excitations in ^{160}Gd	164
5.4 Level scheme showing the decays with calculated reduced transition probabilities for the $K^\pi=2_\gamma^+$ band and low-lying negative parity states in ^{160}Gd	166
5.5 Level scheme showing the decays with calculated reduced transition probabilities for the $K^\pi=4^+$ and 1^+ bands in ^{160}Gd	168
5.6 Level scheme showing the decays with calculated reduced transition probabilities for the levels that are not assigned to rotational bands in ^{160}Gd . Note the neutron and proton pairing gaps drawn as dotted lines ($2\Delta_\nu \sim 1625$ keV and $2\Delta_\pi \sim 1810$ keV).	171
5.7 Singles spectra cuts where remaining 0^+ excitations should be ob- served. Spectra for $0_{4,5}^+$ placements are from the $E_n=1.925$ MeV excita- tion function measurements, with $0_{8,10}^+$ from the $E_n=2.9$ MeV dataset. 177	
5.8 Level scheme outlining all measured lifetimes for $K^\pi=0^+$ bands in ^{162}Dy . New lifetime measurements are shown in red (color online), and new $B(E2;0_i^+ \rightarrow \text{g.s.})$ calculations are expressed in Weisskopf units (W.u.).	178
5.9 Measured angular distribution of 1342 keV γ ray leaving the 2230 keV level, $W(\theta)$ fit is shown with a_2 and a_4 coefficients from the $E_n=3.1$ MeV angular distribution.	184
5.10 Level scheme showing all observed transitions from the lowest-lying 2_γ^+ , 0_2^+ , and 4_1^+ band with all interband ($K^\pi=J_i^+ \rightarrow K^\pi=2_\gamma^+$) decays. Intensities for transitions to the γ -band are taken from [3]. Also shown is a tentative (2^+) state at 2230 keV with a strong decay to the 2_γ^+ band.	186

5.11 $E_\gamma=1195$ & 1275 keV (de-excitations from the $E_x=1275$ keV level) Doppler shifts and excitation functions (color online). The excitation function (in blue) for the 1275 keV γ ray is scaled by a factor of 1.53 to normalize to the branching ratio of the level.	195
5.12 Observed γ -decays from negative parity, $K^\pi=2^-$, 0^- , 2_2^- bands in ^{162}Dy . Transition strengths are drawn proportional in width to their deduced $B(E1)$, with E1 transitions ($B(E1)$ in milli-Weksskopf units) in violet (color online). Literature $B(E3)$ values are drawn in green, expressed in W.u., and are from Refs. [56, 59]	196
5.13 Observed γ -decays from higher lying $K^\pi=5^-$, 3^- , 1^- , 3_2^- bands in ^{162}Dy . Transition strengths are proportional in width, with E2 transi- tions in red and E1 transitions in violet (color online). Hollow (white with colored border) transition arrows indicate that the resulting transi- tion probability is tentatively from an unreliable lifetime measure- ment.	199
5.14 $K^\pi=1^+$ band and the 1^\pm -spin levels part of the isovector M1 scissors mode in ^{162}Dy . $B(E1)$ in violet and in mW.u., $B(M1)$ in green and W.u., and $B(E2)$ in red in W.u.	201
5.15 Levels in ^{162}Dy with no rotational band assignment above the pairing gap ($2\Delta n=1720$ keV & $2\Delta p=1914$ keV). $B(E2)$ strengths drawn in red and in W.u.	202
5.16 Levels in ^{162}Dy with no rotational band assignment above the pairing gap ($2\Delta n=1720$ keV & $2\Delta p=1914$ keV) (continued). $B(E1)$ in violet and in mW.u., and $B(E2)$ in red in W.u.	203
5.17 Levels in ^{162}Dy with no rotational band assignment above the pairing gap ($2\Delta n=1720$ keV & $2\Delta p=1914$ keV) (continued). $B(E1)$ in violet and in mW.u., and $B(E2)$ in red in W.u.	204
6.1 Energies of the lowest-lying 0^+ state as a function of A (top) and N (bottom) for rare earth Sm, Gd, Dy, Er, Yb and Hf isotopes.	212
6.2 Known experimental $B(E2)$ strengths of the lowest-lying 0^+ state as a function of A for rare earth Sm, Gd, Dy, Er, Yb and Hf isotopes.	213

TABLES

1.1	WEISSKOPF CONVERSIONS FOR ^{160}GD AND ^{162}DY	26
2.1	NEUTRON ENERGIES: ^{160}GD	62
2.2	DETECTOR ANGLES: ^{160}GD	63
2.3	NEUTRON ENERGIES: ^{162}DY	63
2.4	DETECTOR ANGLES: ^{162}DY	66
3.1	CALIBRATION LINES: ^{226}RA DECAY-CHAIN	69
3.2	ENERGY CALIBRATIONS: ^{160}GD AND ^{162}DY	71
4.1	$K^\pi=0^+$ BANDS: ^{160}GD	95
4.2	$K^\pi=2^+$ BAND: ^{160}GD	96
4.3	NEGATIVE PARITY BANDS: ^{160}GD	98
4.4	POSITIVE PARITY ($K^\pi=4^+/1^+$ BANDS): ^{160}GD	99
4.5	OTHER LEVELS: ^{160}GD	101
4.6	LITERATURE LIFETIME COMPARISON: ^{162}DY	105
4.7	$K^\pi=0^+$ BANDS: ^{162}DY	111
4.8	$K^\pi=2^+$ AND 4^+ BANDS: ^{162}DY	115
4.9	NEGATIVE PARITY BANDS ($K^\pi=2^-, 0^-, 2^-_2$): ^{162}DY	120
4.10	NEGATIVE PARITY BANDS ($K^\pi=5^-, 3^-, 1^-, 3^-_2$): ^{162}DY	131
4.11	$K^\pi=1^\pm$ AND M1 SCISSORS MODE: ^{162}DY	134
4.12	OTHER LEVELS (NO K ASSIGNMENT): ^{162}DY	137
4.13	ALL DECAYS OBSERVED: ^{162}DY	141
5.1	ALAGA: ^{160}GD	174
5.2	OBSERVED 0^+ STATES: ^{162}DY	176
5.3	OBSERVED/LITERATURE INTENSITIES ($K^\pi=0^+, 2^+, 4^+$): ^{162}DY	187
5.4	ALAGA ($K^\pi=0^+, 2^+, 4^+$): ^{162}DY	189
5.5	B(E2) RATIOS ($K^\pi=0^+, 2^+, 4^+$): ^{162}DY	190
5.6	ABSOLUTE INTENSITIES (NEGATIVE PARITY): ^{162}DY	193

ACKNOWLEDGMENTS

This thesis would be an absolute train-wreck without Ani Aprahamian, my academic advisor and mentor, for giving me the swift kick I needed at periodic times to push me through the revolving door that is graduate school, and for frequently reminding me that “If what you were doing was easy, someone would have already done it long ago”.

Next, I want to thank below-freezing temperatures, without you, I would have stuck around the South Bend/Notre Dame area for a few more years.

I am forever indebted to Jacee Rohlck, for reminding me on numerous occasions that she will eternally love me (read: put up with me), no matter the circumstances.

Although I always pay in a strict monetary sense, I owe Starbucks some degree of success, for supplying me with a near limitless amount of coffee (a necessary tool for good work) throughout graduate school.

I need to acknowledge the best friends I have ever made in my entire life (my fellow graduate students), for keeping me sane and sufficiently distracted throughout my career here at Notre Dame.

I would not be writing this work without the help of Dr. Richard Prior, since he convinced me it was a good idea to come to TUNL with him in 2010, effectively bringing me to the event horizon of the black hole that is experimental nuclear physics research.

I owe thanks to Shelly Lesher, for providing me with the answers to numerous questions about the analysis process and for her gracious use of publication data for part of the results presented in this work (^{160}Gd excitation functions and level

lifetimes below 2.0 MeV excitation energy).

Along the same lines, I thank Ben Crider, Erin Peters, and the entire cadre of nuclear scientists at the University of Kentucky, for answering my inane, incessant, and frankly, unintelligent questions about nuclear physics and the analysis methods I would need to implement to complete the Herculean task of understanding nuclear structure.

Lastly, I am eternally grateful for Mark Caprio's LevelScheme/SciDraw package for Mathematica for the creation of many (read: the majority) figures presented herein. Without this lifesaving program, I would never have been able to express my results in a clean and understandable fashion.

CHAPTER 1

INTRODUCTION

Henri Bequerel and Marie Curie's discovery of natural, spontaneous radiation in 1896 fueled the scientific tinder that erupted into modern physics. This breakthrough in scientific impetus, coupled with the formulation of quantum mechanics and the discovery of the nucleus (the incredibly dense and minuscule core of the atom) in the early 20th Century, led to this brand new field of nuclear science. Initially, the nucleus was modeled as a homogenous core of positive charge, but with continued study, the nucleus was found to be comprised of discrete, \sim 1 femtometer large (or small, depending on perspective) particles, the positively charged proton and the inert neutron, all held together with a very attractive and short-range force, the aptly named the strong interaction.

Knowing that the atomic nucleus is comprised of protons and neutrons, we can study it as a many-body quantum system. Throughout the entirety of nuclear science's history, we have studied countless nuclear structure properties, including the nuclear (and nucleon) masses and properties of excited states in the nucleus. Several observations of phenomena like the spin and parity of the ground state of even-even nuclei being 0^+ led directly to the evolution of the nuclear shell model, which then drove further theories and experiments to describe the nucleus in deeper ways. The nuclear shell model saw incredible success for a great deal of nuclei, particularly at the shell closures, where the spins and parities of the second, third, and onward states agreed exceptionally well, but overall, the shell model did not see unified, complete success for all nuclei.

By describing the nucleus as a geometric shape of a liquid drop (Equation 1.1), the nucleus can be represented as a quantum system with varying degrees of freedom about that spherical shape, by performing a multipole expansion in terms of the spherical harmonics.

$$R = R_{sp}[1 + \sum_{\lambda\mu} \alpha_{\lambda\mu} Y_{\lambda\mu}(\theta, \phi)] \quad (1.1)$$

Here, R_{sp} is the average *spherical* nuclear radius, often given by the well-known approximation of $R_{sp}=R_0 A^{\frac{1}{3}} \approx 1.2 A^{\frac{1}{3}}$ fm. $Y_{\lambda\mu}(\theta, \phi)$ represent the spherical harmonics of order λ , with corresponding expansion coefficients $\alpha_{\lambda\mu}$. These static, permanent geometric deformations can be characterized by an expansion of their multipole order, λ , with $\lambda=2$ being a quadrupole deformation, $\lambda=3$ as an octupole, and so on. Trivially, if $\lambda=0$, we are left with the spherical case. The lowest-order (and most common) static deformation in nuclei, the quadrupole deformation ($\lambda=2$), can be reparameterized into the Euler angles and subsequently the polar-like ‘Hill-Wheeler’ coordinates β and γ , (Equations 1.2 & 1.3), which provides measures of the extent of quadrupole deformation and the departure from axial asymmetry, respectively. Performing this parameterization also allows us to make a convenient convention of dynamic deformation ‘directions’ later on, as well as a categorization of the nuclear shape. So, for each axis ($k=1,2,3$) of our deformed solid nucleus, the deviation from spherical symmetry is given by Equation 1.4, where we also gain this categorization of the various deformed nuclear shapes based on the range of both β and γ .

$$\alpha_{2,\pm 2} = \beta \sin \gamma \quad (1.2)$$

$$\alpha_{2,0} = \beta \cos \gamma \quad (1.3)$$

$$\delta R_k = \sqrt{\frac{5}{4\pi}} \beta \cos\left(\gamma - \frac{2\pi k}{3}\right) \quad (1.4)$$

Figure 1.1 shows the Chart of Nuclides, which displays every isotope of observed nuclei with the number of protons (Z) on the y-axis and the number of neutrons (N) on the x-axis. In this plot, the $R_{\frac{4}{2}}$ values (the ratio of the energies of the first 4^+ state to the 2^+ state) for even- Z /even- N nuclei are shown on as a color gradient; this $R_{\frac{4}{2}}$ ratio is a practical measure of static deformation in the nucleus, with shades of orange (>3) representing well-deformed nuclei and shades of green (<2) representing spherical or near-spherical shape. Throughout the region of deformation (and the entire Nuclear Chart), experimental physicists have observed the various emergent nuclear phenomena of vibrations and rotations to drive experiments and theories further.

The first of such phenomenon is the existence of small surface oscillations of spherical nuclei, in which the nucleus can exhibit a macroscopic, collective motion of nucleons about the spherical equilibrium shape. These vibrations about the spherical shape are well-documented and studied throughout the spherical mass ranges of the Chart of Nuclides as an excellent example of collective degrees of freedom in the nucleus [4, 20]. These vibrational quanta, or phonons, also manifest in higher-order excitations (a two-phonon vibration, a three-phonon vibration, etc) as superimposed vibrations built on top of other vibrations.

Vibrations, however, are not the only collective degree of freedom afforded to the nucleons in the nucleus; collective rotations of nucleons about an axis are abundant in nuclei [20, 79]. For spherical nuclei, a nuclear rotation is energy degenerate, as there is no change in the fundamental frequency of oscillation, but in deformed nuclei, we find strong experimental evidence of collective rotations about the different axes. Whenever a quadrupole deformed nucleus rotates about an axis, it will emit electric quadrupole radiation (E2 type radiation) [26]. We subsequently observe this strong rotational motion in the transition probabilities between nuclear states ($B(E2)$ measurements quantized with a single-particle estimate) in Figure 1.2, where the entire

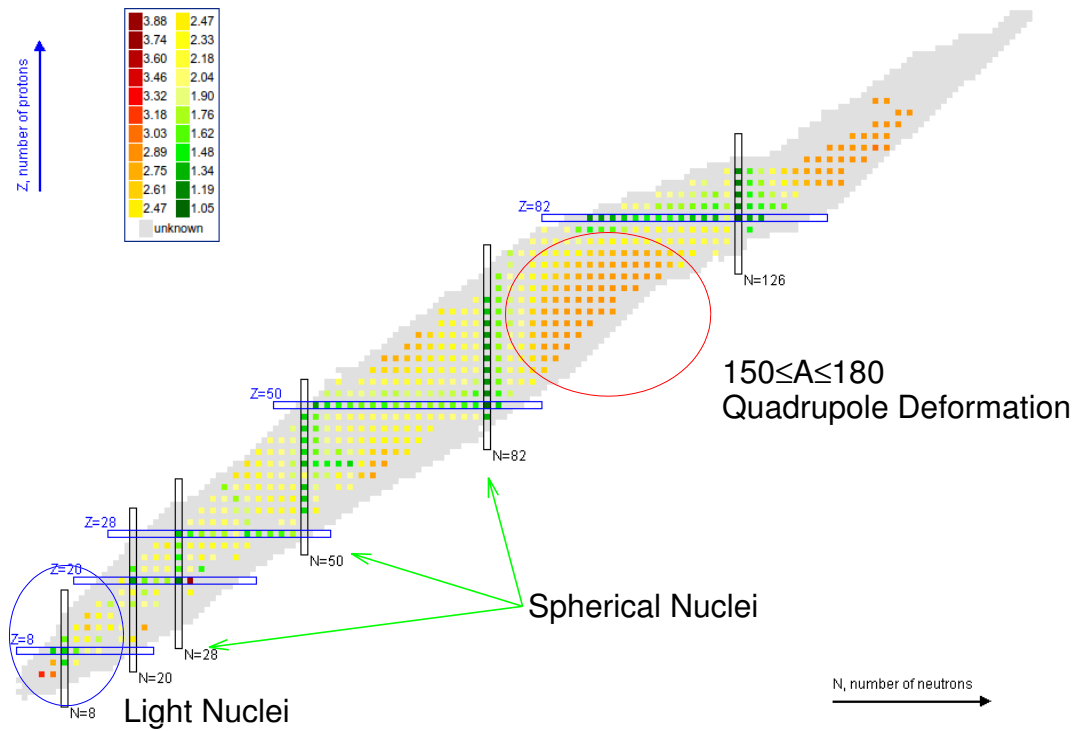


Figure 1.1. Chart of nuclides showing the varying degrees of deformation ($R_{\frac{4}{2}}$ values for even-even nuclei). Orange colored squares mark a well-deformed ground state, with green representing spherical nuclei.

region of deformation exhibits strong (>50 Weisskopf unit strength) transitions, a very strong indication of collective motion.

An open question then arises: are there superimposed vibrations on top of a deformed ground state, much like the vibrations about a spherical shape?

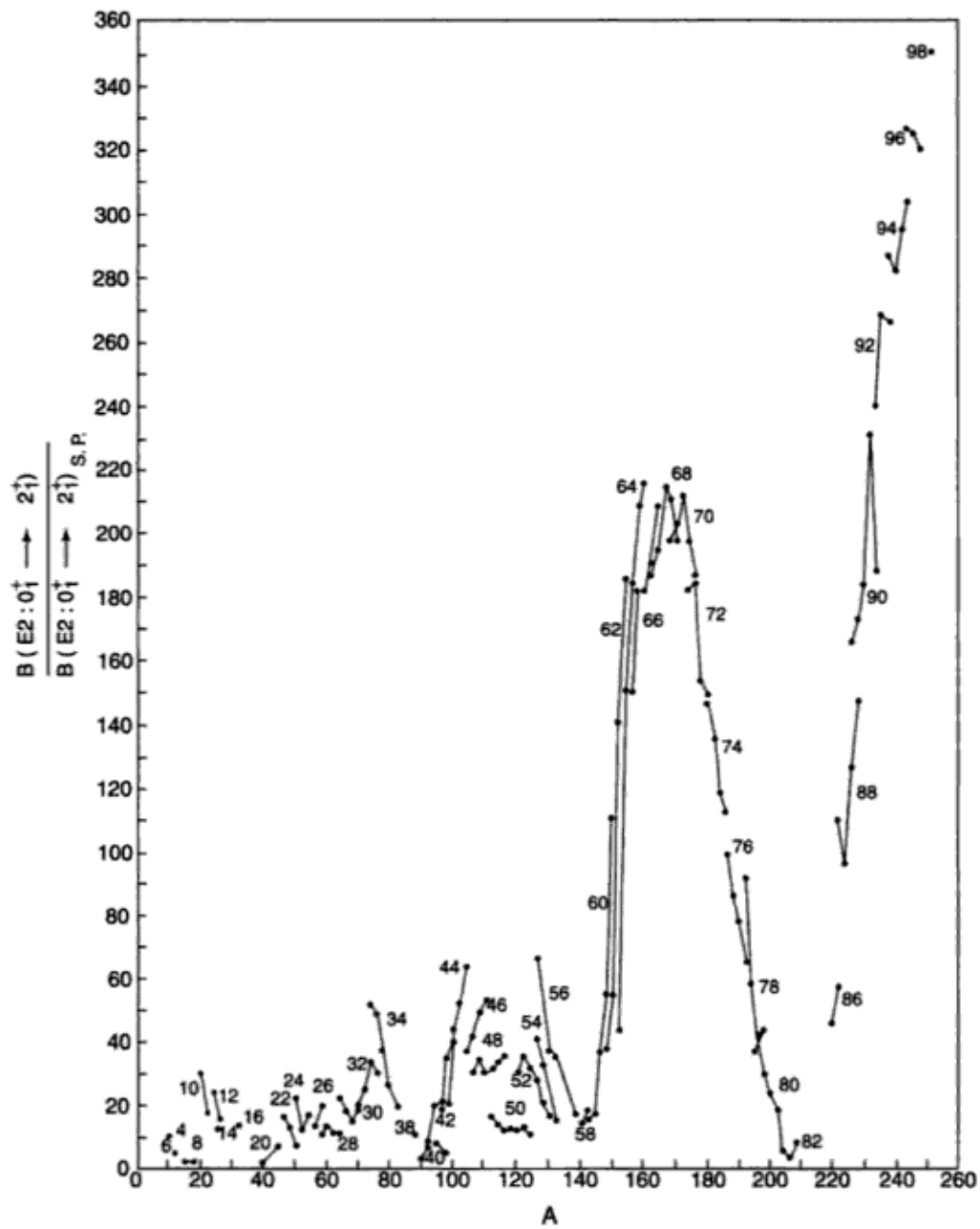


Figure 1.2. Measured $B(E2)$ transition probabilities in single-particle units as a function of A , highlighting the region of deformation (as well as heavier actinide region) where strong nuclear rotations exist [20].

1.1 Deformation in Nuclei

Description of collective motion for a deformed nucleus begins by treating the nuclear radius as a liquid drop with the statically deformed shape shown in Equation 1.1, and then allowing the deformation parameters to deviate in small amplitudes. The work contained in this dissertation is strictly concerned with static, prolately deformed nuclei, or where $\gamma=0$ and $\beta > 0$, although other nuclear shapes exist for negative values of β (oblate, axially asymmetric, etc). This deformed nuclear shape is equivalent to a permanent quadrupole deformation in the ground state, or where $\lambda=2$ from Equation 1.1. It is also convenient and prudent to recast the angular momentum of states in the deformed nucleus as a projection of the total angular momentum along the axis of symmetry (K^π); this is beneficial, as it helps us easily identify and distinguish the different types of collective motion in deformed nuclei. K^π can further be distinguished by the parity of states, as is typical by a $\pi=(-1)^\lambda$ rule, where this is also a clue to the asymmetry of nuclear wave functions.

Effects due to the pairing of nucleons in discrete shells and subshells in the nucleus have a profound effect on the structure of states in the deformed nucleus. In one of the most important pairing effects, the pairing of fermions in discrete shells forbids particles from occupying the same space, so when two protons or neutrons pair together to create an excitation (or as the even-even nucleus resides in the ground state). However, there is an energy intrinsic to the nucleus at which two nucleons will break their tendency to couple together as pairs; this pairing gap for protons and neutrons ($2\Delta_\pi$ & $2\Delta_\nu$, respectively) is taken from [53], and is a measure of the odd-even staggering of energies caused by the pairing interaction in the nuclear binding energy. In the rare-earth region of nuclei, this pairing gap is experimentally observed near $\sim 1.5\text{-}2.0$ MeV, where the states below this energy are the signatures of macroscopic collective motion of nucleons (or in terms of pairing, multiple quasiparticle pairs acting in the form of vibrational phonons) as a whole, in a dramatic shift away

from independent/single particle excitations [13]. These pairing effects then bring rise to the idea of nuclear excitations being created via quasiparticle pairs; this is stated in stark contrast to the rigid rules of the shell model where fermions (in the case of particle-hole states) will have defined occupancy of shells, and instead can exhibit partial occupancies. Above the pairing gap, we notice a sharp increase in level density, where we have state-mixing occurring between the particle, quasiparticle pair, and collective configurations, and as such, finding a ‘pure’ collective vibration becomes increasingly difficult [20, 40].

The pairing gap for a particular nuclei ${}^A_Z X_N$ can be calculated with Equations 1.5 and 1.6, where $E(N,Z)$ is the binding energy of the nucleus X for the particular neutron number N and proton number Z combination, and $E(N,Z+1)$ is the binding energy of a nucleus that has an added proton, $E(N,Z+3)$ is the nuclear binding energy of the nucleus with three added protons, and so on. For example, the proton pairing gap for ${}^{162}\text{Dy}$ would involve the binding energies of ${}^{162}\text{Dy}$, ${}^{163}\text{Ho}$, ${}^{165}\text{Tm}$, ${}^{161}\text{Tb}$, and ${}^{159}\text{Eu}$, for the respective entries in Equation 1.5.

$$2\Delta_\pi = \frac{1}{8}[16E(N, Z) + 9E(N, Z + 1) + E(N, Z + 3) + 9E(N, Z - 1) + E(N, Z - 3)] \quad (1.5)$$

$$2\Delta_\nu = \frac{1}{8}[16E(N, Z) + 9E(N + 1, Z) + E(N + 3, Z) + 9E(N - 1, Z) + E(N - 3, Z)] \quad (1.6)$$

1.1.1 Vibrations in Deformed Nuclei

Given some excitation energy, the deformed nucleus’ excitations are not necessarily treated as single particle excitations, but instead as a movement of multiple nucleons *collectively* (as a whole) throughout the nuclear shape as it rotates. In the mid-20th Century, theoretical treatments to describe a deformed nucleus emerged as

the geometric collective model of Bohr and Mottelson [12], and one of the beauties of this descriptive model was the near-immediate appearance of low-lying surface oscillations (in this case, nuclear vibrations) about the deformed ground shape [12], as well as the prevalence of fundamental nuclear rotations. These two modes of collective motion, vibration and rotation, make up the basic degrees of freedom available to a deformed nucleus, where, in stark contrast to the degenerate vibrations of a spherical nucleus, a vibration in a deformed nucleus can be along any of the axes of symmetry according to a time-dependent multipole expansion of the deformed shape. In its lowest order ($\lambda=2$ expansion of Equation 1.1), the nucleus *can* exhibit quadrupole oscillations around its equilibrium shape in one of two possible types, a γ -vibration or a β -vibration. The notation and phenomenology behind these modes of vibrations alludes to the ‘direction’ of oscillation with respect to the Hill-Wheeler coordinate parameterization mentioned earlier in §1. For example, the γ -vibration is a dynamic oscillation that breaks axial symmetry (the parameter γ) to maintain a $K^\pi=2^+$ projection of angular momentum, while the β -vibration maintains both axial symmetry, as well as a $K^\pi=0^+$ projection of angular momentum (an oscillation of quadrupole deformation β). Note the positive parity, which indicates a reflection symmetry for the nuclear shape and corresponding wave functions. Crude cartoon visualizations of these quadrupole vibrations can be seen in Figures 1.3 and 1.4. In these pictures, the schematic on the left looks down the axis of symmetry (represented by bold, black lines), with the side view on the right. Thin black lines outline the deformed equilibrium shape, with dashed red lines showing the extent of the dynamic, quadrupole oscillations; blue arrows are meant to guide the eye as to how the nucleus changes shape.

If a single vibrational phonon can be superimposed on the collective rotational ground state, how feasible is the two-phonon case for deformed nuclei? Linear combinations of the quadrupole phonon structure would involve the $\gamma\gamma$ (with either a 0^+

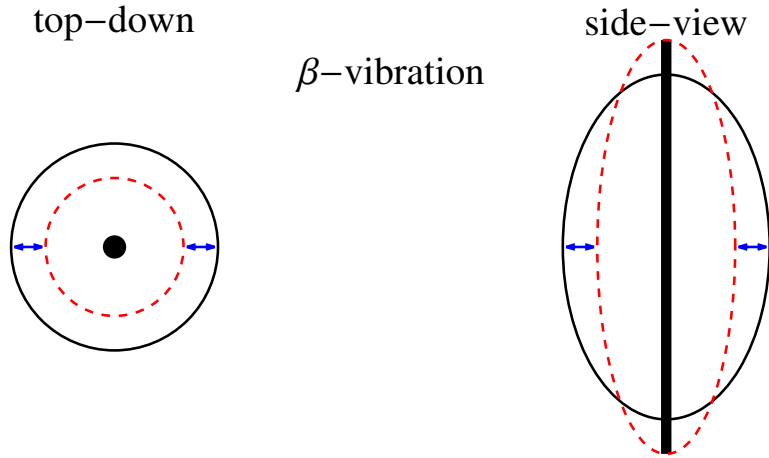


Figure 1.3. Schematic of the β quadrupole vibration about a deformed equilibrium shape.

or 4^+ K^π projection), $\beta\gamma$ ($K^\pi=2^+$), & $\beta\beta$ vibrations (again, $K^\pi=0^+$). As an analogue to the classical harmonic oscillator problem, the addition of multiple phonon quanta will increase the energy of the system by some proportional amount, so we would expect a 2 phonon vibration to be double the energy of the 1 phonon vibration, or that $E_{phonon} \propto N_{phonon}$. *In theory*, all modes of vibration should be obvious and abundant, but we will see that this is not immediately the case for deformed rare-earth nuclei given the current state of experimental data, especially with varying degrees of anharmonicity at play.

A further study in deformed nuclei is on the higher order octupole ($\lambda=3$ expansions of Equation 1.1) vibrations and if they can also exist, but the motions of the nuclear surface are significantly more difficult to envision as a drawing, especially on a 2-dimensional piece of paper. However, qualitatively, the octupole vibration is an asymmetric vibration about the quadrupole deformed nucleus in a ‘pear’-like oscillation. The octupole vibration (in spherical nuclei) manifests as a $K^\pi=3^-$ projection

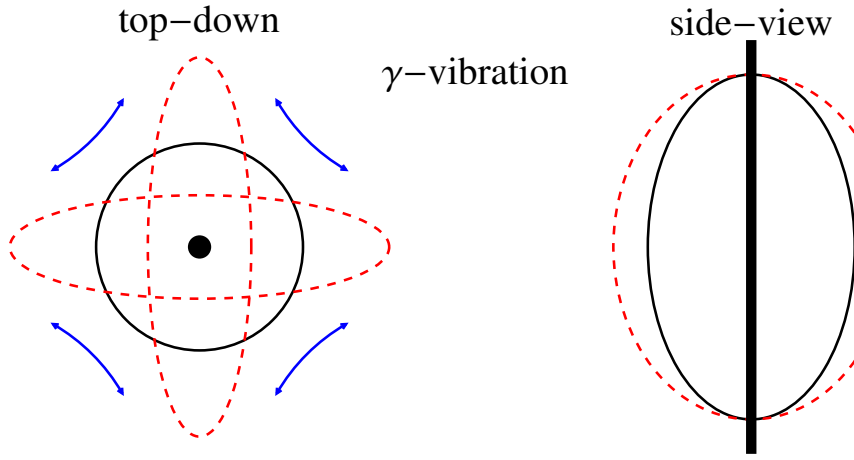


Figure 1.4. Schematic of the γ quadrupole vibration about a deformed equilibrium shape.

on the axis of symmetry, with asymmetric wave functions (and shape) due to the negative parity. However, in contrast to the degenerate quadrupole modes of $K=0,2$ in deformed nuclei, we expect a split-degeneracy of this $K^\pi=3^-$ projection into a quartet of possible projections, $K^\pi=0^-, 1^-, 2^-,$ and 3^- [12] in the deformed nucleus.

1.2 Excited States in Deformed Nuclei

The question then arises: what would these quadrupole and octupole vibrations look like represented as low-lying excited states in the level scheme of a well-deformed rotational nucleus? A cartoon level scheme representing the lowest lying quadrupole and octupole vibrations is given in Figure 1.5, where we can immediately see the ensemble of states corresponding to each vibration, and each vertical ‘band’ lines up with rotational members of a particular vibrational state. Starting in the bottom left, we see the low-lying $K^\pi=2^+$ and 0^+ bands as the γ and β -vibration (where one would

expect near ~ 1 MeV excitation energy). Then, continuing upward, the single-phonon vibrations of γ and β type have their corresponding two-phonon counterparts and combinations ($\beta\beta$, $\beta\gamma$, and $\gamma\gamma$) drawn at twice the excitation energy that assumes a completely harmonic vibration.

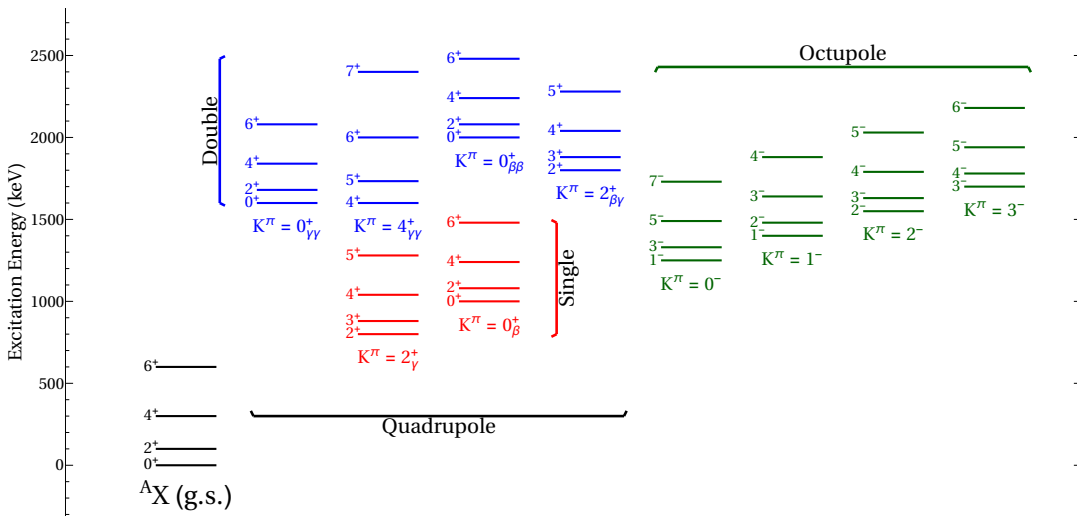


Figure 1.5. Schematic level scheme of the single- and double-phonon vibrational (quadrupole and octupole) bands expected in deformed nuclei (color online).

Nuclear rotations are superimposed on the base vibration expected for each type of phonon as band excitations, (single quadrupole/octupole and double quadrupole) according to the $J(J+1)$ rule set out in Equation 1.7 for low values of K , of which would include the single- and double-phonon vibrational states ($K=0,2,4$). These additions of rotational energy directly correlate to higher-lying members of a band,

with \mathcal{I} being the moment of inertia for the nucleus. The rotational excitations in a band carry a set of spins related to the band's value of K ; for $K \neq 0$, J progresses through $K, K+1, K+2, \dots$ where only even spins occur in a $K=0$ band [36].

$$E_{rot} = \frac{\hbar}{2\mathcal{I}}[J(J+1)] \quad (1.7)$$

In Figure 1.5, we immediately see a key (and long-lived) question in nuclear structure physics: What are the nature of 0^+ excitations? From this ideal, toy picture, we already see three possible ways to make a $K^\pi=0^+$ excitation. Understanding the nature of these common, low-lying excitations in nuclei has been a cornerstone of nuclear structure in the rare-earth region for decades. Experimentally, the searches for the nature of 0^+ have been cloudy from the evidence of double-phonon states across the entire rare-earth region such as the $\gamma\gamma$ -type vibration in several nuclei ([32], [49], [2]) that exhibit strongly collective, anti-aligned combinations of the γ -vibrational phonon.

Experimentally, many deformed rare-earth nuclei exhibit a low-lying excited $K^\pi=0^+$ and $K^\pi=2^+$ band, and were assumed to be the β and γ vibration, respectively. In practice, however, this assumption of vibrational character has come under fire in recent years and tends to fall apart due to several factors. First, we do not have a complete, unambiguous characterization of each 0^+ state in the rare-earth region as a collective β -vibration; this stems from a lack of lifetime information (and thus transition probability information) of the $K^\pi=0^+$ bands in rare-earth nuclei.

Second, examination of the $B(E2)$ transition probabilities and energies of the lowest-lying 0^+ and 2^+ bands yields a contrasted picture for each (assumed to be) vibrational type, shown in Figures 1.6 and 1.7. In the case of γ -vibrational characteristics, we observe a smoothly varying energies across the entire region, with the same behavior for the overall collectivity of these states (falling around 5 Weisskopf unit strength). However, the β -vibrational systematics become quickly obscured,

with both obvious gaps in the lifetime information, an order of magnitude variance of the transition probabilities, and a less than smooth variance in energies like their γ -vibrational cousins!

The emergence of the nuclear data that gives this unclear picture (particularly of the scattered $B(E2)$ strengths) has garnered significant skepticism of *any* vibrational degrees of freedom in the nucleus [30]. The story is *still* unclear on the nature of any vibrational states in deformed nuclei due to the incomplete data surrounding it; if any clarification is to be made, we need lifetime information to say one way or the other.

By a similar merit for the octupole vibration, in Figure 1.5 we see the split quartet of low-lying negative parity states, as expected, yet these $\lambda=3$ excitations are not as well studied as their quadrupole counterparts [20]. Several different phenomena occur in the low-lying negative parity states of deformed nuclei, including an inversion in the energy ordering of states as N increases, irregularities among the transition probabilities (as a function of ΔK) throughout the rare-earth region of nuclei, among others [16, 20]. Continue the multipole expansion to higher-order terms, and the hexadecapole ($\lambda=4$) vibrations appear. Again, we state here that these negative parity states and higher-order vibrational phonons have not seen the same order of experimental rigor and study as their $\lambda=2$ counterparts have; this work hopes to aid in the lack of vital lifetime information on low-lying negative parity states in the deformed region of nuclei. Systematic behavior of negative parity states (as well as the strength of quadrupole vibrations) varies wildly across the entire rare-earth region of nuclei and have been caught in the epicenter of experimental focus in nuclear structure in the past several decades.

Much like the quadrupole counterparts, we can also picture a structure of coupled quadrupole-octupole-type phonons to either octupole or quadrupole phonons, further increasing the possible K -projections available to study [60]. For example, a $2^+ \otimes 3^-$

coupling can produce projections of 1^- , 2^- , 3^- , 4^- & 5^- , if we follow the same parity and triangle selection rules inherent to quantum systems.

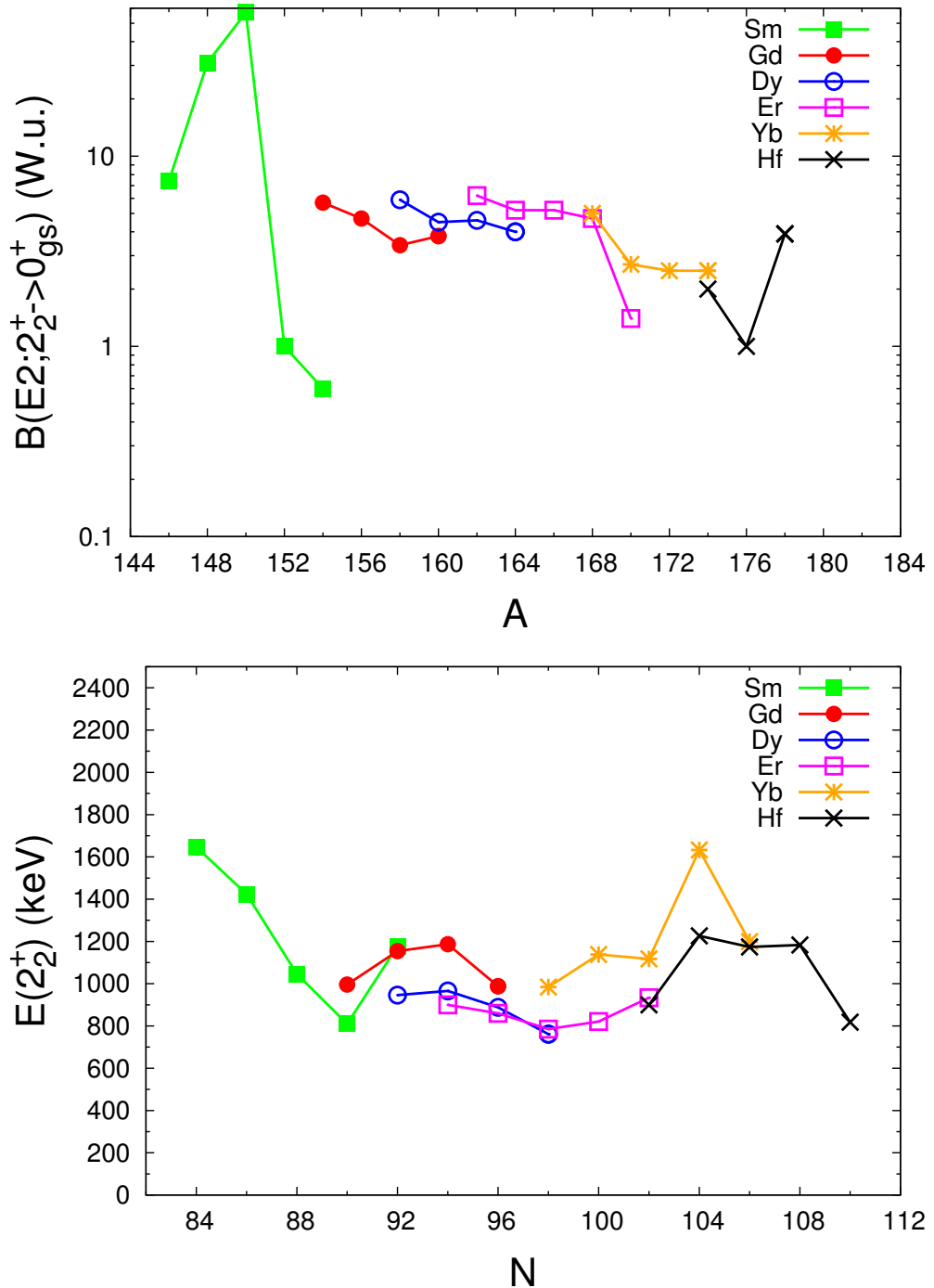


Figure 1.6. Absolute $B(E2; 2_2^+ \rightarrow 0_{gs}^+)$ (in Weisskopf units) measurements for rare-earth nuclei, showing the uniformity of the γ -vibration in a deformed nucleus. The bottom plot shows the energy of the 2^+ bandheads as a function of N , highlighting the smoothly varying energies.

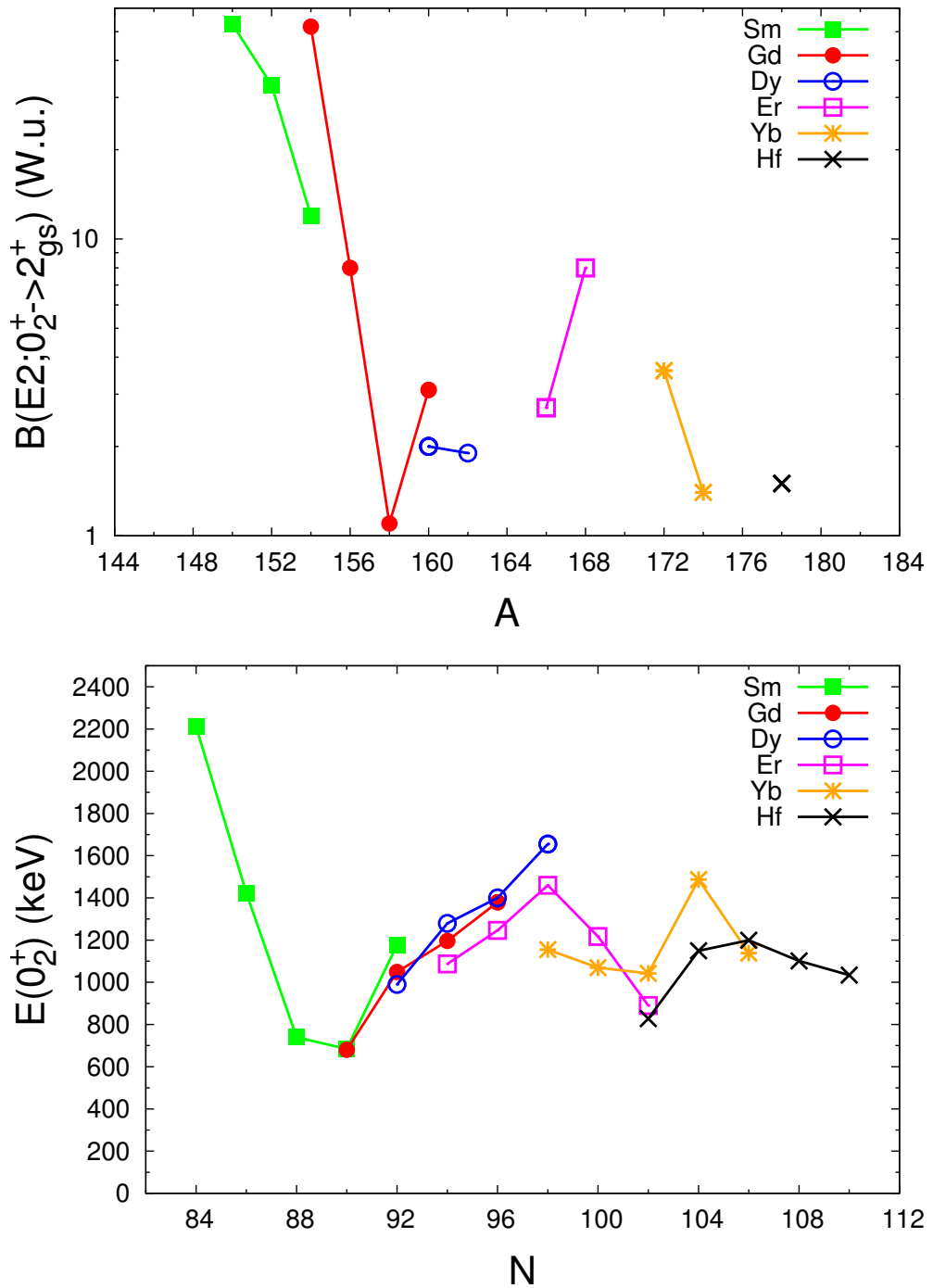


Figure 1.7. Absolute $B(E2; 0_2^+ \rightarrow 2_{gs}^+)$ (in Weisskopf units) measurements for rare-earth nuclei, showing the scattered experimental data that spans an order of magnitude variance. The bottom plot shows the energy of the 0_2^+ bandheads as a function of N , which shows a slightly more variant energy systematic than the 2^+ bandheads.

1.3 Historical Impetus in Experimental Nuclear Structure

Experimentally, how have these low-lying excitations in deformed nuclei been studied in the past? The study of collective vibrational states has been a pressing issue in nuclear structure for decades, with the constant evolution of experimental techniques and theoretical models throughout the mid-to-late 20th Century [20, 39, 48]. Categorization of $2^+ \gamma$ vibrational bands across the region of deformation arose quickly, but their significantly more elusive cousins in the 0^+ states proved to be more difficult to ascertain an origin. A major contributor to their elusiveness stems from the difficulty experimentalists had in detection of these states in the first place; experimentation was simply not sensitive enough to capture signatures of the L=0 states!

Near the turn of the millennium, however, in one of the pioneering (and one of the most-cited) works in the field, Lesher *et. al* found a surprising, completely unprecedented number of excited 0^+ states in deformed ^{158}Gd [50]. This work utilized the Q3D magnetic spectrograph at Münich with two-nucleon transfer reactions, a particularly adept way to find $J^\pi=0^+$ excitations, where seven new 0^+ excitations (of thirteen total) were discovered. The Q3D was to later be used by D. Meyer in 2006 to continue this newly sparked renaissance of nuclear structure studies on the nature of 0^+ excitations in deformed nuclei [58], measuring 84 new 0^+ states.

Recall from [26] the Pauli principle that governs nucleon pairing; first, the pairing of nucleons governs the J=0 ground state of even-even nuclei. Second, in a two nucleon transfer reaction, (p,t) or (t,p), the paired neutrons entering or exiting the nucleus will preferentially couple to $J^\pi=0^+$ states. For an even-even nucleus with a 0^+ ground state, transfer reactions have a high overlap to this mode of excitation to $J^\pi=0^+$, giving the Q3D spectrograph its sensitivity. In the two nucleon transfer reactions angular distributions of outgoing tritons (or protons) are collected at various angles with respect to the beam direction by the opening of the spectrometer and

bent through a series of 3 dipole magnets to a focal-plane detector (see Figure 1.8). Differing energies of ejectiles are bent by various amounts to the focal-plane detector, where positional dependence in the detector is directly related to the energy of the excited state populated (E_x), according to Equation 1.8. The remarkable resolution produced by the setup of quadrupole and dipole magnets propeled the Q3D above previously unattainable levels of discrimination, and has forever changed the field of nuclear structure.

$$E_{ejectile} = E_{projectile} - Q - E_x - E_{C.O.M.} \quad (1.8)$$

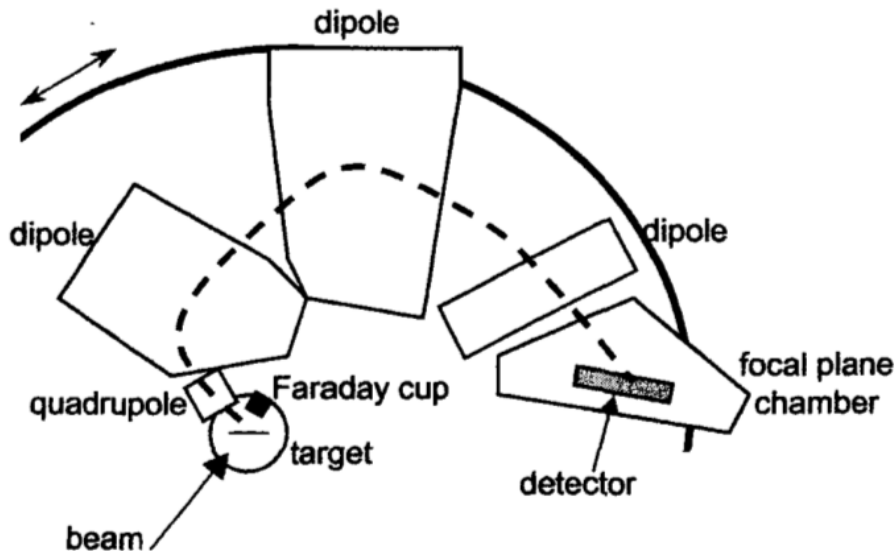


Figure 1.8. Schematic of the Q3D magnetic spectrograph at München used for precision (p,t)/(t,p) spectroscopy [57].

In the case of a $\Delta L=0$ transition, the angular distribution of detected particles will be extremely forward-peaked; this is an easily observed experimental signature, and is completely unique to $\Delta L=0$, as the measured intensity (differential cross section) can drop by an order of magnitude from $\sim 5^\circ$ to $\sim 17^\circ$ [58]. Confirmation of the $J^\pi=0^+$ assignments can be made by comparing the relative cross sections from the experimental data to a Distorted Wave Born Approximation (DWBA) calculation, where an example of this can be seen in Figure 1.9 for the 0^+ states in ^{158}Gd .

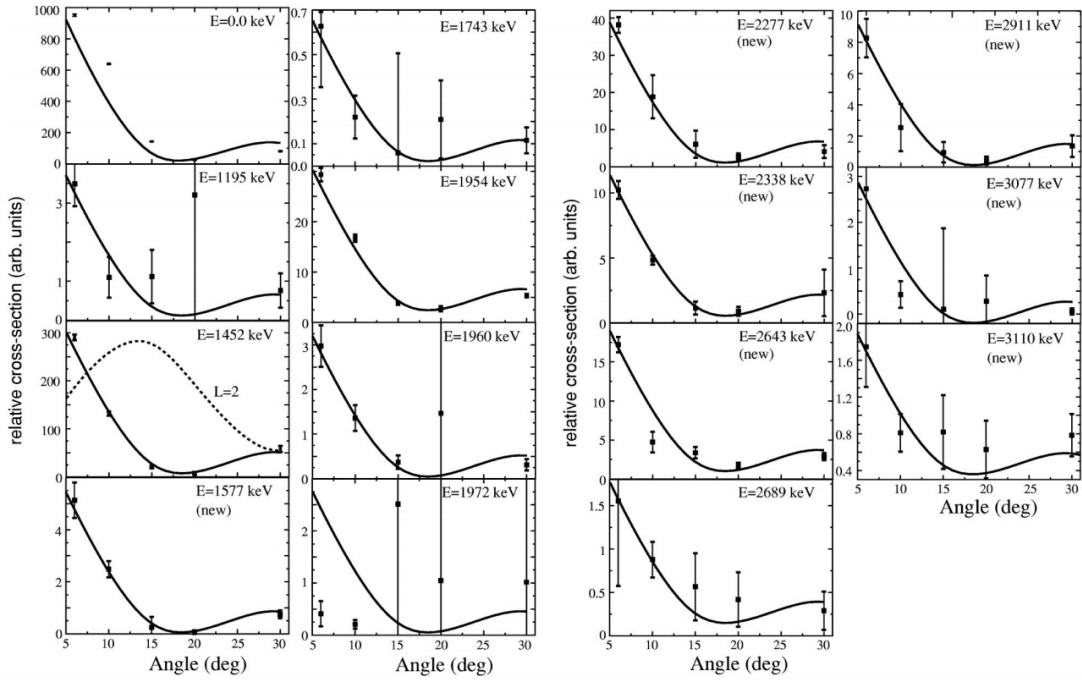


Figure 1.9. Angular distribution data for all 0^+ states in ^{158}Gd observed in the (p,t) reaction in [58]. A DWBA calculation for an $L=2$ transition is shown as a dotted line in the $E=1452$ keV plot to show the unique nature of the $L=0$ transitions (in solid black).

This renaissance of (p,t)/(t,p) reaction studies has emerged in the past decade, as well as a coordinated flurry of theoretical and experimental efforts and campaigns to begin to answer the still open and important query of the nature of 0^+ excitations in the rare-earth region of nuclei [1, 14, 16, 24, 30, 41, 65, 74, 81, 84]. Figure 1.10 shows the number of 0^+ states for rare earth nuclei, due in large part to the two nucleon transfer reaction studies by Meyer and Lesher [50, 58].

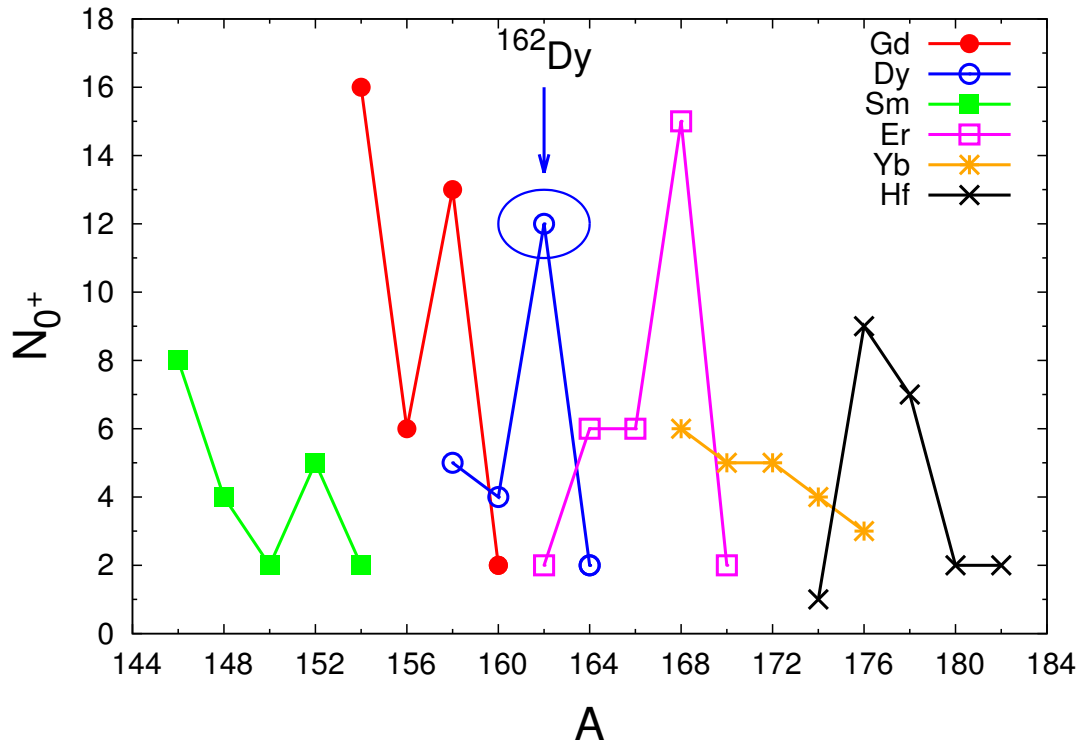


Figure 1.10. Number of 0^+ states in rare earth isotopes of Sm, Gd, Dy, Er, Yb, and Hf. ^{162}Dy is highlighted with a blue circle.

In their recent review [41], Heyde & Wood outline several criteria (key experimental fingerprints) to successfully elucidate the true nature of these 0^+ excitations.

- I. Two nucleon transfer reaction strengths, (p,t) or (t,p)
- II. Monopole E0 strengths, $\rho^2(E0)$
- III. Absolute reduced transition probability measurements, $B(E2;0_i^+ \rightarrow 2_{g.s.}^+)$

Individually, the experimental quantities listed above cannot fully probe any collective nature of excitations within the nucleus, but in tandem, can uncover much of the mystery of the makeup of nuclear states.

In many cases (due in part to the pioneering (p,t) measurements made by [50, 58]) throughout the rare-earth region of nuclei, two nucleon transfer reaction strengths are available; the relative cross sections can provide a clue to pairing configurations in nucleons [41]. This implies that a large relative cross section between two-nucleon transfers will signify a large single- or two-quasiparticle nature of a particular excited state. Historically, inflated two-nucleon transfer reaction cross sections between 0^+ states were observed as evidence of rapid shape change of the nucleus [24]. Multinucleon transfer reactions also offer a double-pronged attack, in that the spectroscopy can also find/confirm the existence of 0^+ excitations, recalling the (p,t) reactions outlined in §1.3.

Monopole E0 transitions, the γ -ray forbidden decay of a $0^+ \rightarrow 0^+$ transition, provide insight into a unique facet of the nuclear structure, as the transition is directly related to the mean-square nuclear radius, and thus, the extent of deformation. The measurement of E0 transitions offers clues to the nature of 0^+ states, but these experimental signatures are far from easy to obtain [40]. Since a γ -ray carries *at least* one unit of angular momentum away from the nucleus, and no angular momentum transfer takes place in a $0^+ \rightarrow 0^+$ transition, the nucleus must decay via internal conversion electrons. The transition probability of an E0 transition differs in form from the traditional γ -ray reduced transition probability (see §1.4.1), but is expressed

by the monopole strength, the internal conversion electron analogue, $\rho^2(E0)$, instead. A similar amount of experimental and theoretical effort is being made in regards to the E0 transitions in rare-earth nuclei [29].

Finally, the absolute $B(E2)$ transition probabilities (inversely proportional to the lifetime of excited states) are the largest clue to the collectivity of states, as they hold a vital part in testing both the IBA and the geometric collective model. The measurement of excited state lifetimes (as seen in the upcoming §1.4) are the main focus on this work.

Strong octupole shape correlations have been experimentally observed in spherical/transitional nuclei (and recently in neutron-rich ^{144}Ba) by the observation of strong E3 multipolarity radiation that decays to the ground state [17, 33]. Similarly, strong quadrupole-octupole coupling has been observed in the form of $2^+ \otimes 3^-$ coupling in several cases by the observation of $K^\pi = 2^- \rightarrow 2_\gamma^+$ transitions [60, 73, 76]. In all of these cases, we see and stress the importance of reduced transition probabilities connecting nuclear states. One experimental observable that points toward any octupole correlation (as a means to measure reflection asymmetry, a signature of octupole deformation) is the measurement of E3-multipolarity radiation, which we do not employ in this work due to the lack of detection of this type of radiation. However, significant (albeit less than straightforward) emphasis is placed in the measurement of E1 radiation to study octupole vibrations in the deformed rare-earth region [60, 76].

1.4 Assessing Nuclear Structure from Decay Radiation

The detection of electromagnetic γ radiation is of great value when studying the structure of the nucleus. Since γ -decay of the nucleus is one of the dominant methods of de-excitation for states below the energy threshold for particle emission, a link (some quantum mechanical operator) between two quantum states can be made

via the electromagnetic Coulomb process. Usually expressed as a matrix element, Equation 1.9 is the manifestation of observables from some corresponding operator (in this case, the electromagnetic operator acting on the nuclear eigenfunctions). In the case of electromagnetic decays, the matrix elements of the E2 multipole transition operators remain a key facet of nuclear structure, as the quadrupole electromagnetic operator drives collective quadrupole transitions in nuclei, lending its importance almost immediately. Similarly, the other multipole expansions of the electromagnetic operator (isovector dipole, isoscalar dipole, octupole, etc.) directly link the charge distributions of two nuclear states, such as the E3 operator for octupole shape change.

$$\mathcal{M}_{fi} = \langle \psi_f | \mathcal{H} | \psi_i \rangle \quad (1.9)$$

When studying excited states in nuclei, measurement of the transition probability (related to the matrix element) becomes the basis for understanding nuclear structure phenomena.

The transition probability (\mathcal{W}) for a γ -decay that de-excites the nucleus from an initial state to a final state can be expressed in terms of the mean lifetime (τ), the average time the nucleus stays in an excited state, or by the half-life ($t_{1/2}$). The exact relationship can be seen in Equation 1.10.

$$\mathcal{W} = \frac{1}{\tau} = \frac{\ln 2}{t_{1/2}} \quad (1.10)$$

For an excited state with multiple γ -decay channels, we can expand the total \mathcal{W} as a sum of all transition probabilities weighted by the branching ratio (BR_i) and internal conversion coefficient (α_i) of each transition (Equation 1.11).

$$\mathcal{W} = \sum_i \frac{BR_i}{\tau(1 + \alpha_i)} \quad (1.11)$$

The number of full mathematical derivations of Fermi's Golden Rule from time-

dependent perturbation theory rivals that of Talmi's estimation of 2^+ configurations in Samarium-154 ($\sim 3 \times 10^{14}$) [20]. The exhaustive treatment can be seen in much greater detail in various sources ([79],[40],[10]), where (in this work) we will start with Fermi's Golden Rule [79] in Equation 1.12.

$$\mathcal{W} = \frac{2\pi}{\hbar} |\langle \psi_f | \mathcal{H}_{EM,int} | \psi_i \rangle|^2 \rho(E_\gamma) \quad (1.12)$$

Here, we can see the direct relationship between the nuclear matrix element and γ -ray energy-dependent density of states ($\rho(E_\gamma)$) to the transition probability, \mathcal{W} . This square of the matrix element describes the coupling of the nuclear-based interaction Hamiltonian to an external electromagnetic field, which brings the nucleus from some initial state $|\psi_i\rangle$ to a final state $|\psi_f\rangle$. This transition, for γ -decay in the nucleus, is represented by the electric or magnetic multipole operator(s) of order λ , \mathcal{O}_λ . From Wigner-Eckhart theory, we can remove any angular momentum dependence from the full matrix element ($|\mathcal{M}_{fi}| = \langle \psi_f | \mathcal{H}_{int} | \psi_i \rangle$) to give us the reduced transition probability in Equation 1.13.

$$B(\pi\lambda; J_i \rightarrow J_f) = |\mathcal{M}_{fi}|^2 = \frac{1}{2J_i + 1} |\langle J_f | \mathcal{O}_\lambda | J_i \rangle|^2 \quad (1.13)$$

Performing a multipole (and subsequent series) expansion of \mathcal{O}_λ into the spherical Bessel functions, spherical harmonics, and the nuclear current density $\mathcal{J}(\vec{r})$ (Equations 1.14 and 1.15) [79], we arrive at Equation 1.16.

$$\mathcal{O}_{\lambda\mu}(E\lambda) = -\frac{(2\lambda+1)!!}{c(\lambda+1)k^{\lambda+1}} \mathcal{J}(\vec{r}) \cdot \vec{\nabla} \times (\vec{r} \times \vec{\nabla})(j_\lambda(kr) Y_{\lambda\mu}(\theta, \phi)) \quad (1.14)$$

$$\mathcal{O}_{\lambda\mu}(M\lambda) = -\frac{(2\lambda+1)!!}{c(\lambda+1)k^\lambda} \mathcal{J}(\vec{r}) \cdot (\vec{r} \times \vec{\nabla})(j_\lambda(kr) Y_{\lambda\mu}(\theta, \phi)) \quad (1.15)$$

$$\mathcal{W} = \frac{8\pi}{\hbar} \frac{(\lambda + 1)}{\lambda[(2\lambda + 1)!!]^2} \left(\frac{E_\gamma}{\hbar c} \right)^{2\lambda+1} B(\pi\lambda; J_i \rightarrow J_f) \quad (1.16)$$

Now, simply recall Equation 1.11 to make Equation 1.17, an extremely important quantity for nuclear structure studies, as every non-constant quantity can be determined in laboratory experiments.

$$B(\pi\lambda; J_i \rightarrow J_f) = \frac{\hbar}{8\pi} \mathcal{F}(\pi\lambda) \frac{BR}{\tau(1+\alpha)} \frac{\lambda[(2\lambda + 1)!!]^2}{(\lambda + 1)} \left(\frac{\hbar c}{E_\gamma} \right)^{2\lambda+1} \quad (1.17)$$

In Equation 1.17, $\mathcal{F}(\pi\lambda)$ is a measure of the mixing from differing multipolarity γ radiation; For pure E1, E2, or M1 transitions, this factor collapses to unity, where $\mathcal{F}(\pi\lambda)$ for mixed E2 & M1 radiation follows the relations in 1.18 & 1.19:

$$\mathcal{F}(E2) = \frac{\delta^2}{1 + \delta^2} \quad (1.18)$$

$$\mathcal{F}(M1) = \frac{1}{1 + \delta^2} \quad (1.19)$$

The multipole mixing fraction δ is an experimentally measured quantity (to be discussed later) as a ratio of the E2/M1 transition strengths.

1.4.1 Importance of Transition Probabilities

To provide a comparison of the relative collectivity of a transition on a meaningful scale, it is generally prudent to express $B(\pi\lambda)$ in terms of a Weisskopf estimate. This formulation assumes that only one nucleon is involved in a particular transition [79], and is given in Equations 1.20 and 1.21 for electric-type transitions and magnetic-type transitions, respectively.

$$B(E\lambda) = \frac{0.12^{2\lambda}}{4\pi} \left(\frac{3}{\lambda + 3} \right)^2 A^{\frac{2\lambda}{3}} \quad (1.20)$$

$$B(M\lambda) = 0.12^{2\lambda-2} \frac{10}{\pi} \left(\frac{3}{\lambda+3} \right)^2 A^{\frac{2\lambda-2}{3}} \quad (1.21)$$

These ‘Weisskopf Units’ (W.u.) act as a normalization or ‘yardstick’ for collective strength in nuclei, as $B(\pi\lambda) \gg 1$ imply strong collective motion in the nucleus. In the rare-earth region, nuclear collectivity is generally dominated by nuclear rotation, an incredibly collective phenomenon with transition rates upwards of 100+ Weisskopf units! However, from our previous observations of vibrational phenomena in deformed nuclei, we observe order(s) of magnitude weaker transition strengths for the rare earth nuclei. Weisskopf units are not universally adopted however, with some (especially older) works relying on the natural units of $e^2 b^\lambda$. Transition probabilities in this work are reported in W.u., but for the purposes of unit conversion, Table 1.1 shows this conversion for E1, M1, E2, and E3 transition probabilities for both ^{160}Gd and ^{162}Dy .

TABLE 1.1

WEISSKOPF CONVERSIONS FOR ^{160}GD AND ^{162}DY

$\pi\lambda$		^{160}Gd	^{162}Dy	
1 mW.u.	E1	= 1.90	1.91	$e^2 b$
1 W.u.	E2	= 5.16E-7	5.25E-7	$e^2 b^2$
1 W.u.	E3	= 1.52E-9	1.56E-9	$e^2 b^3$
1 W.u.	M1	= 1.79	1.79	μ_N^2

Unit conversion for transition probabilities from Weisskopf units to $e^2 b^\lambda$ (μ_N^2 for M1s) for ^{160}Gd and ^{162}Dy .

To give these transition probabilities context in a vibrational sense, the electric and magnetic multipole operator is proportional to the phonon annihilation operator, \mathbf{b} in the vibrational model [79]. This is again, analogous to the classic harmonic oscillator problem in quantum mechanics, where the basis states that make up the eigenfunctions of the phonon creation/destruction operators. Since the matrix element of this annihilation operator and two harmonic oscillator states is $\sqrt{N_{phonon}}$, the reduced transition probability for a γ -decay that destroys an N_{phonon} state will be proportional to the number of phonons in the state, N_{phonon} , outlined in Equation 1.22.

$$\mathcal{O}_\lambda \propto \mathbf{b}_\lambda \rightarrow \langle \psi_f | \mathbf{b}_\lambda | \psi_i \rangle = \sqrt{N_{phonon}} \rightarrow B(\pi\lambda) \propto N_{phonon} \quad (1.22)$$

This fact implies the transition probability for a double phonon vibrational state will be enhanced in relation to the already inflated $B(E2)$ of a single phonon vibration (in W.u.). These high $B(E2)$ values should be a ‘signature’ of collective motion, however, recall that the $B(E2)$ strength is inversely proportional to the energy of the γ -ray ($B(E2) \propto E_\gamma^{-5}$), meaning higher energy transitions will be suppressed in relation to the lower energy transition probabilities. The delicate balance between interband and full de-exciting transitions must be stressed to fully understand the structure of these states.

Transition probabilities can also be compared to the ‘Alaga’ rules to provide a benchmark of relative transition strength. The Alaga rules imply that the intrinsic matrix elements for two transitions leaving the same level will be identical (an assumption that the parent state is a rotational excitation), so the ratio of their reduced transition probabilities are only dependent on the square of the Clebsch-Gordan coefficients (Equation 1.23). As a first-order approximation, these rules agree remarkably well with experimentally measured $B(E2)$ values, especially for the lowest spin members of a rotational band (again, the bulk of this work).

$$\frac{B(E2; J_i \rightarrow J_f)}{B(E2; J_i \rightarrow J'_f)} = \frac{\langle J_i K_i 2(\Delta K) | J_f K_f \rangle^2}{\langle J_i K_i 2(\Delta K) | J'_f K_f \rangle^2} \quad (1.23)$$

Of course, a limitation behind the Alaga rules is that it only gives relative transition probabilities, where the absolute $B(E2)$ is needed, and also can only be used to compare transition probabilities for multiple decays out of the same parent state.

1.5 Decay and Structure Systematics in the $150 < A < 180$ Region

Throughout all of the assertions in [41] and a flurry of experimental and theoretical efforts preceding and succeeding it, the jury is still out on the nature of low-lying excitations in rare-earth nuclei and the evolution of collectivity with nuclear deformation. Globally, the lifetimes presented in this work aim to elucidate some of the mystery behind the systematic behavior (or lack thereof) of quadrupole and octupole vibrations in deformed nuclei. Before the emergence of 0^+ studies with the Q3D spectrometer, there were very few known 0^+ excitations in literature, and even less with accompanying lifetime measurements! Historically, the 0^+ bands are populated far weaker than their 2^+ γ -band cousins, making direct measurement of their lifetimes with techniques like Coulomb Excitation much less straightforward. Many of the lifetime measurements made in this work are new, in an region of nuclei where literature lifetimes (especially lifetimes of 0^+ states) are scarce. Figures 1.11, 1.12, 1.13, 1.14, 1.15, and 1.16 show the even isotopes of rare-earth nuclei throughout varying degrees of deformation (marked by the $R_{\frac{4}{2}}$ value). Each set of level schemes displays the ground state band, excitation energies of the first excited 2^+ bandhead, the energies of all excited 0^+ states, literature $B(E2)$ values (in W.u.) for any 2^+ or 0^+ de-excitations, as well as the proton & neutron pairing gap ($2\Delta_\pi$ in green and $2\Delta_\nu$ in blue) for each isotope (calculated from Equations 1.5 and 1.6 in [6] & [53]).

1.5.1 $K^\pi=0^+, 2^+$ Systematics in Samarium, Gadolinium, and Dysprosium Nuclei

At the low-mass end of the rare-earth region, which includes Sm, Gd, and Dy isotopes, we are presented with a series of rapidly-changing deformations in the nucleus, as well as a sharp drop in collectivity of the 0_2^+ bandheads as they decay to the ground state. The paradigms of the β -vibration seem to be abundant in nuclei like ^{150}Sm and $^{154,156}\text{Gd}$, with distinctly collective decays to the ground state. However, these nuclei are not considered fully deformed (noted by their $R_{\frac{4}{2}} \leq 3$), so their existence as collective vibrations do not answer our question whether or not deformed nuclei can exhibit collective quadrupole vibrations. We also see the same pockets where we lack lifetime information for all 0^+ states in the region, notably ^{146}Sm , ^{154}Gd , and $^{156,158}\text{Dy}$ nuclei. Yet again, the collectivity of the $2^+ \gamma$ bands are consistently well-behaved, speaking to the stability of this vibrational excitation. In all cases except ^{158}Gd , any candidates for the β -vibration are well below the pairing gaps drawn for each nucleus, and is to be expected; this case of ^{158}Gd 's most collective decay from a 0^+ lying above the pairing gap is extremely curious, and unfortunately does not clear up the nature of 0^+ bands in deformed nuclei!

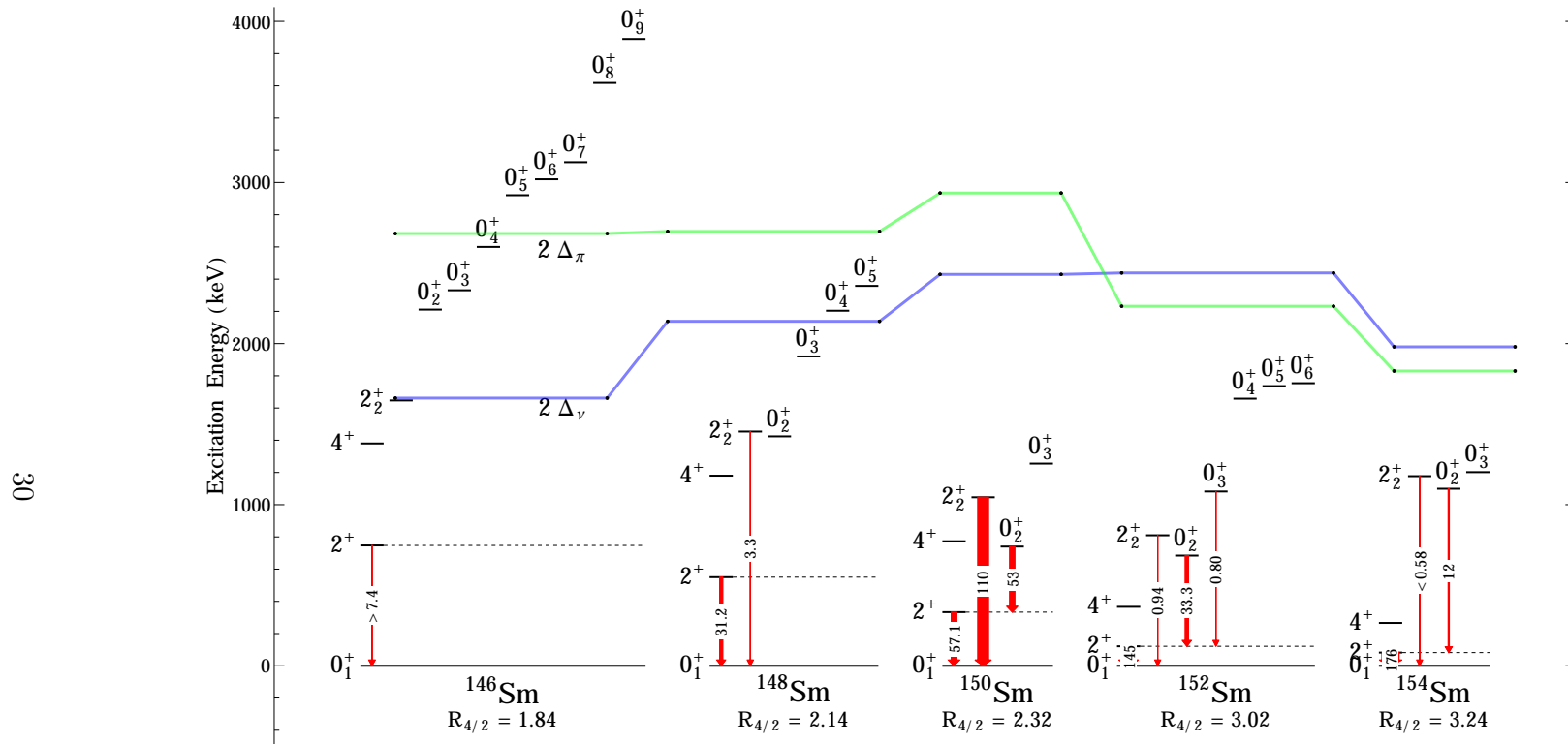


Figure 1.11. Systematics for the energies of excited 0^+ states, the first excited 2^+ bandhead, and low-lying ground state band members for even-even Samarium nuclei. Proton and neutron pairing gaps ($2\Delta_\pi$ and $2\Delta_\nu$, respectively) are drawn in green and blue and are calculated from Equations 1.5 and 1.6. Transition arrows represent known experimental $B(E2)$ measurements for 0^+ bandheads and 2^+ bandheads (in W.u. where known).

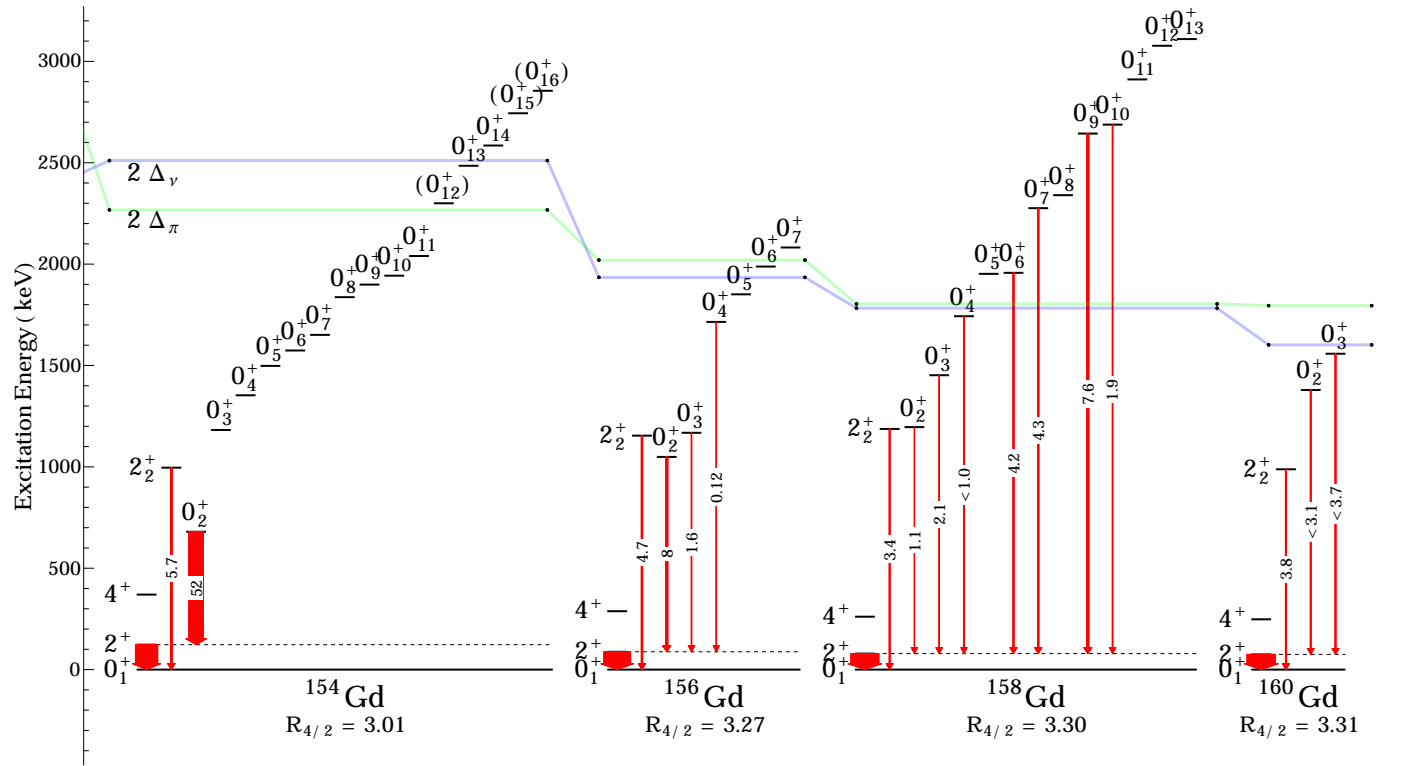


Figure 1.12. Systematics for the energies of excited 0^+ states, the first excited 2^+ bandhead, and low-lying ground state band members for even-even Gadolinium nuclei. Proton and neutron pairing gaps ($2\Delta_\pi$ and $2\Delta_\nu$, respectively) are drawn in green and blue and are calculated from Equations 1.5 and 1.6. Transition arrows represent known experimental $B(E2)$ measurements for 0^+ bandheads and 2^+ bandheads (in W.u. where known).

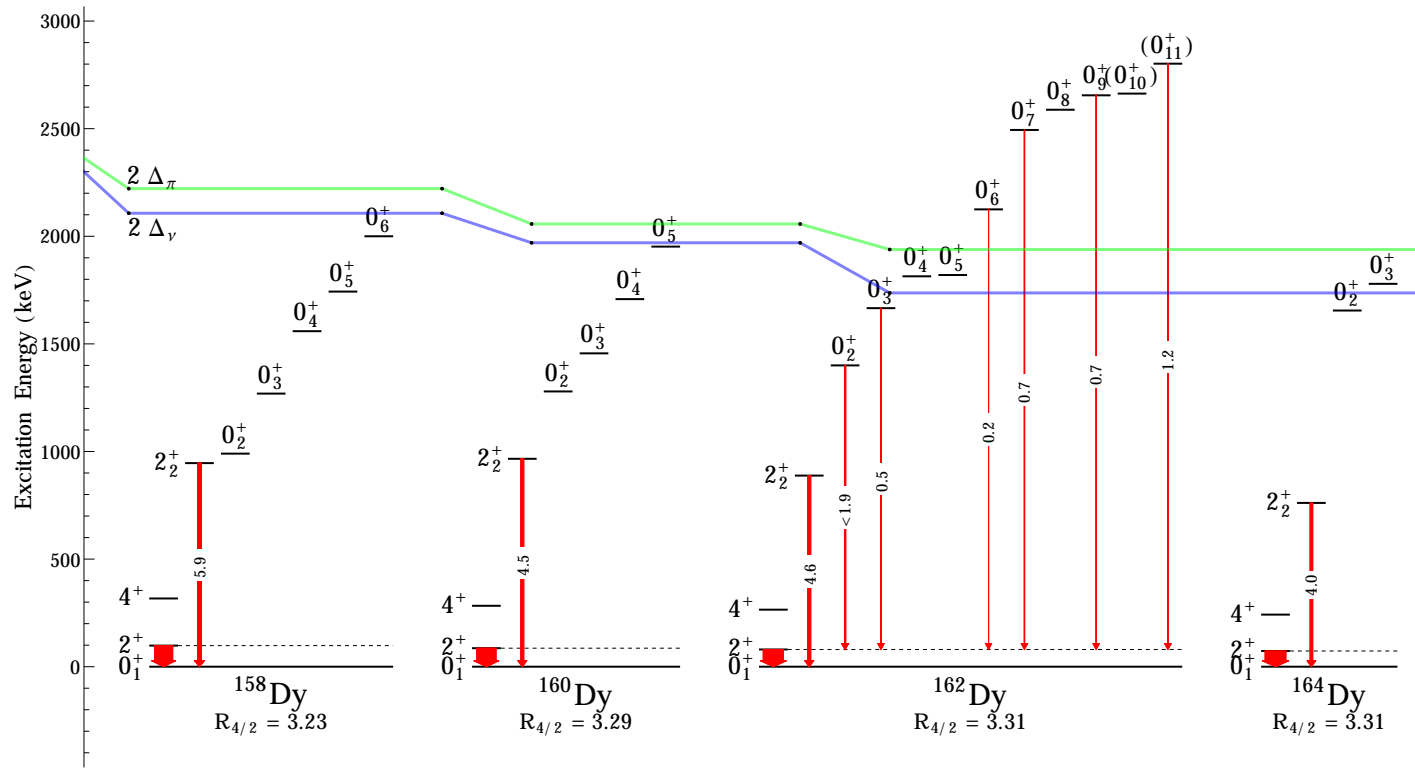


Figure 1.13. Systematics for the energies of excited 0^+ states, the first excited 2^+ bandhead, and low-lying ground state band members for even-even Dysprosium nuclei. New transition probabilities are presented in ^{162}Dy , with the widths proportional to $B(E2)$ values (in W.u.); also shown are the proton and neutron pairing gap ($2\Delta_\pi$ and $2\Delta_\nu$, respectively) for each isotope.

1.5.2 $K^\pi=0^+,2^+$ Systematics in Erbium, Ytterbium, and Hafnium Nuclei

At the heavier end of the region, we echo some of the same rhetoric as the preceding nuclei, in that lifetime information for all 0^+ states is lacking in select places, but we still retain *some* semblance of the β -vibration in nuclei like ^{166}Er and ^{172}Hf , as well as an overall behavior of the γ vibration across the entire chain of isotopes. In contrast, however, these nuclei are all well-deformed, and would be great nuclei to study the feasibility of vibrations on top of deformed ground states (take ^{168}Er for example).

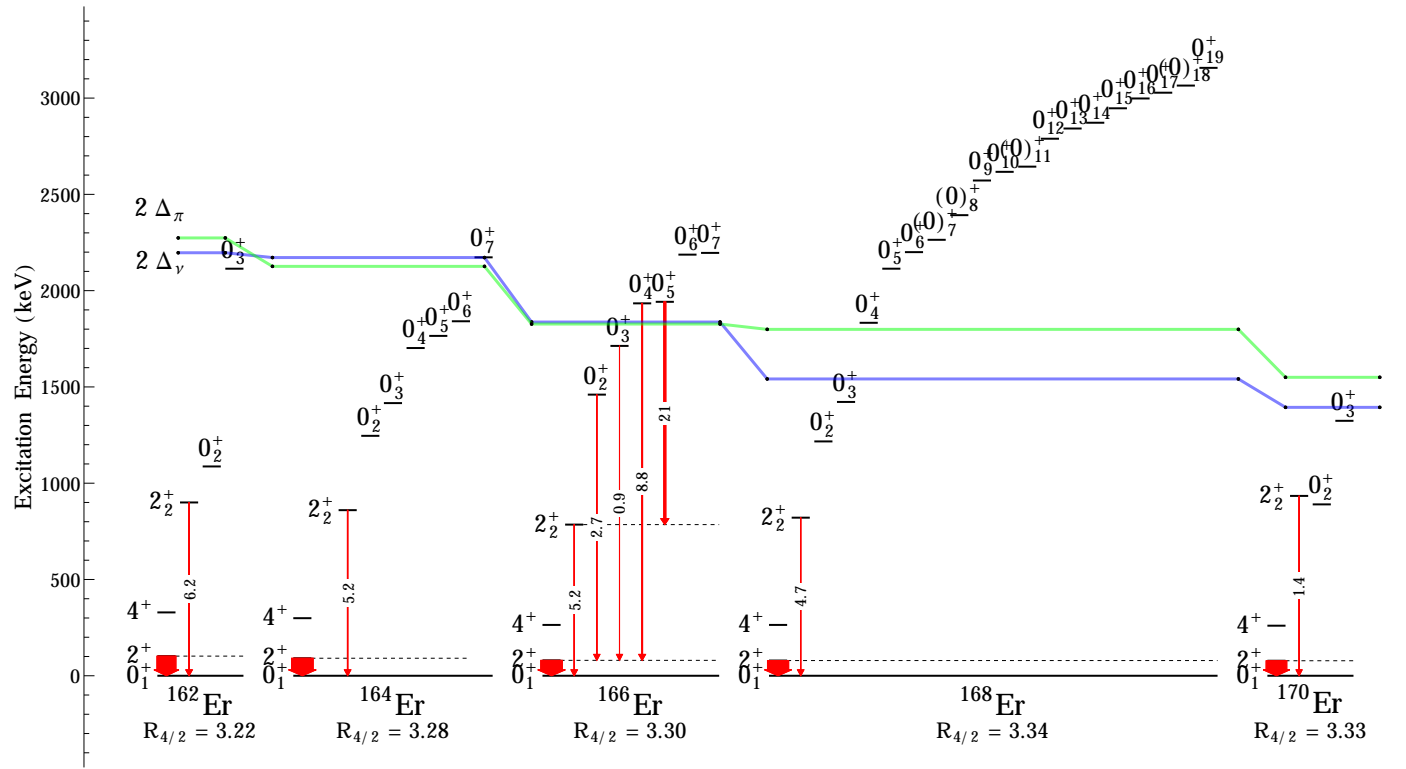


Figure 1.14. Systematics for the energies of excited 0⁺ states, the first excited 2⁺ bandhead, and low-lying ground state band members for even-even Erbium nuclei. Proton and neutron pairing gaps ($2\Delta_\pi$ and $2\Delta_\nu$, respectively) are drawn in green and blue and are calculated from Equations 1.5 and 1.6. Transition arrows represent known experimental B(E2) measurements for 0⁺ bandheads and 2⁺ bandheads (in W.u. where known).

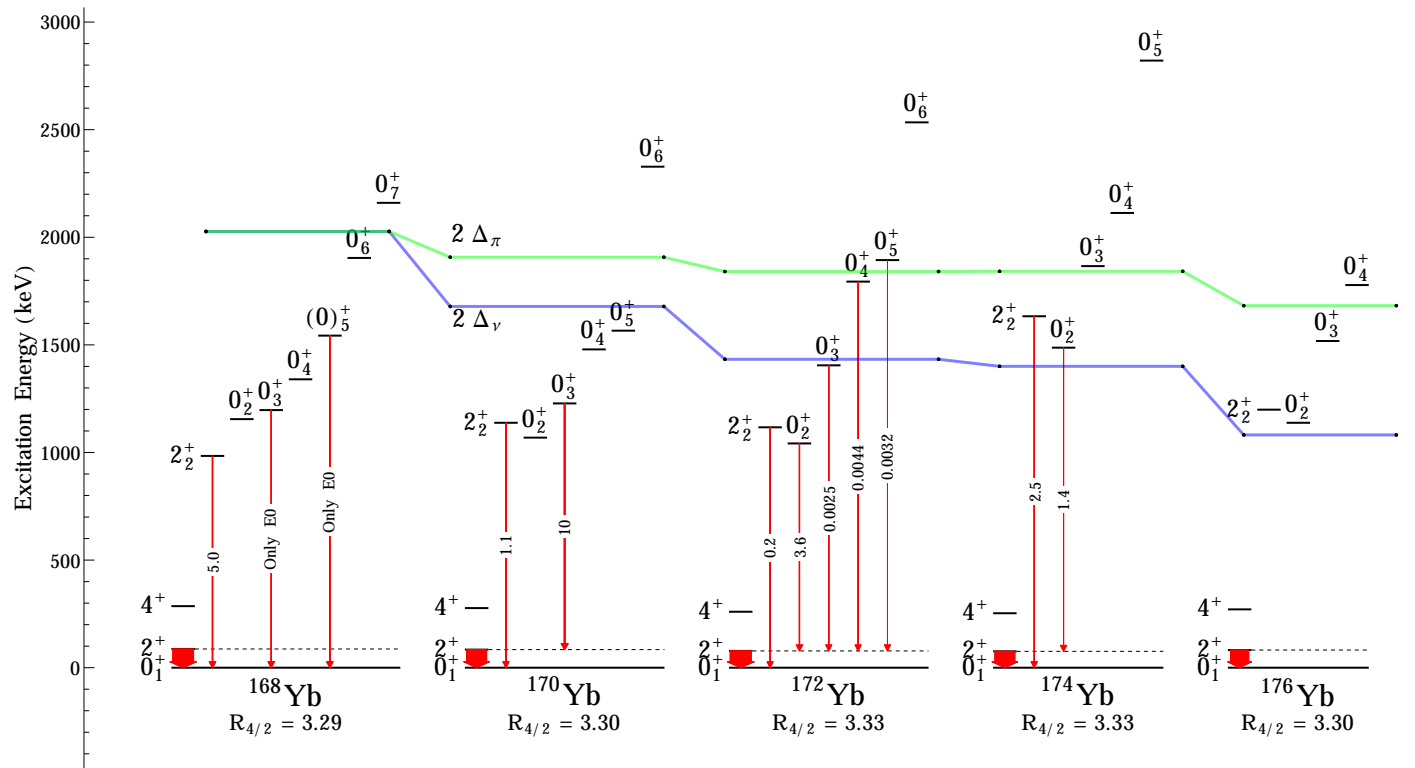


Figure 1.15. Systematics for the energies of excited 0^+ states, the first excited 2^+ bandhead, and low-lying ground state band members for even-even Ytterbium nuclei. Proton and neutron pairing gaps ($2\Delta_\pi$ and $2\Delta_\nu$, respectively) are drawn in green and blue and are calculated from Equations 1.5 and 1.6. Transition arrows represent known experimental $B(E2)$ measurements for 0^+ bandheads and 2^+ bandheads (in W.u. where known).

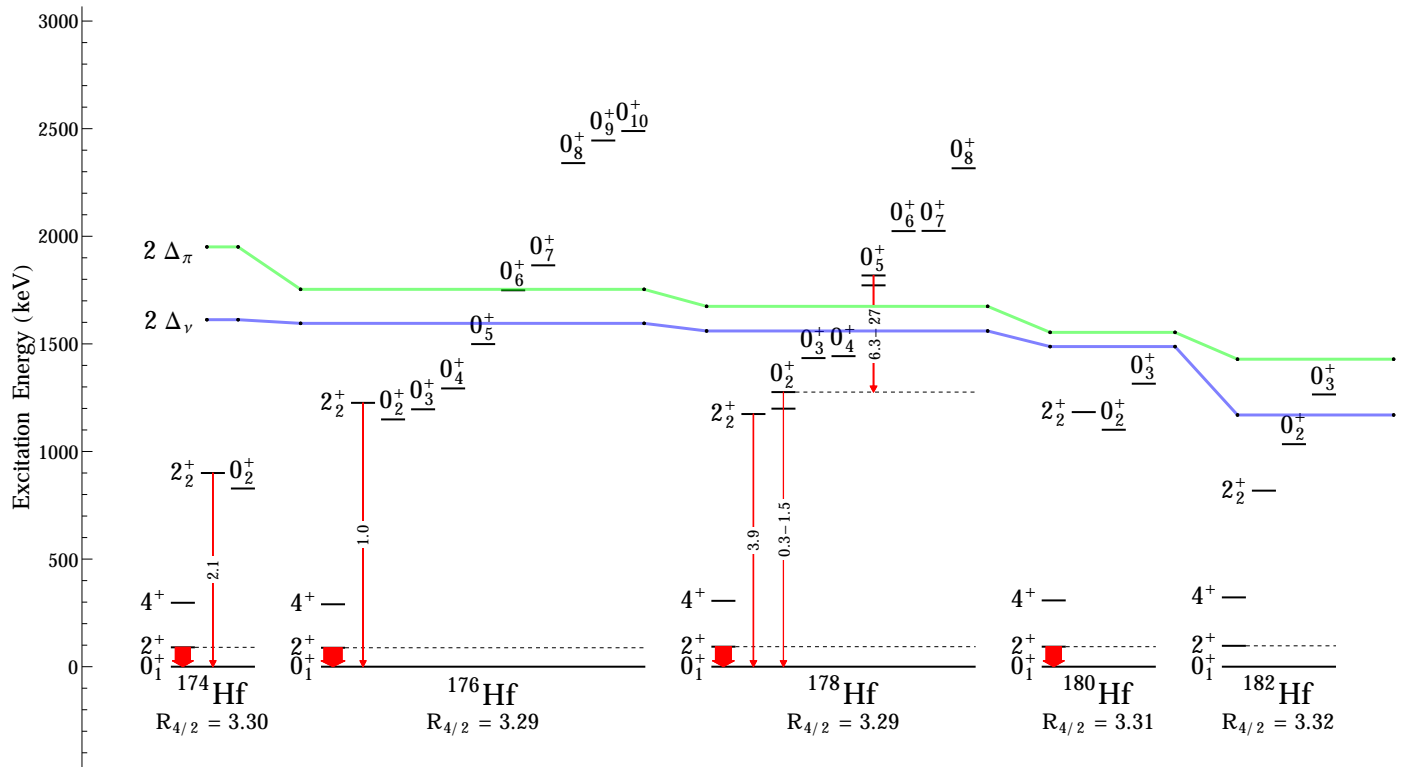


Figure 1.16. Systematics for the energies of excited 0⁺ states, the first excited 2⁺ bandhead, and low-lying ground state band members for even-even Hafnium nuclei. Proton and neutron pairing gaps ($2\Delta_\pi$ and $2\Delta_\nu$, respectively) are drawn in green and blue and are calculated from Equations 1.5 and 1.6. Transition arrows represent known experimental B(E2) measurements for 0⁺ bandheads and 2⁺ bandheads (in W.u. where known).

In these figures, we can immediately observe some key motivations for performing lifetime measurements in the rare earth region. First, there are currently pockets where we lack literature lifetime information for 0^+ excitations in the $150 < A < 180$ region, especially for states below the proton and neutron pairing gaps, where we would expect to find macroscopic collective motion. Second, in the Gadolinium nuclei, a particular suppression of the collectivity of the lowest-lying 0^+ state appears as the static deformation increases. This decrease in collective strength complements the long-standing irregularities in collective strength of 0^+ excitations, highlighted by the otherwise ‘well-behaved’ collectivity of the lowest lying $K^\pi=2^+$ bands [14, 21]. Lastly, this general inconsistency in collective strength of the 0^+ states must be further investigated (previous studies include [31, 69, 70]) to match the assertions provided in [41]. It is entirely reasonable to make the case for strongly collective β -vibrations in spherical or transitionally deformed nuclei with strong $B(E2)$ s to the ground state 2^+ , (see $^{150,152}\text{Sm}$ in Figure 1.11 and ^{154}Gd in 1.12) where $R_{\frac{4}{2}} < 3$, but as we move to the well-deformed, rotational limit of nuclei, the story definitively changes, and the behavior of the lowest-lying 0^+ state changes drastically! Nuclei in the rare-earth region along the line of stability have been hallmarks of spectroscopic knowledge, being some of the most well-studied nuclei for decades, giving us a well-defined goal to characterize the multitude of states where we have a wealth of knowledge as a foundation!

1.5.3 Negative Parity States in Gadolinium and Dysprosium Nuclei

We can also see the lack of lifetime information for low-lying negative parity states in rare-earth nuclei, of which, we will study the same cases (^{160}Gd and ^{162}Dy) for the isotopic chains of even-even rare-earth nuclei. Figures 1.17 and 1.18 show the energy systematics for the lowest-lying negative parity bands across isotopes. Immediately again, we see the energies of the negative parity states mentioned in §1.2

in regards to the shifting and re-ordering of the split negative parity bands. Again, just like the $K^\pi=0^+$ bands, crucial lifetime information for these states is scarce (only 6 lifetimes of negative parity states are known in Dysprosium nuclei); given the number of excitations below the pairing gap (where we expect to see collective excitations), measurement of the $B(E1)$ transition probabilities can allude to any octupole correlations as a phonon excitation in the nuclei discussed in this work, yet the most important piece of experimental evidence (which still remains out of the scope of the experiments performed in this work) is the absolute $B(E3)$ transition probabilities linking states. Enhanced $B(E1)$ strengths have been attributed to the octupole vibration as a type of reflection asymmetry, but are not a smoking gun of the octupole vibration, but more and more nuclei in the rare-earth region display an enhanced degree of dipole strength in the octupole vibration [60, 76].

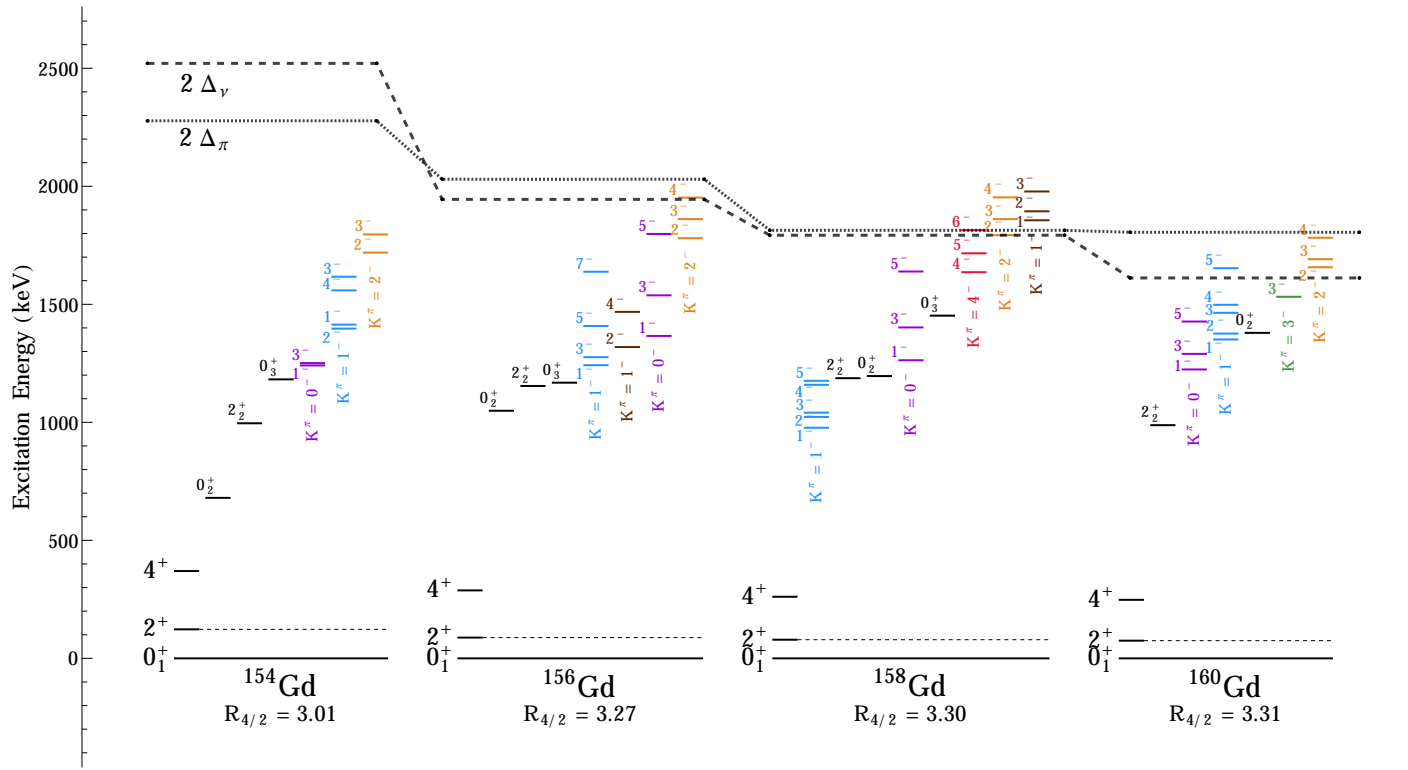


Figure 1.17. Systematics for the energies of excited negative parity states, the first excited 2^+ bandhead, and low-lying excited 0^+ states below the pairing gap ($2\Delta_\pi$ and $2\Delta_\nu$) for even-even Gadolinium nuclei.

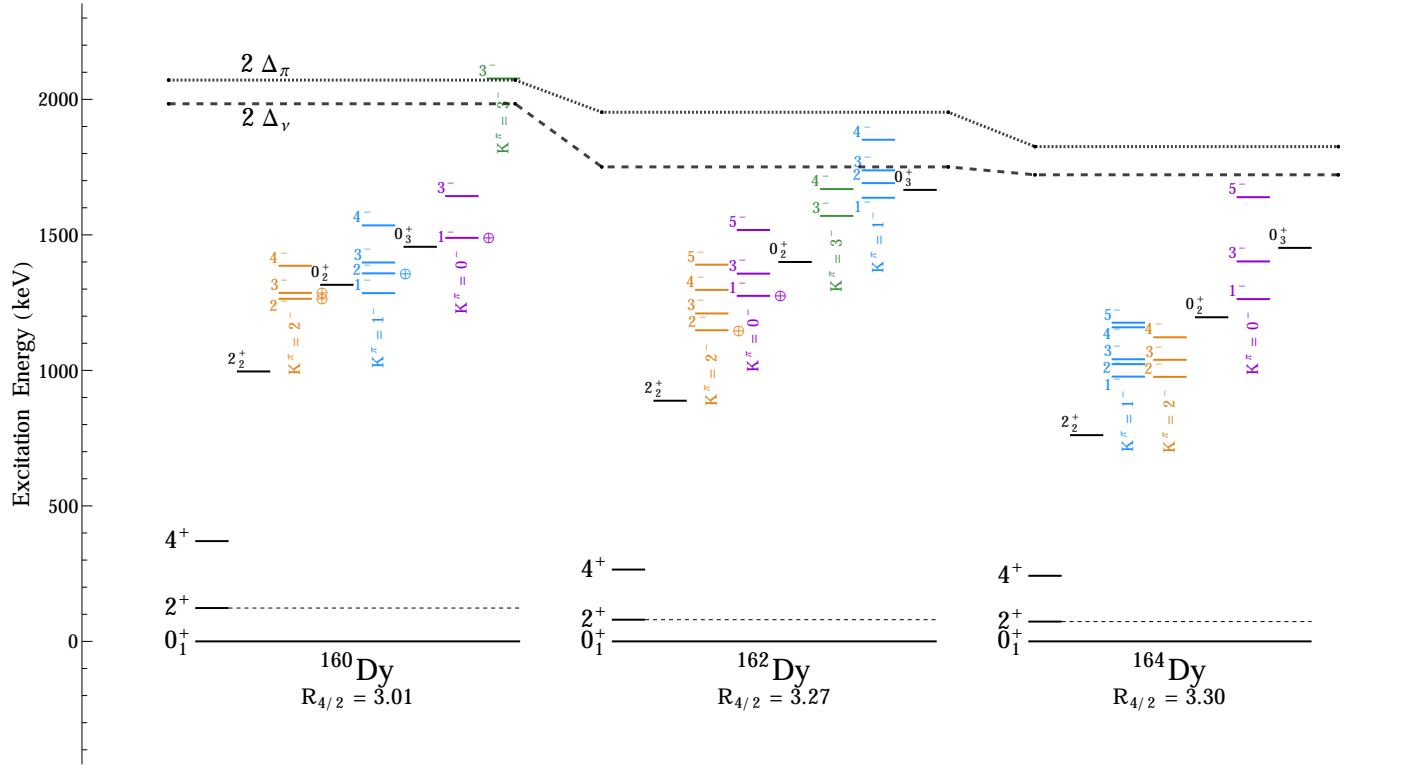


Figure 1.18. Systematics for the energies of excited negative parity states, the first excited 2^+ bandhead, and low-lying excited 0^+ states below the pairing gap ($2\Delta_\pi$ and $2\Delta_\nu$) for even-even Dysprosium nuclei. States with a '+' marker indicate where a literature lifetime measurement exists.

1.5.4 Multiphonon Configurations in Deformed Nuclei

We end discussion of the systematics of rare-earth nuclei with any known multiphonon configurations ($K^\pi=0^+, 4^+ \gamma\gamma$ type, $K^\pi=0^+ \beta\beta$). Figure 1.19 contains a series of level schemes of rare-earth nuclei with measured and confirmed two-phonon states; these states are evident by the observation of collective decays to known collective states. For example, the $4^+ \gamma\gamma$ -vibration in ^{166}Er decays via a 7.4 Weisskopf unit $B(\text{E}2)$ to the bandhead of the $2^+ \gamma$ -vibration (it then subsequently decays via a collective $B(\text{E}2)$ to the ground state). As with previous assertions about the ‘reliability’ of the γ -vibration as a paradigm of nuclear collective vibrations, Figure 1.6 shows the absolute $B(\text{E}2; 2_\gamma^+ \rightarrow 0_{gs}^+)$ measurements in the literature from the $K^\pi=2^+$ bandheads, simply to highlight its uniformity over the entire deformed rare-earth region. The trend for Samarium nuclei is drastic, but these isotopes lie in a region of extremely fast shape-change, from nearly spherical to fully deformed within a few nucleons! In a perplexing change of rhetoric in the rare-earths, we observe (and continue to investigate) that many well-deformed nuclei do not exhibit the traditional Bohr-Mottelson behavior of a collective β -vibration existing as the lowest-lying 0^+ state. Instead, many of these lowest-lying 0^+ states exist as the $\gamma\gamma$ -vibration, with distinctly collective transitions to the $2^+ \gamma$ -band. Truly, whether or not the notion of a traditional β -type vibration is valid seems to be lacking in the deformed case, from the current experimental data. Compare the number of known $0^+ \gamma\gamma$ configurations to the preceding Figures (??) that highlight the status of lifetime measurements of the states and we observe the distinct lack of structure information that still plagues the rare-earth region. No known $\beta\gamma$ -vibrations have been observed in the rare-earth nuclei at any excitation energy via a collective transition to a collective β or γ -vibration. However, the 0_5^+ state in ^{178}Hf *could* be the first experimental evidence of a $\beta\beta$ vibration, pending the confirmation of the 0^+ state as a collective β -vibration; as it stands now, the collectivity of the β -band is tentative, ranging from non-collective

to a distinct level of collectivity. If the lowest 0^+ band in ^{178}Hf is indeed a collective β -vibration, we already have the experimental evidence of a collective transition from another $K^\pi=0^+$ band built on top of it, making the 0_5^+ band a $\beta\beta$ -vibration.

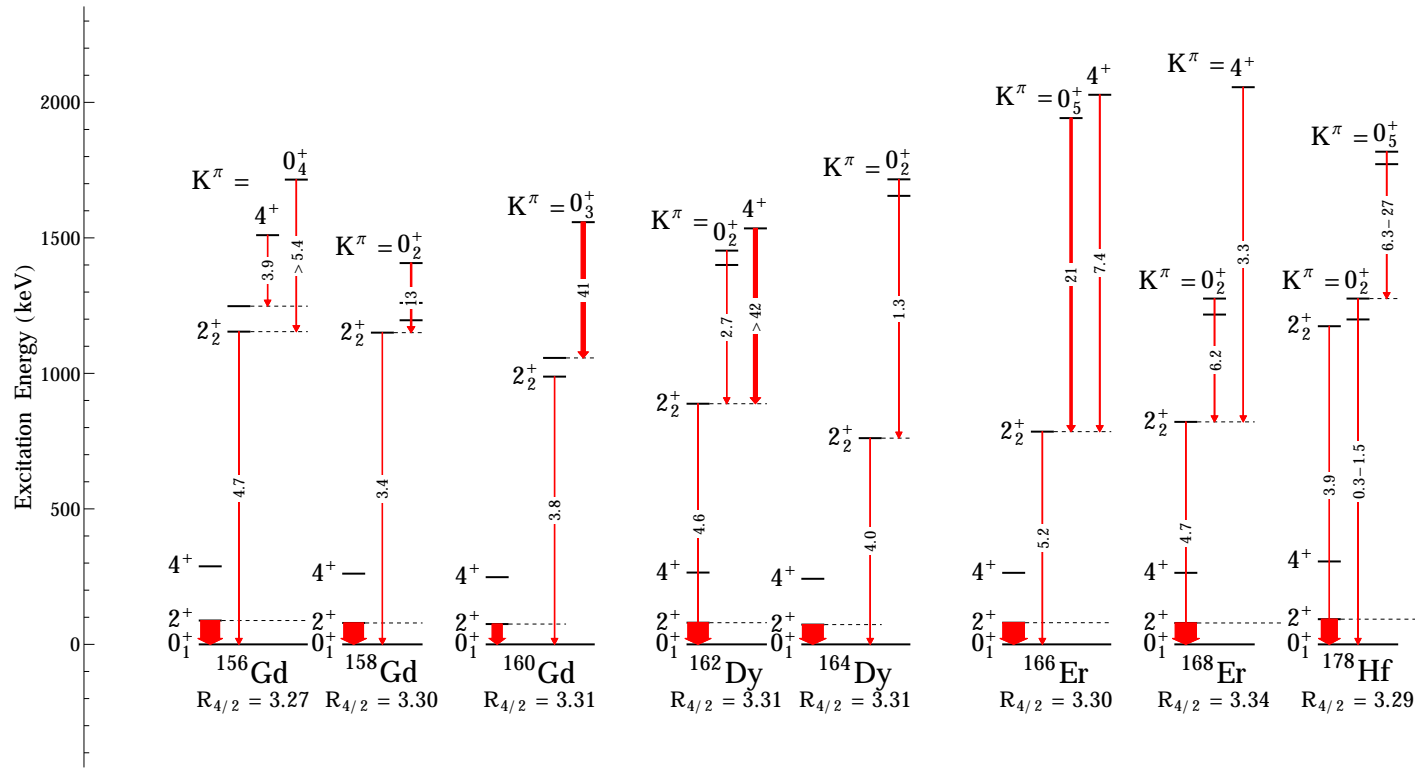


Figure 1.19. Summary of all known multiphonon ($\gamma\gamma$, $\beta\gamma$, or $\beta\beta$) configurations in rare-earth nuclei, absolute $B(E2)$ from literature are shown in Weisskopf units to signify collective decays to γ -vibrational and/or potential β -vibrational states.

Furthermore, we stress that this problem in nuclear structure is very open, with varied systematic behavior of all K=0 bands in deformed nuclei. In some cases, a collective β vibration can be found as the lowest-lying 0^+ state, or at a higher excitation energy, in others, the lowest-lying 0^+ acts like a collective two-phonon vibration built on top of the γ -vibration, and in others, one of the higher excitations acts as a $\gamma\gamma$ -vibration. Surely, the issue at hand of the nature of 0^+ excitations is a wide-open question in nuclear structure, and has been for decades, with a multitude of questions to answer. Can the deformed nucleus act as a near-infinite quantum system with all vibrational degrees available and afforded to it? If we observe well-behaved vibrations in the form of the γ bands as the lowest 2^+ bands, why do we not have the same B(E2) systematics of the β -vibration as the lowest 0^+ bands? Is the β vibration even viable for well-deformed nuclei; if not, what is happening to the β vibration across chains of nuclei in the rare-earth region?

Gadolinium-160 and Dysprosium-162 nuclei both have a very well-deformed shape ($R_{\frac{4}{2}}=3.31$) as well as a modest number of confirmed and tentative 0^+ excitations to study the feasibility of vibrational degrees of freedom superimposed on top of a rotational ground state. Literature lifetimes for most states (especially 0^+ states and the negative parity states of interest for any octupole correlations) in these nuclei are also scarce, further motivating the lifetime measurements. A great deal of effort and importance is placed on the evolution of nuclear structure across isotopic changes, or at least in a regional scale on the chart of nuclides; the emergence of nuclear data aids in the simultaneous evolution of theoretical effort to explain the various nuclear structure phenomena at the forefront of nuclear physics. In order to fully ascertain the nature of low-lying excitations (whether they are macroscopic, collective vibrations superimposed on top of a deformed ground state, multiconfigurative particle-quasiparticle states, or something completely different), consistent, precise, and accurate lifetime measurements of excited states must be performed

in nuclei where we already have a wealth of spectroscopic knowledge to aid in the characterization of states.

CHAPTER 2

EXPERIMENTS AND DATA ACQUISITION

2.1 Lifetime Measurements of Excited States

The measurement of excited state lifetimes remains an integral part in discerning information about the structure of the nucleus. An abundance of techniques, applicable/sensitive lifetime ranges, and facilities can be implemented to measure these lifetimes in the massive landscape of existing isotopes in nuclei. A schematic of experimental measures available for use with several lifetime measurement techniques can be found in Figure 2.1:

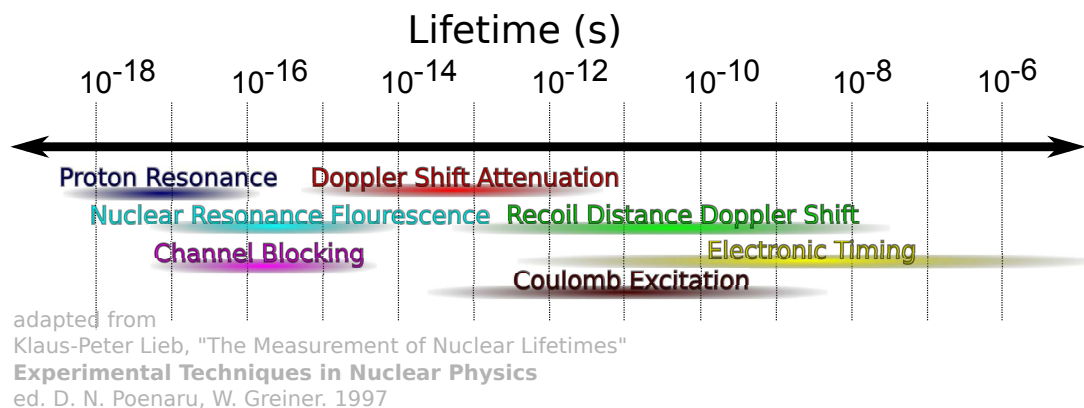


Figure 2.1. Techniques available to nuclear physicists to measure lifetimes as short as a few attoseconds (10^{-18} s) to the more long-lived lifetimes on the order of microseconds (10^{-6} s) (Adapted from [66], courtesy of M. K. Smith).

The various lifetime measurement techniques span a tremendous and continuous range of possible lifetimes for nuclear excitations, from $\sim 10^{-18}$ to $\sim 10^{-6}$ s, and can be applied to the vast majority of the ~ 3339 known nuclei in existence (stable and unstable). Several lifetime measurement techniques directly measure the lifetime (or a lifetime-dependent factor in the case of the Doppler Shift Attenuation Method) via various means; techniques like the Recoil Distance Doppler Shift, Coulomb Excitation, and Electronic Timing rely on fast-timing techniques for multiple γ -ray and/or particle coincidences to measure the lifetimes of metastable states. These direct lifetime measurements apply to the longer-lived excitations (picosecond and above lifetimes), and are contrasted with the more exotic, indirect methods (Proton Resonance, Nuclear Resonance Fluorescence, and Channel Blocking) that measure the partial or total Lorentzian energy ($\Gamma \approx \hbar/\tau$) width(s) to extract the lifetime of a state. Each lifetime measurements also has its own set of experimental advantages and challenges in addition to their respective sensitive ranges of lifetime measurement. For example, Electronic Timing can measure lifetimes over a very broad range of lifetimes by measuring the time between successive decays into and out of a state, but is limited by the requirement that the particular state desired must be populated via a cascade from higher-lying levels or by charged particle decays. Coulomb excitation offers a relatively simple measurement technique, in that it can directly deduce nuclear lifetimes by measuring the reduced transition probability for direct population of a desired state from the ground state, however, for decays that are not directly linked to the ground state via γ decay, this method rapidly increases in complexity. The Recoil Distance Doppler shift method utilizes Doppler-type effects to measure intensities of decay radiation as a function of target position (which then correlates to a nuclear lifetime). This picosecond-range lifetime measurement technique is highly tunable to the precise needs of the experimentalist, yet the methodology and necessary experimental equipment needed can become cumbersome and sophisticated.

Specifically, level lifetimes in the tens to hundreds of femtosecond ($\sim 10^{-15}$ s) range can be measured with the Doppler Shift Attenuation Method (DSAM), a technique that exploits a recoiling nucleus to produce Doppler shifted γ -rays when observed at various laboratory angles. The magnitude of the Doppler shift is reliant on a lifetime-dependent factor, which we can easily extract from experiments in the laboratory. DSAM holds a unique place in the overall landscape of lifetime measurement techniques in that it is almost exclusively sensitive in this near-femtosecond timescale. The level lifetimes from DSAM can then be quickly extracted from the angular energy shift(s) of any γ -rays that de-excite the nucleus. All of the presented lifetimes in this work are measured with this DSAM technique at the University of Kentucky.

2.2 DSAM-INS Formalism

A γ -ray observed from a recoiling nucleus will be energy-shifted linearly as a function of the laboratory angle, θ_{lab} , shown in Equation 2.1. This angular dependence on the energy is due to observation of Doppler shifted energies of the γ -ray, based on the detection angle, θ_{lab} , as a γ ray observed as the nucleus recoils ‘away’ from the observer will be ‘red-shifted’ down in energy, and inversely (energies will be ‘blue-shifted’) for a γ ray observed for nuclei that recoil ‘towards’ the detector.

$$E_\gamma(\theta_{lab}) = E_{\gamma,o}[1 + \beta F(\tau) \cos(\theta_{lab})] \quad (2.1)$$

Here, $E_{\gamma,o}$ is the unshifted γ -ray energy, $F(\tau)$ is an attenuation factor, dependent on the lifetime of the excited state (to be discussed in detail in §3.2.2.2, as this is one of the key experimental quantities we measure), and β is the ratio of the recoil velocity of the target nucleus to the speed of light, c ; this recoil velocity is derived in Pelte and Schwalm [62] from the kinematics involving conservation of momentum and energy in the laboratory frame, and is given by Equation 2.2.

$$\beta = 0.04635 \frac{A_n}{A_n + A_A} \sqrt{\frac{E_n}{A_n}} \quad (2.2)$$

The mass numbers of the bombarding particle and solid target are A_n and A_A , respectively, with the bombarding particle energy given by E_n in MeV. In $(n,n'\gamma)$ experiments, A_n is unity, while A_A must take into account the full molecular weight of the target, *e.g.* for Dysprosium-Oxide powder ($^{162}\text{Dy}_2^{16}\text{O}_3$), $A_A=162\times 2+16\times 3=372$. For rare-earth nuclei and $E_n < 5$ MeV, the nuclear recoil velocities are generally less than 1 % of the speed of light, meaning relativistic effects do not need to be taken into account as they normally would with other lifetime measurement techniques (*e.g.* Recoil Distance Doppler Shift measurements). For example, the recoil velocity β for a $^{162}\text{Dy}_2^{16}\text{O}_3$ molecule recoiling from a bombarding neutron of 3.1 MeV is 2.1878e-4. Lifetimes, then, are measured via the single experimental observable, the energy of the γ ray as a function of angle; this is achieved at the University of Kentucky with High Purity Germanium detectors with high-resolution γ -ray spectroscopy to measure precise energy shifts. This excellent energy resolution provided by HPGe detector systems is ideal to measure the \sim 200-300 eV energy shifts needed, as older fast NaI(Tl) detectors cannot distinguish peaks at such a fine-grain resolution. To highlight this centroid energy shift, Figure 2.2 shows a 1902.055 keV γ -ray Doppler shifting as the detector changes laboratory angle, with the centroids drawn to guide the eye.

From Equation 2.1, the only undetermined parameter is $F(\tau)$, an attenuation factor directly dependent on the specific lifetime of the decaying state, formulated by Blaugrund in ref. [11] to be an effect of the recoil nuclei slowing down in the target medium while they decay. $F(\tau)$ can be calculated via multiple formulations, where all formulations rely on an understanding of the nuclear and electronic stopping power of a medium to produce this lifetime dependent attenuation, as the inelastic interaction of the bombarding particle is directly related to these stopping powers.

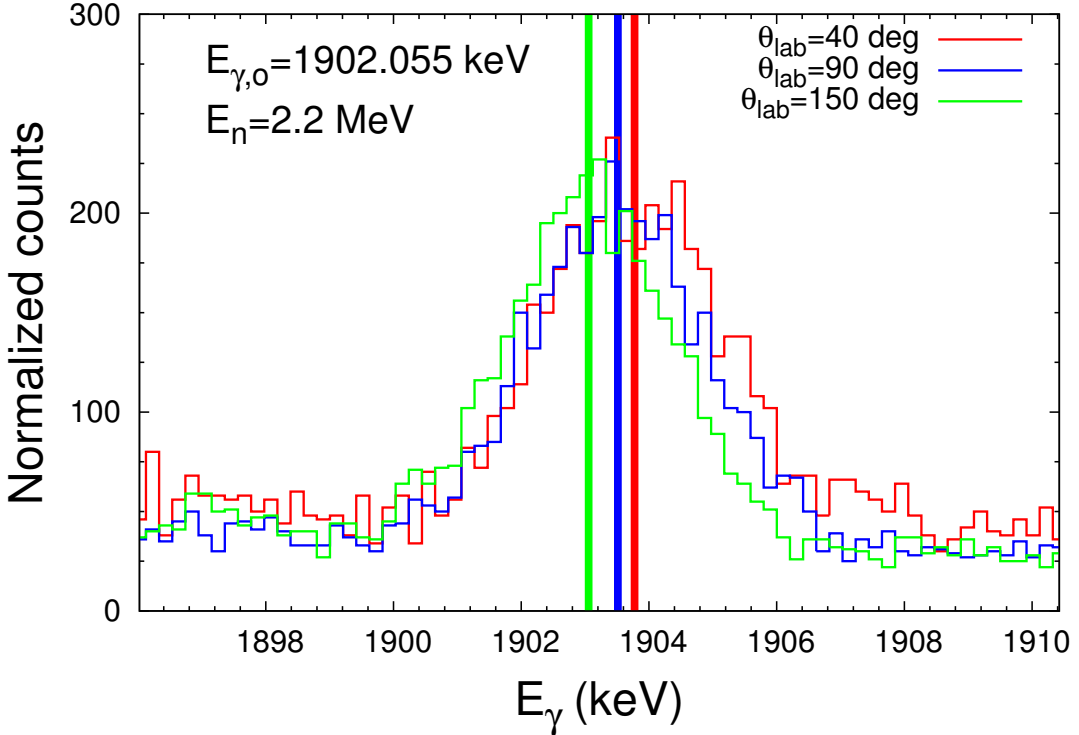


Figure 2.2. Doppler shift of an $E_\gamma=1902.055$ keV de-excitation from the $\theta_{lab}=40$, 90, and 150 degrees in red, blue, and green, respectively. The vertical lines mark the centroid of each peak of corresponding color.

In this work, the Winterbon formalism will be used, where the underlying framework is outlined in [78] and [5], where an exact solution was obtained for the attenuation factor $F(\tau)$ in terms of the electronic stopping power, the nuclear scattering cross sections, and target density. Key improvements were made to this attenuation factor calculation in the early 1970s by taking the possibility of nuclear deflection during the recoil as well as slowing inside the material lattice into account. This refinement is a necessary addition with the use of large, molar amounts and physical weights of target material, where the electronic stopping power of the medium plays a finite aspect in the calculation of the Winterbon curve; previous (Lindhard and Blaugrand) formulations of the theoretical $F(\tau)$ factors were unable to successfully represent

both the nuclear and electronic stopping powers correctly, vastly and systematically underestimating the attenuation. Further advancement of the Winterbon formalism was investigated in [63], with attention being placed on the chemical makeup of the target to better characterize the lattice relaxation needed to quantify the nuclear recoil inside the sample. This placed an important focus on the dependence on the oxide powder's consistency and packing density of the molar quantity of the target material inside a container (in our case, a polyethelene vial) when calculating the Winterbon curve.

Note that energy shifts (and thus $F(\tau)$) must *always* be positive, in that energies of DSAM γ rays are higher at forward angles and lower at backward angles for any realistic system. We will encounter some of the limitations behind measurement of γ ray energies via DSAM shortly, and oftentimes, the measured energy shift is either consistent with zero or negative. These limitations in an extraction of $F(\tau)$ are products of either a lifetime that is outside the range of DSAM, or other factors including sample self-attenuation and/or coincidence with background radiation to blur the centroid energy shift of a particular γ ray.

2.3 $(n,n'\gamma)$ Experiments at the University of Kentucky

DSAM requires the nucleus to be moving as it decays from an excited state for it to be effective, and the preferred probe to excite the nucleus used at the University of Kentucky Accelerator Laboratoy (UKAL) is the inelastic scattering of neutrons. The inelastic scattering reaction imparts some velocity to the target nuclei, fulfilling the base requisite for DSAM, that the target is moving as it decays. In years past, thermal neutrons from various fission sources have been utilized to perform the inelastic scattering reactions, but the accessibility of monoenergetic neutrons has made UKAL a popular and unique setting in the realm of experimental structure physics. Energetic neutrons cannot be accelerated with a standard electrostatic accelerator

due to their neutral charge-state, so non-thermalized neutrons must be produced via a primary reaction. This mechanism is outlined in Equation 2.3.



This $^3\text{H}(\text{p},\text{n})$ reaction produces quasi-monoenergetic neutrons, tunable to a desired energy in a 0.5 - 5.5 MeV bombarding neutron energy range, ideal for studying the low-lying states in nuclei. UKAL uses their on-site 7 MV single-ended Van De Graff accelerator to accelerate a bunched, pulsed beam (at a frequency of 1.875 MHz) of protons to impinge on a pressurized (slightly above atmospheric at ~ 110 kPa) tritium gas cell, prompting the reaction to produce a forward cone of neutrons. A slight energy spread is present in the outgoing neutrons due to a thin molybdenum foil to prevent the gas cell from out-gassing upstream, which would catastrophically contaminate the entire beamline with radioactive ^3H . This energy straggling is minute, however, providing a $\sim 2.5\%$ energy spread on average at 50-100 keV standard deviation on neutron energy [5].

The choice of neutrons as a probe can be justified for multiple reasons, and brings its set of distinct advantages; the inelastic scattering and low-spin transfer leaves the nucleus in excited, aligned states with relatively low angular momentum. Generally, spin 5^\pm states are the practical limit of angular momentum that can be imparted in an inelastic scattering reaction with neutrons at the University of Kentucky. This low-spin population of states is because the spin-1/2 neutron would naturally not be able to produce a higher spin state without the addition of a very large amount of angular momentum during the inelastic scattering reaction. The neutral charge of the neutron also implies that the scattering reaction is not impeded by the Coulomb barrier; this means that levels are populated very close to the bombarding neutron energy. Lastly, the excited states populated by inelastic neutron scattering are generally nonselective,

in that either single-particle excitations or collective states can be populated, allowing the study of both types of excitation. The Doppler Shift method also offers the unique ability to tune bombarding neutron energies to populate states at or very near their threshold energies. This effect is two-fold: first, the experimentally determined $F(\tau)$ factor from Equation 2.1 is directly dependent on the incoming neutron energy, so minimization of the neutron energy is key to extraction of the lifetime, so the ‘observed’ $F(\tau)$ will be inflated for higher neutron energies. Secondly, this ‘dialing-in’ of neutron energy can completely remove any lifetime inflation due to feeding from higher-lying states; DSAM is unique in this aspect because the other methods of measuring a nuclear lifetime will be unable to remove this feeding, or in some cases (such as the Gamma Ray Induced Doppler Broadening technique), the feeding will manifest as a large uncertainty in measurement.

DSAM following inelastic neutron scattering is not without its downsides or experimental challenges to overcome. Since the target has significant thickness and involves molar quantities of target powder, γ rays from deep inside the sample will be attenuated in their trajectory out of the sample. This has a two-fold effect, in that the absolute intensity must be corrected for (explained in detail in §3.1.4) low-energy γ rays that could easily become fully attenuated and absorbed by the target material, and that any lifetimes extracted from the linear shift of energy *may* not be trustworthy, as the energy attenuation is strongly angular dependent, effectively ‘flattening’ the Doppler energy shift.

The ensemble of $(n,n'\gamma)$ experiments performed at UKAL can be achieved with the relatively simple experimental setup, shown in Figure 2.3.

The single 50% relative efficiency Ortec HPGe planar detector (named after the 1904 Kentucky Derby winner Elwood) sits \sim 125 cm away from the end of the beamline on a goniometer equipped circular track \sim 2 m in radius to observe γ -rays at various laboratory angles. In Figure 2.3, the target (a cylindrical polyethelene vial

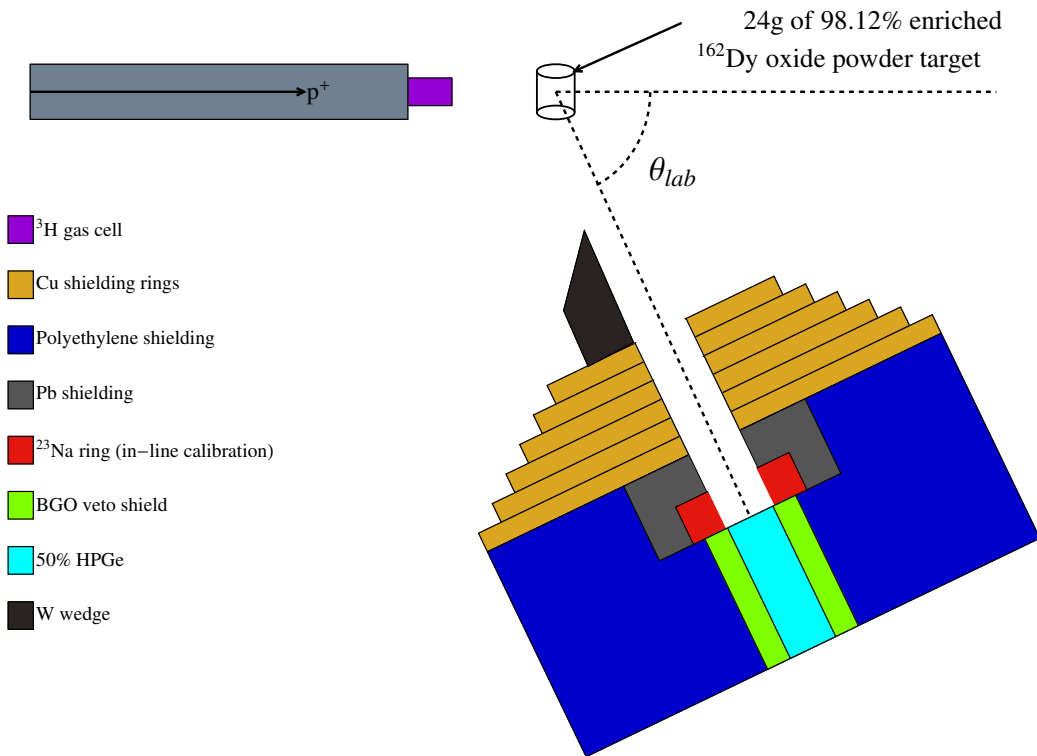


Figure 2.3. Sample Experimental Setup at UKAL for γ -singles measurements (Made in M. Caprio's SciDraw software for Mathematica [19])

of enriched target powder) is suspended a few (~ 4) inches away from the end of the tritium gas cell, where monoenergetic neutrons will inelastically scatter off the target, prompting γ decay from the sample to be observed by the HPGe detector. The proximity of the target in relation to the end of the tritium gas cell ensures that the highest possible neutron flux from the forward cone of neutrons will strike the majority of the target material. The castle of passive shielding materials are two-fold in use: to lower background radiation in spectra and to diminish fast neutron damage to the HPGe detector itself. The viewing channel of the detector is lined with copper

plating to absorb fast neutrons from the tritium gas cell at the end of the beamline. In addition, borated polyethelene surrounds the detector to reduce secondary & tertiary scattering of neutrons and γ -rays from reaching the detector; the typical ensemble of lead rings also aid in regular γ background reduction. Lastly, a wedge of tungsten is placed in direct view of the tritium gas cell to act as a shadow bar to prevent neutrons from directly entering the detector from the gas cell. An ensemble of BGO (Bismuth Germanate Oxide) scintillators are placed annularly around the HPGe detector to further aid in Compton scattering background suppression; these scintillation detectors provide an anti-coincidence to veto background events that occur, actively cleaning spectra.

Spectra are generated from the Time of Flight (TOF) technique to discriminate background events from prompt γ events; a time-to-amplitude converter (TAC) measures the relative time between events in the HPGe detector and a beam pick-off signal near the end of the beamline. At UKAL, the events in the HPGe act as the ‘start’ and the pick-off serves as the ‘stop’ as to not flood the electronics from pick-off signals that do not result in detected radiation. The concept of the TOF technique is that particles and γ -rays require different amounts of time to reach a detector, dependent on their velocity (neutrons of a velocity $\ll c$ take longer to reach a detector than a γ -ray traveling at the speed of light). This time difference between measured events is recorded by the TAC, and TOF spectra are generated through a built-in single channel analyzer (SCA). Specifically at UKAL though, the neutron events occur *first* as they scatter off the various materials (mainly primary scattering off iron) in between the target and detector face, while the speed of light γ -ray events occur in the larger peak. The resultant spectrum is used to properly gate the experimental datasets in the analog-to-digital converter (ADC) by only selecting corresponding prompt γ -ray events from the histogram. An example of a typical TOF spectrum from experiments at UKAL is shown in Figure 2.4.

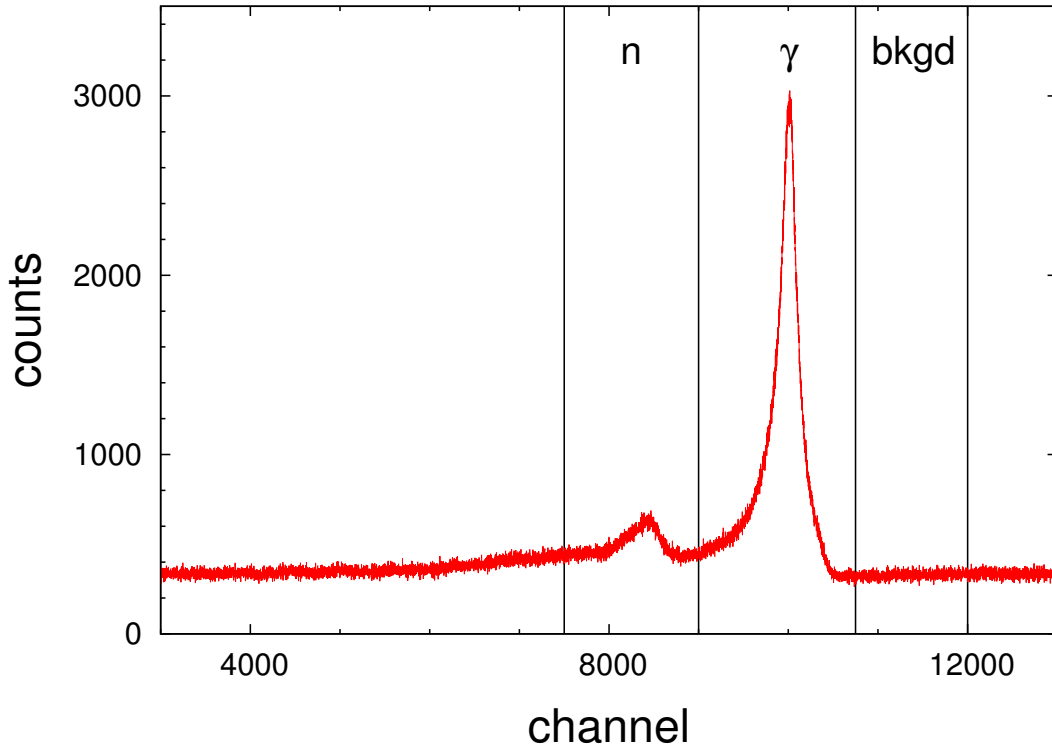


Figure 2.4. Typical TOF spectrum with labeled regions for corresponding γ , neutron, and background events.

The single-detector setup and γ -singles based experiments provide more distinct downsides to lifetime measurements via DSAM at the University of Kentucky in particular. The limitations of not using γ - γ coincidences can have profound implications on the visibility and overall statistics of spectra gathered from the experiment(s); being able to apply timing gates on individual γ -decays is an extremely powerful tool in determining decay patterns, cascades, and lower-intensity peaks for interband decays. One detector setups require a considerable length to the experimental campaign, and is a severe limitation to the facilities, where the experimenters must enter the target room periodically throughout the run to physically move the detector across the entire range of angles used in the measurements, and must systematically scan through the entire range one angle at a time. Given an unlimited amount of beamtime with

little to no deadlines, this is not a problem, however, a modest amount of statistics for γ -decays observed in a typical measurement require up to (in some cases in excess) a week of continuous beamtime for a single neutron energy angular distribution.

2.3.1 Excitation Function Measurements

Typically, the first measurements to be made are excitation function measurements; these supplement the γ -singles nature of the angular distribution measurements, to help infer the ideal bombarding neutron energy for peak γ -ray population rates. In stark contrast to the angular distributions where the neutron energy is kept constant, the excitation functions modulate the bombarding neutron energy to provide the γ -ray population strengths as a function of neutron energy. Similarly in contrast, the HPGe detector is kept at a constant laboratory angle of 90 degrees with respect to the beamline. An extremely powerful tool, these excitation functions provide important insight into the nature of any observed γ -rays; for a particular excited state that de-excites via multiple channels, the corresponding γ -rays will have both the same a) quantitative threshold, and b) qualitative shape. The absolute threshold allows previously unidentified or unplaced γ -ray transitions to be placed into a known level scheme, as the threshold for the de-excitation must match the level energy. If the populated level's spin are high (5^\pm), the threshold will be higher than the level energy, as the bombarding neutron must have higher linear momentum (energy) to successfully provide enough angular momentum transfer during the reaction. The qualitative shape of the excitation functions is heavily dependent on the initial spin and parity of the de-exciting level, making γ -ray discrimination and identification from different levels a trivial task. This identical shape also allows the relative intensities of γ -rays to be inferred (independent of the absolute intensities we can gather from the angular distribution measurements), since we can take the ratio of matched-shape excitation functions. An example of two matching γ -ray transitions

from the same level ($J^\pi=5^-$), contrasted with a γ -ray from another level ($J^\pi=1^-$) is shown in Figure 2.5.

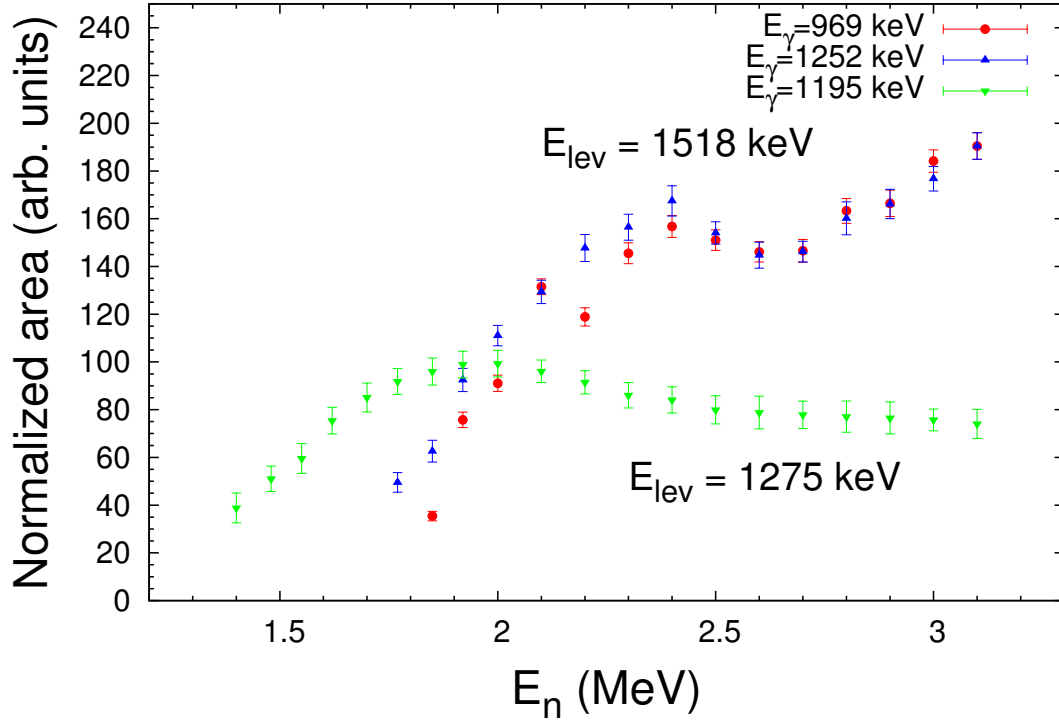


Figure 2.5. Superimposed excitation functions for two gamma rays ($E_\gamma=969$ & 1252 keV) leaving the same level ($E_{lev}=1518$ keV), and a single 1195 keV γ -ray leaving a separate $E_{lev}=1275$ keV level in ^{162}Dy . The different thresholds and shape of the 1195 keV and 969 keV de-excitations imply that these decays are from two different levels, clearly showing their placement in the level scheme.

The excitation function measurements serve as a quasi-replacement for $\gamma\gamma$ coincidences in a particular experiment, as it allows retention of good statistics that one would get from γ -singles spectroscopy. With $\gamma\gamma$ coincidences, a level scheme

can be built extremely easily, because coincident γ -decay chains into and out of levels are unquestionably vivid in multiple HPGe detectors; this is not the case in a γ -singles experiment, since a) particular γ -rays appear only in the single HPGe detector, and b) discrimination of decay chains is impossible with γ -singles. The excitation function allows a level scheme to be built in a similar fashion to $\gamma\gamma$ coincidences, while only requiring a single detector, because threshold energies are obvious, and that the qualitative shape of the excitation functions will be identical. Without either implemented technique (excitation function measurements or $\gamma\gamma$ coincidences), proper γ -spectroscopy would be rendered impossible, as we would no longer be able to confidently place γ decays to levels or assign level lifetimes from the Doppler Shift Attenuation measurements.

2.3.2 Angular Distribution Measurements

To extract the lifetimes of excited states, the angular distribution of gamma rays must be measured, specifically, the energy dependence of γ rays as a function of lab angle; this is achieved at UKAL with the same single High-Purity Germanium detector used in the excitation function measurements. By physically moving the HPGe detector to different laboratory angles on the circular track, we can extract multiple observable quantities from the angular distribution measurements. First, $F(\tau)$ is found by plotting E_γ as a function of $\cos(\theta)$; the relation in Equation 2.1 states that the centroid energy shift of a γ -ray will be linear with cosine, with $F(\tau)$ being the slope. Comparison of this experimental $F(\tau)$ factor with the theoretical calculation for $F(\tau)$ allows extraction of a lifetime τ for the decay radiation and excited state. Special care must be taken when measuring the lifetimes, because higher-lying levels can introduce feeding transitions into lower-lying states, inflating the measured lifetimes. Since the theoretical $F(\tau)$ factor is directly dependent on the recoil velocity (the bombarding neutron energy), additional inflation will also be introduced when

extracting lifetimes for levels far below the bombarding neutron energy. Performing the excitation function measurements first allows for the minimization of lifetime inflation while maximizing population rate for a particular excited state, as we know the approximate population as a function of bombarding neutron energy.

When the nucleus decays from an aligned state, the classical radiation pattern of the γ -ray can be expressed by the sum of even Legendre polynomials as a function of $\cos(\theta)$ (Equation 2.4), where the coefficients for each order polynomial are directly related to the multipolarity of the transition. Realistically, only the coefficients a_2 and a_4 are considered, since the higher order terms correspond to the contributions from the insignificantly intense multipolarities for $\Delta J > 2$.

$$W(\theta) = \sum_{\text{even } k} \alpha_k P_k \cos(\theta) \Rightarrow W(\theta) \approx A_0[1 + a_2 P_2 \cos(\theta) + a_4 P_4 \cos(\theta)] \quad (2.4)$$

The anisotropic nature of the γ radiation produced arises from the fact that parity conserving nuclear reactions, *e.g.* ($n, n'\gamma$), and a defined beam direction, create a plane of interaction . Otherwise, the random orientation of nuclei in space would mean all multipolarities of γ radiation have isotropic angular distributions. By comparing the relative magnitude and sign of the a_2 and a_4 coefficients, limits can be placed on both the spin and parity of the de-exciting level, because dipole and quadrupole radiation patterns have distinct shapes (shown in Figure 2.6). These same Legendre Polynomial coefficients can also be compared to theoretical calculations to extract multipole mixing fractions (δ) for mixed-multipolarity transitions. This multipole mixing fraction is simply the ratio of E2 transition strength to M1 transition strength:

$$\delta = \frac{\langle \eta | E2 | \nu \rangle}{\langle \eta | M1 | \nu \rangle} \quad (2.5)$$

Lastly, the angular distributions allow us to measure the absolute intensity of

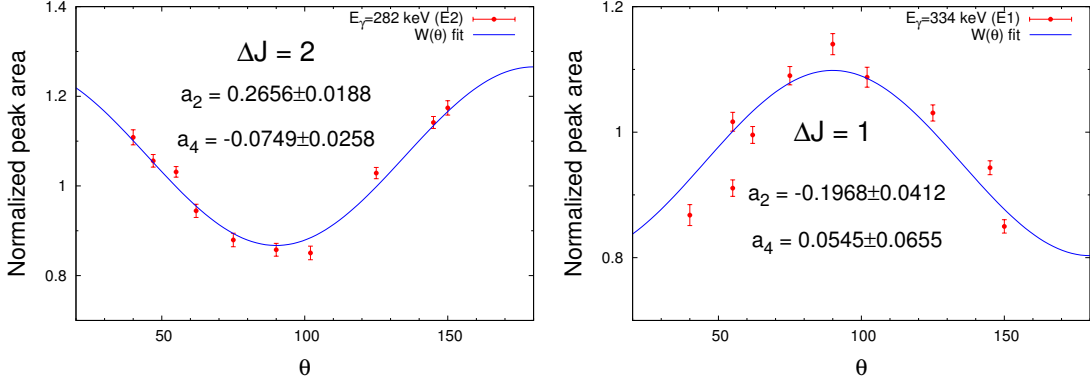


Figure 2.6. Angular distributions for two different multipolarity γ -rays in ^{162}Dy , an E2 transition of $E_\gamma=282$ keV (the $6_{gs}^+\rightarrow 4_{gs}^+$ transition) & an E1 transition of $E_\gamma=334$ keV (a $3^-\rightarrow 2_\gamma^+$ transition), showing distinct, inverted shapes.

emitted γ -rays from the A_0 coefficient. In experiments with static, symmetric detectors (*e.g.* two detectors at 90°), only the relative intensity of γ rays can be extracted. Though seemingly simple in form and function, the γ -singles measurements made at UKAL are an incredibly powerful tool that yield a wealth of knowledge about the structure of the nucleus.

2.4 Experimental Campaigns

Two sets of experimental campaigns were performed at the University of Kentucky to measure the level lifetimes for deformed rare-earth nuclei, ^{160}Gd and ^{162}Dy . Both targets were acquired from Oak Ridge National Laboratory in the form of an isotopically enriched oxide powder (specifically, $^{160}\text{Gd}_2^{16}\text{O}_3$ & $^{162}\text{Dy}_2^{16}\text{O}_3$); the sample powder was then placed into a 1.5" diameter by 3" height cylindrical polyethelene vial for the experiments.

2.4.1 The ^{160}Gd Campaign

In July/August of 2012 and 2013, inelastic neutron scattering experiments were performed to study the low-lying excitations of ^{160}Gd . The 29.4564 g of 98.12 % enriched powder vial was placed 4.82 cm from the end of the ^3H gas cell and 119.3 cm from the face of the detector for all experiments. First, an excitation function measurement was performed at the neutron energies shown in Table 2.1:

TABLE 2.1

NEUTRON ENERGIES: ^{160}GD

E _n (MeV)							
1.40	1.50	1.60	1.70	1.80	1.90	2.00	2.075
2.15	2.225	2.3	2.375	2.45	2.525	2.6	2.625

Bombarding energy of neutrons used to populate the excitation functions for the ^{160}Gd experiment.

Once proper γ -ray identification and placement in the level scheme was completed from examining the excitation functions, angular distributions were measured at three (3) bombarding neutron energies, 1.5, 2.0, and 2.8 MeV at the angles shown in Table 2.2.

2.4.2 The ^{162}Dy Campaign

Throughout August of 2013 and March of 2014, we performed an excitation function measurement and three (3) angular distributions to measure lifetimes of levels

TABLE 2.2

DETECTOR ANGLES: ^{160}GD

θ_{lab}	40°	55°	62°	75°	90°	102°	125°	137°	145°	150°
$E_n = 1.5, 2.0, \& 2.8 \text{ MeV}$										

Angles used for lifetime measurements for the suite of ^{160}Gd experiments at 1.5, 2.0, and 2.8 MeV bombarding neutron energies.

for levels $\leq 1.6, 2.2$, and 3.1 MeV in excitation energy. Similarly to the ^{160}Gd experiments, the 24 g of 98.12 % enriched powder vial was placed 4.80 cm from the end of the ^3H gas cell and 120.2 cm from the face of the detector for all experiments. The excitation function measurement was taken first to discern the population rate for levels and γ -rays similar to the ^{160}Gd ; this allowed us to estimate the beam-on time required to give good statistics for desired and important γ -rays.

TABLE 2.3

NEUTRON ENERGIES: ^{162}DY

$E_n \text{ (MeV)}$									
1.40	1.48	1.55	1.62	1.70	1.775	1.85	1.925	2.0	2.1
2.2	2.3	2.4	2.4	2.5	2.6	2.7	2.8	2.9	3.0

Bombarding energies of neutrons used to populate the excitation functions for the ^{162}Dy experiment. $\sim 75 \text{ keV}$ steps were used at the lower energies ($\leq 2 \text{ MeV}$) to enhance the resolution of the threshold and population shape for low-lying excitations.

Following the procedure of the ^{160}Gd experiments, the angular distributions were measured to extract level lifetimes from ^{162}Dy . The specific angles used for each angular distribution are given in Table 2.4, and are drawn in Figure 2.7, where angles in black are used in all angular distributions, angles in red are used in the $E_n=1.6$ MeV measurements and blue angles correspond to the angles used in $E_n=2.2$ & 3.1 MeV runs.

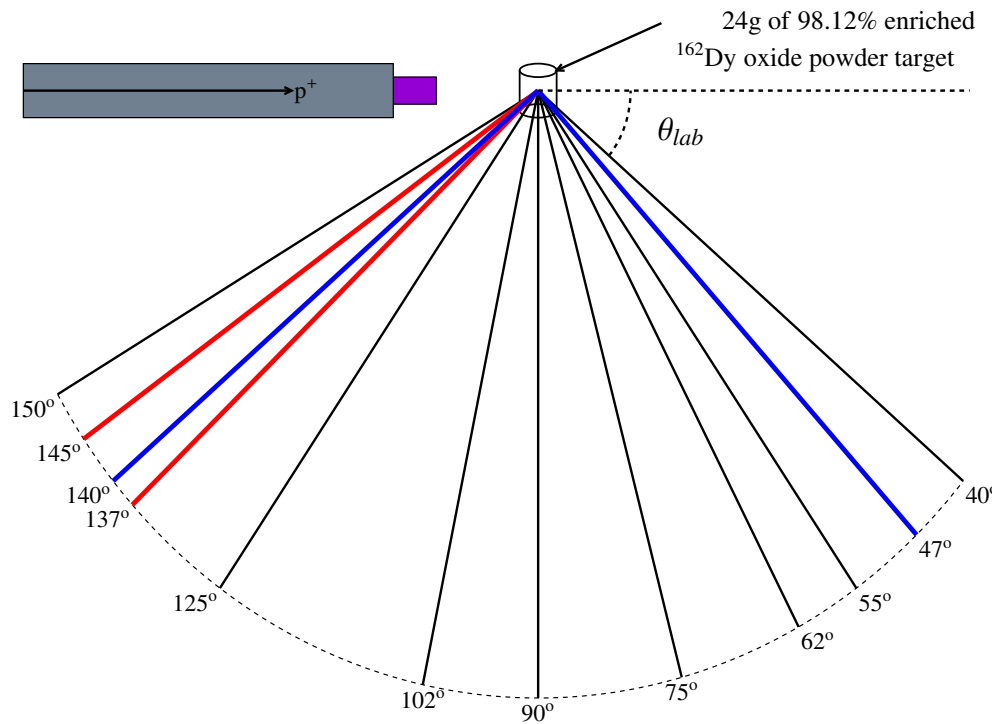


Figure 2.7. Angles used in $^{162}\text{Dy}(n,n'\gamma)$ angular distributions. Angles in black are used in all measurements, while angles in red (137° and 145°) are used for the $E_n=1.6$ MeV measurements and angles in blue are used for both $E_n=2.2$ and 3.1 MeV datasets.

Once data is collected for both experimental campaigns, we carry out the analysis process to extract the various experimental quantities needed for nuclear structure studies (lifetimes of excited states, branching ratios/absolute intensities of γ -rays, etc) outlined in §3.

TABLE 2.4

DETECTOR ANGLES: ^{162}DY

	θ_{lab}									
$E_n = 1.6 \text{ MeV}$	40°	55°	62°	75°	90°	102°	125°	137°	145°	150°
$E_n = 2.2 \text{ MeV}$	40°	47°	55°	62°	75°	90°	102°	125°	140°	150°
$E_n = 3.1 \text{ MeV}$	40°	47°	55°	62°	75°	90°	102°	125°	140°	150°

Angles used for lifetime measurements for the suite of ^{162}Dy experiments at 1.6, 2.2, and 3.1 MeV bombarding neutron energy. Angles in bold are to emphasize differences in measurements.

CHAPTER 3

DATA ANALYSIS

3.1 Calibrations and Corrections

In order to account for systematic errors inherent to the laboratory, several corrections and calibrations must be made to ensure proper γ -ray spectroscopy. A suite of in-beam (^{24}Na & ^{60}Co) and offline calibration (^{226}Ra & ^{152}Eu) sources were implemented during the experimental campaigns to provide the numerous corrections that must be made; successful calibration hinges on the implementation of a wide energy range of strong calibration lines that do not shift. An ADC nonlinearity, a detector efficiency, and a target sample self-absorption correction are all applied to energy calibrated spectra before the analysis of data can begin.

3.1.1 Energy Calibrations

Proper energy calibration is vital to the success of DSAM lifetime measurements; the precision in peak centroid location determines the sensitivity of the lifetime measurement, as centroid energy shifts for longer-lived levels (~ 1 ps) can be as small as 20 eV. With its large range of energetic decays (from 185 keV to 2.4 MeV shown in Table 3.1), ^{226}Ra is an ideal candidate to energy calibrate our spectra; the ^{226}Ra spectrum from the $^{162}\text{Dy}(n,n'\gamma)$ experiments can be seen in Figure 3.1. Angular distribution measurements saw the presence of an in-line calibration source in the form of annular-shaped ring of ^{23}Na that had been irradiated with a separate, on-site neutron source to produce radioactive ^{24}Na . The β -decay to $^{24}\text{Mg}^*$ leads to a cascade

of two intense γ -rays, 1368.626 and 2754.007 keV, providing a calibration point at a higher energy than a typical ^{60}Co source can provide (1173.228 & 1332.492 keV). This sodium ring is placed around the detector crystal to ensure the two calibration γ -rays are not attenuated by the passive shielding from the experimental setup shown in Figure 2.3. While far from an ideal candidate for an energy calibration point, radioactive ^{28}Al from a $^{27}\text{Al}(\text{n},\gamma)$ channel will emit a high intensity γ -ray at 1778.785 keV; this peak originates from the aluminum housing for the HPGe detector and is often not well-defined in width, especially compared to the traditional Radium and Cobalt sources normally used, and as such, the ^{28}Al should not be a main energy calibration point. A table of all online and offline calibrations used in the ^{160}Gd and ^{162}Dy experiments can be found in Table 3.2.

TABLE 3.1
CALIBRATION LINES: ^{226}Ra DECAY-CHAIN

E_γ (keV)	I_γ (rel)						
186.053(4)	3.502(28)	487.090(70)	0.431(6)	1120.287(10)	14.66(103)	1661.280(60)	1.063(17)
241.997(3)	7.130(50)	580.130(30)	0.369(6)	1155.190(20)	1.611(19)	1729.595(15)	2.791(22)
258.870(40)	0.525(5)	609.312(7)	44.83(314)	1238.110(12)	5.750(46)	1764.494(14)	15.03(105)
274.800(50)	0.472(6)	665.453(22)	1.506(12)	1280.960(20)	1.411(16)	1847.420(25)	1.994(20)
295.224(2)	18.09(127)	768.356(10)	4.780(38)	1377.669(12)	3.895(31)	2118.550(30)	1.137(11)
351.932(2)	35.04(245)	785.960(90)	1.097(12)	1385.310(30)	0.782(9)	2204.210(40)	4.820(39)
455.000(70)	0.287(6)	806.174(18)	1.250(13)	1401.500(40)	1.311(12)	2293.400(120)	0.298(8)
480.430(20)	0.336(5)	934.061(12)	3.041(24)	1509.228(15)	2.065(31)	2447.860(100)	1.525(14)

Energies (in keV) and relative intensities (in arbitrary units) for γ -ray emissions from the ^{226}Ra decay chain used in data calibrations for this work.

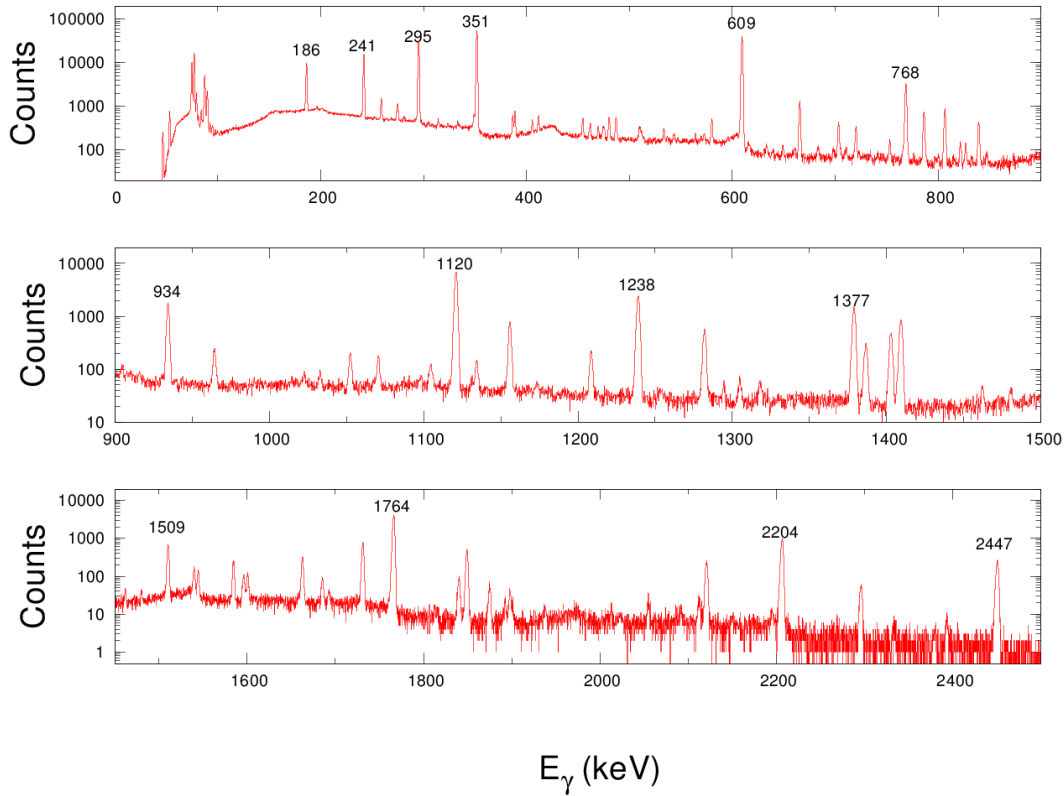


Figure 3.1. Spectrum from a ^{226}Ra calibration run during the ^{162}Dy experiments. Sampled, higher intensity peaks are labeled by their energy in keV (refer to Table 3.1).

TABLE 3.2

ENERGY CALIBRATIONS: ^{160}Gd AND ^{162}Dy

$^{160}\text{Gd}(\text{n},\text{n}'\gamma)$ calibration E_γ (keV)					
$E_n=1.5$ MeV	1173.228	1332.492	2223.245		
$E_n=2.0$ MeV	1173.228	1332.492	2223.245		
$E_n=2.8$ MeV	1173.228	1332.492	1778.885	2223.245	
Excitation Function	185.002	351.932	609.312	1120.287	1764.494
					2223.245

$^{162}\text{Dy}(\text{n},\text{n}'\gamma)$ calibration E_γ (keV)								
$E_n=1.6$ MeV	185.002	1173.228	1332.492	2223.245				
$E_n=2.2$ MeV	185.002	1173.228	1332.492	2223.245				
$E_n=3.1$ MeV	351.932	609.312	1120.287	1173.228	1332.492	1764.494	2223.245	2754.007
Excitation Function	185.002	351.932	609.312	1120.287	1764.494	2223.245		

Calibration points used for all ^{160}Gd and ^{162}Dy spectra energy calibrations, given in keV.

The linear energy calibrations from the $^{162}\text{Dy}(n,n'\gamma)$ experiments can be seen in figure 3.2:

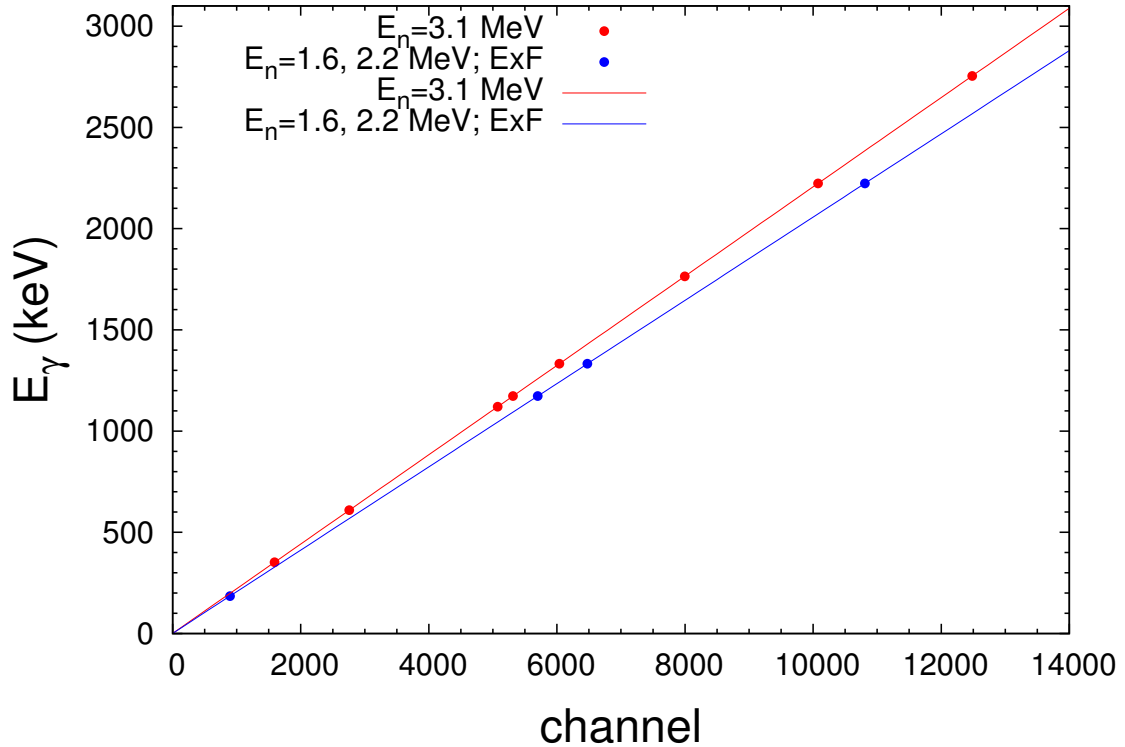


Figure 3.2. Linear energy calibration, taken from the three $^{162}\text{Dy}(n,n'\gamma)$ angular distributions and single excitation function (ExF in the legend).

The difference in linear energy calibrations is the result of a change in gain settings between the two ^{162}Dy experiments; the excitation function measurements and $E_n=1.6$ & 2.2 MeV angular distributions occurred in August of 2013, while the single $E_n=3.1$ MeV angular distribution took place months later, in March of 2014. The specific difference in energy calibration can be seen in Figure 3.2, where the electron-

ics gain settings were changed (a natural, necessary, and sometimes unintentional occurrence in the laboratory).

3.1.2 Nonlinearity Calibrations

The first of these corrections is an ADC nonlinearity calibration, where a binning nonlinearity is introduced in the data acquisition's ADC. In the ideal case, an ADC correlates an analog voltage to a specific bin (in this case, the energy of a γ -ray on the abissca), with the bins being equally spaced and sized. We, of course, do not live in a perfect world, and some bins cover a larger energy range than others, generating an easily correctable error in the measurement of peak centroids. To perform this offline correction, a radioactive ^{226}Ra source is placed at the same location the target is suspended, and is allowed to decay. Since the multitude of decays from ^{226}Ra have very well defined and precise centroids, we can compare the measured position of these peaks to literature values for the peak centroids. By plotting a relationship between the change in channel as a function of energy, we can generate the specific nonlinearity curve to make the correction. Generally, the nonlinearity correction introduces a ± 2 channel difference (at most a 0.5 keV correction), and this nonlinearity can be fit to an order 5 polynomial, shown in Figure 3.3:

Special care must be taken to ensure a realistic polynomial fit for the ADC nonlinearity; polynomials of high order can gravely mis-characterize the ADC behavior outside of the range of calibration points used (in our case, ^{226}Ra decays). In Figure 3.3, the downward turn in the fifth-order extrapolation above 2.5 MeV γ -rays would be magnified for higher order odd polynomials, and would turn upward (at a similarly unrealistic rate) for the even polynomials. To justify the use of an order-5 polynomial, the highest energy γ -ray observed in the ^{162}Dy experiments is a 2779 keV de-excitation, keeping in line with a $\sim \pm 1$ keV nonlinearity correction.

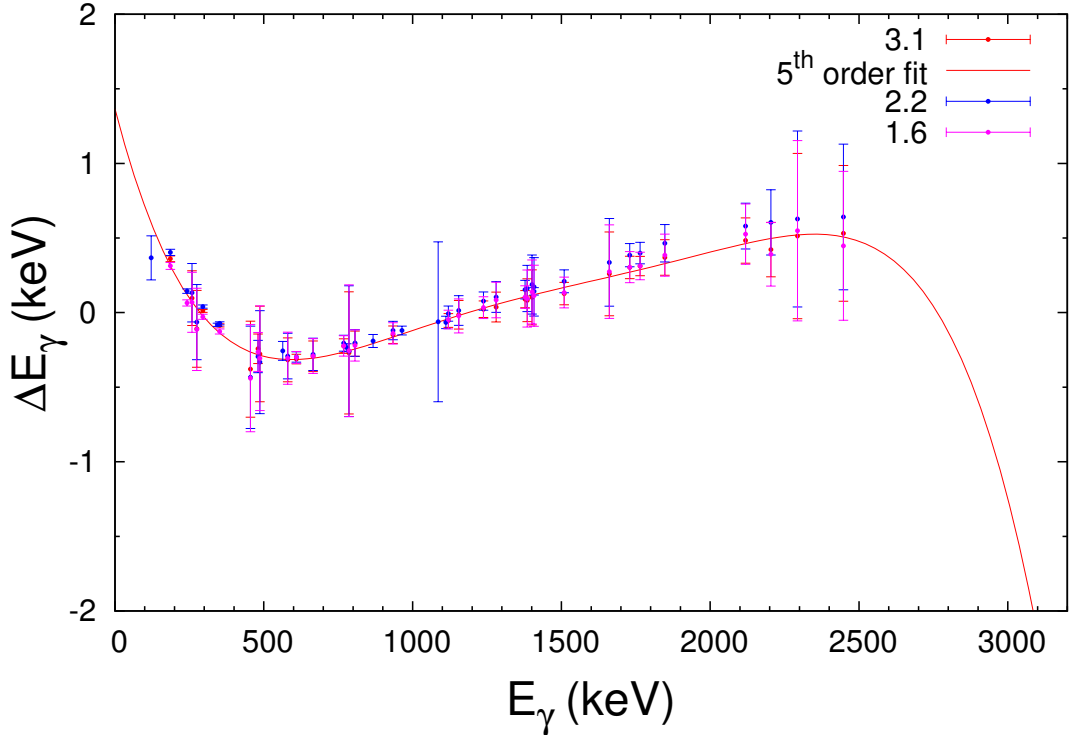


Figure 3.3. Order-5 polynomial nonlinearity correction, taken from the $^{162}\text{Dy}(n,n'\gamma)$ angular distribution with $E_n=3.1$ MeV

3.1.3 Efficiency Calibrations

High Purity Germanium detectors have an intrinsic detection efficiency, dependent on the energy of a particular γ -ray that enters the Ge crystal; higher energy γ -rays have a lower probability of depositing their entire energy into the detector, so this must be accounted for in angular distribution data to get correct γ -ray intensities. The same spectrum from the nonlinearity calibrations is used, as we can simply compare the measured intensities of γ -rays from the ^{226}Ra source to the literature values of γ -ray intensity. This efficiency correction is shown in Figure 3.4 as a function of E_γ :

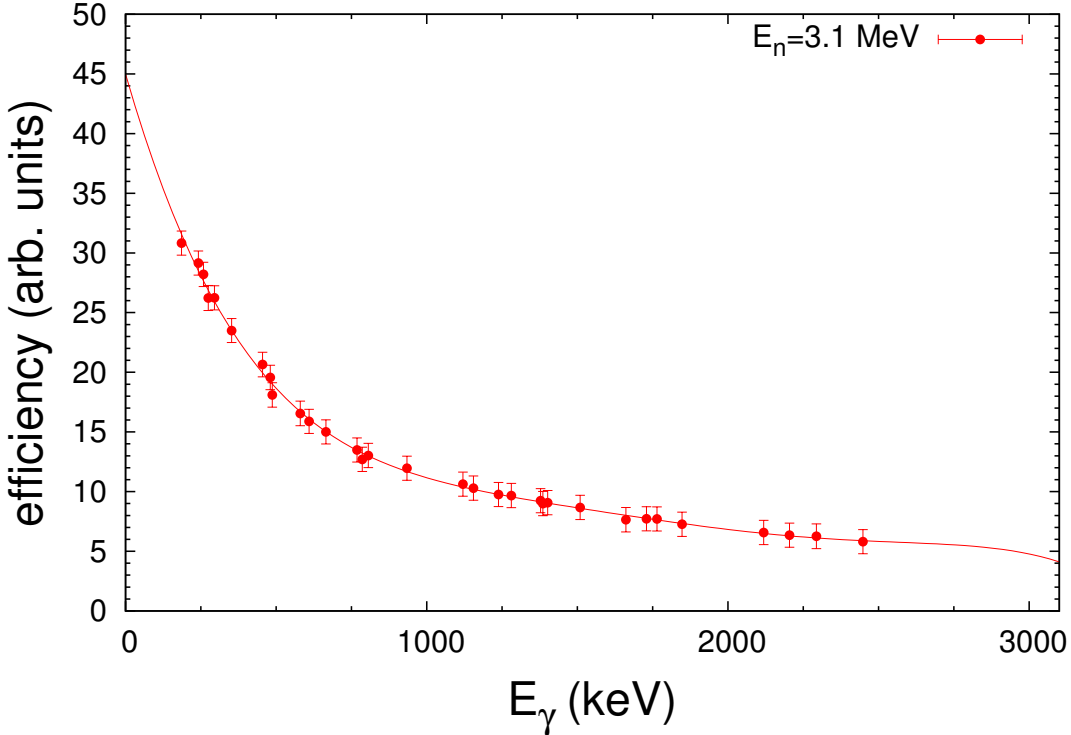


Figure 3.4. Fifth-order relative efficiency curve taken from the $^{162}\text{Dy}(n,n'\gamma)$ angular distribution with $E_n=3.1$ MeV

3.1.4 Self-Absorption Corrections

One of the key characteristics of the Winterbon formalism for determining $F(\tau)$ as a function of τ is the use of large quantities of target material to provide sufficient nuclear and electronic stopping power [78]. Of course, a downside to using these molar quantities of powder targets is that incoming neutrons and outgoing γ -rays will be attenuated by the physical thickness of material. Much like the efficiency calibration, the self-absorption correction must be made to get proper γ -ray intensities, since low-energy gamma rays may be drastically attenuated by the thickness of the sample. Both the physical geometry of the experimental setup and size of the sample affect this highly-angular dependent correction, used solely in the angular distribution data in the presented analysis. The GAMBIT ([27], [67], [15]) codes and subroutines are well-

equipped to perform this correction for any experiment performed at UKAL involving a cylindrical target cell; **GAMBIT** takes into account differential elastic neutron cross sections ($\frac{d\sigma_n}{d\Omega}$ at 0° and 180°), total neutron cross sections ($\sigma_{n,tot}$), elastic neutron scattering cross sections ($\sigma_{n,el.}$), and the photon absorption cross sections (σ_γ for each composite material found in the sample ($^{162}\text{Dy}_2^{16}\text{O}_3$)). Figure 3.5 shows the multiplicative factor needed to give the correct peak areas from this self-absorption of γ -rays as a function of θ_{lab} . Factors near unity indicate little to no correction is needed (at higher energies, a γ -ray can easily escape the physical target), while a significant correction must be made to low-energy (<200 keV) γ -rays that are partially or heavily attenuated by the sample.

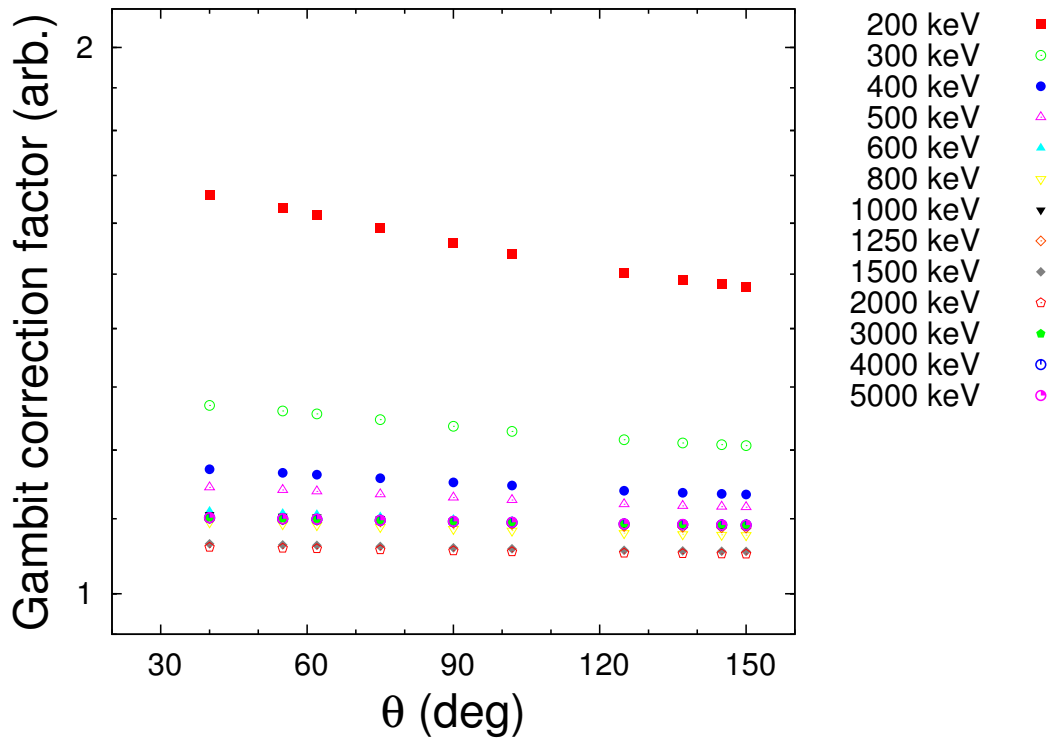


Figure 3.5. Multiplicative factor calculated by **GAMBIT** to correct for the angular dependent γ -ray self-absorption by a finite-size target.

This self-absorption correction given by **GAMBIT** is sufficient and appropriate for use in the $(n, n'\gamma)$ experiments at UKAL, even though much more modern approaches to characterize the self-absorption exist. Molecular dynamics calculations can be made to generate this angularly and energetically dependent attenuation, but require a much higher amount of computational power to complete. Since the newer, refined methods do not offer a more efficient or accurate self-absorption calculation, we can confidently use the more simplistic approach given by the **GAMBIT** code.

3.2 Statistical Analysis

The wealth of information that can be extracted from γ -ray spectroscopy hinges on consistent, precise statistical analysis of spectra. An example of a properly TOF gated, energy calibrated, and background subtracted spectrum can be seen in Figure 3.6:

3.2.1 Fitting Procedures

A γ -ray event recorded in the HPGe detector will manifest itself as a skewed, defined-width gaussian distribution on the histogram of the form shown in Equation 3.1, and is fit according to:

$$y = \sum_k \frac{A_k}{(2\pi)^{\frac{1}{2}}\sigma} e^{-\frac{1}{2}\left(\frac{Z-Z_k}{\sigma}\right)^2} \left[1 + P_{left,1} \left(\frac{Z-Z_k}{\sigma}\right)^4 + P_{left,2} \left(\frac{Z-Z_k}{\sigma}\right)^{12} \right] \quad (3.1)$$

The multiple parameter fitting procedure in Equation 3.1 can be qualitatively described as measures of σ , the width of the peak, Z_k , the centroid location of a peak, A_k , the peak height, and two parameters relating to the low-energy tail (a measure of the skewedness of the gaussian), $P_{left,1}$ & $P_{left,2}$. This trailing edge is the result of Bremsstrahlung escape from the detector itself [47], but is necessary

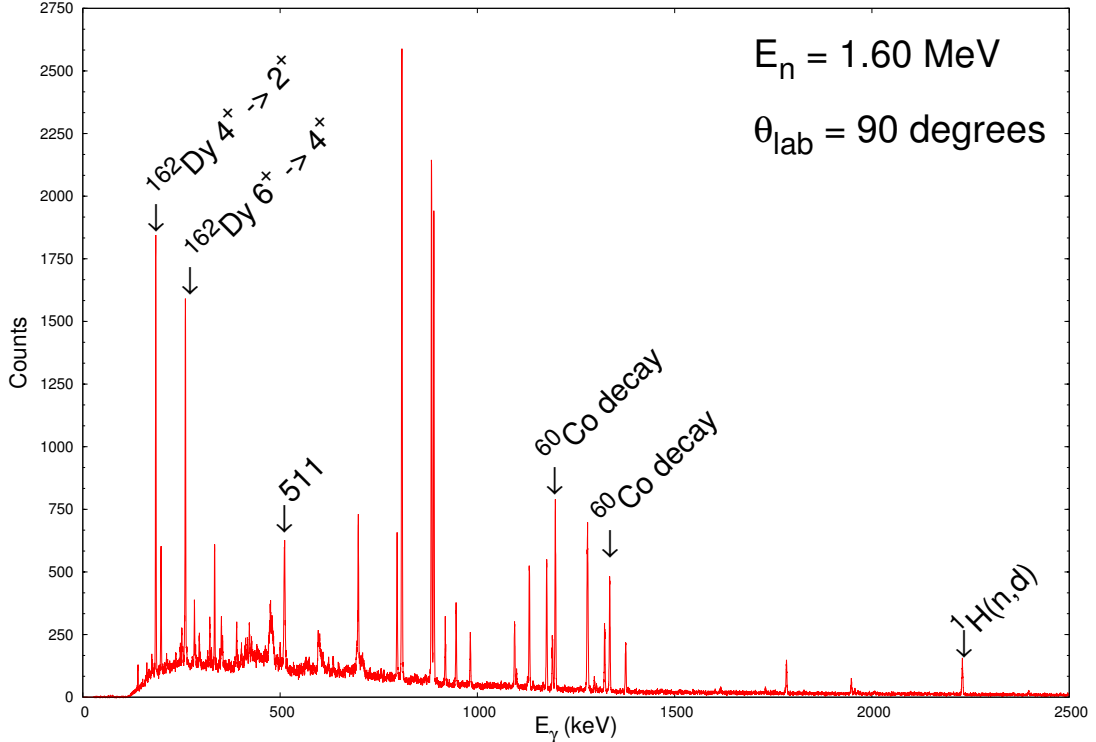


Figure 3.6. Example of an energy-calibrated spectrum from the ^{162}Dy angular distribution at $E_n=1.6$ MeV and $\theta_{lab}=90^\circ$, outlining typical background levels and miscellaneous γ -ray transitions.

to accurately fit low-intensity peaks that exist as a doublet with higher-intensity peaks. For a given peak, three parameters are interpolated separately into a χ^2 fit, the width, σ , and the two left-polynomial terms, $P_{left,1}$ & $P_{left,2}$. Typically, the polynomial terms are a small, but significant contribution ($P_{left,1}<0.010$), and σ is bounded between ~ 2 and ~ 7 channels (~ 0.5 to ~ 1.5 keV energy resolution). These open parameters are iteratively fit one at a time to best recreate the shape of the gaussian distribution in the histogram; once all peaks have been properly fitted, the fit parameters are exported to a peak list with peak areas, centroids (subsequently the energy of the γ -ray), and the associated statistical errors from each parameter. $F_i t P_i c$ [75] was used to interpolate fit parameters for all experimental data in both

^{160}Gd and ^{162}Dy . Peaks are assigned to groups with up to five other peaks to ensure a locally linear background for each gaussian.

3.2.2 Observable Extraction

From the peak list, we can extract a wealth of knowledge about the decay radiation observed, even with the seemingly basic information gained from fitting the peaks in a given histogram.

3.2.2.1 Excitation Functions

Although no direct measurable quantities (γ -ray energies, branching ratios, etc) can be extracted from the excitation function data, previously unplaced γ rays can be assigned to de-exciting levels simply by looking at the raw threshold of γ -ray population. Two plots per γ -ray are generated, the relationship between E_γ and E_n , and peak area as a function of E_n ; the first plot allows confirmation that each peak is fit uniformly, where the relationship between peak area and neutron energy will allow us to determine an approximate threshold energy. Any modulation of the γ -ray energy as a function of bombarding neutron energy is a signature of non-uniform peak fitting or that another γ -ray of similar energy has been populated in the level scheme at a different threshold. When this latter case occurs, the peak area as a function of neutron energy will also show a corresponding bump at the same threshold. An example of this ensemble of plots is shown in Figure 3.7:

The absolute threshold energies for γ -rays are used to determine where a γ -ray comes in, and to determine which level is providing the de-excitation, a problem that would otherwise require γ - γ coincidence measurements. Since the excitation functions give γ -ray placements in the nucleus, we are no longer reliant on the more complex coincidence measurements.

Figure 3.8 shows an example of the population rate of a γ -decay in ^{162}Dy by

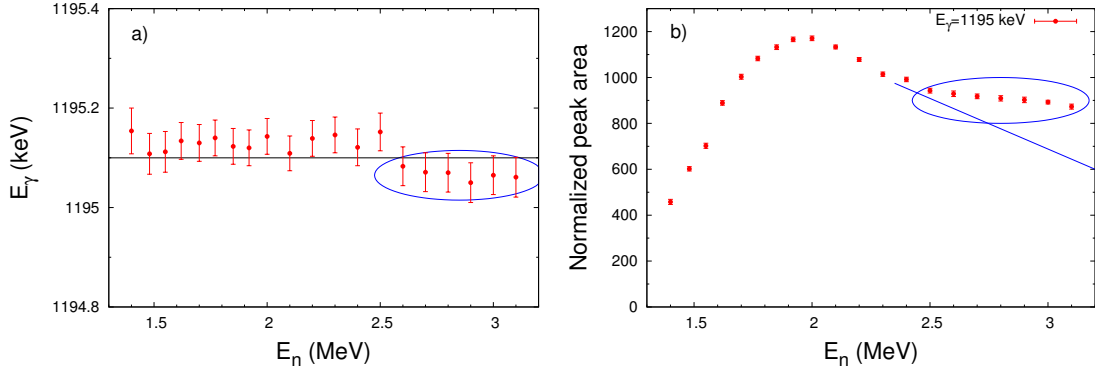


Figure 3.7. A set of plots from a typical excitation function for a single γ -ray transition, in ‘a’), E_γ vs. E_n , and in ‘b’), the peak area vs E_n . Note the dip in γ -ray energy at 2.6 MeV, and corresponding bump in peak area (shown as a blue ellipse to guide the eye), indicating a second transition of a similar (slightly lower) energy being populated.

superimposing multiple neutron energy spectra on top of each other. Take note that the $E_n=1.4$ and 1.7 MeV datasets are below the energy threshold of the level that the 1647 keV decay leaves, with a sharp increase of counted statistics just above the level energy threshold, growing until a well-defined gaussian peak is seen at $E_n=2.3$ MeV.

Proper placement of γ -rays in the level scheme is vital to confident, precise measurement of level lifetimes, absolute intensities, and multipole mixing fractions. Although the experiments at UKAL are not designed to find new $J=0$ states (*e.g.* something the Q3D spectrometer can better achieve with two nucleon transfer reactions), tentative spin assignments and/or confirmation of spin can be placed with information from both the excitation functions and angular distributions. $J=0$ excitations should have a threshold very close to the energy of the state, as there is very little angular momentum needed to populate the state, and since inelastic neutron scattering can only realistically populate up to spin 5^\pm states (a consequence of the limited angular momentum transfer from the spin- $\frac{1}{2}$ neutron to the nucleus during inelastic scattering), stringent upper limits on the spin and parity of a parent level

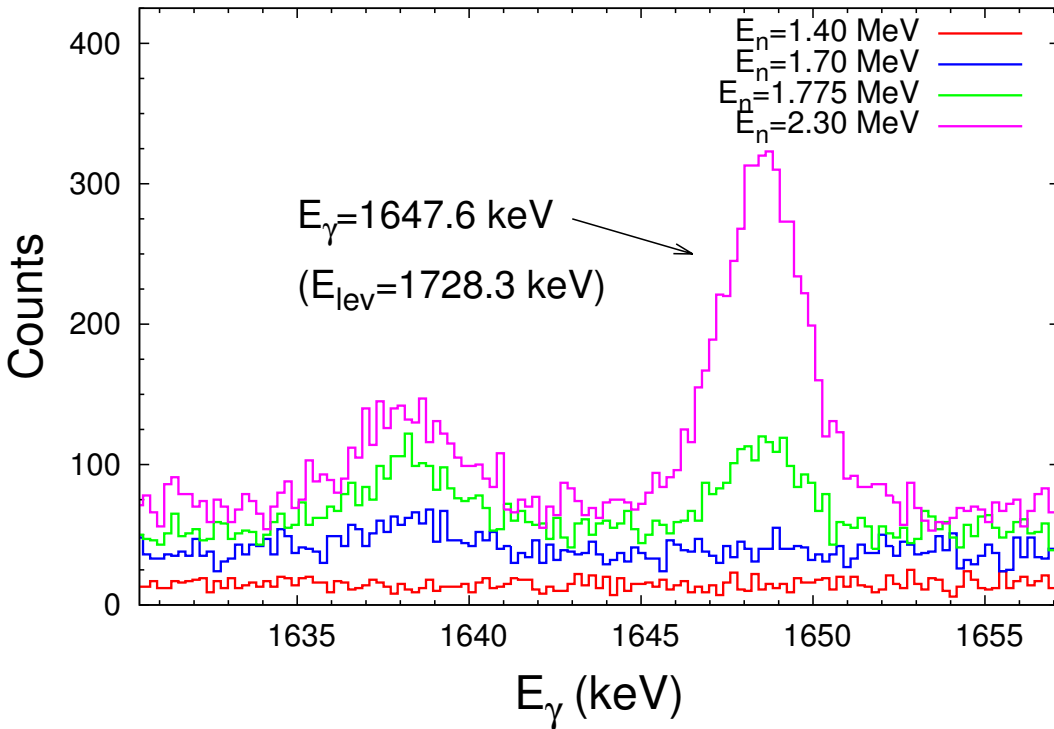


Figure 3.8. Spectra from four bombarding neutron energies ($E_n=1.4$, 1.7, 1.775, and 2.3 MeV datasets) to show the typical increase of statistics for a single peak, a 1647 keV decay from the 1728 keV state in ^{162}Dy . Note the peak area emerge just above the level energy threshold (1.775 MeV neutron dataset), with optimal statistics in the $E_n=2.3$ MeV set.

can be placed by examining the spin and parity of the daughter state. For example, if a transition between two levels is energetically feasible, we know that the spin and parity of the parent state will be within ± 2 units of angular momentum of the daughter level because only $\Delta J < 2$ multipolarities are observed in the laboratory with any appreciable or measurable intensity, as the relative intensity of E3, E4 and higher multipolarities are orders of magnitude less intense than the strong E2 quadrupole radiation observed in the lab. For example, in cases where the daughter level is spin-5, we know that the parent state will be spin-3 or spin-4, due to the low spin-population of inelastic neutron scattering.

3.2.2.2 Angular Distributions

Spectra from the angular distributions have all corrections applied (nonlinearity, detector efficiency, and self-absorption), where the peak list is separated and sorted into groups based on the γ -ray energy as a function of angle. Careful bounding of groups must be made to ensure good γ -ray separation in the event of a close-lying doublets, while maintaining sufficient overhead to account for large-order Doppler energy shifts (very short lifetimes on the order of ~ 10 fs).

In order to extract the lifetime of a particular state, precise calculation of the theoretical values for $F(\tau)$ (Winterbon curve) must be made to compare the extracted $F(\tau)$ from the Doppler shifted γ -rays. This calculation is achieved via `v1pgm`, which takes into account the calculated recoil velocity from Equation 2.2, the target density and atomic weight of each element in the target, and a range of lifetimes to iterate over (from 1 fs to 10 ps). Since the target does not change composition or density, the only input parameter that changes is the nuclear recoil velocity, dependent solely on the bombarding neutron energy. The calculated Winterbon curves for the ^{162}Dy experiments can be seen in Figure 3.9, with an emphasis to highlight the ideal range ($\sim 10 - \sim 600$ fs) to measure lifetimes with DSAM. In general, $F(\tau)$ is constrained by the uncertainties in electronic and nuclear stopping powers, resulting in $\sim 10\%$ uncertainty in the attenuation factor [5]; this uncertainty is propagated to the extracted lifetime's uncertainty.

Direct comparison of the experimental $F(\tau)$ value to the calculated Winterbon curve for a particular γ -ray is straightforward; in Figure 3.10, the measured slope of the Doppler shift of 0.665 correlates to a τ of 21 fs. For excited states with only one de-exciting transition, the extracted γ -ray lifetime is equivalent to the level lifetime, where level lifetimes with multi-channel γ -ray de-excitations are extracted from the weighted average of all de-exciting $F(\tau)$ values, weighted by the uncertainty in each measured $F(\tau)$. This standard statistical average can be explicitly seen in Equation

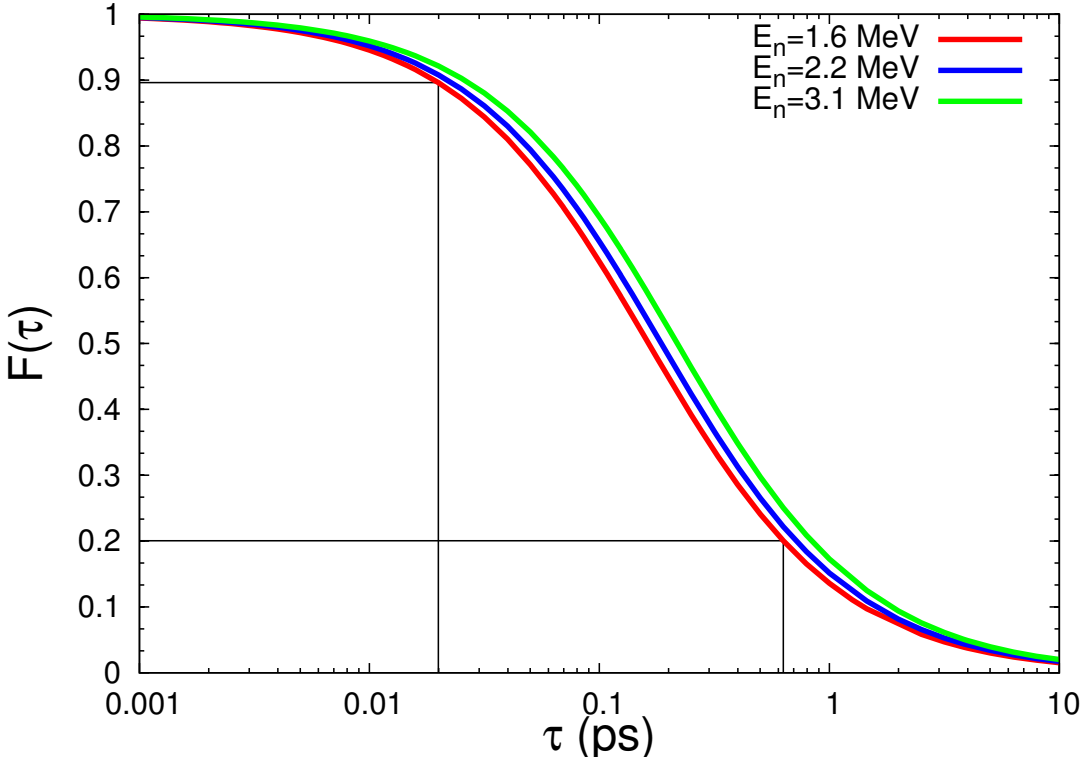


Figure 3.9. Calculated Winterbon curves ($F(\tau)$) as a function of τ) for $E_n=1.6, 2.2$, and 3.1 MeV ^{162}Dy angular distributions. Sensitive lifetime ranges from DSAM are shown as vertical black lines, with the corresponding $F(\tau)$ values as horizontal lines.

3.2 taken from [9]. Special care must be taken, however, to ensure accurate and precise Doppler shifts are obtained from the various de-excitation channels from a level. In several cases for low energy and/or intensity γ rays, the shift (magnitude of $F(\tau)$) will be negative or consistent with zero; in this case, any lifetime deduced from the Doppler shift is not accounted in the weighted average of the level lifetime. The same rules apply when a particular γ ray has the potential to be coincident with a background line, where the $F(\tau)$ value may be unreliable. As a rule of thumb, $F(\tau)$ should be about 1σ variance from zero to be considered a good candidate for DSAM, however, this is sometimes impossible if the physical lifetime is on the precipice of the sensitive range of lifetimes DSAM can measure. Large upper uncertainties

are not uncommon for the near-picosecond lifetimes with ‘shallow’ values for $F(\tau)$ measured with DSAM (e.g. 3000^{+4800}_{-1300} fs for the 1666 keV state in ^{162}Dy), yet another experimental challenge we must overcome when measuring the lifetimes of states.

$$\widehat{F(\tau)} = \frac{\sum_i F_i(\tau) \sigma_i^{-2}}{\sum_i \sigma_i^{-2}}, \sigma^2(\widehat{F(\tau)}) = \frac{1}{\sum_i \sigma_i^{-2}} \quad (3.2)$$

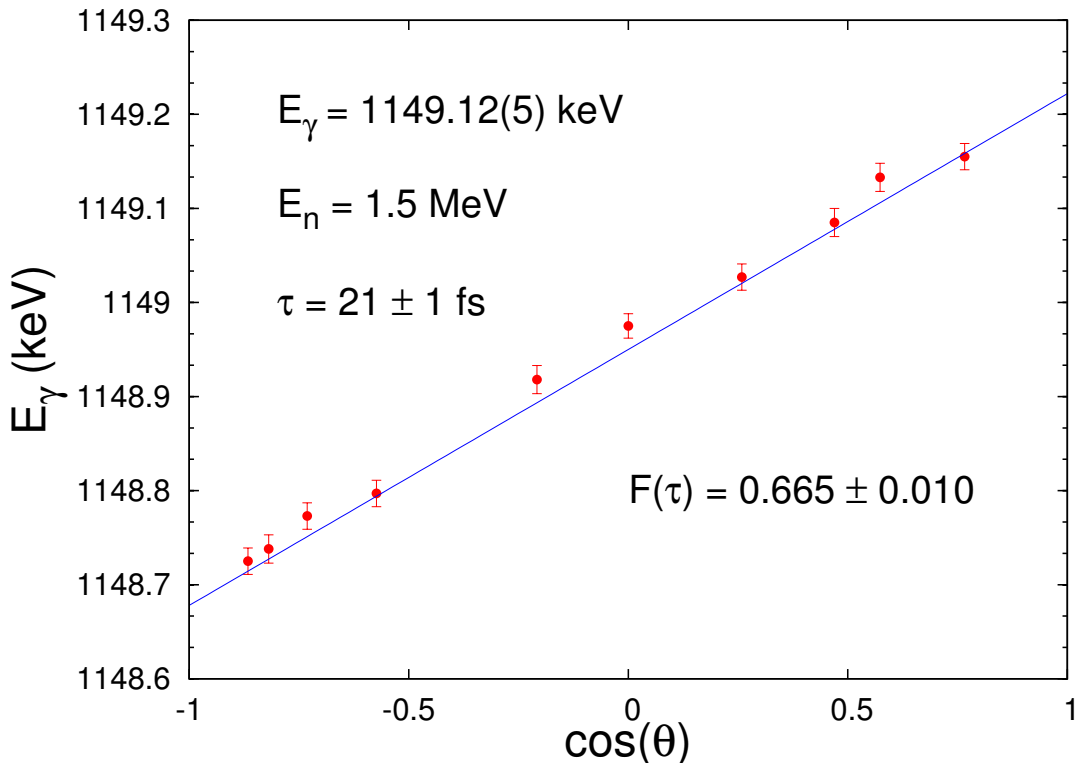


Figure 3.10. Example Doppler Shift for a 1149 keV γ -ray populated in the 1.5 MeV $^{160}\text{Gd}(n,n'\gamma)$ experiment. Here, the $F(\tau)$ value of 0.665 ± 0.010 corresponds to a lifetime of 21 ± 1 fs.

Further refinement of any spin assignments made in the literature can be deduced

by examining the a_2 and a_4 coefficients from Equation 2.4; isotropic or near-isotropic angular distributions could suggest significant multipole mixing of γ radiation, as pure E2, E1, or M1 radiation will mimic the classical radiation patterns displayed in Figure 2.6. The decay radiation pattern leaving a 0^+ excitation will also be isotropic in the angular distribution, as this is the equivalent of an unaligned decaying state. The angular distributions can be used to confirm or deny tentative spin-0 states by examining the angular distribution, but this technique should not be used to find new 0^+ excitations (two nucleon transfer reactions are still a much higher resolution method). For all angular distributions presented in this work, the peak areas are normalized in a way to ensure the angular distribution of the decay from the first excited 0^+ state is isotropic (a_2 consistent with 0). This is justified in [52], where multiple angular distribution normalizations were examined: once with the above normalization, and once where we normalized the peak area to another tentative (now repudiated) 0^+ state with disastrous results. Under this secondary normalization, strong E2 transitions that show no mixing ceased to have the same qualitative shape of a pure quadrupole in Figure 2.6, implying this was not a suitable candidate for normalization (or as an isotropic $0^+ \rightarrow 2^+$ transition). Special care must also be taken with the evaluation of the angular distributions, as there are multiple ways to create an isotropic distribution, via proper mixing of multipole radiation (admixtures of E2 and M1 radiation).

If the angular distribution is not isotropic or indicative of a pure quadrupole or dipole radiation (Figure 2.6), then the γ -ray may be of a mixed multipolarity. This commonly occurs in transitions where $J_i^\pi \approx J_f^\pi$, but is not to be confused with an E0 monopole transition, which is strictly forbidden by γ decay and must occur via internal conversion electrons. In order to characterize this mixing, we compare the a_2 and a_4 coefficients to theoretical calculations of the same a_2 and a_4 coefficients for a particular J^π value for a level, assuming there is no mixing. The statistical model

for a compound nucleus is used to calculate cross sections for a $(n,n'\gamma)$ reaction with the target nucleus being treated as an optical model potential (the combination of a real Woods-Saxon potential with a diffuse, imaginary Gaussian surface potential). The FORTRAN code used to achieve this calculation is **CINDY** (a Hauser-Feschbach formalism taken from [71]). The multipole mixing fraction (effectively a_2 and a_4) is then varied in the statistical model to reproduce the angular distribution for a possible J^π ; the direct comparison of experimental Legendre Polynomial coefficients to those calculated in this statistical model lead directly to χ^2 as a function of δ , the multipole mixing fraction. Any γ -ray observed in our experiments that has a known placement in the level scheme can be added to the optical model to perform this χ^2 minimization, where the smallest value of χ^2 corresponds to the optimal value of δ for a particular de-excitation. These experimental mixing fractions aid in the calculation of the reduced transition probabilities for mixed multipolarity γ decays given in Equation 1.17, also using Equations 1.18 or 1.19. An example extraction of δ from the angular distribution of γ -rays can be seen in Figure 3.11; χ^2 is minimized locally for this γ ray at a δ value ~ 1 , which indicates $\sim 50\%$ E2/M1 mixing. In Figure 3.11, the top left plot shows the measured angular distribution of the 1308 keV γ ray, with **CINDY** calculations for a range of starting spins decaying to a spin-4 state. The intersection of the black ellipse and the colored ellipses (calculations) correspond to the projections in the bottom plot, where we verify the lowest χ^2 value on the y-axis for a particular delta on the x-axis for the $4^+ \rightarrow 4^+$ transition.

To round out the cadre of important experimental information, we can extract the absolute intensity of γ -rays that de-excite the nucleus from the angular distribution data. The A_o coefficient from Equation 2.4 is proportional to the absolute intensity, and simply needs to have the efficiency & self-absorption corrections applied to the measured A_o (gross peak area). The branching ratios immediately follow from the absolute intensities, since we know all γ -decay channels open to a particular level,

and these are used to calculate absolute transition probabilities (Equation 1.17).

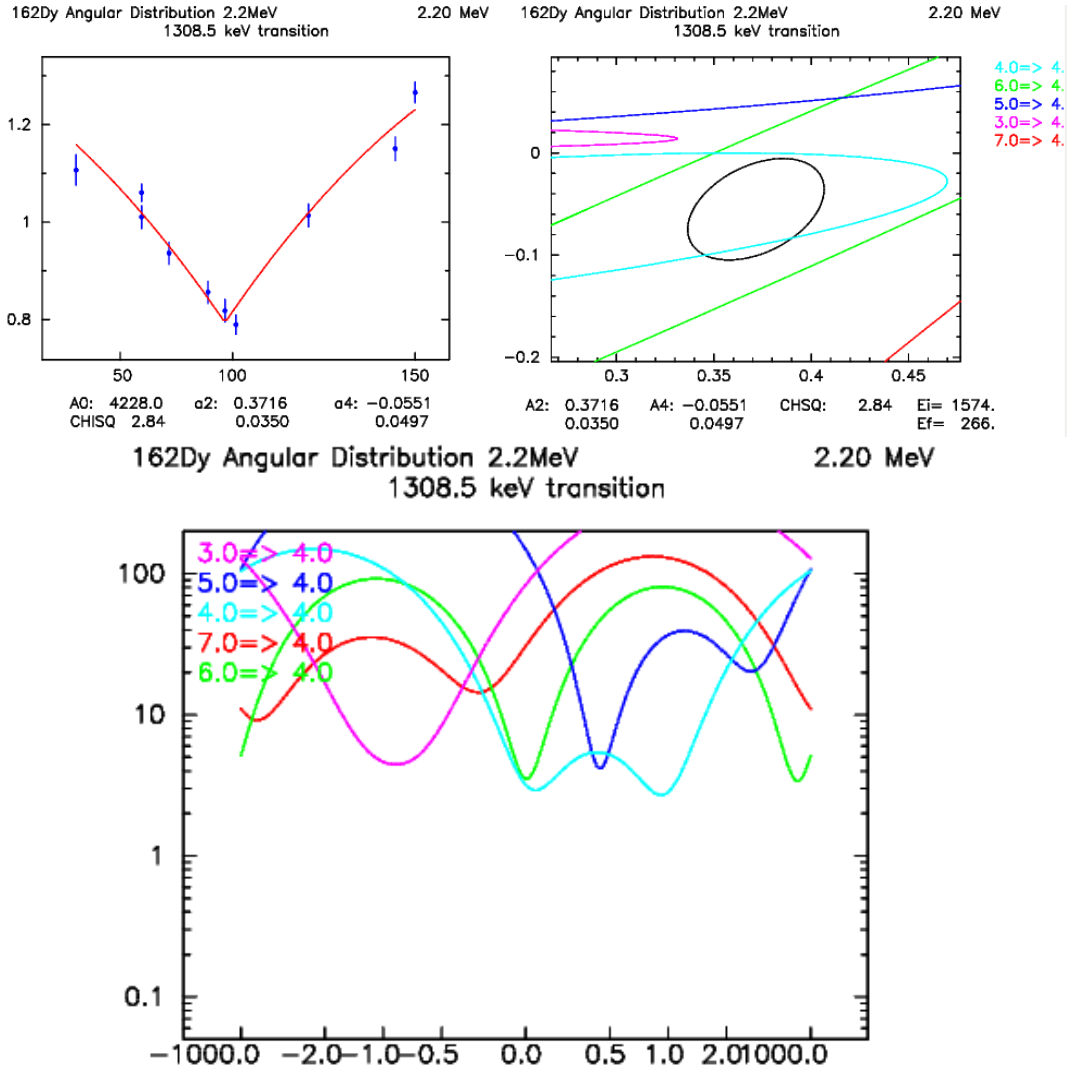


Figure 3.11. Example extraction of multipole mixing fraction (δ) for a $4^+ \rightarrow 4^+$ transition in ^{162}Dy . Top-left plot: angular distribution of the 1308 keV γ ray. Top-right plot: CINDY comparison for a range of initial spins (color online) decaying to the final spin of 4; intersections with the black ellipse mark local/global minima of χ^2 vs δ . Bottom plot: projection of CINDY comparison as χ^2 as a function of δ minimization (note the lowest χ^2 value corresponds to the $\delta \approx 1$ for the cyan-colored $4^+ \rightarrow 4^+$ transition).
 (color online)

CHAPTER 4

RESULTS

When reporting the lifetimes in this work, it is prudent to distinguish which bombarding neutron energy angular distribution is used, as the lifetimes are sensitive to inflation from multiple sources. First, recall Figure 3.9, where we observe inflation of the extracted lifetimes due to the calculation of $F(\tau)$ from a higher neutron energy, and thus, a modified value for the nuclear and electronic stopping powers that allows us to extract the lifetime. To minimize this effect, the neutron energy is carefully chosen under the time constraints imposed by accelerator availability. Specific neutron energies were selected with the aid of the excitation function measurements. Second, the extracted lifetime can be inflated due to level-feeding effects from higher-lying excitations in the nucleus; for these reasons, lifetimes are reported from the *lowest* energy threshold possible to reduce this effect of observed lifetime inflation. As decays from higher-lying levels feed a state, the decay width (and thus lifetime) of the state are artificially inflated; this effect is observed throughout the most fundamental measurements of nuclear lifetimes [20, 79]. An example of the proportional lifetime inflation for two excited states caused by level-feeding and bombarding neutron energy differences can be seen in Figure 4.1.

For the interest of discussion in §5, lifetimes are separated into smaller, more digestable tables based on their corresponding discussion sections (*e.g.* a table containing lifetimes of 0^+ states, one for the 2_γ^+ band, etc). Unless otherwise noted, tables in this chapter will contain experimentally determined level energies, γ -ray energies, branching ratios measured from our angular distributions, multipole mixing

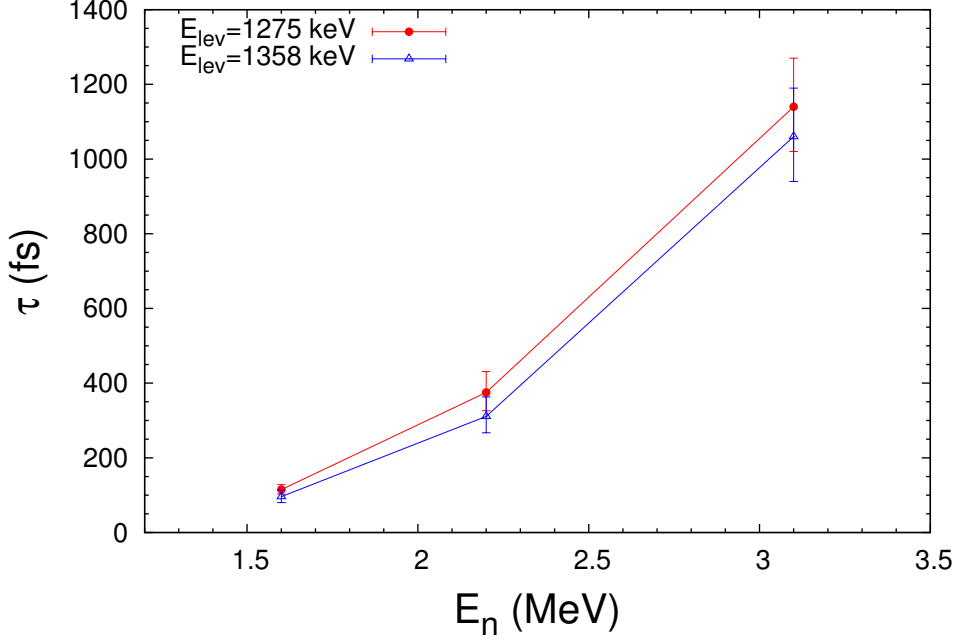


Figure 4.1. Lifetime inflation of the measured lifetimes for two levels ($E_{lev}=1275$ keV and $E_{lev}=1358$ keV) in ^{162}Dy caused by effects due to a higher bombarding neutron energy and unknown level-feeding from higher-lying states.

fractions where applicable, and the lifetime of the state with applicable uncertainties for all of the above quantities.

4.1 ^{160}Gd Results

Results from the ^{160}Gd campaign were published in [52], where this work also outlines and reiterates the major results taken from the suite of experiments in §2.4.1. A level scheme outlining all measured lifetimes in the ^{160}Gd campaign is shown in Figure 4.2, with previously existing literature lifetimes in blue and new lifetime measurements in red. Prior to the presented results in this work, Gadolinium-160 has a complete paucity of lifetime information as a whole (most notably for 0^+ bands and negative parity bands), and as such, we add 29 new lifetimes, a factor of 7 increase,

to the pool of placed literature values.

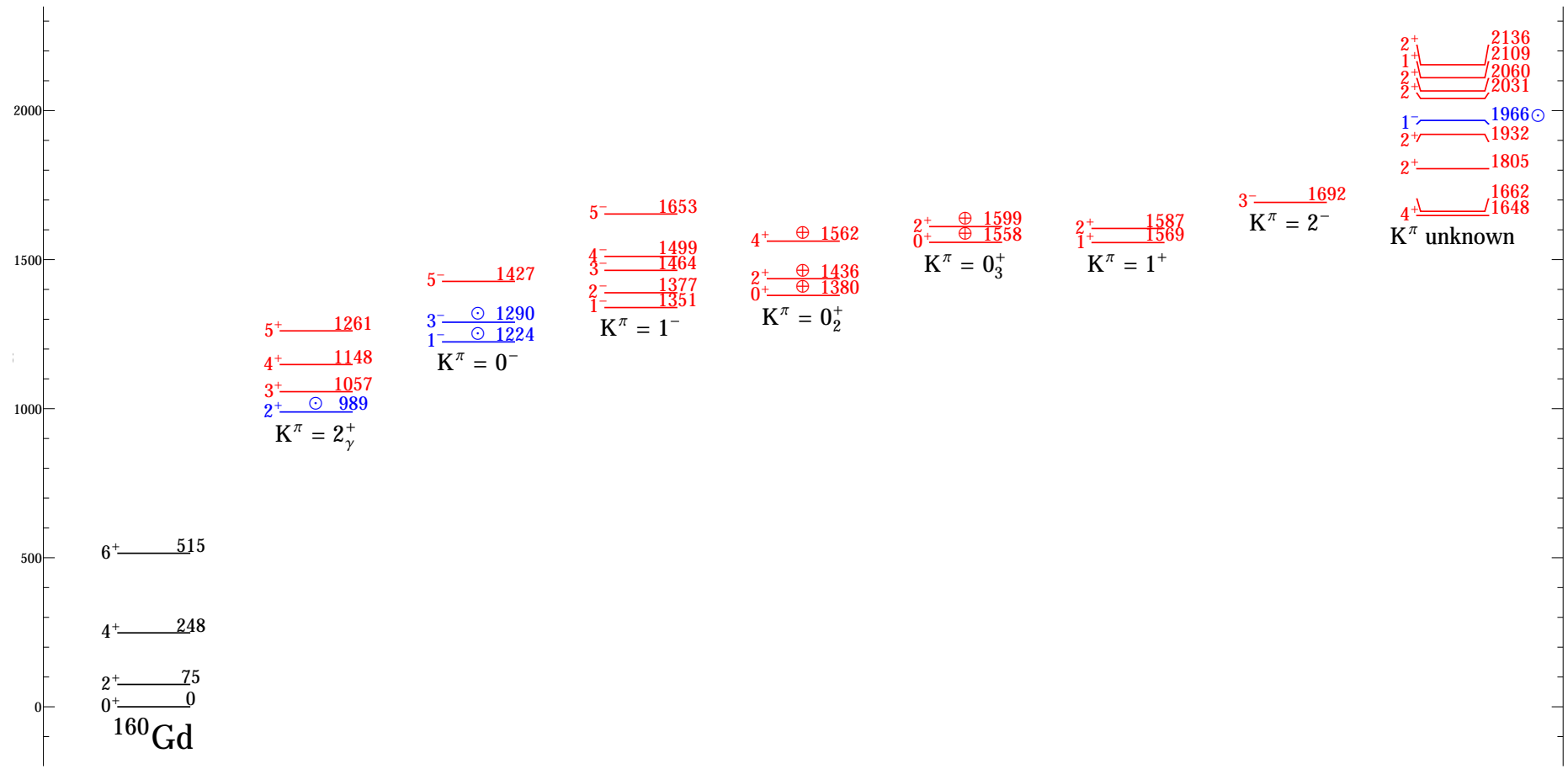


Figure 4.2. Level scheme for all level lifetimes measured in the ^{160}Gd experiments, with confirmed band and spin assignments shown. Previously measured lifetimes are in blue, with newly presented lifetimes in red. Individual levels and bands will be discussed in following sections.

High resolution angular distribution measurements were performed by Govor in [35] and provide us with an overall benchmark for our measurements, and as a whole, our reported γ -ray intensities, angular distribution coefficients, and multipole mixing ratios are found to be in good agreement with the work. One key contrasted element in our work with the Govor paper is the use of monoenergetic neutrons for DSAM-INS rather than the continuum energies of reactor neutrons to extract the lifetimes in addition to any decay information (γ -ray energies, multipole mixing fractions, etc). A visual representation of the all the measured lifetimes in ^{160}Gd is shown in Figure 4.3, with literature values in black and new lifetimes in red (corresponding to lifetime extracted from the $E_n=1.5$ MeV dataset), green for 2.0 MeV neutrons, and blue for the final dataset using 2.8 MeV neutrons bombardement.

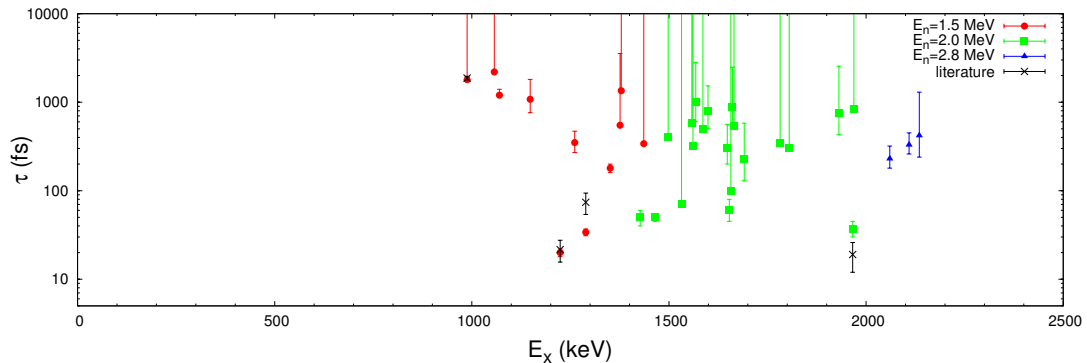


Figure 4.3. Visual representation of all measured lifetimes with respect to literature values (in blue). Each separate color outlines the specific regimes (<1.5 MeV, $1.5 - 2.0$ MeV, and >2.0 MeV excitation energy) of energies studied in the ^{160}Gd angular distributions.

An example of the $E_n=2.0$ MeV angular distribution singles-spectrum for $^{160}\text{Gd}(n,n'\gamma)$ can be seen in Figure 4.4 with select peaks labeled for reference.

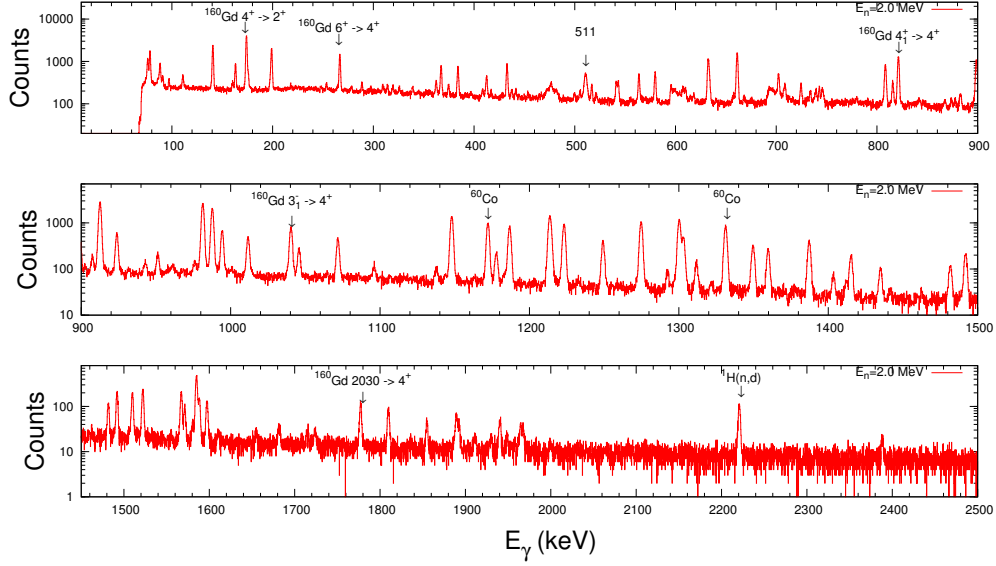


Figure 4.4. Singles spectra from the $\theta_{lab}=90^\circ$ and $E_n=2.0$ MeV angular distributions of ^{160}Gd .

4.1.1 Lifetimes of 0^+ States

The tabulation of lifetimes for the 0^+ bands in ^{160}Gd is given in Table 4.1. In many cases, $F(\tau)$ values for γ rays were small, and as such, we are only able to extract lower limits for the level lifetimes. Further refinement of the level lifetime for the $E_x=1599$ keV state was provided in [TBA REF], where any negative (and consequently impossible) $F(\tau)$ attenuation factors were removed from the weighted average for the level lifetime.

TABLE 4.1

 $K^\pi=0^+$ BANDS: ^{160}GD

E_{level} (keV)	E_γ (keV)	$J_{K_i}^\pi$	$J_{K_f}^\pi$	τ (fs)	BR	Mult.	B(E2) (W.u.)	B(E1) (mW.u.)
1379.70 (7)	1304.46 (5)	$0^+_{0_2^+}$	$2^+_{0_1^+}$	>1350	1.000	E2	<3.10	
1436.47 (4)	1187.81 (5)	$2^+_{0_2^+}$	$4^+_{0_1^+}$	>340	0.667	E2	<13.1	
	1361.05 (6)	$2^+_{0_2^+}$	$2^+_{0_1^+}$		0.243	E2/M1 ^[a]	<2.42	
	1436.34 (6)	$2^+_{0_2^+}$	$0^+_{0_1^+}$		0.090	E2	<0.68	
1561.59 (6)	1046.67 (6)	$4^+_{0_2^+}$	$6^+_{0_1^+}$	>320	0.572	E2	<22	
	1313.03 (6)	$4^+_{0_2^+}$	$4^+_{0_1^+}$		0.428	E2/M1 ^[b]	<0.4	
1558.30 (7)	1483.06 (6)	$0^+_{0_3^+}$	$2^+_{0_1^+}$	>590	1.000	E2	<3.74	
1599.00 (4)	309.32 (6)	$2^+_{0_3^+}$	$3^-_{0_1^-}$	800^{+730}_{-300}	0.037	E1		$0.34^{+0.13}_{-0.31}$
	374.78 (6)	$2^+_{0_3^+}$	$1^-_{0_1^-}$		0.062	E1		$0.32^{+0.12}_{-0.29}$
	541.53 (6)	$2^+_{0_3^+}$	$3^+_{2\gamma}$		0.154	E2/M1 ^[c]	41^{+16}_{-37}	
	1523.59 (6)	$2^+_{0_3^+}$	$2^+_{0_1^+}$		0.418	E2/M1 ^[d]	$0.34^{+0.68}_{-0.32}$	
	1598.85 (6)	$2^+_{0_3^+}$	$0^+_{0_1^+}$		0.329	E2	$0.41^{+0.15}_{-0.37}$	

Lifetimes of excited 0^+ bands in ^{160}Gd , with experimentally determined B(E2) in W.u and B(E1) in mW.u. ^[a] $\delta=0.00^{+0.08}_{-0.08}$, ^[b] $\delta=0.28^{+0.34}_{-0.12}$, ^[c] $\delta=-5.57^{+1.91}_{-5.00}$, ^[d] $\delta=-1.04^{+0.72}_{-2.10}$, 1 W.u.(E2)= $5.16\text{E-}7 \text{ e}^2\text{b}^2$, 1 mW.u.(E1)= $1.90 \text{ e}^2\text{b}$

4.1.2 Lifetimes of 2_{γ}^{+} Band

We have measured lifetimes for the 4 lowest-lying members of the $K^{\pi}=2^{+}$ band in ^{160}Gd in our campaign of experiments. Throughout the rare-earth region of nuclei, the 2^{+} band lifetimes are generally well known and fall in the near-picosecond lifetime range [18, 39, 44, 56]. Due to the sensitive range of DSAM, these near-picosecond lifetimes manifest as lower-limits due to the shallow $F(\tau)$ values observed in our experiments; however, we obtain well-defined values for the 4^{+} and 5^{+} members of the 2^{+} band via some well-defined energy shifts, all shown in Table 4.2.

TABLE 4.2

$K^{\pi}=2^{+}$ BAND: ^{160}GD

E_{level} (keV)	E_{γ} (keV)	$J_{K_i^{\pi}}^{\pi}$	$J_{K_f^{\pi}}^{\pi}$	τ (fs)	BR	Mult.	$B(E2)$ (W.u.)
988.72 (6)	913.43 (5)	$2_{2\gamma}^{+}$	$2_{0_{gs}^{+}}^{+}$	>1800	0.530	E2/M1 ^[a]	<1.2
	988.68 (5)	$2_{2\gamma}^{+}$	$0_{0_{gs}^{+}}^{+}$				
1057.42 (6)	809.06 (5)	$3_{2\gamma}^{+}$	$4_{0_{gs}^{+}}^{+}$	>2200	0.171	E2/M1 ^[b]	<0.04
	982.28 (5)	$3_{2\gamma}^{+}$	$2_{0_{gs}^{+}}^{+}$				
1148.15 (7)	899.59 (5)	$4_{2\gamma}^{+}$	$4_{0_{gs}^{+}}^{+}$	1080^{+730}_{-320}	0.631	E2/M1 ^[d]	16^{+5}_{-10}
	1072.85 (5)	$4_{2\gamma}^{+}$	$2_{0_{gs}^{+}}^{+}$				
1261.24 (9)	746.34 (5)	$5_{2\gamma}^{+}$	$6_{0_{gs}^{+}}^{+}$	350^{+120}_{-80}	0.164	E2/M1 ^[e]	31^{+7}_{-11}
	1012.65 (5)	$5_{2\gamma}^{+}$	$4_{0_{gs}^{+}}^{+}$				

Lifetimes of $K^{\pi}=2_{\gamma}^{+}$ band in ^{160}Gd , with experimentally determined $B(E2)$ in W.u. and multipole mixing fractions δ taken from the $E_n=1.5$ MeV angular distributions.
^[a] $\delta=-0.45^{+0.04}_{-0.05}$, ^[b] $\delta=0.11^{+0.03}_{-0.03}$, ^[c] $\delta=47^{+18}_{-10}$, ^[d] $\delta=21^{+21}_{-7}$, ^[e] $\delta=8^{+13}_{-4}$, ^[f] $\delta=15^{+17}_{-6}$
1 W.u.(E2)= $5.16\text{E-}7 \text{ e}^2\text{b}^2$

4.1.3 Lifetimes of Negative Parity Bands

Population of the $K^\pi=0^-$ bands in rare-earth nuclei is abundant [85], showing up as some of the strongest peaks in our γ -singles spectra, with a very low angular momentum transfer needed to populate the states ($\Delta K=0$). Typically, since the lowest-lying negative parity states are collective octupole vibrations on top of the deformed ground state, the mean lifetimes of these states are comparatively short, acting as a practical benchmark for lifetimes measurable by DSAM-INS. All three level lifetimes from the $K^\pi=0^-$ band in ^{160}Gd were measured from the inelastic scatter of 1.5 MeV neutrons, using the five γ -rays listed in Table 4.3.

Similar to the $K^\pi=0^-$ band, the $K^\pi=1^-$ band in ^{160}Gd is richly populated in our $(n,n'\gamma)$ experiments, with four band members ($1^-, 2^-, 3^-, 4^-$) all proposed by Govor in another $(n,n'\gamma)$ study [35] using continuum energy reactor neutrons in contrast to our monoenergetic probe. Of the specific lifetimes measured from the Doppler shifting γ -rays, we observe a weak decay from the 2^- state to the γ -vibrational band; this branching ratio is so weak that it *could* be misplaced, however, the threshold of the de-excitation in our excitation function does not place it leaving any other level. The resulting lifetime from the 1301 keV γ ray is only a lower-limit due to the shallow $F(\tau)$ value.

Grigoriev [37] places a $K^\pi=2^-$ assignment on the band with the $E_x=1691$ & 1782 keV members that was tentatively either a 2^- or 3^- . We adopt this 2^- assignment from our observed γ -decay channels, even without the measurement or observation of the 2^- bandhead in our data.

4.1.4 Lifetimes of Positive Parity Bands

In addition to the measurement of lifetimes of $K=0,2$ and negative parity bands, we are also able to populate the vast majority of states below $J=5$. Lifetimes of

TABLE 4.3

NEGATIVE PARITY BANDS: ^{160}GD

E_{level} (keV)	E_γ (keV)	$J_{K_i}^\pi$	$J_{K_f}^\pi$	τ (fs)	BR	Mult.	B(E1) (mW.u.)
1224.33 (6)	1149.12 (5)	$1_{0_1^-}^-$	$2_{0_1^+}^+$	20_{-2}^{+2}	0.597	E1	$6.5_{-0.6}^{+0.6}$
	1224.38 (5)	$1_{0_1^-}^-$	$0_{0_1^+}^+$		0.403	E1	$3.6_{-0.4}^{+0.4}$
1289.90 (7)	1041.37 (5)	$3_{0_1^-}^-$	$4_{0_1^+}^+$	34_{-3}^{+3}	0.353	E1	$3.0_{-0.3}^{+0.3}$
	1214.79 (5)	$3_{0_1^-}^-$	$2_{0_1^+}^+$		0.647	E1	$3.5_{-0.3}^{+0.3}$
1427.40 (12)	1214.79 (5)	$5_{0_1^-}^-$	$4_{0_1^+}^+$	50_{-10}^{+10}	1.000	E1	$4.0_{-0.8}^{+0.8}$
1351.30 (6)	1276.06 (5)	$1_{1_1^-}^-$	$2_{0_1^+}^+$	180_{-20}^{+20}	0.833	E1	$0.74_{-0.08}^{+0.08}$
	1351.30 (5)	$1_{1_1^-}^-$	$0_{0_1^+}^+$		0.167	E1	$0.12_{-0.01}^{+0.01}$
1376.70 (8)	319.38 (6)	$2_{1_1^-}^-$	$3_{2\gamma}^+$	>550	0.017	E1	<0.18
	1301.46 (5)	$2_{1_1^-}^-$	$2_{0_1^+}^+$		0.982	E1	<0.27
1464.00 (10)	1388.75 (5)	$3_{1_1^-}^-$	$2_{0_1^+}^+$	50_{-5}^{+5}	1.000	E1	$2.5_{-0.2}^{+0.2}$
1498.94 (10)	1250.39 (5)	$4_{1_1^-}^-$	$4_{0_1^+}^+$	>400	1.000	E1	<0.41
1691.68 (7)	543.45 (6)	$3_{2_1^-}^-$	$4_{2\gamma}^+$	230_{-100}^{+350}	0.226	E1	2_{-3}^{+1}
	634.56 (6)	$3_{2_1^-}^-$	$3_{2\gamma}^+$		0.370	E1	$2.1_{-3.2}^{+0.9}$
	702.84 (6)	$3_{2_1^-}^-$	$2_{2\gamma}^+$		0.372	E1	$1.5_{-2.3}^{+0.7}$
	1442.93 (8)	$3_{2_1^-}^-$	$4_{0_1^+}^+$		0.032	E1	$0.01_{-0.02}^{+0.01}$
1782.67 (10)	521.53 (8)	$4_{2_1^-}^-$	$5_{2\gamma}^+$	>350	0.208	E1	<2.0
	725.19 (6)	$4_{2_1^-}^-$	$3_{2\gamma}^+$		0.792	E1	<1.4

Lifetimes of excited negative parity bands in ^{160}Gd , with experimentally determined B(E1) in mW.u.

positive parity bands were measured in ^{160}Gd , namely of the $K^\pi=4^+$ and 1^+ bands.

The full tabulation of measured lifetimes can be found in Table 4.4.

TABLE 4.4

POSITIVE PARITY ($K^\pi=4^+/1^+$ BANDS): ^{160}GD

E_{level} (keV)	E_γ (keV)	$J_{K_i}^\pi$	$J_{K_f}^\pi$	τ (fs)	BR	Mult.	$B(\pi\ell)$
1070.57 (7)	555.45 (8)	$4_{4_1^+}^+$	$6_{0_1^+}^+$	>1200	0.010	E2	<2.4
	822.06 (5)	$4_{4_1^+}^+$	$4_{0_1^+}^+$				<7.2
	995.30 (5)	$4_{4_1^+}^+$	$2_{0_1^+}^+$				<5.2
1568.77 (6)	217.51 (6)	$1_{1_1^+}^+$	$1_{1_1^-}^-$	1000^{+1800}_{-400}	0.030	E1	$0.97^{+0.7}_{-1.8}$
	580.20 (6)	$1_{1_1^+}^+$	$2_{2_1^+}^+$		0.305	E2/M1 ^[b]	$5.3^{+6.7}_{-13}$
	1493.40 (6)	$1_{1_1^+}^+$	$2_{0_1^+}^+$		0.323	E2/M1 ^[c]	$0.44^{+0.23}_{-0.88}$
	1568.70 (6)	$1_{1_1^+}^+$	$0_{0_1^+}^+$		0.342	E2/M1 ^[*]	$0.56^{+0.22}_{-1.01}$
	1586.61 (12)	$2_{1_1^+}^+$	$2_{0_1^+}^+$	>500	1.000	E2	<4.01
	1665.16 (8)	$3_{1_1^+}^+$	$2_{1_1^-}^-$	>540	0.115	E1	<2.9
	1416.59 (6)	$3_{1_1^+}^+$	$4_{0_1^+}^+$		0.462	E2/M1 ^[d]	<0.73
	1589.81 (6)	$3_{1_1^+}^+$	$2_{0_1^+}^+$		0.423	E2/M1 ^[e]	<0.95

Lifetimes of excited positive parity bands in ^{160}Gd , with experimentally determined $B(E2)$ in W.u and $B(E1)$ in mW.u.

^[a] $\delta = -0.72^{+0.06}_{-0.05}$, ^[b] $\delta = 0.28^{+0.25}_{-0.18}$, ^[c] $\delta = 1.34^{+1.6}_{-0.6}$, ^[d] $\delta = 0.67^{+0.11}_{-0.08}$, ^[e] $\delta = -1.87^{+0.18}_{-0.18}$

^[*] Full E2 strength is reported (no δ was calculated)

1 W.u.(E2)=5.16E-7 e²b², 1 mW.u.(E1)=1.90 e²b

4.1.5 Lifetimes of States with No K^π Assignment

The remaining lifetimes of states with no rotational band assignment are tabulated in Table 4.5 and presented with deduced transition probabilities in Figure 5.6. We place stringent limits on the spin and parity of these states by confirming all de-excitations exhibit the same qualitative shape in the excitation functions, and by examining the Legendre polynomial coefficients to ascertain changes in angular

momentum. In many cases, this is easily done if the radiation pattern is strongly E2 or E1; for mixed-multipolarity γ rays, comparison to the CINDY code is possible to restrict possible spin assignments. Generally, CINDY is used as a baseline, rough assignment, as the statistical model behaves much better at lower mass nuclei, such as ^{76}Ge or ^{106}Pd [25, 64], where the density of states above the pairing gap is smaller, and as such are tentative assignments placed by our $(n,n'\gamma)$ study.

TABLE 4.5

OTHER LEVELS: ^{160}GD

E_{level} (keV)	E_γ (keV)	$J_{K_i}^\pi$	$J_{K_f}^\pi$	τ (fs)	BR	Mult.	$B(\pi\ell)$
1805.13 (9)	734.50 (6)	$2^+_{[\Upsilon]}$	$4^+_{4_1^+}$	>300	0.307	E2	<76
	816.46 (6)	$2^+_{[\Upsilon]}$	$2^+_{2_1^+}$				
1931.96 (7)	874.51 (6)	$2^+_{[\Upsilon]}$	$3^+_{2_1^+}$	760^{+1800}_{-330}	0.197	E2/M1 ^[b]	$8^{+3.5}_{-19}$
	1683.45 (7)	$2^+_{[\Upsilon]}$	$4^+_{0_1^+}$		0.206	E2	$0.32^{+0.14}_{-0.75}$
	1856.65 (6)	$2^+_{[\Upsilon]}$	$2^+_{0_1^+}$		0.454	E2/M1 ^[c]	$0.20^{+0.17}_{-0.47}$
	1932.00 (7)	$2^+_{[\Upsilon]}$	$0^+_{0_1^+}$		0.143	E2	$0.11^{+0.05}_{-0.26}$
1966.66 (10)	1891.33 (6)	$1^+_{[\Upsilon]}$	$2^+_{0_1^+}$	37^{+8}_{-7}	0.637	E1	$0.84^{+0.28}_{-0.21}$
	1966.97 (13)	$1^+_{[\Upsilon]}$	$0^+_{0_1^+}$		0.363	E1	$0.43^{+0.16}_{-0.11}$
1969.84 (9)	1894.50 (6)	$2^+_{[\Upsilon]}$	$2^+_{0_1^+}$	>830	0.582	E2/M1 ^[*]	<0.45
	1969.93 (7)	$2^+_{[\Upsilon]}$	$0^+_{0_1^+}$				
2030.90 (9)	1782.14 (6)	$2^+_{[\Upsilon]}$	$4^+_{0_1^+}$	>255	0.139	E2/M1 ^[*]	<0.47
	1955.93 (7)	$2^+_{[\Upsilon]}$	$2^+_{0_1^+}$				
2060.43 (11)	2060.42 (6)	$2^+_{[\Upsilon]}$	$6^+_{0_1^+}$	230^{+90}_{-50}	1.000	E2	$1.82^{+0.40}_{-0.71}$
	2109.32 (7)	$1^+_{[\Upsilon]}$	$3^+_{2_1^+}$				
	1119.71 (13)	$1^+_{[\Upsilon]}$	$2^+_{2_1^+}$	330^{+120}_{-70}	0.170	E2	$6.23^{+1.34}_{-2.28}$
	2034.26 (6)	$1^+_{[\Upsilon]}$	$2^+_{0_1^+}$				
	2109.31 (6)	$1^+_{[\Upsilon]}$	$0^+_{0_1^+}$	420^{+880}_{-180}	0.263	E2/M1 ^[*]	$0.30^{+0.06}_{-0.11}$
	2135.76 (13)	2135.74 (7)	$2^+_{[\Upsilon]}$				

Lifetimes of excited states in ^{160}Gd that have no K band assignment, with experimentally determined $B(E2)$ in W.u and $B(E1)$ in mW.u.

^[a] $\delta = -0.76^{+0.10}_{-0.13}$, ^[b] $\delta = -3.3^{+1.1}_{-2.4}$, ^[c] $\delta = 0.92^{+0.41}_{-0.64}$

^[*] Full E2 strength is reported (no δ was calculated)

1 W.u.(E2)= 5.16×10^{-7} e²b², 1 mW.u.(E1)= 1.90×10^{-6} e²b

$[\Upsilon]$: No rotational K $^\pi$ band assignment given in literature.

4.2 ^{162}Dy Results

^{162}Dy , one of the most studied nuclei on the chart of nuclides, with over 24 different reactions and probes (from electron capture, stripping/pickup (t,p)/(p,t) reactions, neutron capture, (α ,2n) reactions, and ($^3\text{He},\alpha$) reactions, to name a few) which have been implemented to extract information on the structure of ^{162}Dy [3]. Several previous (n,n' γ) campaigns were carried out to measure level lifetimes of the isovector M1 scissors mode in ^{162}Dy ([46]), as well as a series of precision angular distribution measurements by Govor *et. al* ([34]) to extract multipole mixing fractions and γ -ray intensities. Analogous to the ^{160}Gd case study, the angular distributions carried out by Govor act as a complimentary guide and benchmark for our measurements. While the initial and chief goal is to measure the lifetimes of 0^+ excitations and low-lying negative parity states, we are also able to populate and measure the lifetimes of the vast majority of low spin ($J < 5$) states under the bombarding neutron energy threshold. The full result of all measured lifetimes in the ^{162}Dy experimental campaign (§2.4.2) is displayed in the level scheme in Figure 4.5.

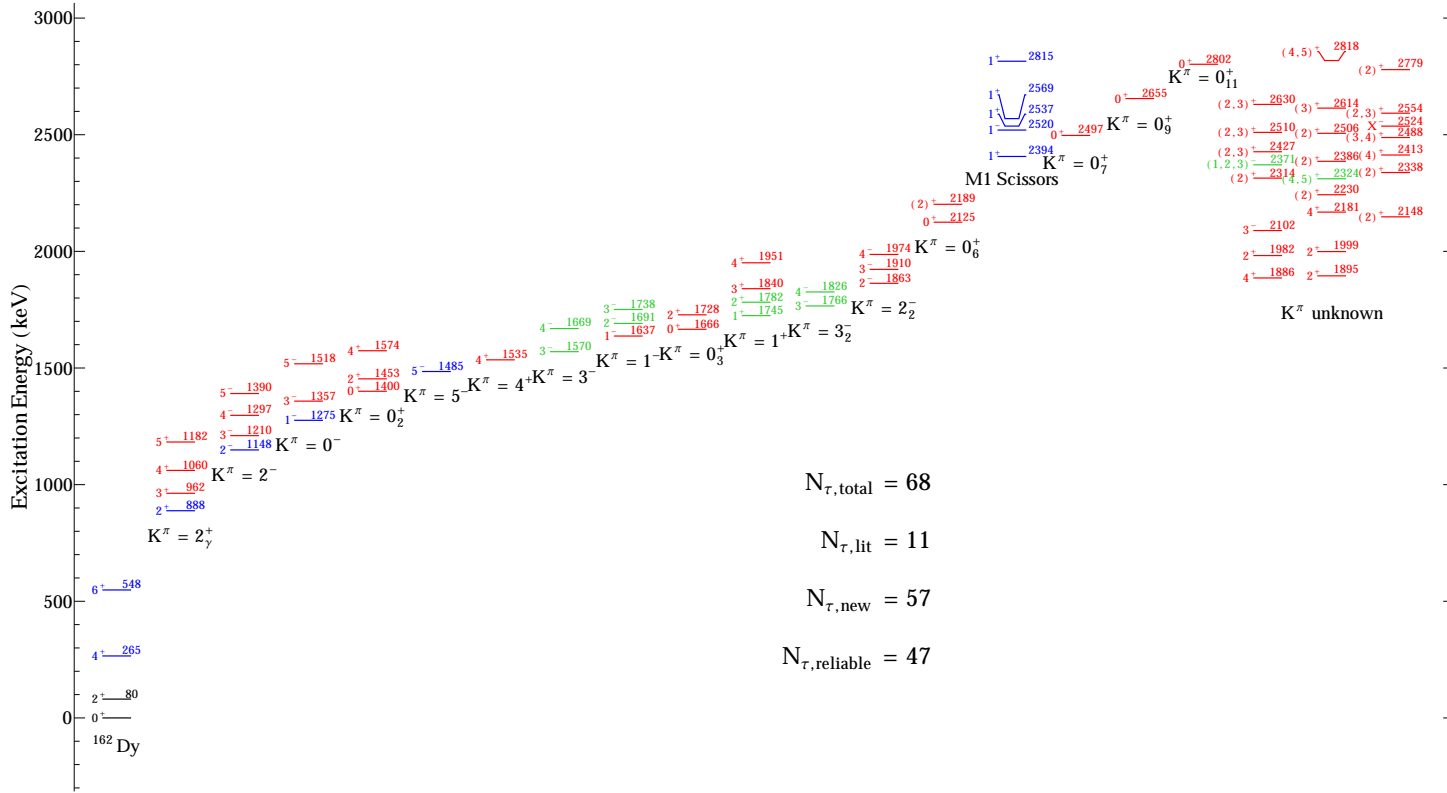


Figure 4.5. Level scheme for all level lifetimes measured in the ^{162}Dy experiments, with confirmed band and spin assignments shown. Previously measured lifetimes are in blue, with newly presented lifetimes in red, levels in green constitute an unreliable lifetime measurement from our data, where $F(\tau) < 0$ or is consistent with zero.

In Figure 4.5, levels colored blue are pre-existing lifetimes in literature, where the levels in red are newly presented lifetime measurements in this work. Due to the limitations of DSAM outlined in §3.2.2.2, cases where $F(\tau)$ is strictly less than zero or consistent with 0 within 1σ , unreliable lifetimes are colored green. Again, it must be reiterated that while these lifetimes do not have previously measured literature values, our $(n,n'\gamma)$ lifetimes should not be trusted as a good measurement. Other techniques must be implemented to fully measure the lifetime of these states (Coulomb Excitation, RDDM plunger method, etc). Excitations are placed into bands where available, along with the well-measured and studied isovector M1 scissors mode lifetimes at ~ 2.4 MeV that results in $J^\pi=1^\pm$ excitations [46, 54, 77]. In total, we observed 108 discrete γ -rays to measure sixty eight (68) lifetimes, fifty seven (57) of which were measured for the first time. Of the newly measured lifetimes, however, only forty seven (47) are considered reliable from our measurement of Doppler energy shifted γ rays. These measured lifetimes were extracted from the three angular distribution measurements ($E_n=1.6, 2.2, \& 3.1$ MeV), with three effective ranges of lifetime sensitivity, in the hopes of limiting any lifetime feeding from higher levels and bombarding neutron energy. Visually, the ranges of lifetimes reported can be seen in Figure 4.6, where we have a comparison of the presented lifetimes (and corresponding errors) in to literature lifetimes in the three separate ranges of lifetime sensitivity (excitation energies of <1.6 MeV in red, 1.6 - 2.2 MeV in green, and 2.2 MeV - 3.1 MeV in blue).

The discrepancies from the literature lifetimes are clearly visible in Figure 4.6, where we can attribute slight inflation of the lifetimes as a result of either feeding from higher-lying states, or from the bombarding neutron energy effects mentioned at the beginning of §4. We can make the justification that our lifetimes agree reasonably with literature because the accuracy of measurement is roughly on the same order

TABLE 4.6

LITERATURE LIFETIME COMPARISON: ^{162}DY

E_{lev} (keV)	$\tau_{(n,n'\gamma)}$ (fs)	τ_{lit} (fs)
265	>1500[†]	0.190E6 (7) [⊕]
548	>960[†]	26.5E3 (14) [⊕]
888	>3700	2840 (3) [⊕]
1148	2100^{+7200}_{-1200}	0.30E6 (6) [⊖]
1275	120^{+10}_{-10}	28.8 (6) [‡][⊕]
1485	400^{+210}_{-140}	2.76E6 (16) [‡][⊗]
2394	14^{+13}_{-11}	16^{+10}_{-10} [Ω]
2520	110^{+30}_{-20}	11^{+9}_{-9} [Ω]
2537	460^{+160}_{-120}	141^{+30}_{-30} [Ω]
2569	90^{+30}_{-20}	56^{+6}_{-6} [Ω]
2815	200^{+130}_{-60}	56^{+19}_{-19} [Ω]

Comparison of lifetimes measured in the campaign of $^{162}\text{Dy}(n,n'\gamma)$ experiments with literature lifetimes. [†]: Measured lifetime not reliable ($F(\tau)$ within 1σ of 0) - resulting lifetimes fall well outside the range of DSAM. [‡]: Lifetime called into question in this work. [⊖]: from ^{162}Tb β^- decay [68]. [⊗]: from ^{162}Ho ε -decay [42]. [⊕]: from $B(E2)\uparrow$ via Coul. Ex [38]. [Ω]: from (γ,γ') [54] and $(n,n'\gamma)$ [46]

of magnitude for every sensitive range of lifetimes measured, with scattered cases of good agreement. In other words, the lifetimes measured at intermediate energies (~ 900 keV, ~ 1850 keV, and ~ 2400 keV) are inflated by the same proportional amount for each bombarding neutron energy. Further discrepancies in our measured lifetimes to those in literature stem from the differences in measurement techniques (DSAM-INS versus deduction of lifetimes via direct $B(E1/M1)\uparrow$). For example, the weighted average of the $F(\tau)$ values for multi-channel decays out of a state can result in a lower

average $F(\tau)$ if only one γ -ray decay is used in the determination of the lifetime, resulting in a longer lifetime.

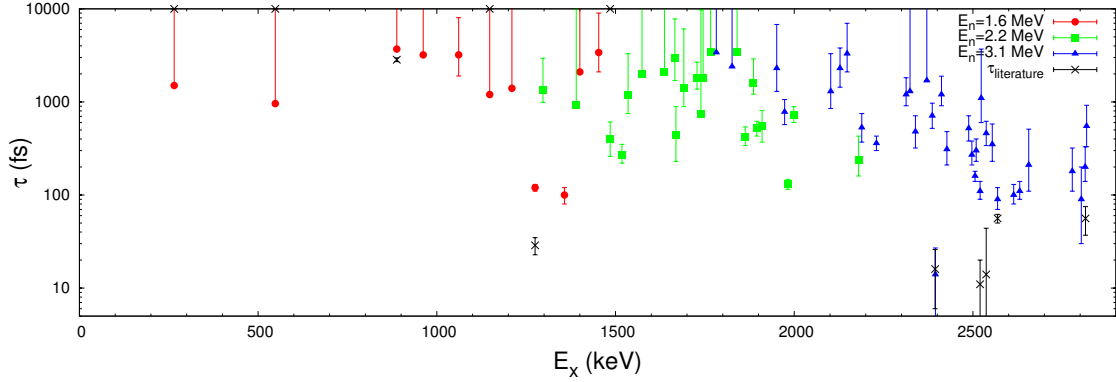


Figure 4.6. All measured lifetimes in ^{162}Dy (in femtoseconds) plotted as a function of excitation energy in keV. Data points in red are extracted from the $E_n=1.6$ MeV angular distributions, points in green correspond to lifetimes extracted from the 2.2 MeV angular distributions, and blue points are lifetimes from the 3.1 MeV dataset. (color online)

An example of the $E_n=2.2$ MeV angular distribution singles-spectrum for $^{162}\text{Dy}(n,n'\gamma)$ can be seen in Figure 4.7 with select peaks labeled for reference.

4.2.1 Lifetimes of 0^+ States

In stark contrast to the results of the ^{160}Gd experiments (namely the lower limit lifetimes and existence of anisotropies in angular distributions), we are able to determine definite level lifetimes for the majority of 0^+ bands and confirm isotropic angular distributions from the ^{162}Dy data. DSAM plots and angular distributions for the full $0_i^+ \rightarrow 2_{g.s.}^+$ de-excitations are seen in Figures 4.9 and 4.8, respectively. We also do not exclude any of the proposed 0^+ states from our observation of isotropic

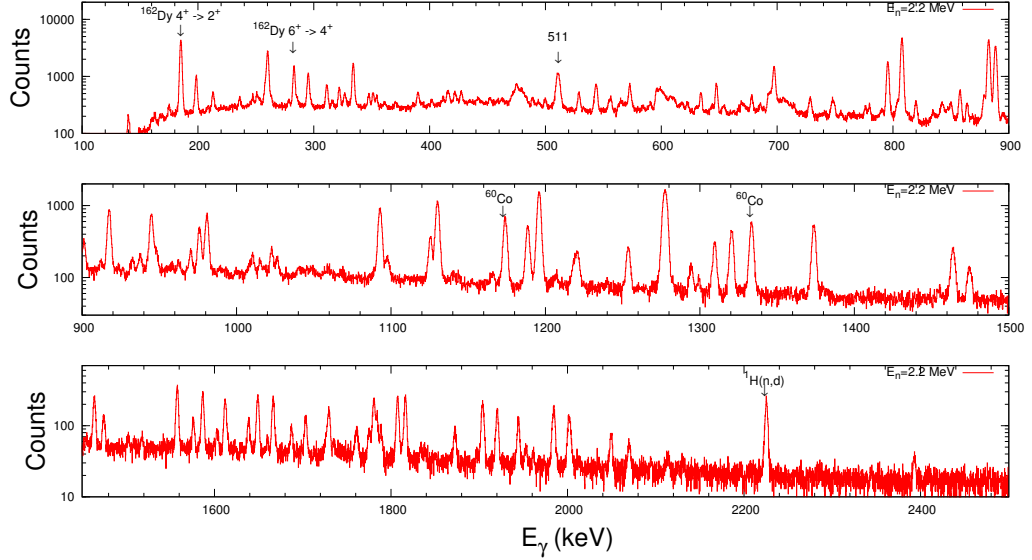


Figure 4.7. Singles spectra from the $\theta_{lab}=90^\circ$ and $E_n=2.2$ MeV angular distributions of ^{162}Dy .

or anisotropies in the angular distributions similar to our ^{160}Gd results.

Lifetimes for six (6) of the eleven (11) confirmed and tentative excited 0^+ states [58] were measured in the campaign of experiments (shown in Table 5.2). We have also measured lifetimes (including a few lower limits) of the five lowest-lying rotational members of the $K^\pi=2^+$ band, the bandheads of both $K^\pi=4^+$ bands, and a total of 52 other states in ^{162}Dy . The absolute intensities of decays discussed in this work were extracted from the angular distributions and are shown in Table 5.3, with unobserved transition intensities taken from literature [3, 80, 83] to provide pertinent discussion later in this manuscript.

The full tabulation of γ decays observed for the de-excitation of $K^\pi=0^+$ bands is shown in Table 4.7, which includes experimentally measured lifetimes in femtoseconds, branching ratios, and γ -ray energies in keV. Mixed multipolarity de-excitations

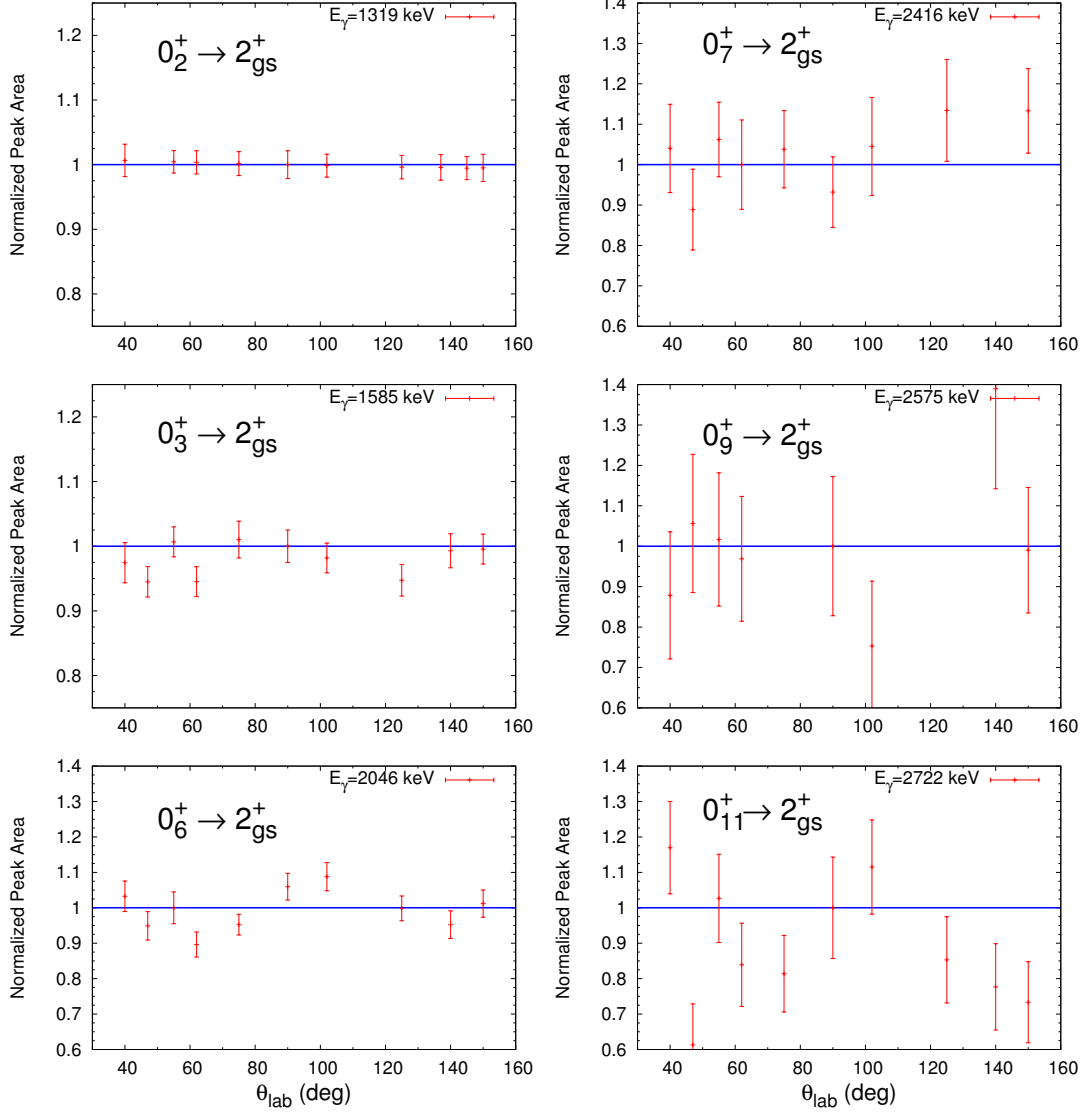


Figure 4.8. Angular distributions of $0_i^+ \rightarrow 2_{g.s.}^+$ γ -rays observed in ^{162}Dy , highlighting their isotropic nature (color online).

are assigned a multipole mixing fraction (δ_{mixing}) from comparison of our gathered angular distributions to a statistical model calculation, performed with CINDY [71]. A level scheme outlining all observed decays from 0^+ bands to the ground state band is also shown in Figure 5.8.

Lifetimes for the three lowest-lying rotational members of the 0_2^+ band were mea-

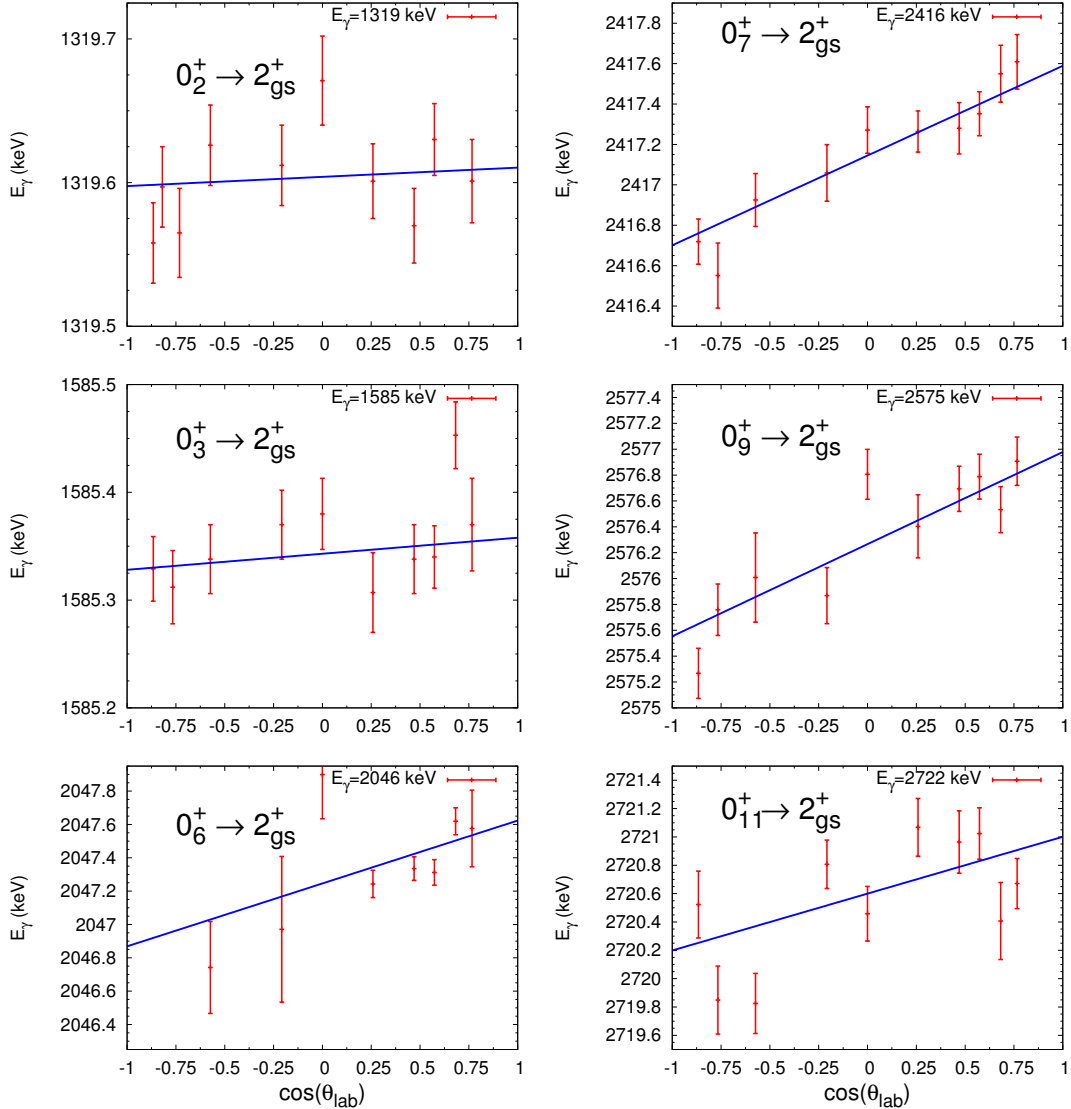


Figure 4.9. Doppler energy shifts of $0_i^+ \rightarrow 2_{g.s.}^+$. γ -rays observed in ^{162}Dy (color online).

sured; the single, most intense γ ray at 1319 keV was used to measure (a shallow) $F(\tau)$ to extract the lifetime from the $E_n=1.6$ MeV dataset. The weighted average of $F(\tau)$ from both the 1187 & 1372 keV γ ray is used to measure the lifetime of the 2^+ state. Only the 1308 keV de-excitation contributes to the lifetime of the 4^+ state at $E_x=1574$ keV, as the 1025 keV transition exhibits a negative $F(\tau)$ value.

We have measured the lifetime of the bandhead and 2^+ member of the 0_3^+ band at $E_x=1666$ keV, with good lifetime resolution extracted from the $E_n=2.2$ MeV dataset. The single 1585 keV transition from the bandhead to the ground state yields a 3000^{+4800}_{-1300} fs lifetime, while only the 1647 and 1728 keV γ rays offer contributions to the 2^+ lifetime of 1800^{+880}_{-430} fs, as the decay at 1462 keV is coincident with a background line, making that particular $F(\tau)$ unreliable. Large uncertainties exist for the bandhead of this 0^+ band due to the natural limits of lifetimes measurable with DSAM; this large error stems from the uncertainties on the measured $F(\tau)$ value.

We adopt the placement [8] of the (2^+) state at 2189 keV as the 2^+ rotational band member of the 0_6^+ band at $E_x=2128$ keV, and have measured lifetimes for these two states from the single-channel decays of 2109 & 2047 keV, respectively. The lifetime of the bandhead was found to be 2300^{+1500}_{-860} fs, and 530^{+220}_{-160} fs for the 2^+ member.

The seventh and ninth 0^+ states decay via full energy de-excitations to the ground state at $E_\gamma=2417$ & 2575 keV, respectively. These corresponding lifetimes extracted from the $E_n=3.1$ MeV dataset are 270^{+110}_{-60} fs for the 0^+ state at 2497 keV, and 210^{+300}_{-100} fs at 2655 keV.

Due to the isotropic radiation observed for the 2721 keV γ -ray that depopulates the (0_{11}^+) state at 2802 keV, we support the assignment of this state as a 0^+ excitation, where further mentions of this state are considered as a confirmed 0^+ state. The Doppler shift from this 2721 keV decay gives us our shortest 0^+ lifetime of 90^{+110}_{-60} fs.

TABLE 4.7

 $K^\pi=0^+$ BANDS: ^{162}DY

K^π	E_{level} (keV)	E_γ (keV)	$J^\pi_{K_i^\pi}$	$J^\pi_{K_f^\pi}$	$F(\tau)_{av}$	τ (fs)	BR	$\pi\ell$	$B(\pi\ell)$ (W.u.)
III	<u>$K^\pi=0_2^+$:</u>	1400.29(36)	512.0(2)	$0^+_{0_2^+}$	$2^+_{2_1^+}$	0.031 ± 0.038	$>2100^{[\vartheta]}$	[†]	E2 (<16)
		1319.60(51)		$0^+_{0_2^+}$	$2^+_{0_1^+}$		1.000	E2	<1.9
	1453.50(30)	395.49 (10)	$2^+_{0_2^+}$	$4^+_{2_1^+}$	0.042 ± 0.026	$3400^{+5600}_{-1300} [\vartheta]$	[†]	E2	$(2.7^{+1.7}_{-1.7})$
		565.32 (12)	$2^+_{0_2^+}$	$2^+_{2_1^+}$			[†]	E2[‡]	$(0.9^{+0.6}_{-0.6})$
	1187.81(51)		$2^+_{0_2^+}$	$4^+_{0_1^+}$			0.425(4)	E2	$0.8^{+0.5}_{-0.5}$
		1372.80(51)	$2^+_{0_2^+}$	$2^+_{0_1^+}$			0.575(4)	E2/M1 ^[aς]	$0.3^{+0.2}_{-0.2}$
	1574.34(29)	513.31 (2)	$4^+_{0_2^+}$	$4^+_{2_1^+}$	0.043 ± 0.031	$>2000^{[\varsigma]}$	[†]	E2[‡]	(<3.7)
		611.23 (5)	$4^+_{0_2^+}$	$3^+_{2_1^+}$			[†]	E2[‡]	(<0.4)
	686.15 (6)		$4^+_{0_2^+}$	$2^+_{2_1^+}$			[†]	E2	(<0.5)
		1025.84(58) ^[\emptyset]	$4^+_{0_2^+}$	$6^+_{0_1^+}$			0.157(5)	E2	<1.1
	<u>$K^\pi=0_3^+$:</u>	1308.65(51)	$4^+_{0_2^+}$	$4^+_{0_1^+}$			0.843(5)	E2/M1 ^[b,ς]	<0.8
		1666.01(33)	1585.35(51)	$0^+_{0_3^+}$	$2^+_{0_1^+}$	0.051 ± 0.033	$3000^{+4800}_{-1300} [\varsigma]$	1.000	E2
	1728.31(20)	1462.70(51) ^[\otimes]	$2^+_{0_3^+}$	$4^+_{0_1^+}$	0.081 ± 0.023	$1800^{+880}_{-430} [\varsigma]$	0.334(5) ^[★]	E2	$0.4^{+0.1}_{-0.1}$

Continued

TABLE 4.7

 $K^\pi=0^+$ BANDS: ^{162}DY

K^π	E_{level} (keV)	E_γ (keV)	$J_{K_i}^\pi$	$J_{K_f}^\pi$	$F(\tau)_{av}$	τ (fs)	BR	$\pi\ell$	$B(\pi\ell)$ (W.u.)
	1647.64(51)		$2^+_{0^+_3}$	$2^+_{0^+_1}$			0.407(5)	$E2/M1^{[c,\varsigma]}$	$0.01^{+0.01}_{-0.01}$
	1728.29(53)		$2^+_{0^+_3}$	$0^+_{0^+_1}$			0.259(4)	E2	$0.2^{+0.1}_{-0.1}$
$K^\pi=0^+_6:$	2128.02(33)	2047.34(61)	$0^+_{0^+_6}$	$2^+_{0^+_1}$	0.071 ± 0.031	2300^{+1500}_{-860} [ϖ]	1.000	E2	$0.2^{+0.1}_{-0.1}$
	2189.65(52)	2109.10(50)	$(2)^+_{0^+_6}$	$2^+_{0^+_1}$	0.267 ± 0.058	530^{+220}_{-160} [ϖ]	1.000	$(E2/M1)^{[d,\varpi]}$	$0.7^{+0.3}_{-0.2}$
$K^\pi=0^+_7:$	2497.77(52)	2417.22(50)	$0^+_{0^+_7}$	$2^+_{0^+_1}$	0.376 ± 0.055	270^{+110}_{-60} [ϖ]	1.000	E2	$0.7^{+0.2}_{-0.2}$
$K^\pi=0^+_9:$	2655.83(33)	2575.28(53)	$0^+_{0^+_9}$	$2^+_{0^+_1}$	0.436 ± 0.164	210^{+300}_{-100} [ϖ]	1.000	E2	$0.7^{+0.6}_{-0.4}$
$K^\pi=0^+_{11}:$	2802.04(61)	2721.48(55)	$0^+_{0^+_{11}}$	$2^+_{0^+_1}$	0.653 ± 0.200	90^{+110}_{-60} [ϖ]	1.000	E2	$1.2^{+2.3}_{-0.6}$

Lifetimes of excited 0^+ bands in ^{162}Dy , with calculated $B(E2)$ in W.u., from our measured multipole mixing fractions, branching ratios, γ -ray energies, and lifetimes, all extracted from the angular distributions. $B(E2)$ strengths in parentheses are calculated using literature intensities.

[*a*]: $\delta = 1.3_{-0.2}^{+0.2}$, [*b*]: $\delta = 0.93_{-0.15}^{+0.14}$, [*c*]: $\delta = -0.22_{-0.08}^{+0.08}$, [*d*]: $\delta = 2.7_{-0.9}^{+1.8}$

[†]: Intensity information taken from [3, 83] (γ -ray not seen in this work), [‡]: Mixing information not available, full E2 strength reported, [\emptyset]: γ ray not used in $F(\tau)$ calculation ($F(\tau) < 0$).

[ϑ]: $F(\tau)$ or δ_{mixing} extracted from $E_n = 1.6$ MeV angular distributions, [ς]: $F(\tau)$ or δ_{mixing} extracted from $E_n = 2.2$ MeV angular distributions, [ϖ]: $F(\tau)$ or δ_{mixing} extracted from $E_n = 3.1$ MeV angular distributions, [\otimes]: γ ray coincident with background, not used in calculation of lifetime.

1 W.u.=5.25E-7 e²b²

4.2.2 Lifetimes of $K^\pi=2^+$ and 4^+ Bands

In the eight decays from the 2^+ band, two of the γ rays (the 697 keV and 634 keV de-excitations) are not used in the calculation of the level lifetime, as they have Doppler shifts that correspond to an $F(\tau)<0$. Lower limits for the lifetime are measured in several cases due to the inherent limitations of sensitive lifetimes DSAM can measure (up to a few picoseconds).

TABLE 4.8

 $K^\pi=2^+$ AND 4^+ BANDS: ^{162}DY

K^π	E_{level} (keV)	E_γ (keV)	$J_{K_i^\pi}^\pi$	$J_{K_f^\pi}^\pi$	$F(\tau)_{av}$	τ (fs)	BR	$\pi\ell$	$B(\pi\ell)$ (W.u.)
115 <u>$K^\pi=2_\gamma^+:$</u>	888.18(22)	807.54(50)	$2_{2\gamma}^+$	$2_{0_1^+}^+$	0.022 ± 0.018	>3700 [θ]	0.524(3)	E2/M1 ^[a,θ]	<1.1
		888.18(50)	$2_{2\gamma}^+$	$0_{0_1^+}^+$			0.476(3)	E2	<3.6
	962.96(27)	697.30(50) ^[∅]	$3_{2\gamma}^+$	$4_{0_1^+}^+$	0.021 ± 0.025	>3200 [θ]	0.159(3)	E2/M1 ^[b,θ]	<0.2
		882.31(50)	$3_{2\gamma}^+$	$2_{0_1^+}^+$			0.841(3)	E2/M1 ^[c,θ]	<7.6
	1061.05(29)	795.35(50)	$4_{2\gamma}^+$	$4_{0_1^+}^+$	0.047 ± 0.030	3200^{+4800}_{-1300} [θ]	0.637(3)	E2/M1 ^[d,θ]	$4.5^{+2.7}_{-3.1}$
		980.36(51)	$4_{2\gamma}^+$	$2_{0_1^+}^+$			0.363(3)	E2	$2.0^{+1.3}_{-1.2}$
	1182.88(26)	634.24(61)	$5_{2\gamma}^+$	$6_{0_1^+}^+$	0.034 ± 0.030	>2500 [s]	0.239(5)	E2/M1 ^[e,θ]	<14
		917.18(51)	$5_{2\gamma}^+$	$4_{0_1^+}^+$			0.761(5)	E2/M1 ^[f,θ]	<7.3
<u>$K^\pi=4_1^+:$</u>	1535.97(23)	475.27(54) ^[∅]	$4_{4_1^+}^+$	$4_{2\gamma}^+$	0.124 ± 0.077	1200^{+2100}_{-450} [s]	0.186(10) ^[★]	E2/M1 ^[g,s]	44^{+34}_{-40} (23^{+18}_{-21})
		572.96(50)	$4_{4_1^+}^+$	$3_{2\gamma}^+$			0.317(6)	E2/M1 ^[h,s]	66^{+42}_{-40} (98^{+63}_{-59})
		647.61(50) ^[∅]	$4_{4_1^+}^+$	$2_{2\gamma}^+$			0.497(7)	E2	57^{+34}_{-36} (120^{+74}_{-78})
<u>$K^\pi=4_2^+:$</u>	2180.69(53)	1217.73(58)	$4_{4_2^+}^+$	$3_{2\gamma}^+$	0.383 ± 0.095	240^{+190}_{-80} [s]	1.000 (113(24) ^[†])	E2/M1 ^[i,s]	$1.3^{+1.0}_{-0.9}$ ($0.7^{+0.6}_{-0.5}$)
		1292.51(58) ^[†]	$4_{4_2^+}^+$	$3_{2\gamma}^+$			(100 ^[†])	E2	$(8.3^{+4.2}_{-3.7})$

Continued

TABLE 4.8

 $K^\pi=2^+$ AND 4^+ BANDS: ^{162}DY

K^π	E_{level} (keV)	E_γ (keV)	$J_{K_i^\pi}^\pi$	$J_{K_f^\pi}^\pi$	$F(\tau)_{av}$	τ (fs)	BR	$\pi\ell$	$B(\pi\ell)$ (W.u.)
$K^\pi=(2^+)$:	2231.06(38)	1342.57(50)	$(2,3,4)^+_{[\Upsilon]}$	$2^+_{2^+_1}$	0.333 ± 0.031	360^{+70}_{-60} [ϖ]	0.577(9)	E2/M1 [j,ϖ]	$5.2^{+0.9}_{-1.2}$

116

Lifetimes of excited 2^+ band, both 4^+ bands, and tentative 2^+ state at 2230 keV in ^{162}Dy , with calculated $B(E2)$ in W.u., from our measured multipole mixing fractions, branching ratios, γ -ray energies, and lifetimes, all extracted from the angular distributions. $B(E2)$ strengths in parentheses are calculated using literature intensities.

[a]: $\delta = -0.45^{+0.05}_{-0.06}$, [b]: $\delta = 0.20^{+0.06}_{-0.06}$, [c]: $\delta < -21$, [d]: $\delta = -0.92^{+0.04}_{-0.05}$

[e]: $\delta < -7$, [f]: $\delta < -21$, [g]: $\delta = -0.89^{+0.32}_{-0.80}$, [h!]: $\delta < -21$, [i]: $\delta = 0.24^{+0.07}_{-0.06}$, [j]: $\delta = 3.1^{+2.1}_{-1.0}$

[\oslash]: γ ray not used in $F(\tau)$ calculation ($F(\tau) < 0$), [\otimes]: γ ray not used in $F(\tau)$ calculation (doublet with background line), [$*$]: Measured branching ratio unreliable (γ -ray on top of background)

[ϑ]: $F(\tau)$ or δ_{mixing} extracted from $E_n = 1.6$ MeV angular distributions, [\natural]: $F(\tau)$ or δ_{mixing} extracted from $E_n = 2.2$ MeV angular distributions, [ϖ]: $F(\tau)$ or δ_{mixing} extracted from $E_n = 3.1$ MeV angular distributions

[Υ]: No K^π band assignment for this level, [\dagger]: Intensity information taken from Ref. [80] (γ -ray not seen in this work)

1 W.u.=5.25E-7 e²b²

The lifetime of the bandhead 4^+ state at 1535 keV is extracted from the Doppler shift of the 572 keV γ ray, as the 475 keV decay lies on top of a background, and as such, the Doppler shift is unreliable; the 647 keV line exhibits a negative $F(\tau)$ value, and is not used in the lifetime calculation. Evidence for the existence of a background contaminant can be seen in the branching ratios for the decays, as they are not consistent with literature intensities. In Table 4.8, deduced $B(E2)$ values from our experiments are reported alongside calculations using the literature intensities from [3] in parentheses.

We have measured the lifetime of the second 4^+ state at 2181 keV, via a 1217 keV γ ray to the 3^+ member of the γ band, but we have not observed the 1294 keV decay to the bandhead (this line would also be coincident with an inherent $^{115}\text{In}(n,n'\gamma)$ background). The $\tau=240^{+190}_{-80}$ fs lifetime and mostly M1 radiation observed from the 1217 keV decay

4.2.3 Lifetimes of Negative Parity Bands ($K^\pi=2^-$, 0^- , and 2_2^-)

A total of 10 well-convergent level lifetimes were measured (8 of which are new) for three negative parity bands in ^{162}Dy . All observed transitions from negative parity bands can be seen in Figure 5.12, with corresponding transition strengths from Table 4.9. Absolute intensities of γ -decays reported in this work can be seen in Table 5.6. The traditional picture of octupole collectivity in well-deformed nuclei exists with the initial, lowest-lying and quartet of states of $K^\pi=0^-$, 1^- , 2^- , & 3^- . However, the current ordering of negative parity bands in ^{162}Dy is difficult (read: impossible) to predict with modern models [3]. We have measured lifetimes for two bands of this lowest-lying set of states in ^{162}Dy , where we provide individual discussion on our measurements.

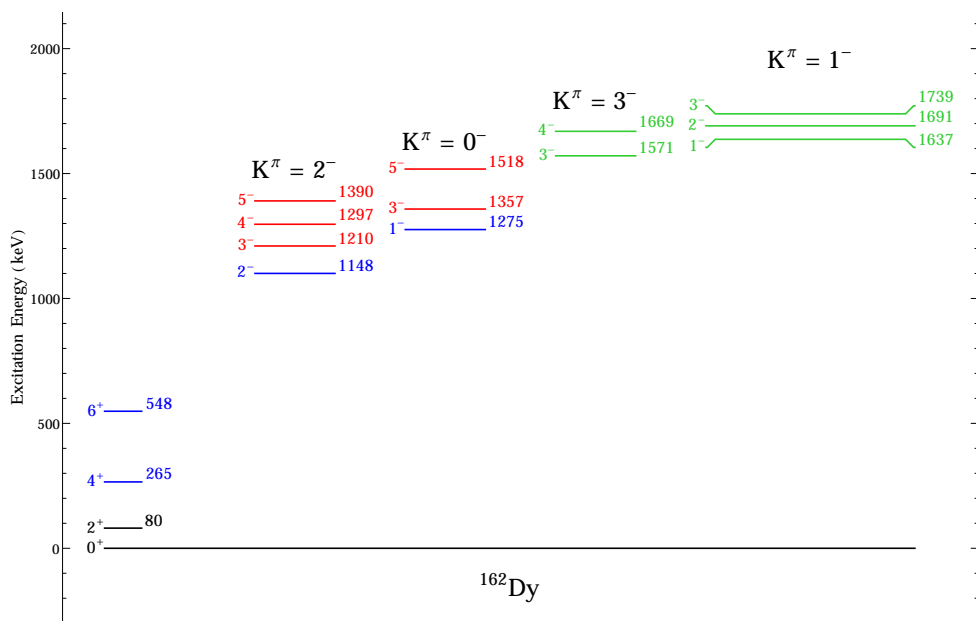


Figure 4.10. Lowest-lying negative parity bands in ^{162}Dy with reliable lifetimes measured in our experiments in red, existing literature values in blue, and unreliable lifetimes measured in green (color online).

TABLE 4.9

NEGATIVE PARITY BANDS ($K^\pi=2^-, 0^-, 2^-_2$): ^{162}DY

E_{level} (keV)	E_γ (keV)	$J_{K_i^\pi}^\pi$	$J_{K_j^\pi}^\pi$	$F(\tau)_{av}$	τ (fs)	BR	B(E1) (mW.u.)
1148.20(20)	260.16(50)	$2^-_{2^-_1}$	$2^+_{2^+_1}$	0.074 ± 0.058	2100^{+7200}_{-950} [s]	1.000	$8.9^{+7.3}_{-6.9}$
1210.05(18)	247.27(55) $[\emptyset]$	$3^-_{2^-_1}$	$3^+_{2^+_1}$	0.052 ± 0.030	3100^{+3700}_{-1200} [s]	0.056(2)	$0.2^{+0.2}_{-0.1}$
	322.05(51) $[\emptyset]$	$3^-_{2^-_1}$	$2^+_{2^+_1}$			0.083(2)	$0.2^{+0.1}_{-0.1}$
	944.48(50)	$3^-_{2^-_1}$	$4^+_{0^+_1}$			0.310(4)	$0.04^{+0.03}_{-0.02}$
	1129.46(50) $[\emptyset]$	$3^-_{2^-_1}$	$2^+_{0^+_1}$			0.552(4)	$0.04^{+0.03}_{-0.02}$
1297.06(27)	236.09(60) $[\emptyset]$	$4^-_{2^-_1}$	$4^+_{2^+_1}$	0.103 ± 0.049	1400^{+1500}_{-350} [s]	0.150(5)	$2.7^{+0.9}_{-1.4}$
	334.15(50)	$4^-_{2^-_1}$	$3^+_{2^+_1}$			0.850(5)	$5.3^{+1.8}_{-2.8}$
1390.52(35)	1124.88(88)	$5^-_{2^-_1}$	$4^+_{0^+_1}$	0.090 ± 0.082	>920 [s]	1.000	<0.3
1275.81(24)	1195.10(50)	$1^-_{0^-_1}$	$2^+_{0^+_1}$	0.568 ± 0.028	120^{+10}_{-10} [ϑ]	0.605(6)	$1.0^{+0.1}_{-0.1}$
	1275.82(53)	$1^-_{0^-_1}$	$0^+_{0^+_1}$			0.395(6)	$0.5^{+0.1}_{-0.1}$
1358.00(30)	1092.27(71)	$3^-_{0^-_1}$	$4^+_{0^+_1}$	0.612 ± 0.043	100^{+20}_{-20} [ϑ]	0.429(9)	$1.1^{+0.3}_{-0.2}$
	1277.33(58)	$3^-_{0^-_1}$	$2^+_{0^+_1}$			0.571(9)	$0.9^{+0.2}_{-0.2}$
1518.47(29)	970.01(55)	$5^-_{0^-_1}$	$6^+_{0^+_1}$	0.372 ± 0.041	270^{+80}_{-50} [s]	0.294(7)	$0.4^{+0.1}_{-0.1}$

Continued

TABLE 4.9

NEGATIVE PARITY BANDS ($K^\pi=2^-, 0^-, 2_2^-$): ^{162}DY

E_{level} (keV)	E_γ (keV)	$J_{K_i}^\pi$	$J_{K_j}^\pi$	$F(\tau)_{av}$	τ (fs)	BR	$B(E1)$ (mW.u.)
	1252.74(51)	$5_{0_1^-}^-$	$4_{0_1^+}^+$			0.706(7)	$0.4_{-0.1}^{+0.1}$
1863.85(26)	900.90(55)	$2_{2_2^-}^-$	$3_{2_1^+}^+$	0.297 ± 0.035	420_{-80}^{+120} [s]	0.251(5)	$0.3_{-0.1}^{+0.1}$
	975.65(50)	$2_{2_2^-}^-$	$2_{2_1^+}^+$			0.749(5)	$0.6_{-0.1}^{+0.1}$
1910.50(26)	947.51(56)	$3_{2_2^-}^-$	$3_{2_1^+}^+$	0.250 ± 0.063	550_{-180}^{+260} [s]	0.552(8)	$0.4_{-0.1}^{+0.2}$
	1022.33(53)	$3_{2_2^-}^-$	$2_{2_1^+}^+$			0.448(8)	$0.3_{-0.1}^{+0.1}$
1972.99(66)	912.09(50)	$4_{2_2^-}^-$	$4_{2_\gamma^+}^+$	0.205 ± 0.053	780_{-210}^{+280} [ϖ]	0.246(13)	$0.1_{-0.1}^{+0.1}$
	1010.19(50)	$4_{2_2^-}^-$	$3_{2_\gamma^+}^+$			0.754(13)	$0.3_{-0.1}^{+0.1}$

121

Lifetimes of negative parity bands ($2^-, 0^-, 2_2^-$) in ^{162}Dy , with experimentally deduced $B(E1)$ in mW.u.

[\emptyset]: γ ray not used in $F(\tau)$ calculation ($F(\tau) < 0$).

[ϑ]: $F(\tau)$ extracted from $E_n=1.6$ MeV angular distributions, [s]: $F(\tau)$ extracted from $E_n=2.2$ MeV angular distributions, [ϖ]: $F(\tau)$

extracted from $E_n=3.1$ MeV angular distributions

[†]: Lifetime not reliable ($F(\tau)$ consistent with zero within 1σ)

1 mW.u.= $1.91 e^2 b$

We are immediately presented with some of the limitations of DSAM with our measurement of the lifetime of the bandhead of the $K^\pi=2^-$ band. Firstly, γ -ray energies can be heavily attenuated in the physical size of the near-molar-weight target; while we correct for this γ absorption in the peak area/intensity, lifetimes from the Doppler shift of γ -rays sub-500 keV are difficult to extract, as $F(\tau)$ can be within 1 or 2σ of 0. Normally, DSAM measurements are taken at the lowest possible bombarding neutron energy, but due to this attenuation of low-energy γ rays, a more precise measurement of the lifetimes in this band are taken from the 2.2 MeV bombarding neutron dataset. While we expect a natural inflation of the lifetimes because of this choice of neutron energy, the vast majority of observed transitions displayed negative (or consistent with zero within 1σ uncertainty) $F(\tau)$ values. This justification is supported by Figure 4.11, which shows all excitation functions for γ rays that both de-excite this band and contribute to the lifetime; take note that the gain in statistics by a factor of ~ 2 by increasing the neutron energy, where we are exempt from higher-lying decays acting as a contaminant (see the trajectories as the neutron energy increases to 3.1 MeV). Extraction of the lifetime for the bandhead at 2100^{+7200}_{-950} fs involves the measurement of a 260 keV γ ray, shown in Figure 4.11, and does not agree with the literature value of 303 ps [68], as the shallow $F(\tau)$ is just over 1σ away from 0, making this lifetime partially unreliable. We do not observe the other decay channel to the 3^+ member of the γ -band, as that decay energy is 185 keV, directly on top of our strongest line in our spectra, the ground state $4^+ \rightarrow 2^+$ transition. With no higher energy decays observed to the ground state, we report this measurement of the bandhead's lifetime, but it should be taken as a tentative, cautious measurement, given the very large discrepancy from literature. However, we regain good lifetime resolution on the measurement of the 3^- and 4^- bandmembers; the former state's lifetime of 3100^{+3700}_{-1200} fs comes from the 944 keV γ ray, where the other exit channels have either a negative $F(\tau)$ value.

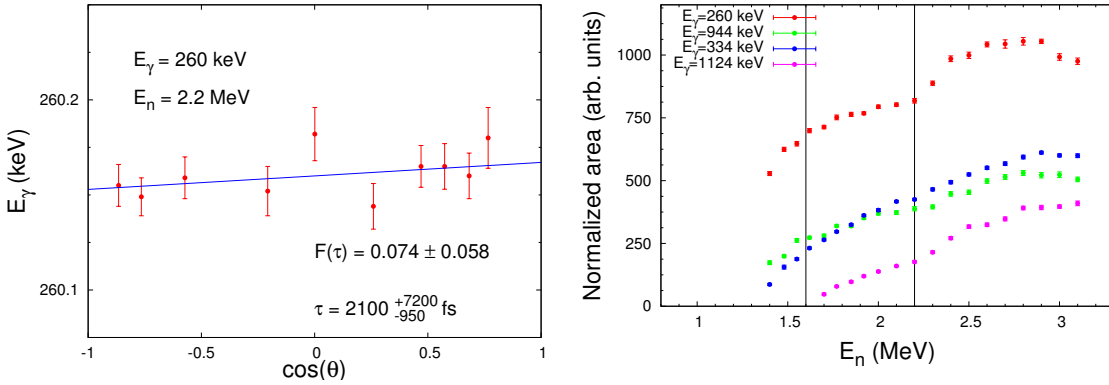


Figure 4.11. $E_\gamma=260$ keV γ ray (from the $E_x=1148$ keV level) Doppler shift and excitation functions for decays from the first 2^- band (color online). The vertical black lines highlight our justification for using a slightly higher bombarding neutron energy, for the sake of better statistics, without the potential for contaminant decay channels from other states.

We have measured lifetimes for the 3 lowest-lying members of the 0^- band, currently assigned as the single octupole vibration in ^{162}Dy from the clearly collective literature $B(E3;3^- \rightarrow 0^+_{gs})$ measurements ranging from 1.4-4.7 W.u. [48, 59]. The deduced lifetime from the direct $B(E1)\uparrow$ measurement in [85] of the bandhead of the $K^\pi=0^-$ band has been called into question by the NDS evaluator, with the distinct comment that the γ -branches of E1 radiation depopulating the state differs drastically from the adopted values. We are confident in our lifetime measurement from the extremely well-defined Doppler energy-shifts of the two de-excitations from this $E_x=1275$ keV level (shown in Figure 5.11). The 5^- state at 1518 keV is below the threshold to be populated by $E_n=1.6$ MeV neutrons, the de-excitations are not observed until the $E_n=2.2$ MeV dataset; this implies that the resulting lifetime will be inflated, as $F(\tau)$ is directly related to the bombarding neutron energy.

The final set of lifetime measurements of negative parity states is the second $K^\pi=2^-$ band. Two γ -ray placements from [3] are made into the bandhead of this 2^- band, the 900 and 975 keV transitions, both showing a well-behaved Doppler shift to

yield a level lifetime of 420^{+120}_{-80} fs. We have also placed two γ -ray transitions from the $E_x=1974$ keV 4^- state [8], a 912 keV and a 1010 keV decay to the γ -vibrational band. Confirmation of the placement of these de-excitations is made with the measurement of the excitation functions, shown in Figure 4.12; these γ -rays were also observed in [3], but were unplaced in their level scheme. Our absolute intensities are in reasonable agreement with the literature values in [3, 8], further justifying their correct placement in the level scheme.

4.2.4 Lifetimes of Other Negative Parity Bands ($K^\pi=5^-, 3^-, 1^-$ and 3_2^-)

Our discrepancy in lifetime measurement with respect to the literature value for the $K^\pi=5^-$ bandhead is striking, much like the case for the $E_x=1148$ keV level, yet we repeat the same assertions made in the previous section. The two de-exciting γ -rays exhibit a rather unambiguous placement in the level scheme from our measurement of the excitation function (both $E_\gamma=937$ & 1220 keV γ rays match qualitative shape and have the same threshold, consistent with a 5^- state at 1485 keV), and show well-defined Doppler energy-shifts that correspond to a lifetime of 450 fs, compared to the literature value of 1.92 ns [42]. We contest this lifetime measurement via delayed-coincidence from the β -decay of ^{162m}Ho , from our unambiguous placement of de-exciting γ rays in the level scheme, accurate branching ratios in comparison to literature intensities, and well-behaved DSAM shifts. In scrutinization of the literature, it is found that the 1.92 ns lifetime measurement by [42] is explicitly placed for the nearby 1490 keV state, and very little discussion is made on the delayed-coincidence measurements made in [23]. It is not entirely unreasonable that the measured lifetime in [23, 42] are instead seeing this nearby state at 1490 keV. This 7^+ state de-excites via a very similar energy (940 keV versus 937 keV) γ ray, and is populated via first-forbidden Fermi-type β -decay, in contrast to the preferred Gamov-Teller decay to the 5^- at 1485 keV.

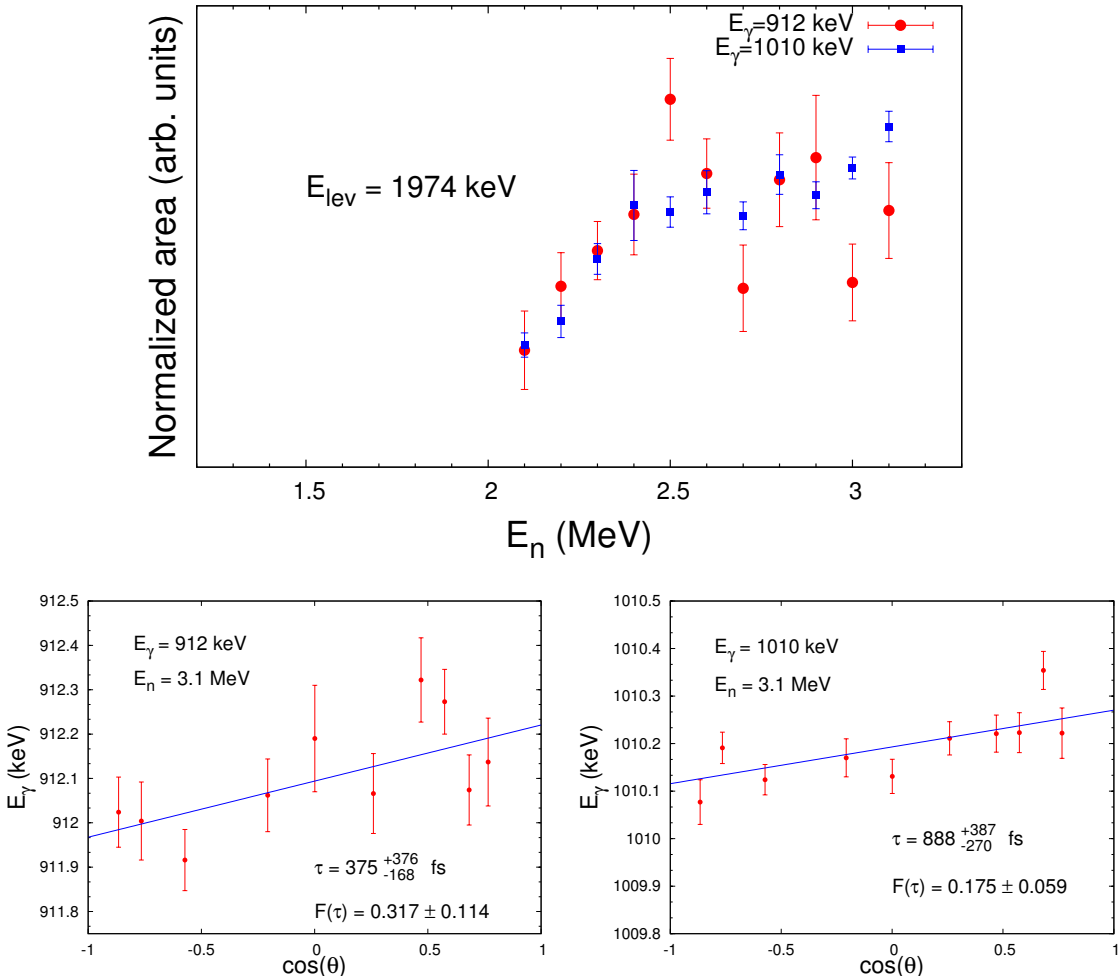


Figure 4.12. $E_{\gamma}=912$ & 1010 keV (de-excitations from the $E_x=1974$ keV level) Doppler shifts and excitation functions (color online). The excitation function (in blue) for the 1010 keV γ ray is scaled by a factor of 0.33 to normalize to the branching ratio of the level.

Absolute intensities from γ rays depopulating the $K^{\pi}=3^-$ band at 1570 keV show an obvious preference to the previously established 0^- octupole band [3] in the literature, where we do not observe the full $3^- \rightarrow g.s.$ transitions due to the low branching ratios listed. Shallow shifts in the DSAM fitting only gives a lower limit to the lifetime of the 3^- bandhead of >3050 fs, where, in contrast, we get good lifetime resolution on the 4^- member. That being said, we yet again encounter some of

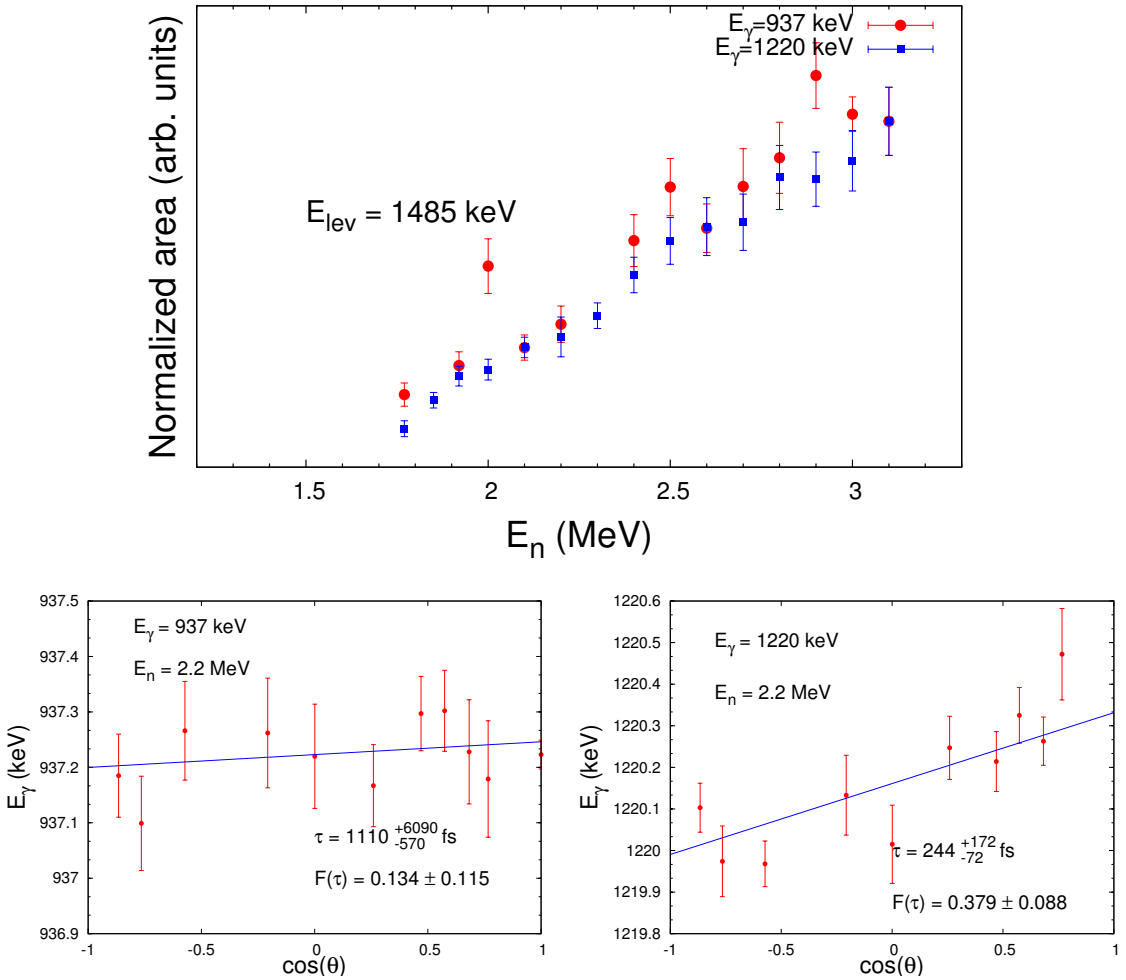


Figure 4.13. $E_\gamma=937$ & 1220 keV (de-excitations from the $E_x=1485$ keV level) Doppler shifts and overlaid excitation functions (color online). The excitation function (in blue) for the 1220 keV γ ray is scaled by a factor of 0.291.

the limitations behind the Doppler Shift Attenuation Method, in that lower energy γ rays (<500 keV) are easily attenuated by the sample size and may not exhibit reliable energy shifts. Further investigation of this level lifetime with another measurement technique (Coulomb excitation, ‘plunger’ method with RDDM, etc) is desired to more confidently understand the transition probabilities here, as the lifetimes measured in our campaign of experiments seem to be fairly unreliable.

The $K^\pi=1^-$ band at 1637 keV provides some of the least consistent and reliable results from our experimental campaign to measure lifetimes in ^{162}Dy . Starting with the bandhead, the only γ ray to attribute to the lifetime measurement is the de-excitation of $E_\gamma=1637$ keV. The questionability of this γ -ray placement is an issue, in that (n,γ) reactions by [3] do not observe it, yet other $(n,n'\gamma)$ experiments do. Nevertheless, the other two observed decays cannot be used because the 427 keV line is coincident with a background line, and as such, the extracted $F(\tau)$ is not reliable; the 489 keV γ provides an alternate discussion on its exclusion from the level lifetime. First, the relative intensity of the radiation does not fall in line with the other de-excitations according to the literature, and second, the extracted $F(\tau)$ from the 427 keV line varies wildly (by more than 2σ) from the 1637 keV line, and lastly, the excitation function(s) (Figure 4.14) for de-excitations out of the bandhead show an inconclusively similar pattern, qualitatively. These reasons are indicative of a bad placement of this decay in the level scheme, and is indicated by parentheses in Table 4.10. Further proof of the 489 keV γ ray being a contaminant can be seen in the nonconvergence of a multipole mixing fraction (ranging from 33-91% E2, with a large χ^2 value on the angular distribution).

The 2^- member of the band also yields some less than stellar resolution on the nuclear lifetime. With two decays observed at intermediate energies (but still below 1 MeV), we are only able to rely on the 728 keV γ ray to measure the lifetime, as the 416 keV decay lies on top of a background. The resulting lifetime limit of >1000 fs extracted from the Doppler Shift is not reliable, with $F(\tau)$ being consistent with zero within 1σ uncertainty. Since the 416 keV γ ray is coincident with a background, a reliable multipole mixing fraction cannot be extracted from the angular distributions, as we do not know the distribution of the background as a function of angle.

The 3^- member offers a slight tangent from the echoed rhetoric of lifetime measurements in the 1^- band, but still does not provide well-defined DSAM lifetimes.

The extracted average level $F(\tau)$ value is just over 1σ deviant from 0, giving both a) a borderline unreliable lifetime extraction, and b) an extremely low magnitude lower limit of >740 fs. In this sea of delinquent behavior, the branching ratios for the 3^- state of the 1^- band agree well with literature [3], but the multipole mixing fraction for the 529 keV γ is deviant from literature ($\sim 50\%$ mixed, vs $>99\%$ M1 in literature).

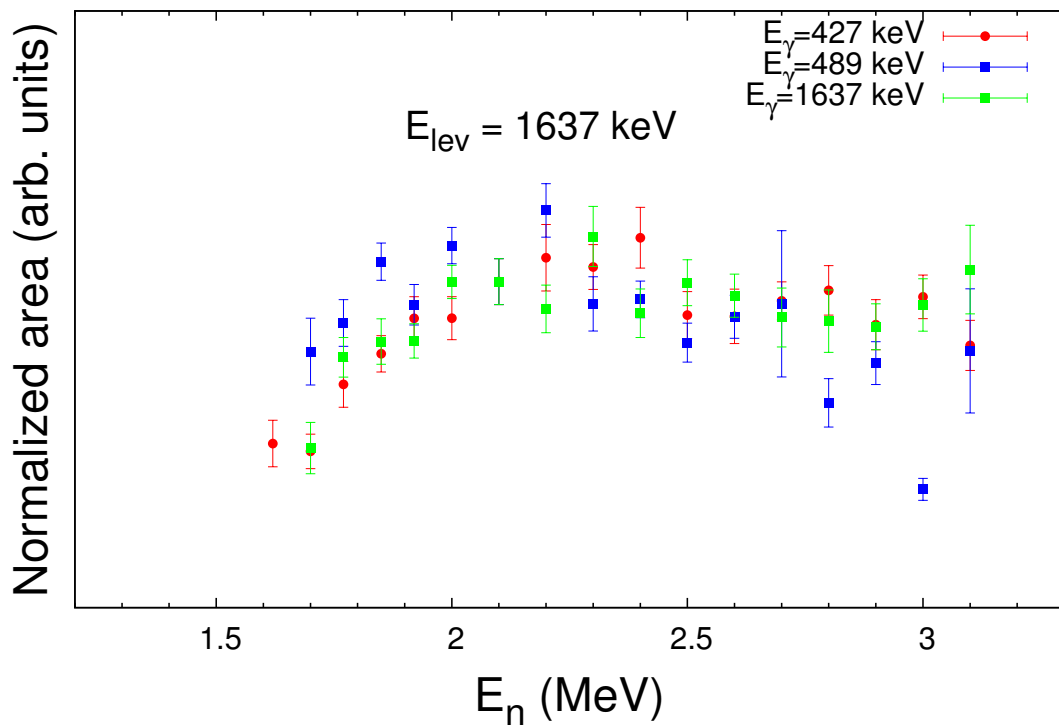


Figure 4.14. Excitation functions for the decays leaving the $E_x=1637$ keV state. Note the differing population threshold energies for each γ -ray.
(color online)

$F(\tau)$ values for the bandhead of the second $K^\pi=3^-$ band at 1766 keV fail to display

any definite shift in energy, in fact, having a negative (completely unphysical) value with a very large error. The unreliable lifetime reported in this work is simply the lower limit where $F(\tau)$ is the most positive, at a value of 0.044, but this extracted lifetime of 3400 fs should not be taken with any amount of confidence. The same can be said about the 4^- member at 1826 keV: the extracted $F(\tau)$ is *very* consistent with zero, as the only available transition to γ -band at 863 keV transition energy gives an appreciably nonzero shift (though not by much). Again, the lower limit of the lifetime is taken at the very edge of what $F(\tau)$ can be (at a value of 2400 fs). The statistical model employed (CINDY [71]) to calculate multipole mixing fractions was able to converge on a value for the mixing ratio from the 556 keV γ ray's angular distribution, however.

TABLE 4.10

NEGATIVE PARITY BANDS ($K^\pi=5^-, 3^-, 1^-, 3_2^-$): ^{162}DY

E_{lev} (keV)	E_γ (keV)	J_i	J_f	$F(\tau)_{av}$	τ (fs)	BR	$\pi\ell$	δ_{mix}	$B(\pi\ell)$
1485.79(29)	937.23(56)	$5_{5_1}^-$	$6_{0_1^+}^+$	0.310 ± 0.070	400_{-140}^{+210} [s]	0.257(10)	E1		$0.3_{-0.1}^{+0.1}$
	1220.16(56)	$5_{5_1}^-$	$4_{0_1^+}^+$			0.743(10)	E1		$0.3_{-0.1}^{+0.2}$
1570.82(27)	212.89(51) $[\emptyset]$	$3_{3_1^-}^-$	$3_{0_1^-}^-$	0.015 ± 0.036	$>3200^{[\varpi,\dagger]}$	0.348(9)	E2/M1	$-0.48_{-0.16}^{+0.13}$ [s]	<720
	295.23(50)	$3_{3_1^-}^-$	$1_{0_1^-}^-$			0.652(9)	E2		<1400
1669.26(38)	311.27(50)	$4_{3_1^-}^-$	$3_{0_1^-}^-$	0.289 ± 0.116	440_{-210}^{+450} [s]	1.000	E2/M1	$-6.9_{-2.2}^{+1.6}$ [s]	12000_{-11000}^{+6000} [\ddagger]
1637.52(20)	427.62(52) $[\otimes]$	$1_{1_1^-}^-$	$3_{2_1^-}^-$	0.081 ± 0.052	2000_{-800}^{+3500} [ϖ]	0.418(8) $[*]$	E2		230_{-140}^{+150}
	(489.05(56) $[\emptyset]$)	$1_{1_1^-}^-$	$2_{2_1^-}^-$			0.157(9)	E2/M1	$0.7 < \delta < 3.2$ [s]	40_{-27}^{+25}
	1637.68(55)	$1_{1_1^-}^-$	$0_{0_1^+}^+$			0.425(9)	E1		$0.02_{-0.01}^{+0.01}$
1691.72(23)	416.00(51) $[\otimes]$	$2_{1_1^-}^-$	$1_{0_1^-}^-$	0.060 ± 0.087	>1000 [s, \dagger]	0.483(8) $[\star]$	E2/M1	$—^{[\ddagger]}$	<630
	728.50(51)	$2_{1_1^-}^-$	$3_{2_1^+}^+$			0.517(8)	E1		<0.4
1739.02(21)	529.06(51) $[\emptyset]$	$3_{1_1^-}^-$	$3_{2_1^-}^-$	0.107 ± 0.098	>740 [s]	0.375(6)	E2/M1	$1.4_{-0.2}^{+0.2}$ [s]	<130
	590.74(54)	$3_{1_1^-}^-$	$2_{2_1^-}^-$			0.139(5)	E2/M1	$1.2_{-0.3}^{+0.5}$ [s]	<24
	678.12(53)	$3_{1_1^-}^-$	$4_{2_1^+}^+$			0.238(5)	E1		<0.3

Continued

TABLE 4.10

NEGATIVE PARITY BANDS ($K^\pi=5^-, 3^-, 1^-, 3^-_2$): ^{162}DY

E_{lev} (keV)	E_γ (keV)	J_i	J_f	$F(\tau)_{av}$	τ (fs)	BR	$\pi\ell$	δ_{mix}	$B(\pi\ell)$
	1473.36(53) $[\emptyset]$	$3^-_{1^-}$	$4^+_{0^+}$			0.248(5)	E1		<0.03
1766.56(26)	556.67(59) $[\emptyset]$	$3^-_{3^-_2}$	$3^-_{2^-_1}$	-0.061 ± 0.105	>3400 $[\varsigma, \dagger]$	0.310(12)	E2/M1	$-0.54^{+0.16}_{-0.21}$ $[\varsigma]$	<6 $[\dagger]$
	878.21(55) $[\emptyset]$	$3^-_{3^-_2}$	$2^+_{2^+_1}$			0.690(12)	E1		<0.1 $[\dagger]$
1826.64(28)	643.99(54) $[\otimes]$	$4^-_{3^-_2}$	$5^+_{2^+_1}$	0.002 ± 0.066	>2400 $[\varpi, \dagger]$	0.265(9) $[\star]$	E1		<0.1
	863.84(54)	$4^-_{3^-_2}$	$3^+_{2^+_1}$			0.735(9)	E1		<0.2

Lifetimes of 5^- , 3^- , 1^- , and second 3^- bands in ^{162}Dy , with experimentally deduced $B(E1)$ in mW.u. and $B(E2)$ in W.u. $[\emptyset]$: γ ray not used in $F(\tau)$ calculation ($F(\tau)<0$).

$[\vartheta]$: $F(\tau)$ extracted from $E_n=1.6$ MeV angular distributions, $[\varsigma]$: $F(\tau)$ extracted from $E_n=2.2$ MeV angular distributions, $[\varpi]$: $F(\tau)$ extracted from $E_n=3.1$ MeV angular distributions

$[\dagger]$: Lifetime not reliable ($F(\tau)$ consistent with zero within 1σ), $[\otimes]$: γ ray not used in $F(\tau)$ calculation (coincident with background), $[\star]$: branching ratio not reliable due to background contamination. 1 W.u.(E2)=5.25E-7 $e^2 b^2$, 1 mW.u.(E1)=1.91 $e^2 b$

4.2.5 Lifetimes of $K^\pi=1^+$ Band and Members of M1 Scissors

Our measurement of lifetimes in the 1^+ band can be seen in Table 4.11, where we have two good $F(\tau)$ shifts, and two unreliable measurements of the lifetime of states. The bandhead is the first of the unreliable lifetimes measured. Here, the only γ decay that contributes to the calculation of a level lifetime is the 857 keV γ ray, but the energy shift is consistent with zero within 1σ uncertainty. While this is not a low-energy decay that would be more susceptible to attenuation in the sample, it *may* be a contaminant, as the angular distribution does not yield a reliable mixing ratio for the decay.

The 2^+ member of this band echoes a similar story; one de-excitation is not used in the determination of the nuclear lifetime, as the $F(\tau)$ measured is negative. However, unlike the bandhead, this γ -ray angular distribution that is excluded (1701 keV) converges on a good, reliable value for E2/M1 mixing, at just under 50% mixing. That being said, the extracted lifetime is still not reliable, since $F(\tau)$ for this level is negative.

The decays to both the ground state 4^+ and the γ -band 4^+ are used to extract the lifetime of 1400^{+4500}_{-1000} fs for this 3^+ state at 1840 keV. To round out the $K^\pi=1^+$ band, the 4^+ state at 1951 keV offers good lifetime resolution, similar to the 3^+ state.

TABLE 4.11

 $K^\pi=1^\pm$ AND M1 SCISSORS MODE: ^{162}DY

E_{lev} (keV)	E_γ (keV)	J_i	J_f	$F(\tau)_{av}$	τ (fs)	BR	$\pi\ell$	δ_{mix}	$B(\pi\ell)$	
134	1745.80(25)	857.65(50)	$1^+_{1^+}$	$2^+_{2^+}$	0.039 ± 0.044	>1800 [ς, \dagger]	0.538(5)	E2/M1	— [\ddagger]	<0.02 [\dagger]
	1665.09(51) $[\emptyset]$	$1^+_{1^+}$	$2^+_{0^+}$				0.462(5)	E2/M1	$0.41^{+0.27}_{-0.19}$ [ς]	<0.04 [\dagger]
	1782.54(22)	1701.90(53) $[\emptyset]$	$2^+_{1^+}$	$2^+_{0^+}$	0.013 ± 0.033	>3400 [ϖ, \dagger]	0.389(10)	E2/M1	$0.33^{+0.24}_{-0.13}$ [ς]	<0.01
	1782.63(53)		$2^+_{1^+}$	$0^+_{0^+}$			0.611(10)	E2		<0.2
	1840.44(21)	630.51(68) $[\emptyset]$	$3^+_{1^+}$	$3^-_{2^-}$	0.104 ± 0.074	1400^{+3500}_{-500} [ς]	0.180(10)	E1		$0.2^{+0.1}_{-0.1}$
	779.58(60)		$3^+_{1^+}$	$4^+_{2^+}$			0.283(11)	E2/M1	<-4.8 [ς]	10^{+8}_{-6}
	1574.82(57)		$3^+_{1^+}$	$4^+_{0^+}$			0.262(12)	E2/M1	$4.4^{+18}_{-2.1}$ [ς]	$0.3^{+0.2}_{-0.2}$
	1759.60(75) $[\emptyset]$		$3^+_{1^+}$	$2^+_{0^+}$			0.276(16)	E2/M1	$0.21^{+0.15}_{-0.13}$ [ς]	$0.01^{+0.01}_{-0.01}$
	1951.17(34)	1685.80(56)	$4^+_{1^+}$	$4^+_{0^+}$	0.071 ± 0.048	2300^{+4500}_{-1000} [ϖ]	1.000	E2/M1	$-0.38^{+0.14}_{-0.17}$ [ϖ]	$0.1^{+0.1}_{-0.1}$
	2395.60(39)	2395.00(50)	1^+_Ω	$0^+_{0^+}$	0.926 ± 0.061	14^{+13}_{-11} [ϖ]	1.000	M1		$0.14^{+0.61}_{-0.08}$
	2519.43(36)	2438.00(51)	1^-_Ω	$2^+_{0^+}$	0.595 ± 0.054	110^{+30}_{-20} [ϖ]	0.564(27)	E1		$0.1^{+0.1}_{-0.1}$
	2520.27(51)		1^-_Ω	$0^+_{0^+}$			0.436(27)	E1		$0.1^{+0.1}_{-0.1}$
	2537.26(30)	2537.24(51)	1^+_Ω	$0^+_{0^+}$	0.290 ± 0.049	460^{+160}_{-120} [ϖ]	1.000	M1		$0.004^{+0.001}_{-0.001}$

Continued

TABLE 4.11

$K^\pi=1^\pm$ AND M1 SCISSORS MODE: ^{162}Dy

E_{lev} (keV)	E_γ (keV)	J_i	J_f	$F(\tau)_{av}$	τ (fs)	BR	$\pi\ell$	δ_{mix}	$B(\pi\ell)$
2569.35(22)	2568.83(51)	1^+_Ω	$0^+_{0^+_1}$	0.653 ± 0.066	90^{+30}_{-20} [ω]	1.000	M1		$0.021^{+0.006}_{-0.005}$
2814.80(33)	2734.24(55)	1^+_Ω	$2^+_{0^+_1}$	0.442 ± 0.099	200^{+130}_{-60} [ω]	1.000	M1		$0.008^{+0.003}_{-0.003}$

135

Lifetimes of 1^+ band and 1^\pm members of the isovector M1 scissors mode ($[\Omega]$ marker) in ^{162}Dy , with experimentally deduced $B(E1)$ in mW.u., $B(M1)$ in μ_N^2 and $B(E2)$ in W.u. [∅]: γ ray not used in $F(\tau)$ calculation ($F(\tau)<0$).

[∅]: $F(\tau)$ extracted from $E_n=1.6$ MeV angular distributions, [∅]: $F(\tau)$ extracted from $E_n=2.2$ MeV angular distributions, [ω]: $F(\tau)$ extracted from $E_n=3.1$ MeV angular distributions

[†]: Lifetime not reliable ($F(\tau)$ consistent with zero within 1σ)

1 W.u.(E2)=5.25E-7 e²b², 1 mW.u.(E1)=1.91 e²b

4.2.6 Lifetimes of States with No K^π Assignment

We direct the reader to the fact that lifetimes above the pairing gap in ^{162}Dy exhibit very well-behaved and precise lifetime measurements; this is an artifact of the DSAM measurements at UKAL, where, generally, the higher energy γ rays that completely de-excite the nucleus fare better in escaping the sample size and displaying a noticeable energy shift than those at lower energy thresholds. Tables 4.12 and ?? list these ‘miscellaneous’ lifetimes for which there is no rotational band assignment for the state. In many of these states, we place liberal limits on the spin/parity, based solely on our measurement of the angular distributions. Because of the tentative spin assignments, multipole mixing fractions extracted from the angular distributions are often unavailable, as the statistical model employed requires known spins and parities to be known.

TABLE 4.12

OTHER LEVELS (NO K ASSIGNMENT): ^{162}DY

E_{lev} (keV)	E_γ (keV)	J_i	J_f	$F(\tau)_{av}$	τ (fs)	BR	$\pi\ell$	δ_{mix}	$B(\pi\ell)$
1886.53(33)	1805.86(52)	$4^+_{[\Upsilon]}$	$2^+_{0_1^+}$	0.086 ± 0.034	1600^{+1300}_{-390} [s]	1.000	E2		$0.5^{+0.2}_{-0.2}$
1895.44(26)	747.34(57) ^[⊗]	$2^+_{[\Upsilon]}$	$2^-_{2_1^-}$	0.258 ± 0.029	530^{+100}_{-90} [s]	$0.249(6)^{[*]}$	E1		$0.4^{+0.1}_{-0.1}$
	1814.69(52)	$2^+_{[\Upsilon]}$	$2^+_{0_1^+}$			0.751(6)	E2/M1	$-0.58^{+0.07}_{-0.08}$ [s]	$0.3^{+0.1}_{-0.1}$
1982.61(22)	1902.06(53)	$2^+_{[\Upsilon]}$	$2^+_{0_1^+}$	0.547 ± 0.031	130^{+17}_{-15} [s]	0.522(5)	E2/M1	— ^[‡]	$2.5^{+0.3}_{-0.3}$
	1982.50(56)	$2^+_{[\Upsilon]}$	$0^+_{0_1^+}$			0.478(5)	E2		$1.9^{+0.2}_{-0.2}$
1999.23(33)	1918.57(52)	$2^+_{[\Upsilon]}$	$2^+_{0_1^+}$	0.203 ± 0.031	730^{+160}_{-130} [s]	1.000	E2/M1	$-0.12^{+0.03}_{-0.04}$ [s]	$0.01^{+0.01}_{-0.01}$
2102.42(57)	584.22(50)	$(3)^-_{[\Upsilon]}$	$5^-_{0_1^-}$	0.122 ± 0.073	1300^{+2000}_{-450} [ϖ]	1.000	(E2)		180^{+93}_{-110}
2148.47(33)	2067.92(50)	$(2)^{\pm}_{[\Upsilon]}$	$2^+_{0_1^+}$	0.048 ± 0.026	3300^{+3700}_{-1200} [ϖ]	1.000	(E2/M1)	— ^[‡]	$0.1^{+0.1}_{-0.1}$
2180.69(53)	1217.73(58)	$4^+_{[\Upsilon]}$	$3^+_{2_1^+}$	0.383 ± 0.095	240^{+190}_{-80} [s]	1.000	E2/M1	$0.24^{+0.07}_{-0.06}$ [s]	$1.3^{+1.0}_{-0.9}$
2231.06(38)	955.75(50)	$(2,3,4)^+_{[\Upsilon]}$	$1^-_{0_1^-}$	0.333 ± 0.031	360^{+70}_{-60} [ϖ]	0.423(9)	E1		$0.4^{+0.1}_{-0.1}$
	1342.57(50)	$(2,3,4)^+_{[\Upsilon]}$	$2^+_{2_1^+}$			0.577(9)	E2/M1	$3.1^{+2.1}_{-1.0}$ [ϖ]	$5.2^{+0.9}_{-1.2}$
2313.75(52)	2233.20(50)	$(2)^+_{[\Upsilon]}$	$2^+_{0_1^+}$	0.133 ± 0.048	1200^{+620}_{-290} [ϖ]	1.000	(E2/M1)	— ^[‡]	$0.2^{+0.1}_{-0.1}$

Continued

TABLE 4.12

OTHER LEVELS (NO K ASSIGNMENT): ^{162}DY

E_{lev} (keV)	E_γ (keV)	J_i	J_f	$F(\tau)_{av}$	τ (fs)	BR	$\pi\ell$	δ_{mix}	$B(\pi\ell)$
2324.59(39)	1141.96(50)	(4,5) $^+_{[\gamma]}$	$5^+_{2_1^+}$	0.051 ± 0.063	>1300 [ϖ, \dagger]	1.000	(E2/M1)	—[‡]	<6.16
2339.31(50)	2339.29(50)	(2) $^+_{[\gamma]}$	$0^+_{0_1^+}$	0.285 ± 0.067	480^{+230}_{-160} [ϖ]	1.000	(E2)	—	$0.5^{+0.2}_{-0.2}$
2371.55(52)	2291.00(50)	(1,2,3) $^-_{[\gamma]}$	$2^+_{0_1^+}$	0.011 ± 0.079	>1700 [ϖ, \dagger]	1.000	E1	—	<0.02
2386.48(52)	2305.92(50)	(2) $^+_{[\gamma]}$	$2^+_{0_1^+}$	0.217 ± 0.053	710^{+260}_{-190} [ϖ]	1.000	(E2/M1)	—[‡]	$0.3^{+0.1}_{-0.1}$
2411.96(36)	2331.40(50)	(4) $^+_{[\gamma]}$	$2^+_{0_1^+}$	0.126 ± 0.046	1200^{+690}_{-290} [ϖ]	1.000	(E2)	—	$0.2^{+0.1}_{-0.1}$
2427.02(52)	2346.46(50)	(2,3) $^+_{[\gamma]}$	$2^+_{0_1^+}$	0.355 ± 0.074	310^{+170}_{-100} [ϖ]	1.000	(E2/M1)	—[‡]	$0.7^{+0.3}_{-0.3}$
2487.99(33)	2407.43(50)	(3,4) $^+_{[\gamma]}$	$2^+_{0_1^+}$	0.270 ± 0.052	520^{+190}_{-140} [ϖ]	1.000	(E2/M1)	—[‡]	$0.4^{+0.1}_{-0.1}$
2505.75(26)	2240.40(50)	(2) $^+_{[\gamma]}$	$4^+_{0_1^+}$	0.500 ± 0.032	160^{+20}_{-20} [ϖ]	0.530(16)	(E2)	—	$0.9^{+0.1}_{-0.1}$
	2505.66(51)	(2) $^+_{[\gamma]}$	$0^+_{0_1^+}$			0.470(16)	(E2)	—	$0.5^{+0.1}_{-0.1}$
2509.43(33)	2428.88(50)	(2,3) $^+_{[\gamma]}$	$2^+_{0_1^+}$	0.361 ± 0.050	300^{+100}_{-70} [ϖ]	1.000	(E2/M1)	—[‡]	$0.6^{+0.2}_{-0.2}$
2523.76(85)	952.94(50)	(1,2,3,4) $^\pm_{[\gamma]}$	$3^-_{3_1^-}$	0.151 ± 0.109	1100^{+2600}_{-500} [ϖ]	1.000	(E2/M1)	—	18^{+15}_{-13}
2555.66(33)	2475.11(51)	(2,3) $^+_{[\gamma]}$	$2^+_{0_1^+}$	0.330 ± 0.082	350^{+230}_{-130} [ϖ]	1.000	(E2/M1)	—[‡]	$0.3^{+0.2}_{-0.1}$

Continued

TABLE 4.12

OTHER LEVELS (NO K ASSIGNMENT): ^{162}DY

E_{lev} (keV)	E_γ (keV)	J_i	J_f	$F(\tau)_{av}$	τ (fs)	BR	$\pi\ell$	δ_{mix}	$B(\pi\ell)$
2613.30(33)	2532.75(51)	(3) $^+_{[\gamma]}$	$2^+_{0^+}$	0.613 ± 0.059	100^{+30}_{-20} [⊗]	1.000	(E2/M1)	—[‡]	$0.02^{+0.01}_{-0.01}$
2630.66(30)	2630.63(52)	(2,3) $^+_{[\gamma]}$	$2^+_{0^+}$	0.602 ± 0.056	110^{+30}_{-20} [⊗]	1.000	(E2/M1)	—[‡]	$1.1^{+0.3}_{-0.2}$
2777.62(60)	2777.59(56)	(2) $^+_{[\gamma]}$	$0^+_{0^+}$	0.465 ± 0.117	180^{+140}_{-70} [⊗]	1.000	(E2/M1)	—[‡]	$0.5^{+0.3}_{-0.2}$
2816.53(43)	2551.00(55)	(4,5) $^+_{[\gamma]}$	$4^+_{0^+}$	0.256 ± 0.085	550^{+370}_{-220} [⊗]	1.000	(E2/M1)	—[‡]	$0.3^{+0.2}_{-0.1}$

Lifetimes of states with no rotational K^π band assignment in ^{162}Dy , with experimentally deduced $B(E1)$ in mW.u., $B(M1)$ in μ_N^2 and $B(E2)$ in W.u. [⊗]: γ ray not used in $F(\tau)$ calculation ($F(\tau) < 0$).

[θ]: $F(\tau)$ extracted from $E_n=1.6$ MeV angular distributions, [c]: $F(\tau)$ extracted from $E_n=2.2$ MeV angular distributions, [π]: $F(\tau)$ extracted from $E_n=3.1$ MeV angular distributions

[‡]: Lifetime not reliable ($F(\tau)$ consistent with zero within 1σ)

[⊗]: γ ray not used in $F(\tau)$ calculation (coincident with background)

1 W.u.(E2)=5.25E-7 e²b², 1 mW.u.(E1)=1.91 e²b

4.2.7 All Decays Observed (Intensities)

As a capstone for the experimental campaign to measure lifetimes in ^{162}Dy , Table 4.13 lists every γ -ray observed in our experiments with all possible origins (prompt Dy decay, background, or unknown), its intensity from the 3.1 MeV neutron energy dataset, its placement in the level scheme if applicable, and any notes for the reader as justification for any assignments.

TABLE 4.13

ALL DECAYS OBSERVED: ^{162}DY

E_γ (keV)	Thresh. (MeV)	I_γ abs.	Origin	E_{level} (keV)	Notes
185.002 (3)	<1.4	11831.273 (291.130)	^{162}Dy	265	$F(\tau)$ 'calibrant' ($\tau=190$ ps)
212.856 (9)	1.62	257.926 (8.709)	^{162}Dy	1570	
236.061 (11)	<1.6	48.538 (5.613)	^{162}Dy	1297	
247.173 (14)	<1.6	265.174 (5.347)	^{162}Dy	1210	
250.903 (13)	[†]	205.447 (4.354)	bkg	???	
253.098 (18)	[†]	124.111 (3.481)	bkg	$^{74}\text{Ge}(n,\gamma)$	
258.157 (11)	[†]	92.943 (8.501)	bkg	$^{72}\text{Ge}(n,\gamma)$	
260.136 (3)	<1.4	280.854 (7.729)	^{162}Dy	1148	
262.929 (19)	<1.4	3027.698 (52.841)	[‡]		[★] [A^2] Isotropic
278.131 (26)	~2.0	106.087 (2.859)	[‡]		probable background
282.937 (5)	<1.4	2679.570 (45.708)	^{162}Dy	548	
295.233 (6)	1.62	482.315 (0.539)	^{162}Dy	1571	

Continued

TABLE 4.13

ALL DECAYS OBSERVED: ^{162}Dy

E_γ (keV)	Thresh. (MeV)	I_γ abs.	Origin	E_{level} (keV)	Notes
311.252 (7)	1.70	297.539 (5.342)	^{162}Dy	1669	
322.012 (7)	<1.4	321.899 (6.243)	^{162}Dy	1210	
326.260 (18)	[†]	268.417 (4.960)	bkg		Doublet with $^{70}\text{Ge}(\text{n},\gamma)$ and $^{72}\text{Ge}(\text{n},\gamma)$
328.363 (129)	[†]	73.814 (3.512)	bkg	$^{72}\text{Ge}(\text{n},\gamma)$	
334.120 (4)	<1.4	1470.283 (33.471)	^{162}Dy	1297	
347.482 (11)	<1.4	273.997 (5.784)	[‡]		[A^2]
351.276 (11)	[†]	90.213 (2.284)	bkg	???	
354.259 (15)	[†]	65.674 (2.019)	bkg	???	
411.787 (38)	~1.6	46.863 (3.657)	[‡]		Unidentified UKY bkg
416.221 (17)	[†]	89.239 (3.162)	bkg	$^{115}\text{In}(\text{n},\gamma)$	
422.011 (19)	[†]	89.692 (3.627)	[‡]		
427.504 (14)	1.7	138.412 (3.312)	^{162}Dy	1637	coinc. with a background, $F(\tau)$ not reliable

Continued

TABLE 4.13

ALL DECAYS OBSERVED: ^{162}Dy

E_γ (keV)	Thresh. (MeV)	I_γ abs.	Origin	E_{level} (keV)	Notes
441.529 (41)	1.775	40.169 (2.790)	^{162}Dy	1738	low statistics
475.215 (18)	~ 1.62	186.404 (12.199)	^{162}Dy	1535	a little low threshold for 4^+ population
489.120 (24)	1.7	51.876 (3.312)	[#]	???	$[A^2]$
493.991 (38)	[†]	55.272 (3.010)	bkg		$^{73}\text{Ge}(n,\gamma)$ & $^{74}\text{Ge}(n,n'\gamma)$
529.034 (13)	1.85	227.886 (5.240)	^{162}Dy	1738	
543.660 (10)	1.85	318.589 (7.364)	[#]	???	ExF does not support 1691 placement
556.023 (23)	1.85	136.124 (4.082)	^{162}Dy	1766	
572.944 (9)	~ 1.62	624.137 (13.351)	^{162}Dy	1535	
584.247 (28)	2.2	163.025 (5.805)	^{162}Dy	2102	
590.633 (36)	1.85	79.883 (3.454)	^{162}Dy	1739	
622.528 (23)	[†]	95.089 (4.721)	^{162}Dy		low intensity, should be part of 888
630.455 (54)	1.85	45.621 (3.320)	^{162}Dy	1840?	

Continued

TABLE 4.13

ALL DECAYS OBSERVED: ^{162}Dy

E_γ (keV)	Thresh. (MeV)	I_γ abs.	Origin	E_{level} (keV)	Notes
634.131 (11)	<1.4	394.139 (11.353)	^{162}Dy	1182	
643.548 (46)	1.925	66.334 (2.786)	^{162}Dy	1826	
647.537 (8)	1.7	993.135 (16.799)	^{162}Dy	1535	
669.640 (22)	1.775	115.485 (22.367)	bkg	$^{63}\text{Cu}(n,\gamma)$	
671.516 (44)	1.775	214.988 (4.646)	$^{162}\text{Dy}?$	1634?	too low threshold for a 5^+ population
678.113 (18)	1.85	125.946 (3.396)	^{162}Dy	1739	
697.283 (7)	<1.4	1277.950 (31.781)	^{162}Dy	963	
728.490 (17)	1.775	170.713 (4.611)	^{162}Dy	1691	
748.235 (20)	1.925	126.131 (4.586)	^{162}Dy	1895	
768.763 (58)	~2.3	112.711 (5.692)	[#]		$[A^2]$
770.711 (51)	2.2	75.373 (10.643)	^{162}Dy	2129	$[A^2]$ ($^{65}\text{Cu}(n,n'\gamma)$)
776.014 (19)	1.925	299.865 (6.510)	^{162}Dy	1324?	could be a doublet

Continued

TABLE 4.13

ALL DECAYS OBSERVED: ^{162}Dy

E_γ (keV)	Thresh. (MeV)	I_γ abs.	Origin	E_{level} (keV)	Notes
779.515 (27)	1.925	76.857 (2.643)	^{162}Dy	1840	$F(\tau)$ likely not reliable (doublet)
795.370 (6)	<1.4	2534.118 (51.240)	^{162}Dy	1060	
803.596 (27)	1.85	191.698 (4.408)	^{162}Dy	1766	
807.544 (6)	<1.4	5603.611 (108.346)	^{162}Dy	888	
819.633 (18)	1.85	117.917 (4.035)	^{162}Dy	1782	
842.393 (20)	~1.62	353.148 (9.502)	[‡]		$^{73}\text{Ge}/^{27}\text{Al}(n,n'\gamma)$
846.561 (43)	[†]	70.108 (6.611)	bkg	^{56}Fe	
849.768 (42)	2.0	111.364 (4.651)	[‡]		$F(\tau)=0.137\pm0.179$
857.590 (12)	1.775	210.646 (4.502)	^{162}Dy	1745	
863.833 (21)	1.925	184.136 (4.102)	^{162}Dy	1826	
878.039 (24)	1.85	305.545 (9.103)	^{162}Dy	1766	
882.316 (6)	<1.4	6774.521 (135.466)	^{162}Dy	963	

Continued

TABLE 4.13

ALL DECAYS OBSERVED: ^{162}Dy

E_γ (keV)	Thresh. (MeV)	I_γ abs.	Origin	E_{level} (keV)	Notes
888.195 (6)	<1.4	5140.372 (102.292)	^{162}Dy	888	
894.849 (37)	2.0	234.163 (7.245)	[‡]		Doublet with Pb background
896.295 (74)	[†]	120.660 (14.171)	bkg		$^{207}\text{Pb}(n,n'\gamma)$
901.014 (26)	1.925	150.159 (8.600)	^{162}Dy	1863	
912.030 (27)	2.1	82.148 (3.125)	^{162}Dy	1974	
917.116 (8)	<1.4	1809.219 (33.885)	^{162}Dy	1183	
932.237 (35)	1.925	68.438 (4.803)	[⊗]		[★] $F(\tau) < 0$
937.110 (23)	1.775	240.267 (7.937)	^{162}Dy	1485	5 ⁻ population ✓
944.438 (8)	<1.4	1160.957 (24.752)	^{162}Dy	1210	
947.415 (28)	2.0	173.498 (4.547)	^{162}Dy	1910	
953.210 (103)	2.6	86.864 (3.249)	^{162}Dy	2524	[A ²]-placed
955.939 (32)	2.3	175.548 (4.160)	^{162}Dy	2230	[A ²]-placed

Continued

TABLE 4.13

ALL DECAYS OBSERVED: ^{162}Dy

E_γ (keV)	Thresh. (MeV)	I_γ abs.	Origin	E_{level} (keV)	Notes
962.080 (16)	[†]	189.023 (48.170)	bkg	$^{63}\text{Cu}(\text{n},\text{n}'\gamma)$	
969.756 (20)	1.775	227.299 (4.847)	^{162}Dy	1518	
975.597 (12)	1.925	490.458 (7.426)	^{162}Dy	1863	
980.359 (8)	<1.4	1554.147 (25.227)	^{162}Dy	1060	
1007.010 (34)	2.2	126.177 (7.111)	[⊗]		[★] $[A^2]$ $F(\tau)=0.221\pm 0.074$
1010.050 (21)	2.1	251.922 (15.219)	^{162}Dy	1974	$[A^2]$ -placed
1014.672 (19)	2.0	174.587 (9.489)	bkg	$^{27}\text{Al}(\text{n},\text{n}'\gamma)$	
1017.626 (35)	2.2	149.667 (3.812)	[⊗]		[★] $F(\tau)=0.205\pm 0.063$
1022.172 (19)	1.925	216.003 (6.133)	^{162}Dy	1910	
1025.861 (32)	~1.7	98.003 (5.045)	^{162}Dy	1574	
1092.277 (9)	1.4	1066.432 (20.498)	^{162}Dy	1357	
1096.904 (14)	[†]	172.976 (4.071)	bkg	$^{115}\text{In}(\text{n},\gamma)$	

Continued

TABLE 4.13

ALL DECAYS OBSERVED: ^{162}DY

E_γ (keV)	Thresh. (MeV)	I_γ abs.	Origin	E_{level} (keV)	Notes
1114.721 (57)	2.4	109.426 (32.990)	[\otimes]		[\star] [A^2] ($F(\tau)$ also looks like a background)
1124.974 (12)	1.7	925.209 (24.488)	^{162}Dy	1390	
1129.427 (8)	<1.4	1970.898 (45.151)	^{162}Dy	1210	
1133.244 (42)	2.4	181.084 (5.630)	[\nexists]		[\star] [A^2] $F(\tau)=0.133\pm 0.077$
1141.793 (36)	2.4	263.234 (6.981)	^{162}Dy	2324	[A^2]-placed
1160.958 (102)	2.7	55.458 (3.187)	[\nexists]		[\star]
1164.954 (23)	[\dagger]	87.576 (3.279)	bkg		Unidentified UKY bkg
1169.142 (83)	2.8	80.855 (3.944)	[\nexists]		[\star] [A^2]
1187.759 (10)	1.5	477.002 (10.302)	^{162}Dy	1453	
1195.113 (8)	<1.4	1817.697 (38.720)	^{162}Dy	1276	
1204.352 (50)	[\dagger]	81.093 (3.574)	bkg		$^{73}\text{Ge}(n,\gamma)$ & $^{74}\text{Ge}(n,n'\gamma)$
1207.069 (45)	2.2	205.221 (6.721)	[\nexists]	1754?	[A^2] $F(\tau)>0$, assigned (7^-), could only be 5^-

Continued

TABLE 4.13

ALL DECAYS OBSERVED: ^{162}Dy

E_γ (keV)	Thresh. (MeV)	I_γ abs.	Origin	E_{level} (keV)	Notes
1217.733 (32)	2.2	300.230 (5.134)	^{162}Dy	2181	[A^2]-placed
1219.971 (20)	1.775	687.409 (10.737)	^{162}Dy	1485	
1222.787 (49)	2.3	182.663 (4.252)	^{162}Dy	2283	[A^2]-placed
1231.897 (75)		71.342 (4.794)			[A^2]
1252.721 (15)	1.775	407.559 (11.873)	^{162}Dy	1518	
1275.847 (16)	<1.4	1268.297 (29.632)	^{162}Dy	1275	
1277.317 (19)	<1.4	1601.847 (35.621)	^{162}Dy	1357	
1293.539 (14)	<1.4	319.833 (9.558)	bkg	$^{115}\text{In}(\text{n},\text{n}'\gamma)$	
1298.577 (29)	[†]	374.596 (69.27)	bkg	$^{70}\text{Ge}(\text{n},\gamma)$	
1308.563 (14)	1.7	534.359 (11.016)	^{162}Dy	1574	
1311.851 (42)	2.5	216.796 (6.529)	^{162}Dy	2494	[A^2]-placed
1317.544 (92)	2.4	114.659 (4.166)	[\otimes]		[\star] [A^2]

Continued

TABLE 4.13

ALL DECAYS OBSERVED: ^{162}Dy

E_γ (keV)	Thresh. (MeV)	I_γ abs.	Origin	E_{level} (keV)	Notes
1319.617 (12)	1.4	390.315 (5.095)	^{162}Dy	1400	
1342.508 (27)	2.3	239.620 (6.282)	^{162}Dy	2230	
1350.928 (36)	2.3	164.208 (5.629)	[‡]		[★]
1355.959 (42)	2.3	106.563 (4.235)	[⊗]		[★]
1363.757 (60)	2.4		[⊗]		[★]
1372.781 (12)	1.48	617.669 (7.637)	^{162}Dy	1453	
1390.598 (298)	2.4	107.377 (11.778)	[⊗]		[★]
1404.315 (39)	2.5	167.399 (7.776)	[⊗]		[A^2]
1408.437 (75)		82.543 (2.747)			potentially $^{54}\text{Fe}(\text{n},\text{n}'\gamma)$
1412.530 (91)	2.5	109.346 (26.646)	[⊗]		[★] [A^2] ($F(\tau) < 0$)
1415.814 (131)	2.5	45.376 (2.745)	[‡]		[★]
1421.871 (44)	2.4	124.074 (3.683)	[⊗]		[★]

Continued

TABLE 4.13

ALL DECAYS OBSERVED: ^{162}DY

E_γ (keV)	Thresh. (MeV)	I_γ abs.	Origin	E_{level} (keV)	Notes
1427.853 (56)	2.4	90.089 (3.362)	[\otimes]		[\star] [A^2]
1438.444 (33)	2.4	201.808 (4.037)	[\otimes]		[\star] [A^2]
1462.818 (17)	1.775	175.495 (4.773)	^{162}Dy	1728	
1473.398 (26)	1.85	122.538 (4.393)	^{162}Dy	1738	
1556.569 (14)	1.7	357.876 (8.297)	^{162}Dy	1637	
1574.796 (27)	1.925	109.935 (3.331)	^{162}Dy	1840	
1585.360 (16)	1.7	263.215 (5.591)	^{162}Dy	1666	
1610.972 (26)		266.080 (15.360)			
1637.372 (25)	1.7	140.831 (3.488)	^{162}Dy	1637	
1647.687 (16)	1.775	361.040 (8.131)	^{162}Dy	1728	
1665.078 (18)	1.775	223.042 (5.032)	^{162}Dy	1745	
1685.695 (33)	2.0	129.259 (3.760)	^{162}Dy	1951	

Continued

TABLE 4.13

ALL DECAYS OBSERVED: ^{162}Dy

E_γ (keV)	Thresh. (MeV)	I_γ abs.	Origin	E_{level} (keV)	Notes
1701.886 (26)	1.85	52.493 (2.679)	^{162}Dy	1782	
1725.354 (39)	[†]	136.405 (4.725)	bkg	$^{208}\text{Pb}(\text{n},\text{n}'\gamma)$	
1728.321 (29)	1.85	129.035 (4.985)	^{162}Dy	1728	
1757.250 (102)	2.0	132.588 (4.867)	[⊗]		[★] $[A^2]$
1759.795 (63)	1.925	105.035 (2.993)	^{162}Dy	1840	
1773.654 (30)	2.2	246.807 (5.247)	[⊗]		[★] $[A^2]$
1778.848 (14)	[†]	503.480 (8.628)	bkg	$^{27}\text{Al}(\text{n},\gamma)$	
1782.541 (29)	1.85	214.099 (4.790)	^{162}Dy	1782	$[A^2]$ -placed
1787.095 (31)	2.0	177.804 (6.700)	[⊗]		[★] $[A^2]$
1805.890 (20)	1.925	476.203 (9.733)	^{162}Dy	1886	
1814.670 (20)	2.0	511.834 (11.294)	^{162}Dy	1895	
1902.017 (23)	2.0	366.455 (9.911)	^{162}Dy	1982	

Continued

TABLE 4.13

ALL DECAYS OBSERVED: ^{162}Dy

E_γ (keV)	Thresh. (MeV)	I_γ abs.	Origin	E_{level} (keV)	Notes
1918.538 (23)	2.1	401.636 (7.254)	^{162}Dy	1999	potentially $^{73}\text{Ge}(\text{n},\text{n}\gamma)$ doublet with background (unidentified)
1939.217 (81)	2.3	78.670 (3.337)	[‡]		
1942.544 (19)	[†]	204.334 (7.313)	bkg		
1950.812 (26)	~2.3	194.064 (4.664)	[‡]		
1982.342 (24)	2.0	429.197 (12.363)	^{162}Dy	1982	
1999.951 (28)	2.2	516.006 (12.427)	[⊗]		
2047.329 (30)	2.2	286.080 (6.065)	^{162}Dy	2125	
2067.759 (30)	2.2	294.084 (6.351)	[‡]		
2109.243 (95)	2.4	140.677 (3.860)	^{162}Dy	2189	
2111.981 (57)	<2.3	132.805 (4.279)	[‡]		
2124.122 (41)	2.3	159.010 (5.192)	[⊗]		
2128.643 (92)	2.2		[⊗]		[★] very low statistics

Continued

TABLE 4.13

ALL DECAYS OBSERVED: ^{162}Dy

E_γ (keV)	Thresh. (MeV)	I_γ abs.	Origin	E_{level} (keV)	Notes
2223.245 (21)	[†]	705.920 (22.408)	bkg	$^1\text{H}(\text{n},\text{d})$	used as a long-lived $F(\tau)$ 'calibrant'
2232.738 (95)	2.5	119.372 (3.553)	^{162}Dy	2314	
2239.929 (108)	2.6	141.186 (3.724)	^{162}Dy	2506	
2290.397 (104)	2.5	150.971 (4.446)	^{162}Dy	2371	
2305.762 (96)	2.5	171.415 (6.605)	^{162}Dy	2386	
2310.392 (89)	2.5	294.379 (9.312)	[‡]		
2315.363 (103)	2.4	91.237 (4.904)	[‡]	???	ExF does not match 2395
2323.726 (156)		66.339 (3.358)			
2331.301 (184)	2.7	121.744 (3.916)	^{162}Dy	2413	
2339.223 (134)	2.7	131.612 (5.132)	^{162}Dy	2338	
2346.871 (99)	2.5		^{162}Dy	2427	
2350.287 (175)		225.186 (13.310)			

Continued

TABLE 4.13

ALL DECAYS OBSERVED: ^{162}Dy

E_γ (keV)	Thresh. (MeV)	I_γ abs.	Origin	E_{level} (keV)	Notes
2360.440 (113)	2.5	105.996 (6.241)	[#]		[*]
2382.239 (120)	2.6		[#]		[*]
2390.254 (58)	[†]	74.443 (4.035)	bkg		
2395.010 (112)	2.4	114.428 (4.232)	^{162}Dy	2394	
2399.305 (134)	[†]	122.468 (6.482)	bkg		
2407.410 (127)	2.6	124.465 (5.250)	^{162}Dy	2488	
2417.161 (118)	2.6	116.520 (4.933)	^{162}Dy	2497	
2424.728 (166)	2.5	160.604 (4.627)	[⊗]		
2428.689 (107)	2.6	188.999 (6.585)	^{162}Dy	2510	
2438.349 (99)	2.6	184.794 (18.924)	^{162}Dy	2520	
2455.969 (295)	2.7	98.061 (3.800)	^{162}Dy	2537	
2470.100 (421)		140.857 (6.639)			

Continued

TABLE 4.13

ALL DECAYS OBSERVED: ^{162}Dy

E_γ (keV)	Thresh. (MeV)	I_γ abs.	Origin	E_{level} (keV)	Notes
2473.841 (112)	2.6	147.281 (11.689)	^{162}Dy	2554	
2479.469 (118)		117.953 (5.147)			
2489.552 (128)	2.6	187.124 (6.513)	[‡]	???	ExF does not match 2569
2492.495 (279)	2.7	96.375 (8.575)	[⊗]		[★]
2505.770 (143)	2.6	125.320 (7.327)	^{162}Dy	2506	
2511.291 (161)		106.273 (4.584)			
2516.713 (1392)		48.648 (5.320)			
2519.586 (115)	2.6	142.992 (4.806)	^{162}Dy	2520	
2527.923 (128)	[†]		bkg		UKY background
2532.614 (159)	2.7	117.331 (4.261)	^{162}Dy	2614	
2536.782 (147)	2.6	136.463 (4.552)	^{162}Dy	2537	
2552.567 (137)	2.9	123.938 (4.342)	^{162}Dy	2818	

Continued

TABLE 4.13

ALL DECAYS OBSERVED: ^{162}Dy

E_γ (keV)	Thresh. (MeV)	I_γ abs.	Origin	E_{level} (keV)	Notes
2554.600 (150)	2.7	106.138 (4.030)	^{162}Dy	2614	
2563.244 (341)		89.539 (4.989)			
2568.615 (141)	2.6	103.737 (4.847)	^{162}Dy	2569	
2576.711 (207)		59.373 (5.424)			
2586.345 (164)		147.886 (6.975)			
2590.526 (247)	2.6	87.177 (6.186)	^{162}Dy	2656	
2630.032 (230)	2.8	62.653 (3.161)	^{162}Dy	2630	low statistics
2655.583 (172)	2.8	106.138 (4.030)	[\otimes]		
2720.684 (176)	2.9	50.490 (15.032)	^{162}Dy	2802	
2734.232 (286)	2.9	56.949 (2.991)	^{162}Dy	2815	
2777.299 (271)	2.9	48.416 (4.752)	[\otimes]		
2783.474 (331)	2.9	54.723 (3.180)	[\otimes]		

Continued

TABLE 4.13

ALL DECAYS OBSERVED: ^{162}Dy

E_γ (keV)	Thresh. (MeV)	I_γ abs.	Origin	E_{level} (keV)	Notes
2959.198 (204)	2.9				not realistic
3101.594 (306)	3.0				not realistic

^{158}Gd

All γ rays observed in ^{162}Dy experimental campaign, with approximate energy threshold where first observed, the absolute intensity of the observed decay (taken from the $E_n=3.1$ MeV dataset), the origin and/or placement of the de-excitation in the level scheme (whether it is a prompt ^{162}Dy decay or a background), and any notes for the reader.

[†]: γ -ray excitation function is flat (definitive background)

[⊗]: γ -ray does not belong to ^{162}Dy (not populated by inelastic neutron scattering or energetically between any level in ^{162}Dy)

[★]: γ -ray does not fit energetically inbetween levels in ^{162}Dy , or with favored spin for $(n,n'\gamma)$ reactions.

[A²]: γ -ray observed, but not placed in [3].

[∅]: Origin of γ ray unknown (presumed to *not* be ^{162}Dy from energetics considerations)

CHAPTER 5

DISCUSSION AND INTERPRETATION

Lifetimes of the 13 positive parity states belonging to 4 positive parity bands and 11 negative parity states across the 4 negative parity bands in ^{160}Gd are discussed in this chapter, along with the 19 positive parity states spread across 9 positive parity bands and 18 negative parity states belonging to 7 negative parity bands in ^{162}Dy . Lifetimes are converted to transition probabilities in Weisskopf units to provide context to the transition rates between any collective states observed. Unless otherwise noted, transition probabilities are deduced from the experimentally measured quantities (γ -ray energies, γ -ray intensities, lifetimes, multipole mixing fractions, and associated measured uncertainties); particular cases where we do not observe a γ ray, and thus do not have intensities, energies or mixing information, use literature decay information where available (these cases are explicitly stated).

5.1 ^{160}Gd Discussion

5.1.1 Excited 0^+ States and the $K^\pi=2_2^+$ Band

The 0^+ excitations in ^{160}Gd serve to highlight some of the distinct advantages of $(n,n'\gamma)$ studies performed at UKAL. Previous literature assertions list four 0^+ excitations in ^{160}Gd , from various experiments, two of which are tentative assignments [7, 28]. In [52], we exploit two facets from the angular distribution and excitation function measurements to rule out the two tentative assignments. First, angular distributions for γ radiation leaving a 0^+ state must be isotropic, and secondly, that

energy thresholds of a γ -ray leaving a 0^+ state will come in at precisely the level energy (recall that there is no extra energy needed to make non-zero angular momentum transfers).

The previous assignment of a 0^+ excitation at $E_{lev}=1325.73$ keV was made by [7] in a $(n,n'\gamma)$ reaction using continuous energy reactor neutrons, with a refutation of this assignment made in this work and by angular distribution measurements performed in [35]. The justification for this refutation of a $J=0$ assignment is shown in Figure 5.1, a clearly anisotropic angular distribution of the $E_\gamma=1250.4$ keV de-excitation, explicitly stating that this radiation cannot stem from a 0^+ excitation. A similar check was made via the normalization of angular distributions; absolute intensities of γ rays were normalized so that radiation from the lowest-lying 0^+ state is isotropic. In the case where we used a normalization to this $E_\gamma=1250.4$ keV γ ray, angular distributions of well-behaved dipole and quadrupole radiation (*e.g.* E2 radiation from strong ground-state band transitions) ceased to exhibit the expected behavior of a classically oscillating charge distribution from Figure 2.6. Contrast this catastrophic result from this normalization attempt to the one in use by normalizing to the $E_\gamma=1304.46$ keV from the 1379 keV state, and we see the return of ‘concave-up’ angular distributions for quadrupole radiation, leaving us with a clear choice for normalization and furthermore pointing away from the assignment of the 1325 keV state as a 0^+ excitation.

The second tentative 0^+ excitation at $E_{lev}=2236$ keV was placed in [28] via a (t,p) transfer reaction study; we also reject this assignment based on, again, the non-isotropic nature of γ -radiation from the single observed $E_\gamma=2162.74$ keV de-excitation, as well as a threshold energy below that of the excitation energy of the state. This creates a completely illogical and unphysical system, where a γ -ray is populated below the energy of the state, and as such, cannot be attributed to this

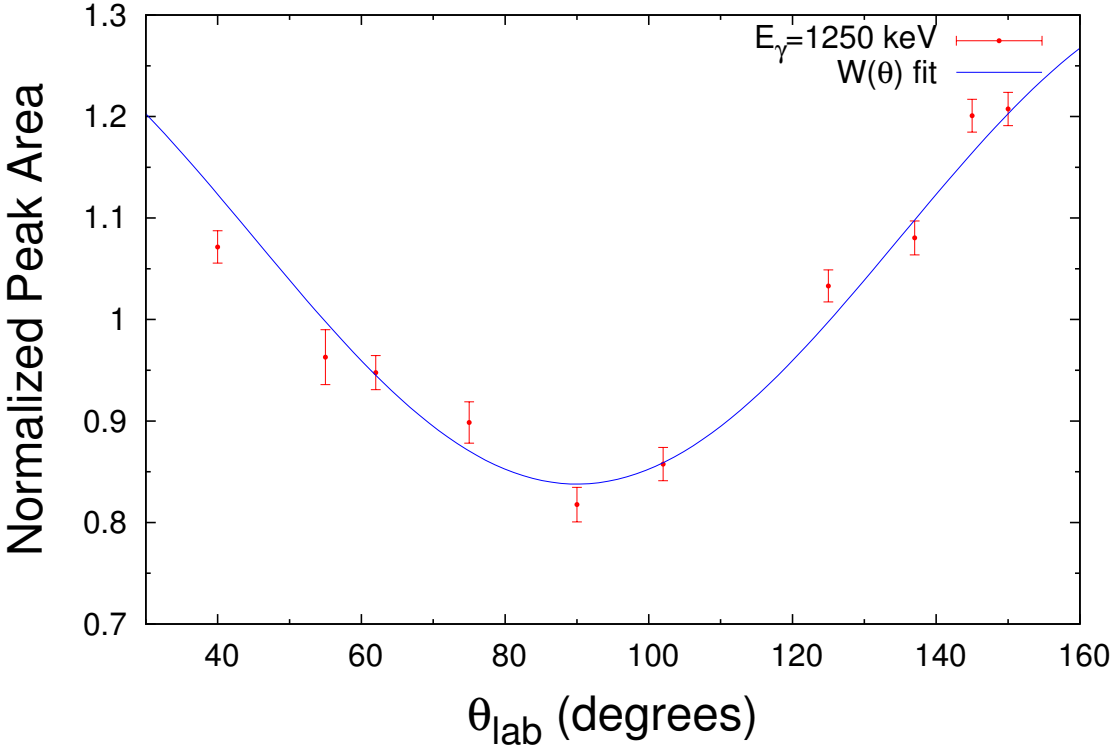


Figure 5.1. Non-isotropic decay from the tentative 0^+ state in ^{160}Gd at $E_x=1325$ keV.

excitation. The excitation function measurement for this decay can be seen in Figure 5.2, with a threshold clearly below 2100 keV.

This leaves only two 0^+ excitations remaining in ^{160}Gd as candidates for either a single-phonon β vibration or a double-phonon ($\gamma\gamma$, double octupole, etc) type, now labeled as the 0_2^+ and 0_3^+ bands. A corresponding level scheme with the decays out of $K^\pi=0^+$ bandmembers is shown in Figure 5.3.

Six (6) γ rays were detected to determine the lifetimes of three levels in the $K^\pi=0_2^+$ band in our $^{160}\text{Gd}(n,n'\gamma)$ experiments. Decays leaving the 0_2^+ band display varying levels of collectivity based off our lower-limit lifetime measurements in the band (at least >320 fs for each state). In terms of offering a concrete case for

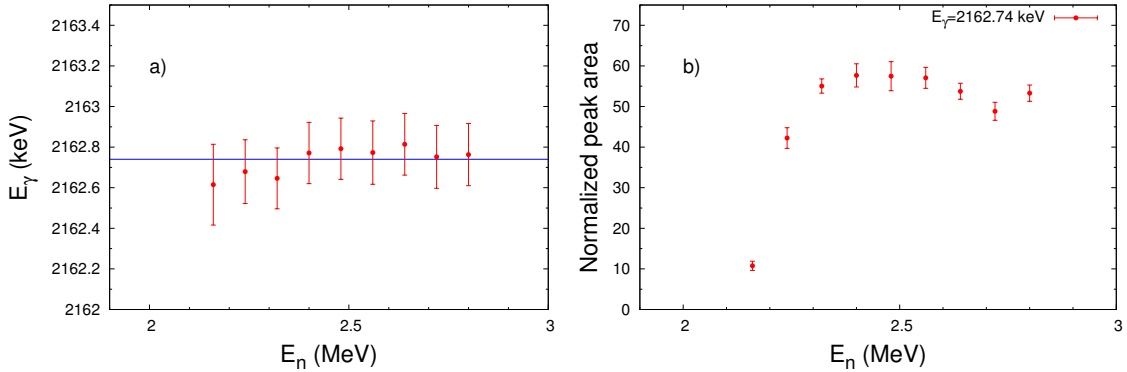


Figure 5.2. Excitation function measurement from the tentative 0^+ state in ^{160}Gd at $E_x=2236$ keV.

assessing this band as a β -vibration, we can tentatively point to this band as a single-phonon quadrupole vibration from its potentially strong transition probabilities to the ground state (or from our measurement of upper limits on the collectivity). Given the limitations of what lifetimes DSAM can measure, we are left with an obviously murky picture for any possible β -vibration in ^{160}Gd due to our measurement of lifetime limits, although the potentially collective decays to the ground state tend to suggest some (albeit weak) β -vibrational interpretation of this band at $E_x=1379$ keV. Due to the lack of intraband transitions observed in our experiment, we cannot place any two-phonon characteristics to this set of excitations, as we should expect strong $B(E2)$ values connecting the 0_2^+ band to the 2_γ^+ band at $E_x=988$ keV. An ideal situation for further study includes the refinement of the lifetime measurements of this band via another measurement technique to concretely assign a β -vibration to this band, as the collective upper limit is *indicative* of a β -vibration, but is not conclusive enough to say for certain.

A similar, yet also contrasted story emerges with the discussion of any single-phonon characteristics in the 0_3^+ band at $E_x=1558$ keV; six (6) γ rays were detected to measure the lifetime of two states in the $K^\pi=0^+$ band. The decays to the ground

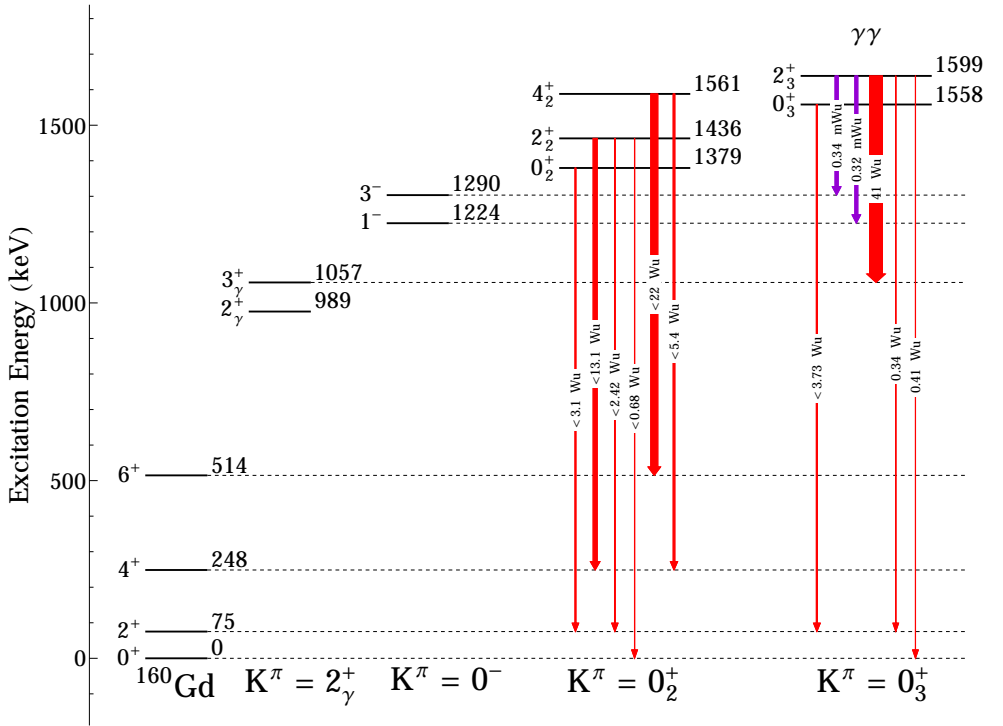


Figure 5.3. Level scheme showing the calculated B(E2) in W.u. and B(E1) in mW.u. for the confirmed 0^+ excitations in ^{160}Gd .

state exhibit characteristically weak collectivity (<4 W.u. for the bandhead and <0.5 W.u. for the 2^+ member), pointing away from the interpretation as a β -vibration. However, the refinement of the 1599 keV state's lifetime opens up key discussion for the 0_3^+ band. We have measured a γ ray that corresponds to an intra-band transition, namely to the $K^\pi=2^+$ γ -vibrational band, with an inflated B(E2) value of 41_{-37}^{+16} Weisskopf units. While the uncertainty of this transition probability is large due to the measured lifetime's uncertainty, this strong, preferential decay is indicative of signatures for the antialigned ($K=0$) double-phonon $\gamma\gamma$ -vibration. Our measurement of the angular distribution for this γ ray led to our overwhelmingly

E2-type mixing ratio ($\delta = -5.57_{-5.00}^{+1.91} \rightarrow 96.8\%$ E2). Of further note, the 0_3^+ band displays some slightly inflated transition probabilities to the lowest lying $K^\pi=0^-$ band at ~ 0.3 mW.u. strength. These somewhat inflated $B(E1)$ probabilities would otherwise be indicative of some double-octupole phenomena in the nucleus, but with the presence of the extraordinarily large $B(E2)$ to the γ -vibrational band, more interest and a higher feasibility is placed on the interpretation of this band as a double quadrupole vibration ($K^\pi=0^+$, $\gamma\gamma$ -type).

Staying within the same vein of quadrupole excitations, we turn our attention to any γ -vibrational characteristics of ^{160}Gd . While the nature of $K^\pi=2^+$ bands is not as heavily debated as the 0^+ bands [18, 39, 44, 56], our lifetime measurements of the states in this γ -vibrational band warrant discussion, as any collective excitations built on-top of this band should be a multiphonon configuration. The decays observed from the lowest $K^\pi=2_\gamma^+$ band are shown in Table 4.2 and Figure 5.4. Overall, we see systematically expected behavior (inflated levels of collectivity averaging about 5-10 W.u.) in terms of the strength of the other 2_γ^+ excitations in the rare-earth region of nuclei [38, 48, 55, 56], and as such, we can assign and confirm this band as a quadrupole γ -vibration in ^{160}Gd . Generally, it is prudent to obtain this base-level of collectivity in the nucleus to compare the feasibility of other phonon excitations, or to make claims on any two-phonon characteristics in ^{160}Gd . We are yet again presented with the well-behaved γ -vibration that has stood the test of time for and has been a figurehead in nuclear structure in deformed rare-earth nuclei.

5.1.2 Negative Parity States

The determination of any reflection-asymmetry and thus, potential octupole shape correlations in ^{160}Gd will lie in the measurement of $B(E1)$ transition probabilities of de-excitations from the low-lying negative parity states. The decays from all observed negative parity bands in ^{160}Gd are shown in Figure 5.4 alongside the $K^\pi=2_\gamma^+$ decays

from the previous section. The tabulated results from all E1 decays observed in the experiments can be seen in Table 4.3.

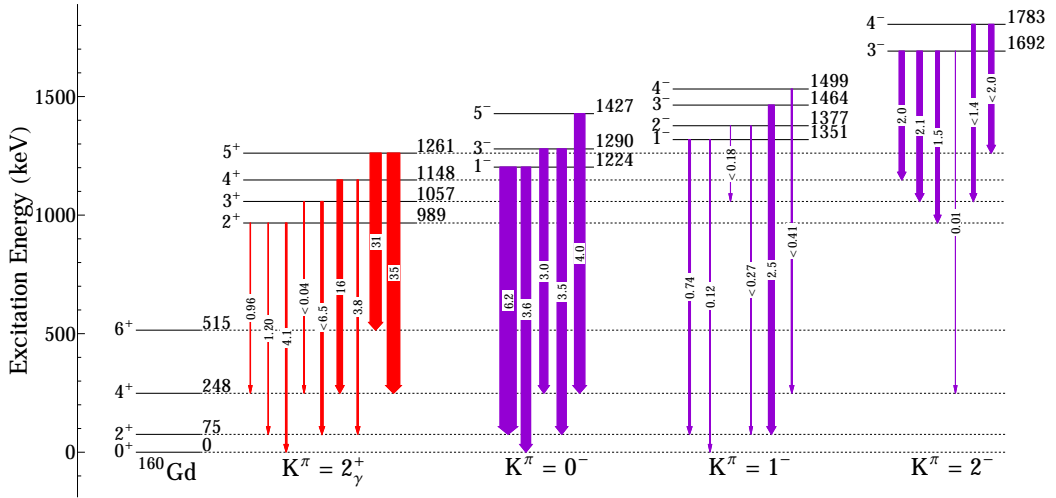


Figure 5.4. Level scheme showing the decays with calculated reduced transition probabilities for the $K^\pi=2^+_\gamma$ band and low-lying negative parity states in ^{160}Gd .

The deduced $B(\text{E}1)$ s from the $K^\pi=0^-$ band show large inflation of collectivity from these states, strongly indicating a well-behaved octupole vibration in ^{160}Gd . This octupole collectivity in the $B(\text{E}1)$ s are corroborated by the experimentally measured and distinctly collective $B(\text{E}3; 0^+ \rightarrow 3^-)$ transition probability ($0.118(7) \text{ e}^2\text{b}^3$) by [56].

We also measure comparably short lifetimes for two of the four members that result in distinctly collective (yet not as collective as the $K^\pi=0^-$ band), indicating that this band could indeed be a part of the fragmented octupole vibration in ^{160}Gd .

The shallow values for $F(\tau)$ in this state cannot offer a concrete idea of the collectivity of the state. A similar argument applies for the 4^- state at 1498 keV, where we only observe a shallow shift from the Doppler plots; luckily, these other members of the 1^- band can offer some insight from the well-defined lifetime measurements. Overall, the observation of moderately inflated levels of collectivity in the band seems to indicate that these rotational members of the $K^\pi=1^-$ band are indeed a part of the octupole vibration.

We measure distinct collectivity from the 3^- member of the $K^\pi=2^-$ band connecting to the γ -vibrational band, following a recent trend of observation by [60, 73] of strong E1 radiation in $2^- \rightarrow 2^+$ transitions. The same trend of (potentially) collective E1s to the γ -vibrational band occur in the 4^- member of the band, where we only have a lower limit to the lifetime. This is obviously a curious behavior and needs more work to assign any conclusive detail to the rotational band. B(E3) transition probabilities to the γ -band are critical in achieving this goal; barring those measurements, only the ideas presented in current, developing works can be applied, but this is still a significant contribution to the total E1 strength in deformed nuclei, whether or not it is a part of the octupole vibration. Furthermore, we can safely adopt this $K^\pi=2^-$ assignment from the well-behavedness and agreement of the deduced B(E1)s in comparison to the Alaga rules (Table 5.1).

Our measurement of lifetimes in the lowest-lying negative parity bands begs the question: where is the 3^- member of the traditional octupole multiplet? Or at least, if this band is *not* the $K^\pi=2^-$ band and instead the $K^\pi=3^-$ band, where is the missing part of the octupole quartet of states? Population of $\Delta K=3$ states is difficult (but not impossible) to accomplish with $(n,n'\gamma)$ reactions, but the states would be very weak, and we may simply lack the statistics needed to observe such states with any reliability. In a soon to be echoed tone throughout this work, more sensitive experiments (or much higher statistics in terms of beam time, reaction

rates, etc) are needed to have fully spectroscopy and measurement of lifetimes in ^{160}Gd . Especially from our observation of negative parity states that do not decay strongly to the ground state (the $K^\pi=2^-$ band), the traditional picture of fragmented octupole collectivity seems tentative as we approach the rotational limit ($R_{\frac{4}{2}} \sim 3.3$).

5.1.3 Other Lifetime Measurements in ^{160}Gd

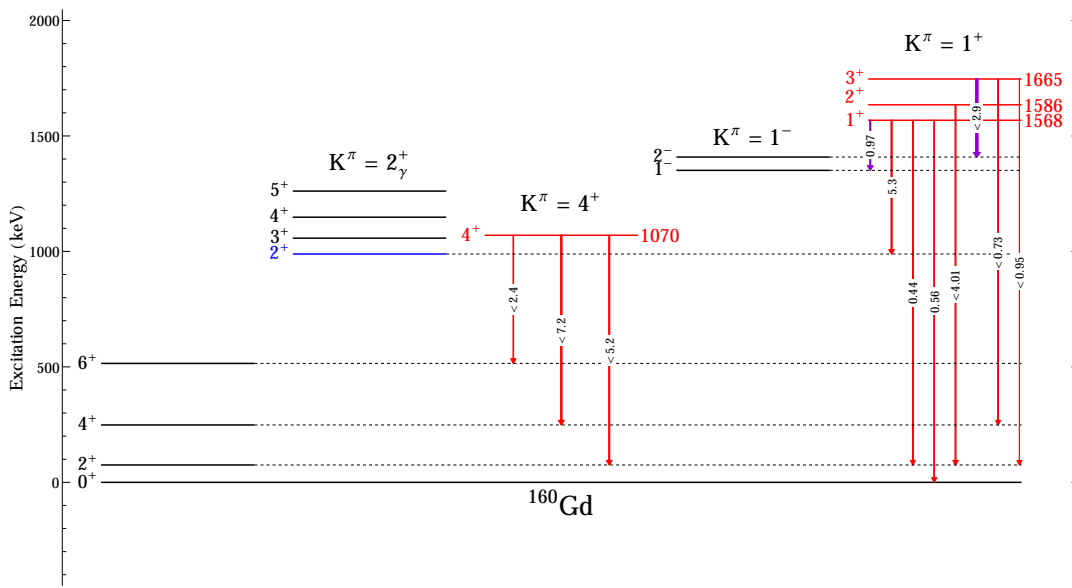


Figure 5.5. Level scheme showing the decays with calculated reduced transition probabilities for the $K^\pi=4^+$ and 1^+ bands in ^{160}Gd .

5.1.3.1 $K^\pi=4^+$ Band as a Hexadecapole Vibration?

The study of even, positive parity states continues into the interpretation of $K^\pi=4^+$ bands in deformed nuclei. We know from earlier assertions, that a $\gamma\gamma$ two-phonon vibration can have this $K=4$ angular momentum projection, but must also exhibit strongly collective decays to the γ -band, as each phonon must be ‘broken’ individually, and in single steps. Any existence of this $\gamma\gamma$ -type behavior in ^{160}Gd is already dubious from energy considerations, as the expected energy for a harmonic two-phonon state should be roughly double the energy of the single-phonon counterpart. The $E_x=1070$ keV state lies 100 keV above the γ -vibrational band, and in our measurement of the lifetime of this single 4^+ bandhead of the $K^\pi=4^+$ band, we find somewhat enhanced $B(E2)$ transition probabilities to the ground state, with no de-excitations or preference of decay to the γ -vibrational band. This implies a lack of two-phonon characteristic in this excitation, and instead points towards a single phonon vibration of order $\lambda=4$; this hexadecapole nature is yet another expansion of the dynamic deformation in the geometric model set out by Bohr and Mottelson, and has been investigated in several works [18, 61, 76] for spherical and nearly-spherical nuclei. Again, much like the need for strong $B(E3)$ radiation in determining octupole characteristics, the direct observation of $E4$ radiation depopulating $K=4$ bands would fully elucidate any hexadecapole nature in these states. We can, however, not say anything about hexadecapole vibrational characteristics in ^{160}Gd with $B(E2)$ measurements alone. Any assertions made would be tentative, as we are only able to extract a lower limit to the lifetime of this state at 1070 keV; further spectroscopy is needed to concretely say anything about the makeup of this state. That being said, Soloviev has produced quasiparticle-phonon calculations that surmise this 4^+ state to be mostly hexadecapole in nature [76]. Tangible experimental evidence for hexadecapole phonon behavior is nearly unprecedented in well-deformed nuclei, which our data could be one of the first signatures of this structure. This curious behavior in

^{160}Gd begs further research, and, if this band is confirmed as a hexadecapole vibration built on top of the deformed ground state, it would be one of the lowest excitation energies of its kind, especially in a well-deformed nucleus.

5.1.3.2 $K^\pi=1^+$ Band

Our measurement of lifetimes for the $K^\pi=1^+$ band yields some interesting discussion in a potential quasiparticle-phonon coupling to either the established 1^- band mentioned in §5.1.2, as well as the γ -vibrational band. We measured lifetimes for the 1^+ , 2^+ , and 3^+ members of this band, with several intraband transitions. Overall, we observe generally weak collectivity from members of this band to the ground state, with enhanced E1 transitions to the weakly collective $K^\pi=1^-$ band; normally and at first glance, this would imply some double-phonon collectivity, but this picture is obscured with a discretely preferential decay to the γ -vibrational band. This ~ 5 W.u. B(E2) is hard to ignore, given its large branching ratio (30%), especially in the context of strong intra-band transitions to known vibrational states in deformed nuclei. The most realistic outcome of interpretation of this band is of purely quasiparticle nature, where there is a strong implication that a majority of the corresponding nuclear wavefunction overlaps with the predominant configuration of the γ -vibrational band. Following in line with the major contributions to γ -vibrational bands in deformed nuclei from [20], we should expect and there is implication that significant overlap with the Nilsson neutron wavefunctions of $\nu(\frac{3}{2}[521]+\frac{1}{2}[521])$ exist for these states.

The inflated level density, uncertain spin-assignment, and higher probability for state-mixing to occur [20] make band-assignments for these states well above the pairing gap increasingly difficult. That does not imply that the lifetimes measured are of diminished value; several instances of subtle nuclear structure exist at the higher energies studied in our experiments, such as the upcoming isovector dipole resonance in

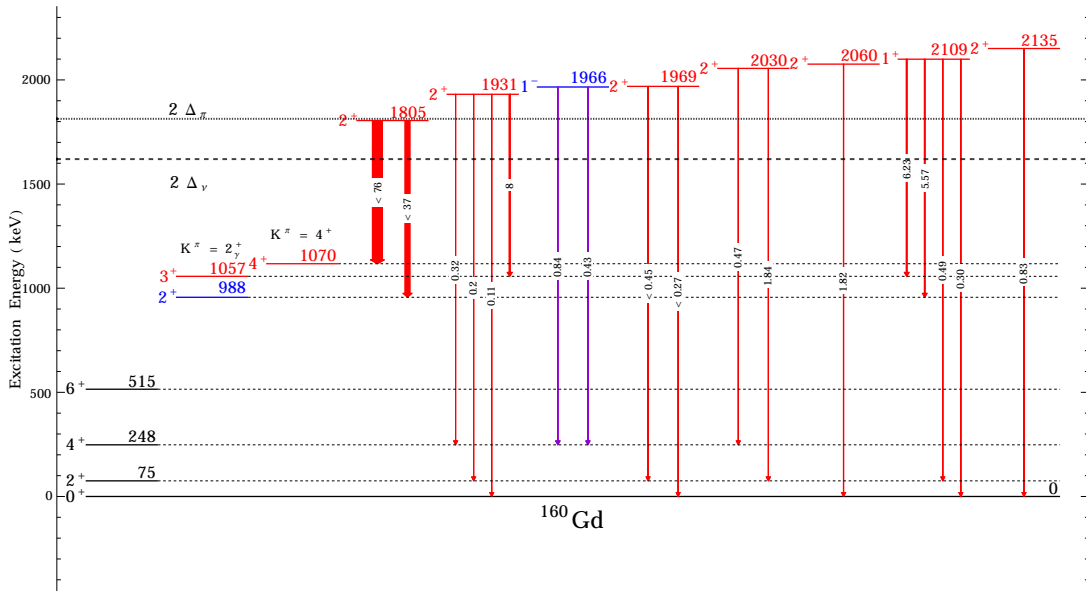


Figure 5.6. Level scheme showing the decays with calculated reduced transition probabilities for the levels that are not assigned to rotational bands in ^{160}Gd . Note the neutron and proton pairing gaps drawn as dotted lines ($2\Delta_\nu \sim 1625$ keV and $2\Delta_\pi \sim 1810$ keV).

^{162}Dy . We have also not exhausted every possible two-phonon candidates in deformed nuclei, as the excessively rare ‘ $\beta\gamma$ ’-type that would have a K-projection of 2^+ . The signatures for this excitation follow the case for any two-phonon vibration, enhanced E2 transitions to a well-established vibrational band (in this case either a ‘ γ ’ or ‘ β ’ vibration). The best such candidate for a $\beta\gamma$ vibration is the 2^+ state at 1931 keV. We measure four decays from this state, and have a very well-defined lifetime from the Doppler Shifted γ rays. The $B(\text{E}2)$ probabilities here are very indicative of collective behavior built on top of the γ -band, with a collective 8 Weisskopf unit transition to the γ -band via a mostly ($\sim 92\%$) E2 decay to the 3^+ member. To say that this is indeed a two-phonon collective vibration would be cavalier, of course, since we do not have complete and unambiguous assignment of the β vibration. Since there are no other decays to the γ -vibrational band, we cannot make an Alaga comparison

of transition strengths, and unfortunately, the large error (upper bound) shows the limiting power of DSAM near picosecond lifetimes. That all being said, given any rotational band assignment of this state, it could be a key asset in the search for a $\beta\gamma$ -type vibration, and as we will see, the viability for anharmonic multiphonon configurations below an energy ratio of 2.

In the remaining states, we see some more of the mirrored assertions on any $K^\pi=1^+$ bands, with a strong coupling to the γ -vibrational band coming from another 1^+ state at 2109 keV. Of course, the macroscopic treatment of quadrupole vibrations by Bohr and Mottelson do not attribute any $K^\pi=1^+$ bands [12], so these states *must* be of single- or multi-quasiparticle configurations. Yet again, the significantly preferred branching ratio and $B(E2)$ strengths to the 2^+ band implies a dominant quasiparticle configuration involving the $\nu(\frac{3}{2}[521]+\frac{1}{2}[521])$ shell using Nilsson model considerations.

5.1.4 Implications and Further Discussion

In terms of a vibrational phonon model, we have measured new lifetimes for key states in ^{160}Gd , the first being a potential (read: tentative) β -vibration existing as the lowest 0^+ state at 1379 keV. However, our assignment here is not conclusive enough to say for certain, as we only have upper limits to the collectivity, yet the potential for large $B(E2)$ probabilities exists (>7 W.u. in strength for some transitions). This level of collectivity above 5 W.u. strength is in line with the assertions made by Garrett [30] on a concrete β -vibration assignment, however, this is only one possible interpretation, and again, we only have limits for measured $B(E2)$ s in this lowest 0^+ band. This certainly does not spell doom for the feasibility of the β vibration, as we can still imagine a distinctly collective transition strength from the members of the 0_2^+ band. For multiphonon quadrupole vibrations in ^{160}Gd , we do see a fairly definitive excitation of the $\gamma\gamma$ -vibration as the third 0^+ state at 1558 keV via a highly collective

transition from the 2^+ member of the band to the γ -vibrational band. Speaking of the γ -vibration, we measured lifetimes for the four lowest-lying members of the $K^\pi=2^+$ band that leads to the trademark $\sim 6\text{-}7$ W.u. collectivity for the γ -vibrational band.

The measurement of lifetimes in the negative parity bands yields some expected results from the systematic study of states in the region, with two well-defined octupole members (0^- and 1^-), and a curious emerging decay pattern of $K^\pi=2^-$ bands to the γ -vibrational state. In all of these states, we measured distinctly inflated $B(E1)$ transition probabilities, indicating some amount of dipole strength or asymmetry in the nuclear shape. In the case of the 0^- and 1^- bands, literature $B(E3)$ values aid in the assessment of an octupole vibration built on top of the deformed ground state, and we have opened the question to find the remaining members of the vibration expected from the base Bohr-Mottelson formulation of the geometric model.

Comparisons of the deduced $B(E2)$ and $B(E1)$ transition probabilities to the Alaga rules round out our discussion of the lifetimes measured in ^{160}Gd . The ratios of our experimental transition probabilities and the Clebsch-Gordan coefficients squared are shown in Table 5.1, where we observe somewhat mixed agreement for the various bands in ^{160}Gd . The comparison of our deduced $B(E2)$ limits for the 0_2^+ band seems to be in stark disagreement, however, our measurement of upper limits of $B(E2)$ s does not exclude agreement for *any* combination of $B(E2)$ value. For the 0_3^+ band, we note reasonable agreement (within the full range of uncertainty) for the Alaga comparisons; this includes both the decay channels to the $K^\pi=0^-$ octupole band and to the ground state band. The 2_γ^+ band is in reasonable agreement within error where we have convergent lifetimes (the 4^+ and 5^+ members), but we mirror the same assertions as the 0_2^+ band, where the disagreement for the upper limits of $B(E2)$ do not offer much insight. Lastly, all of the negative parity band comparisons to the Alaga rules offer good agreement! Furthermore, the agreement of the $K^\pi=2^-$ band's measured $B(E1)$ s imply that the $K^\pi=2^-$ assignment is valid, since a $K^\pi=3^-$ assignment would produce

wildly variant Alaga expectations (*e.g.* the ratio of Clebsch-Gordan coefficients in the K=3 case are 0.14, 0.05, 0.35 and 0.11 going down the table in the same order).

TABLE 5.1

ALAGA: ^{160}GD

K^π	$\frac{J_i \rightarrow J'_f}{J_i \rightarrow J''_f}$	CG ²	Exp
$K^\pi = 0_2^+$	$\frac{2^+ \rightarrow 4^+}{2^+ \rightarrow 2^+}$	1.8	5.4
	$\frac{2^+ \rightarrow 4^+}{2^+ \rightarrow 0^+}$	2.6	19
	$\frac{2^+ \rightarrow 2^+}{2^+ \rightarrow 0^+}$	1.4	3.6
	$\frac{4^+ \rightarrow 6^+}{4^+ \rightarrow 4^+}$	1.8	4.1
$K^\pi = 0_3^+$	$\frac{2^+ \rightarrow 3^-}{2^+ \rightarrow 1^-}$	1.5	1.1
	$\frac{2^+ \rightarrow 2^+}{2^+ \rightarrow 0^+}$	1.4	0.8
$K^\pi = 2_\gamma^+$	$\frac{2^+ \rightarrow 2^+}{2^+ \rightarrow 0^+}$	1.4	0.3
	$\frac{3^+ \rightarrow 4^+}{3^+ \rightarrow 2^+}$	0.4	0.01
	$\frac{4^+ \rightarrow 4^+}{4^+ \rightarrow 2^+}$	2.9	4.2
	$\frac{5^+ \rightarrow 6^+}{5^+ \rightarrow 4^+}$	0.6	0.9
$K^\pi = 0^-$	$\frac{1^- \rightarrow 2^+}{1^- \rightarrow 0^+}$	2.0	1.8
	$\frac{3^- \rightarrow 4^+}{3^- \rightarrow 2^+}$	1.3	0.9
$K^\pi = 1^-$	$\frac{1^- \rightarrow 2^+}{1^- \rightarrow 0^+}$	0.5	0.7
$K^\pi = 2^-$	$\frac{3^- \rightarrow 4_\gamma^+}{3^- \rightarrow 3_\gamma^+}$	1.3	1.0
	$\frac{3^- \rightarrow 4_\gamma^+}{3^- \rightarrow 2_\gamma^+}$	1.8	1.4
	$\frac{3^- \rightarrow 3_\gamma^+}{3^- \rightarrow 2_\gamma^+}$	1.4	1.3
	$\frac{4^- \rightarrow 5_\gamma^+}{4^- \rightarrow 3_\gamma^+}$	1.4	1.4

Alaga comparisons of $B(\pi\ell)$ transition probabilities in ^{160}Gd measured in our experiments.

5.2 ^{162}Dy Lifetimes

In the remaining level schemes in Chapter 5, the widths of transitions are proportional to the calculated reduced transition probabilities for a particular γ -ray and are scaled and normalized to guide the eye; for example, a 1 mW.u. B(E1) is approximately equal in width to a 5 W.u. B(E2) transition strength and ~ 0.1 W.u. for a B(M1), unless otherwise noted in a particular section of discussion. This scaling is in line with the understanding that enhanced E1 transitions are ~ 1 mW.u., large E2 transition strengths are > 5 W.u., and inflated M1 transitions are ~ 0.1 W.u. in strength. To further aid the eye, E1, E2, and M1 multipolarities are colored discretely, with E1 transitions being violet, E2 transitions colored red, and M1 transitions in green.

5.2.1 0^+ Excitations Not Observed in $(n,n'\gamma)$

γ rays were not observed for every excited 0^+ state seen in (p,t) experiments by [58] in ^{162}Dy , namely the excitations at 1814.6, 1820.3, 2588, and 2663 keV (Table 5.2). Figure 5.7 shows cuts of our γ -singles spectra above the level energy thresholds where we would expect to see the full energy ($0_i^+ \rightarrow 2_{gs}^+$ transitions at the drawn vertical lines) de-excitations of the aforementioned states. Locally, there are no obvious peaks above our background, with the exception of the expected γ -ray leaving the 2588 keV state; if this peak exists, it would be a doublet with a γ at 2506 keV, belonging to a state of the same energy, making its energy shift unreliable and thus difficult to extract a lifetime with DSAM.

The tentative 0^+ assigned in [58] as a probable contaminant at $E_x=774.2$ keV was not observed in our experiment. The only decay channel available to such a state was not observed at $E_\gamma \approx 693.5$ keV ($(0_{774.2}^+ \rightarrow 2_{g.s.}^+)$), due to the prominent Ge(n, γ) detector background at the expected peak location. A generous upper limit can be

TABLE 5.2

OBSERVED 0^+ STATES: ^{162}DY

0_i^+	E_x	Observed?
[†]	774.2 (3)	[†]
0_2^+	1398.3 (3)	✓
0_3^+	1666.3 (4)	✓
0_4^+	1814.6 (5)	
0_5^+	1820.3 (5)	
0_6^+	2126.5 (6)	✓
0_7^+	2496.7 (7)	✓
0_8^+	2588.8 (7)	
0_9^+	2655.3 (7)	✓
(0_{10}^+)	2663.0 (7)	
(0_{11}^+)	2802.9 (7)	✓

Observed 0^+ states in our $(n,n'\gamma)$ experiments compared with (p,t) experiments from [58], with [†] as the labeled ‘contaminant’ at $E_x=774.2$ keV.

set to the intensity of any peak on top of this background of 3% of the intensity of the strong 807 keV γ ray that de-excites the γ -band bandhead. This upper limit is well below half of the intensity of the lowest intensity γ rays observed in this $(n,n'\gamma)$ study, and as such, we are unable to measure a lifetime for this state using the Doppler Shift Attenuation Method. Govor in [34] observes an unplaced γ ray at 694.19 keV (well within the detector resolution to consider this γ ray as a candidate) at a lower intensity than our upper limit discussed above; it is entirely possible that this state exists, but the experiments so far have lacked the sensitivity to detect the de-excitation at \sim 693.5 keV. The ‘contaminant’ state at 774.2 keV is not observed in any other ^{162}Dy studies ($(\alpha,2n)$, (n,γ) , $(n,n'\gamma)$, etc [3]), further justifying its lack of

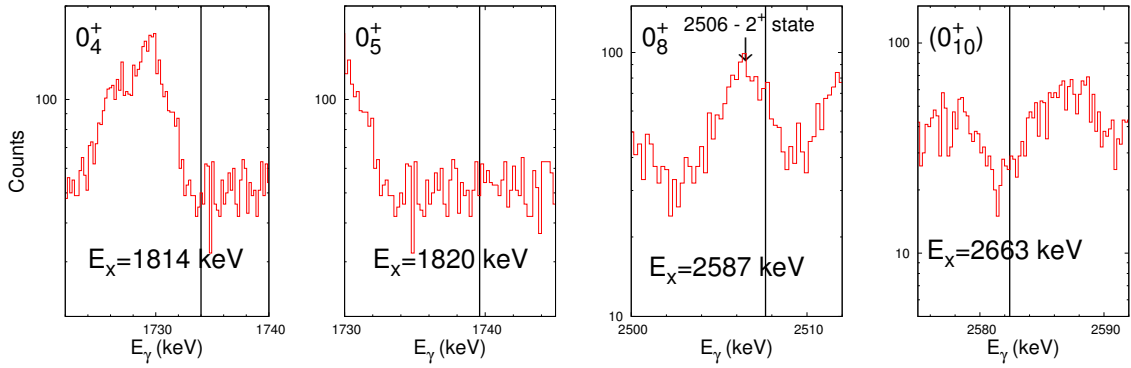


Figure 5.7. Singles spectra cuts where remaining 0^+ excitations should be observed. Spectra for $0_{4,5}^+$ placements are from the $E_n=1.925$ MeV excitation function measurements, with $0_{8,10}^+$ from the $E_n=2.9$ MeV dataset.

detection in this campaign of experiments. We emphasize the use of other reactions such as $(\alpha,\alpha'\gamma)$ to remove the (n,γ) background in hopes of finding this state at 774.2 keV.

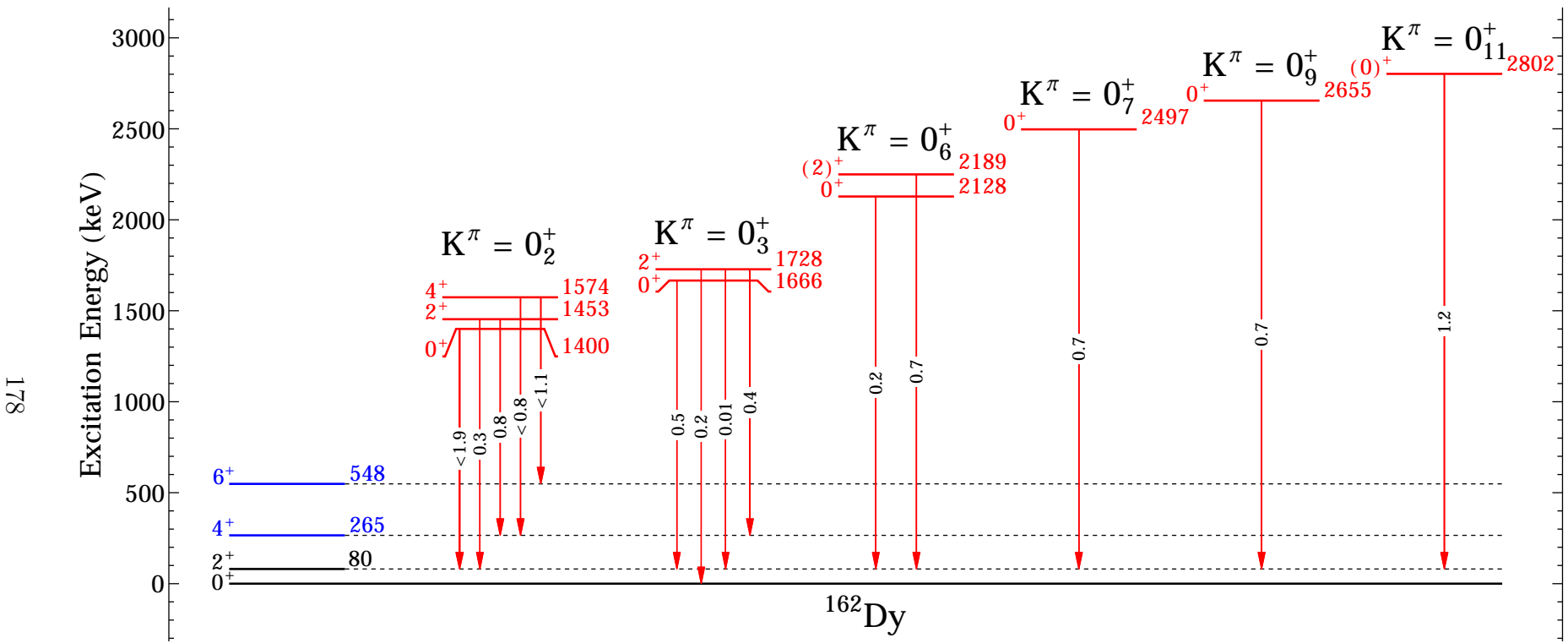


Figure 5.8. Level scheme outlining all measured lifetimes for $K^\pi=0^+$ bands in ^{162}Dy . New lifetime measurements are shown in red (color online), and new $B(E2;0_i^+ \rightarrow \text{g.s.})$ calculations are expressed in Weisskopf units (W.u.).

5.2.2 A Lack of Strong β Vibrations in ^{162}Dy

As it stands from our measurement of the lifetimes, the generally weakly-collective ($B(E2) < 2$ W.u.) transitions to the ground state band point away from a single-phonon β -vibration assignment for *any* observed 0^+ state in ^{162}Dy , shown in Table 4.7. Common allegations on the collectivity of a β -vibration are that the $B(E2; 0_i^+ \rightarrow 2_{g.s.}^+) \sim 12\text{-}33$ W.u. [30], with decays from higher-lying members of the band falling around 6-10 W.u. in strength, when in reality, this behavior is far from common across the nuclear landscape. While the E0 strengths are not available for the states in the 0^+ bands of ^{162}Dy , and the two nucleon transfer reaction cross sections to all but one 0^+ excitation are small (<10.6% of the ground state cross section [58]), order of magnitude differences in the above assertions on $B(E2)$ strength, and the low absolute value of our $B(E2)$ measurements do not lend credence to this β -vibration picture. In addition, the evaluation of upper limits to the $B(E2)$ strength in a few cases is not conclusive enough to confirm any band as a β -vibration, even in the face of a potentially collective transition to the ground state at 1.9 Weisskopf units. Traditionally, the lowest lying $K=0,2$ bands were tenaciously defended as quadrupole vibrations, but this paradigm has evolved as the experimental data trickles in, and as the unclear nature of 0^+ excitations in deformed nuclei is noted [31, 70]. The search for higher-lying collective 0^+ excitations in ^{162}Dy has merit, as both ^{166}Er and ^{158}Gd show signs of strong (> 2 W.u.) collectivity in states above the first excited 0^+ band [32, 51], but again, the findings fail to reveal any concrete signature of a strongly collective β -vibration at *any* excitation energy in ^{162}Dy . The most likely candidate and correspondingly most collective $B(E2)$ ($1.2_{-0.6}^{+2.3}$ W.u.) to the ground state lies in the 0_{11}^+ state at 2802 keV excitation energy. *If* this state is the true β vibration in ^{162}Dy and the state at 774.2 keV is *not* the lowest 0^+ , it follows the empirical behavior of well-deformed rare-earth nuclei, where the β mode of quadrupole vibration does not exist as the lowest-lying $K^\pi = 0^+$ band. The curious lack of an observed collective

β vibration in our data is alarming, but must not forget the unobserved excitations below the pairing gap(s) at 774, 1814, & 1820 keV, as any one of these states *could* be the collective β -vibration in ^{162}Dy .

5.2.3 On the Two-Phonon Characteristics

With the experimental evidence of two-phonon quadrupole vibrations in nearby rare-earth nuclei (^{178}Hf), impetus is given to further examine any multiphonon configurations in the 0^+ states in ^{162}Dy .

5.2.3.1 2_γ^+ Band

The axial symmetry-breaking γ vibration has stood up as one of the benchmarks and cornerstones of quadrupole surface vibrations in the geometric model. While not as enigmatic in behavior as their $K^\pi=0^+$ counterparts (the proposed β vibration), the lowest $K^\pi=2^+$ band provides the basis of understanding nuclear collective motion in deformed nuclei. Lifetimes of the $K^\pi=2^+$ band up to $J=5$ were measured and are shown in Table 4.8 and Figure 5.10. Systematics for the γ -vibrational band decays to the ground state across the even Dysprosium nuclei show inflated levels of collectivity on the order of ~ 5 W.u. in strength [38, 56], where similarly collective (~ 4 W.u.) transitions in the $(n,n'\gamma)$ experiments is observed; this gives a reasonable, unambiguous assignment as the $K^\pi=2^+$ γ -vibration in ^{162}Dy , and provides the foundation for the multiphonon configurations in the nucleus. Since the deduced $B(E2)$ does not offer refinement beyond the previously measured transition probabilities from Coulomb Excitation, the measured value is reported, but literature values are adopted in the discussion.

5.2.3.2 0_2^+ Band $\gamma\gamma$ -Vibration

Considerable theoretical and experimental focus [8, 39, 58, 83] has been placed into the assessment of the 0_2^+ band as a $\gamma\gamma$ -vibration, and its confirmation is contingent on the measurement of level lifetimes and the $0^+ \rightarrow \gamma$ -vibration interband transitions: a weak $E_\gamma=565$ keV line decaying from the 2^+ member of the band, a $E_\gamma=686$ keV line leaving the 4^+ member, and the elusive $E_\gamma=512$ keV line from the 0^+ bandhead, to name a few. The broad annihilation peak in our spectra prevents detection of this latter γ ray in our γ -singles-based experiments, and the low literature intensities of the other two make detection less than straightforward. Transition probabilities can be calculated using the measured lifetimes, the literature values for the intensities [3, 83], and with assumption that no multipolarity mixing is present. The existence of this double-phonon characterization in the 0_2^+ seems fairly evident as a $\gamma\gamma$ -vibration from our lifetime measurements (with lower limits of lifetimes in a few cases), with calculated $B(E2;2^+ \rightarrow 4_\gamma^+)=2.7$, $B(E2;4^+ \rightarrow 4_\gamma^+)<3.7$, and $B(E2;0^+ \rightarrow 2_\gamma^+)<16$ W.u. Clearly, the $B(E2)$ probabilities greater than 1 are plausible in the interband cases for decays of the 2^+ member, and the upper limit of a 16 Weisskopf unit $B(E2)$ for the 512 keV γ ray is difficult to ignore, which points toward some collective behavior built on top of the γ -vibrational band. However, the overall $B(E2)$ strength observed is not blatantly conclusive, so we emphasize a *tentative* two-phonon ($\gamma\gamma$) vibration characterization of the $K^\pi=0_2^+$ band. That being said, the relative inflation and enhancement of transition probabilities to the γ -vibrational band is evident in Table 5.5, where we see more than a factor of 2 increase in $B(E2)$ for like-spin changing transitions ($2^+ \rightarrow 2_\gamma^+$ versus $2^+ \rightarrow 2_{gs}^+$, for example), strengthening our argument for this $\gamma\gamma$ assignment in ^{162}Dy . Comparison of our deduced transition probabilities out of the 0_2^+ band to the Alaga rules (Table 5.4) yield some mixed results; for decays to the ground state, we observe good agreement, but the decays to the γ -vibrational band are in stark disagreement. The disagreement cannot be explained

due to multipole mixing in any case (recall that our reported $B(E2)$ s to the γ -band assume no mixing and are practically upper limits). An inset level scheme for the 0_2^+ band is shown in Figure 5.10, showing the measured decays and the interband decays (with literature intensities). These interband transition strengths are also seen in Table 4.7, marked by a $[\dagger]$ symbol in the column for the branching ratio, corresponding to literature branching ratios taken from [3]. The measurement and confirmation of $\gamma\gamma$ collectivity in this 0_2^+ band also implies certain degrees of anharmonicity at work in the two-phonon vibration, as the 0_2^+ band lies 375 keV below the expected excitation energy for a harmonic $\gamma\gamma$ -vibration (at 1.6 times the energy of the single γ -vibrational phonon case). Anharmonic double-phonon vibrations are not completely unprecedented in the literature (^{178}Hf [2] & ^{232}Th [48]), but this is one of the lowest-lying $\gamma\gamma$ vibrations in well-deformed rare-earth nuclei at $E_x=1400$ keV. On top of this, the nuclei in the actinides (Th and Os) that exhibit two-phonon vibrations have energy ratios very close to the expected value of 2, with ^{232}Th less than 2, yet ^{162}Dy is contrasted with the intriguing evidence of other rare-earth two-phonon vibrations that have a $\frac{E_{\gamma\gamma}}{E_\gamma}$ ratio >2 [82].

5.2.3.3 $K^\pi=4_{1,2}^+$ Bands at 1535,2181 keV as $\gamma\gamma$ -Vibrations

In the case of an aligned $K^\pi=4^+$ $\gamma\gamma$ -vibration, strong $B(E2)$ transition probabilities are expected between the 4^+ band and the existing γ -vibration. In our experiments, the full-energy de-excitations of the $K^\pi=4^+$ band to the ground state were not observed due to K-forbiddenness, but instead with transitions to the previously mentioned γ -vibrational band (shown in Figure 5.10). The level of collectivity in these interband transitions (in either our deduced $B(E2)$ strengths or the ones calculated with literature intensities) is striking and extremely hard to ignore! Due to the preferential decays observed and the collective transitions to the $2^+\gamma$ -band, it seems definitive that this lowest-lying $K^\pi=4^+$ band is the second $\gamma\gamma$ -vibration in ^{162}Dy , at

a slightly anharmonic energy ($R_{\frac{E_{\gamma\gamma}}{2E_\gamma}} \approx 0.86$).

Wu *et. al* characterizes the $\gamma\gamma$ vibration in ^{162}Dy as a highly fragmented excitation, with significant collective strength lying in the two 4^+ states at 1535 & 2181 keV [80]. The M1 mixing present in the $4^+ \rightarrow 3^+$ decay translates to a deduced $B(E2)$ of 1.3 W.u.; this deduced value from our experiments does not account for the $\sim 50\%$ branch of the 1294 keV decay, where in reality, this $B(E2)$ is cut in half by using literature intensities [8, 80]. Using the literature intensities from [80], a distinctly collective E2 transition was observed from this higher-lying 4^+ state to the bandhead of 8.5 W.u., however, this degree of collectivity is contrasted with the lower-lying 4^+ state that we assign as a $\gamma\gamma$ -vibration, where the authors in [80] imply that there is a significant component of a two-phonon vibration in this state at 2181 keV. Instead, an overwhelming portion of collectivity in the lower-lying 4^+ state was observed, with the calculated transition strengths leaving this higher-lying state in Table 4.8. This is not to imply complete disagreement with [80], as a highly fragmented and collective $\gamma\gamma$ -vibration in these two states at 1535 and 2181 keV was observed. Falling in line with other 4^+ $\gamma\gamma$ -vibrations in rare-earth nuclei, the two-phonon vibrational state at 2181 keV is anharmonic, with a $R_{\frac{E_{\gamma\gamma}}{E_\gamma}} = 2.5$ [32].

5.2.3.4 $(2,3,4)^+$ State at 2230 keV

The comprehensive lifetime measurements of $J \leq 5$ states below 3.1 MeV has yielded an interestingly strong transition from a state at 2230 keV excitation energy to the γ -vibrational band. From our measurement of a mixed E2/M1 multipolarity γ -ray ($\sim 89\%$ E2 if the state is a 2^+) at $E_\gamma = 1342$ keV that decays to the bandhead of the γ -band, we can place a tentative $(2,3,4)^+$ spin assignment on this level. Aprahamian observed a similar energy γ -ray, but places an E1 multipolarity assignment, where our angular distribution is consistent with a $\Delta L=2$ transition (Figure 5.9) [3] *et. al.* Given any of the tentative positive parity, low-spin assignments, the measured $B(E2)$

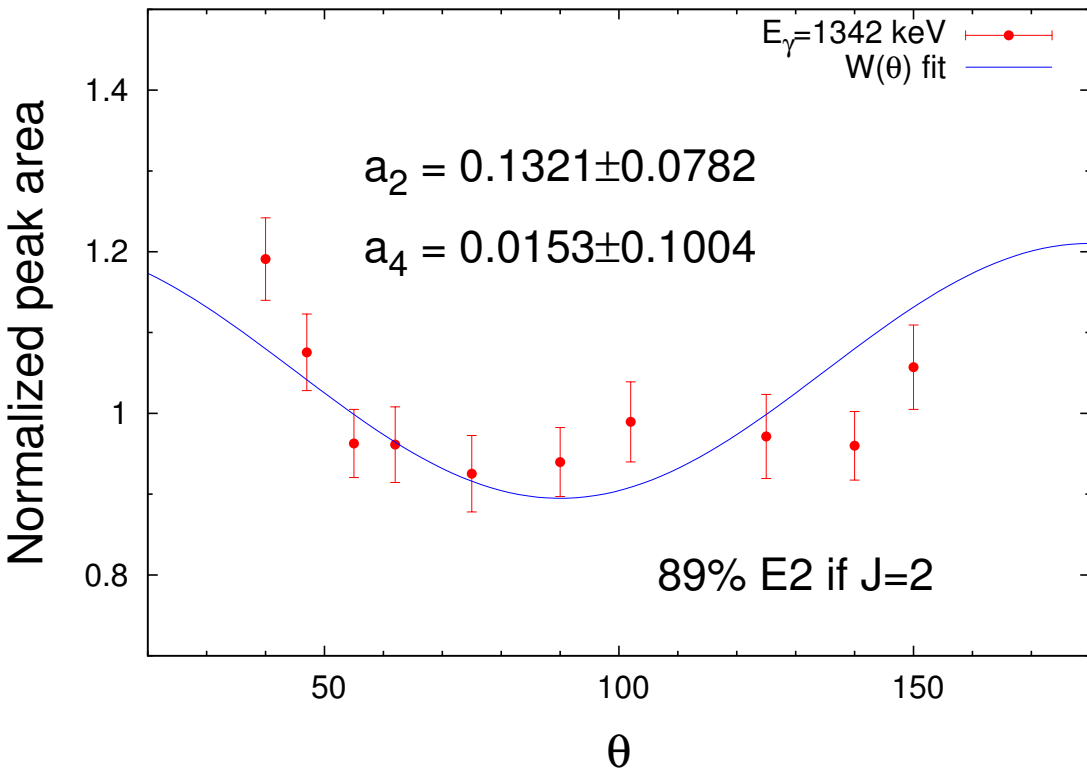


Figure 5.9. Measured angular distribution of 1342 keV γ ray leaving the 2230 keV level, $\text{W}(\theta)$ fit is shown with a_2 and a_4 coefficients from the $E_n = 3.1 \text{ MeV}$ angular distribution.

is distinctly collective, at 5.2 W.u. in strength; this behavior of distinct collectivity is completely expected for a two-phonon $\beta\gamma$ -vibration in structure, and would be one of the first experimental evidences of this mode of multiphonon configuration. These are, of course, large assumptions to make about the rotational band assignment of this state, but provide an interesting avenue to continue research into the structure of this nucleus.

This begs the question, once again: where is the single-phonon β vibration in ^{162}Dy ? If we take this state at 2230 keV as part of the $\beta\gamma$ -vibration and with close to harmonic vibrations, the β vibration *should* be around $E_x \approx 1350 \text{ keV}$; this is clearly not the case based on our lifetime measurements of the 0_2^+ band and its

characterization as the K=0 $\gamma\gamma$ -vibration. That being said, it is entirely possible that a strong β -vibration exists at either of the 0^+ excitations at 1814 or 1820 keV (or at the unobserved and elusive state at 774 keV). In the case of a β vibration at \sim 1800 keV, it would imply that the $\beta\gamma$ is fairly anharmonic, clocking in at \sim 80% of the expected two-phonon energy, which is reasonable, considering that the $K^\pi=0^+$ $\gamma\gamma$ -vibration in ^{162}Dy is \sim 79% harmonic ($R_{\frac{E_{\gamma\gamma}}{2E_\gamma}} \approx 0.79$), and the $K^\pi=4^+$ $\gamma\gamma$ -vibration is similarly anharmonic at $R_{\frac{E_{\gamma\gamma}}{2E_\gamma}} \approx 0.86$. We strongly emphasize further study on the 0^+ states in ^{162}Dy to find the collective β -vibration at 774, 1814, or 1820 keV (if the β -vibration even exists in this nucleus).

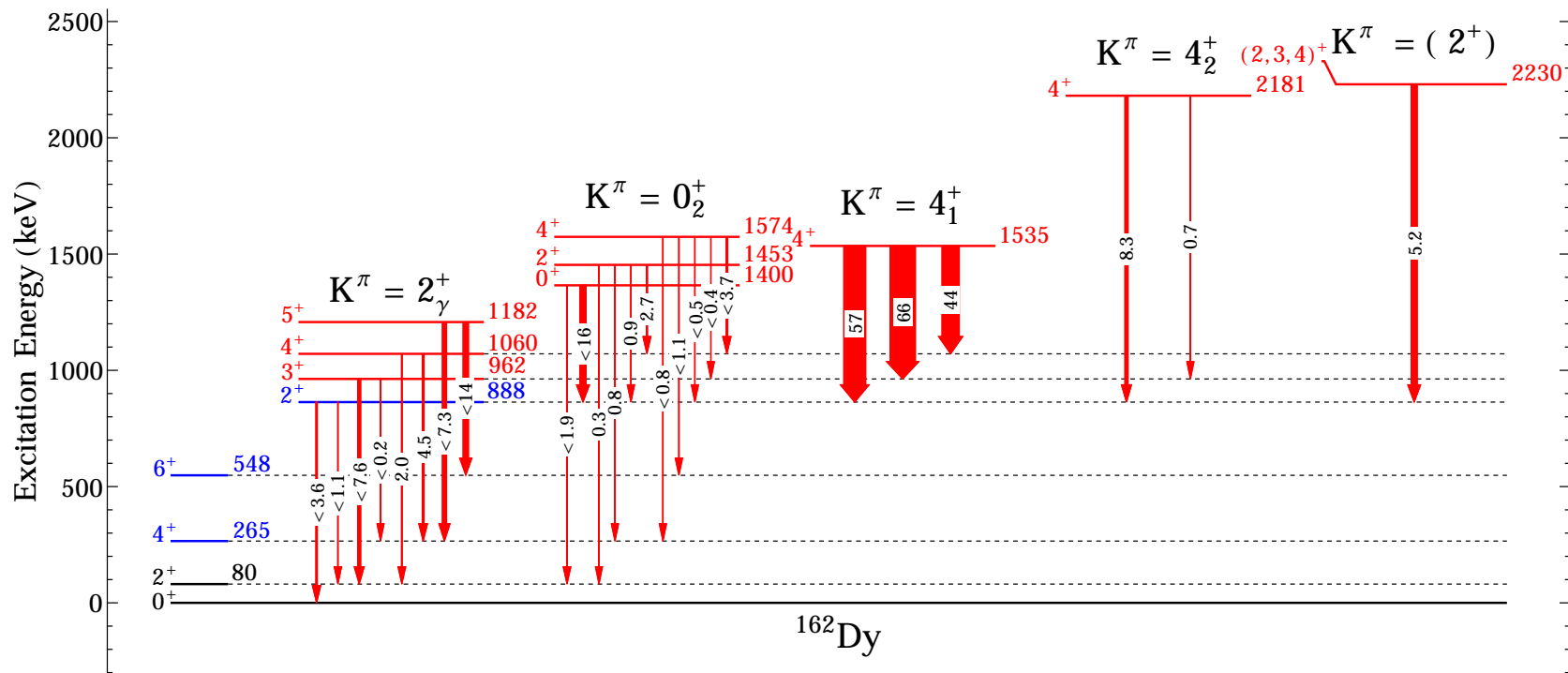


Figure 5.10. Level scheme showing all observed transitions from the lowest-lying 2^+_γ , 0^+_2 , and 4^+_1 band with all interband ($K^\pi = J_i^+ \rightarrow K^\pi = 2^+_\gamma$) decays. Intensities for transitions to the γ -band are taken from [3]. Also shown is a tentative (2^+) state at 2230 keV with a strong decay to the 2^+_γ band.

TABLE 5.3

OBSERVED/LITERATURE INTENSITIES (K^π=0⁺,2⁺,4⁺): ¹⁶²DY

E _{lev} (keV)	E _γ (keV)	I _{γ,abs} (n,n'γ)	I _γ (lit.)
888.18(22)	807.54(50)	976.596(9.252)	
	888.18(50)	887.460(7.953)	
962.96(27)	697.30(50) ^[∅]	166.366(2.981)	
	882.31(50)	877.632(9.095)	
1061.05(29)	795.35(50)	213.256(1.374)	
	980.36(51)	121.782(1.166)	
1182.88(26)	634.24(61)	67.548(1.514)	
	917.18(51)	214.971(2.635)	
1400.29(36)	512.0(2)	[†]	11(5)* [83]
	1319.60(51)	163.971(1.238)	133(3)* [83]
1453.50(30)	395.49 (10)	[†]	0.18(2) [3]
	565.32 (12)	[†]	0.37(6) [3]
	1187.81(51)	125.506(1.610)	12.7(3) [3]
	1372.80(51)	169.820(1.989)	18.1(8) [3]
1535.97(23)	475.27(54) ^[⊗]	53.276(3.388)	4.5(3) [3]
	572.96(50)	90.678(1.588)	21.8(9) [3]
	647.61(50) ^[∅]	141.966(2.084)	50.1(8) [3]
1574.34(29)	513.31 (2)	[†]	0.51(3) [3]
	611.23 (5)	[†]	0.12(2) [3]
	686.15 (6)	[†]	0.29(8) [3]
	1025.84(58) ^[∅]	25.251(0.916)	5.0(2) [3]
	1308.65(51)	135.879(1.997)	24(2) [3]

TABLE 5.3

Continued

OBSERVED/LITERATURE INTENSITIES ($K^\pi=0^+, 2^+, 4^+$): ^{162}DY

E_{lev} (keV)	E_γ (keV)	$I_{\gamma,abs}$ (n,n'γ)	I_γ (lit.)
1666.01(33)	1585.35(51)	131.018(1.476)	
1728.31(20)	1462.70(51) ^[⊗]	110.002(1.779)	0.81(6) [34]
	1647.64(51)	133.790(2.206)	1.21(7) [34]
	1728.29(53)	85.273(1.611)	0.66(6) [34]
2128.02(33)	2047.34(61)	286.080(6.065)	
2180.69(53)	1217.73(58)	300.230(5.134)	1.13(24) [80]
	1292.51(58) ^[⊗]	319.833(9.558)	1.00 [80]
2189.65(52)	2109.10(50)	140.677(3.860)	
2231.06(38)	1342.57(50)	239.620(6.282)	
2497.77(52)	2417.22(50)	116.520(4.933)	
2655.83(33)	2575.28(53)	59.373(5.424)	
2802.04(61)	2721.48(55)	50.490(15.032)	

Absolute intensities for γ -decays observed in (n,n'γ) experiments. [†]: γ ray not observed, reporting literature intensity ([3, 34] gives absolute intensities, while [80, 83] report relative intensities).

TABLE 5.4

ALAGA ($K^\pi=0^+, 2^+, 4^+$): ^{162}DY

K^π	$\frac{J_{K_i} \rightarrow J'_{K_f}}{J_{K_i} \rightarrow J''_{K_f}}$	Exp	CG ²
$K_i^\pi = 2_\gamma^+:$	$\frac{4^+ \rightarrow 4^+}{4^+ \rightarrow 2^+}$	2.3	2.9
$K_i^\pi = 0_2^+:$	$\frac{2^+ \rightarrow 4^+}{2^+ \rightarrow 2^+}$	1.5	1.8
	$\frac{4^+ \rightarrow 6^+}{4^+ \rightarrow 4^+}$	1.4	1.7
	$\frac{2^+ \rightarrow 4_\gamma^+}{2^+ \rightarrow 2_\gamma^+}$	3.1	0.8
	$\frac{4^+ \rightarrow 4_\gamma^+}{4^+ \rightarrow 2_\gamma^+}$	10	44
	$\frac{4^+ \rightarrow 4_\gamma^+}{4^+ \rightarrow 3_\gamma^+}$	9.3	3.2
	$\frac{4^+ \rightarrow 3_\gamma^+}{4^+ \rightarrow 2_\gamma^+}$	0.8	14
$K_i^\pi = 4_1^+:$	$\frac{4^+ \rightarrow 4^+}{4^+ \rightarrow 3^+}$	0.5 ^[*] (0.2)	0.4
	$\frac{4^+ \rightarrow 4^+}{4^+ \rightarrow 2^+}$	0.8 ^[*] (0.2)	0.2
$K_i^\pi = 4_2^+:$	$\frac{4^+ \rightarrow 3^+}{4^+ \rightarrow 2^+}$	0.1	0.6

Alaga rule comparisons of measured $B(E2)$ strengths for the $K^\pi=2_\gamma^+$, 0_2^+ , and 4_1^+ band in ^{162}Dy . ^[*]: Alaga comparison shown in parentheses uses literature intensities to calculate $B(E2)$ strengths.

TABLE 5.5

B(E2) RATIOS ($K^\pi=0^+, 2^+, 4^+$): ^{162}DY

K	$\frac{J_i \rightarrow J_f}{J_i \rightarrow J_f}$	$\frac{B(E2 \rightarrow \gamma)}{B(E2 \rightarrow g.s.)}$
$K^\pi=0_2^+:$		
	$\frac{0^+ \rightarrow 2_\gamma^+}{0^+ \rightarrow 2_{g.s.}^+}$	8.4
	$\frac{2^+ \rightarrow 2_\gamma^+}{2^+ \rightarrow 2_{g.s.}^+}$	3.0
	$\frac{2^+ \rightarrow 4_\gamma^+}{2^+ \rightarrow 4_{g.s.}^+}$	3.4
	$\frac{4^+ \rightarrow 4_\gamma^+}{4^+ \rightarrow 4_{g.s.}^+}$	4.6

Ratios of B(E2) probabilities of the transitions to the γ -band over the ground state band transitions, highlighting an enhancement or preference of decay to the $K^\pi=2^+\gamma$ -band.

5.2.4 Negative Parity States

5.2.4.1 $K^\pi=2^-$ Band at 1148 keV

Modestly collective transitions to the known γ -vibrational states are observed leaving the 2^- band at 1148 keV. This highly-favored trend of γ -rays to the $K^\pi=2^+$ band is difficult to ignore in the face of notably strong ($\sim 2\text{-}5$ mWu), absolute B(E1) measurements between these two modes of excitations. Pascu [60] stresses the importance of this preferential $K^\pi=2^- \rightarrow K^\pi=2^+$ decay in nearby nuclei via the measurement of direct E3 radiation as a potential octupole-quadrupole coupling, however, this decay pattern could be a product of K-forbiddenness, as any decays to the ground state involve $\Delta K=2$ versus the $\Delta K=0$ transitions to the γ -band. We also mirror these same concerns on the continued study of interband decay radiation in the rare-earth region to fully understand this band; B(E3; $5^- \leftrightarrow 2_\gamma^+$) strengths would be remarkably useful in this aspect. ^{162}Dy offers some distinct challenges in terms of the detection of radiation for low-lying excitations; for example, measurement of the interband $2^- \rightarrow 3_\gamma^+$ transition lies at 185 keV, placing it directly on top of our most strongly populated $4_{g.s.}^+ \rightarrow 2_{g.s.}^+$ transition. This experimental challenge is out of the scope of the γ -singles-based experiments performed in this work at UKAL, and would require much more discriminating coincidence measurements to observe the γ -decays.

5.2.4.2 $K^\pi=0^-$ Band at 1275 keV

Overall in the $K^\pi=0^-$ band, we observe inflated, clearly collective B(E1) transition probabilities to the ground state (Table 4.9), with excellent agreement to Alaga predictions (Table 5.7). Although these B(E1)s are weaker overall than other confirmed single-phonon octupole vibrations in the region (^{168}Er [55]), the transition probabilities are well above the threshold for what is considered generally non-collective in the mass region ($\sim 10^{-5}$ mWu strengths). Furthermore, our measured

$B(E1; 1_{K^\pi=0^-}^- \rightarrow 0_{g.s.}^+)$ of $0.002 \text{ e}^2\text{fm}^2$ compares very nicely with the systematic behavior of E1 strengths leaving the bandhead of $K^\pi=0^-$ bands in deformed rare-earth nuclei ($B(E1) \sim 0.002\text{-}0.004 \text{ e}^2\text{fm}^2$) [16]. From these measured collective E1 strengths, this suggests some significant reflection asymmetry in this $K^\pi=0^-$ band, which is especially and notably consistent with the picture of well-behaved octupole collectivity.

5.2.4.3 $K^\pi=2_2^-$ Band at 1863 keV

Much like the lower 2^- band, our measurement of mildly inflated $B(E1)$ transition probabilities to the γ -band is striking, and supports the arguments in numerous works of new, emerging decay patterns [22, 60, 73] of enhanced E1 transitions to the 2^+ band as a differing form of collective dipole excitation built on top of the γ -vibration. Along the same lines, assertions from IBM considerations with the inclusion of p and f bosons imply that the structure of the lowest-lying negative parity bands *may not* be of purely collective nature [3, 43], which supports our experimental findings. Deduced $B(E1)$ s behave well when compared to Alaga considerations (Table 5.7), giving us confidence of correct lifetime measurements. Of particular note, however, is the lower relative $B(E1)$ strength than its lower-energy cousins in the first 2^- band, however, the decays from this band are still above the threshold for what would be considered non-collective. Once again, the interband $B(E3)$ strengths to/from these negative parity bands would be invaluable in the further discussion and feasibility of this pattern.

TABLE 5.6

ABSOLUTE INTENSITIES (NEGATIVE PARITY): ^{162}DY

E_{lev} (keV)	E_γ (keV)	$I_{\gamma,abs}$ ($n,n'\gamma$)
1148.20(20)	260.16(50)	658.762(7.577)
1210.05(18)	247.27(55)	38.973(1.420)
	322.05(51)	57.699(1.240)
	944.48(50)	216.160(3.227)
	1129.46(50)	384.769(5.182)
1297.06(27)	236.09(60)	43.374(1.380)
	334.15(50)	245.585(4.666)
1390.52(35)	1124.88(88)	94.848(2.193)
1275.81(24)	1195.10(50)	429.944(4.249)
	1275.82(53)	280.443(6.356)
1358.00(30)	1092.27(71)	134.371(1.271)
	1277.33(58)	178.995(6.684)
1518.47(29)	970.01(55)	32.453(0.775)
	1252.74(51)	78.039(1.893)
1863.85(26)	900.90(55)	47.527(1.219)
	975.65(50)	141.639(1.587)
1910.50(26)	947.51(56)	48.580(0.955)
	1022.33(53)	39.474(0.978)
1972.99(66)	912.09(50)	82.148(3.125)
	1010.19(50)	251.922(15.219)

Absolute intensities for γ -decays from the $K^\pi=2^-, 0^-,$ and 2_2^- bands observed in $(n,n'\gamma)$ experiments, taken from the $E_n=3.1$ MeV angular distributions.

TABLE 5.7

ALAGA ($K^\pi=2^-, 0^-, 2^-_2$): ^{162}DY

K^π	$\frac{J_{K_i} \rightarrow J'_{K_f}}{J_{K_i} \rightarrow J''_{K_f}}$	Exp	Th
<u>$K_i^\pi = 2^-$:</u>	$\frac{3^- \rightarrow 3\gamma^+}{3^- \rightarrow 2\gamma^+}$	1.0	1.4
	$\frac{4^- \rightarrow 4^+}{4^- \rightarrow 3^+}$	0.5	0.6
<u>$K_i^\pi = 0^-$:</u>	$\frac{1^- \rightarrow 2^+}{1^- \rightarrow 0^+}$	2.0	2.0
	$\frac{3^- \rightarrow 4^+}{3^- \rightarrow 2^+}$	1.2	1.3
	$\frac{5^- \rightarrow 6^+}{5^- \rightarrow 4^+}$	1.0	1.2
<u>$K_i^\pi = 2^-_2$:</u>	$\frac{2^- \rightarrow 3^+}{2^- \rightarrow 2^+}$	0.5	0.5
	$\frac{3^- \rightarrow 3^+}{3^- \rightarrow 2^+}$	1.6	1.4
	$\frac{4^- \rightarrow 4^+}{4^- \rightarrow 3^+}$	0.3	0.6

Comparison of E1 transition probabilities from the $K^\pi=2^-$, 0^- , & 2^-_2 bands with the Alaga rules.

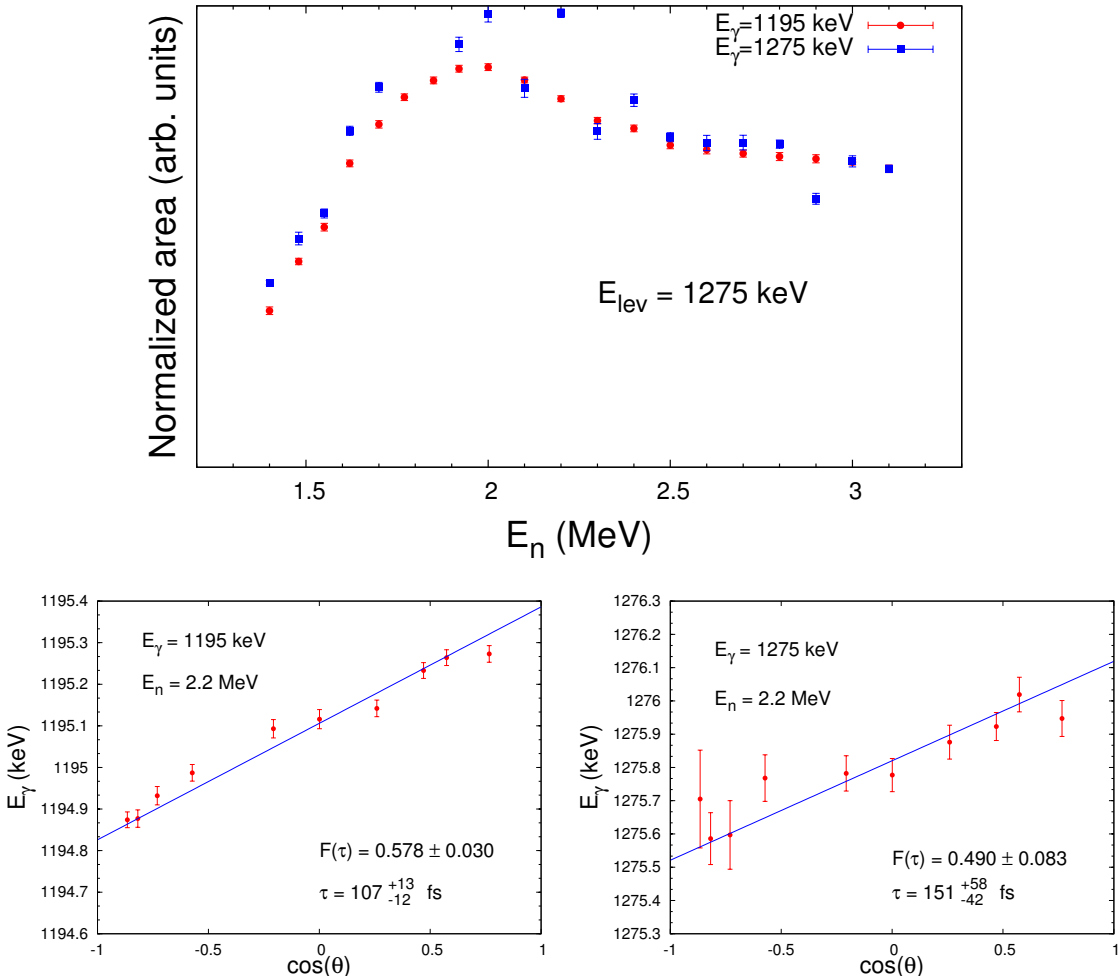


Figure 5.11. $E_\gamma=1195$ & 1275 keV (de-excitations from the $E_x=1275$ keV level) Doppler shifts and excitation functions (color online). The excitation function (in blue) for the 1275 keV γ ray is scaled by a factor of 1.53 to normalize to the branching ratio of the level.

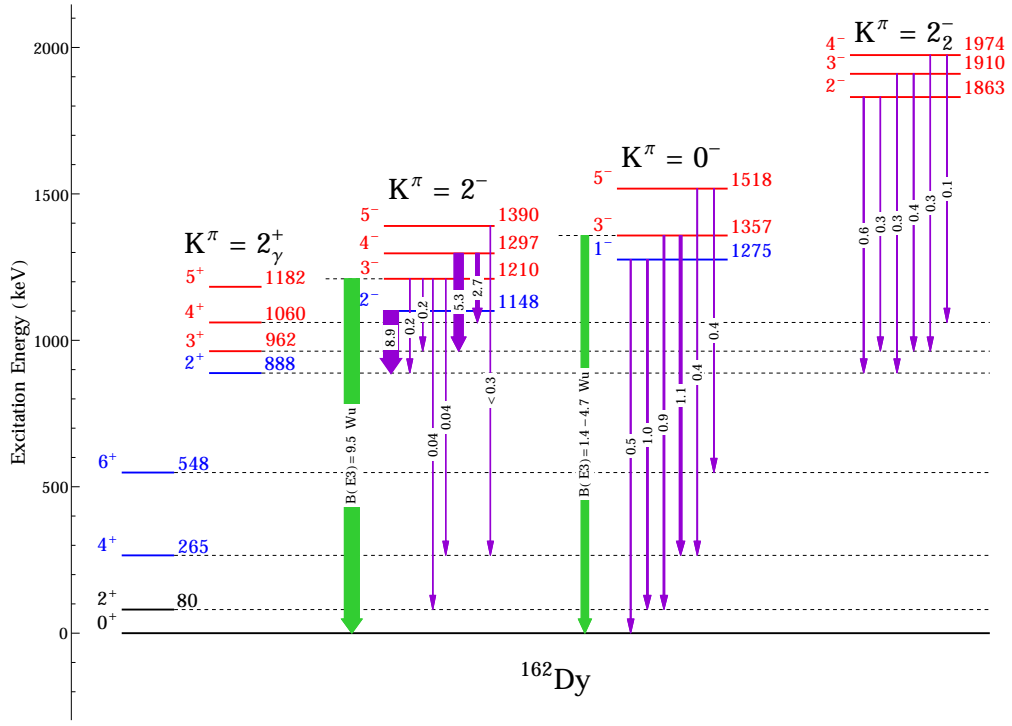


Figure 5.12. Observed γ -decays from negative parity, $K^\pi=2^-$, 0^- , 2_2^- bands in ^{162}Dy . Transition strengths are drawn proportional in width to their deduced $B(\text{E}1)$, with E1 transitions ($B(\text{E}1)$ in milli-Weksskopf units) in violet (color online). Literature $B(\text{E}3)$ values are drawn in green, expressed in W.u., and are from Refs. [56, 59]

5.2.5 Other Negative Parity Bands

5.2.5.1 $K^\pi=5^-$ Band

The current status/insight of this $K^\pi=5^-$ band is of a two-quasiparticle origin [3], where we can verify this interpretation with the (albeit slightly inflated at ~ 0.3 mWu) weak E1 transition strengths to the ground state. Furthermore, $K^\pi=5^-$ bands are not surmised to be a part of the octupole vibration splitting in a deformed nucleus, yet the refinement of this lifetime from older literature values is important nonetheless.

Assertions from IBM considerations with the inclusion of p and f bosons imply that the structure of the lowest-lying negative parity bands may not be of purely collective nature [3, 43], where the traditional picture of octupole collectivity in well-deformed nuclei exists with the initial, lowest-lying and fragmented quartet of states of $K^\pi=0^-, 1^-, 2^-, \& 3^-$. However, the current ordering of negative parity bands in ^{162}Dy is difficult (read: impossible) to predict with modern models [3]. Lifetimes for a few other of the lowest-lying set of states in ^{162}Dy have been measured, and individual discussion of the measurements is provided below.

5.2.5.2 $K^\pi=3^-$ Band

This creates a somewhat murky picture for any interpretation of the $K^\pi=3^-$ band. The $E_\gamma=311$ keV de-excitation from the 4^- member is overwhelmingly E2 radiation, based on our measurement of a mixing ratio of $-6.9_{-2.2}^{+1.6}$ ($\sim 98\%$ E2), but the very large (potentially) E2 transition probabilities that de-excite the bandhead are impressive, even in the face of heavy M1 mixing for the 212 keV γ ray that leaves the bandhead at 1570 keV. Whether this band is some higher collective behavior on top of the existing octupole vibration or if it is even part of the $0^-, 1^-, 2^-, 3^-$ quartet is still an open question, however, the preference of decay to the lower-lying octupole band ($K^\pi=0^-$ band) should not be understated.

5.2.5.3 $K^\pi=1^-$ Band

As such, the deduced transition probabilities should not be taken without careful attention and heavy skepticism. Interband B(E2) strengths of 630 W.u. are unprecedented in *any* nuclear transition, flagging a clear departure from a consistent measurement of the lifetime. The generally low limits for lifetimes measured do not offer vast insight into the collectivity of the band.

5.2.5.4 $K^\pi=3_2^-$ Band

Decays from the second $K^\pi=3^-$ band have the potential for some interesting structure effects, with the extremely preferential branching ratios to the γ -band and the $K^\pi=2^-$ band. However, measurements of the second $K^\pi=3^-$ band's lifetimes cannot reveal any insight to the octupole collectivity in these levels. In the case of mostly E2 radiation and the lowest possible lifetime, the alarmingly large $B(E2)\sim 6$ Wu to the 2^- band could indicate some collectivity on top of the $K^\pi=2^-$ octupole band, based solely on the decay pattern, but nothing concrete can be said, barring a reliable measurement of the actual lifetime of the states in the band.

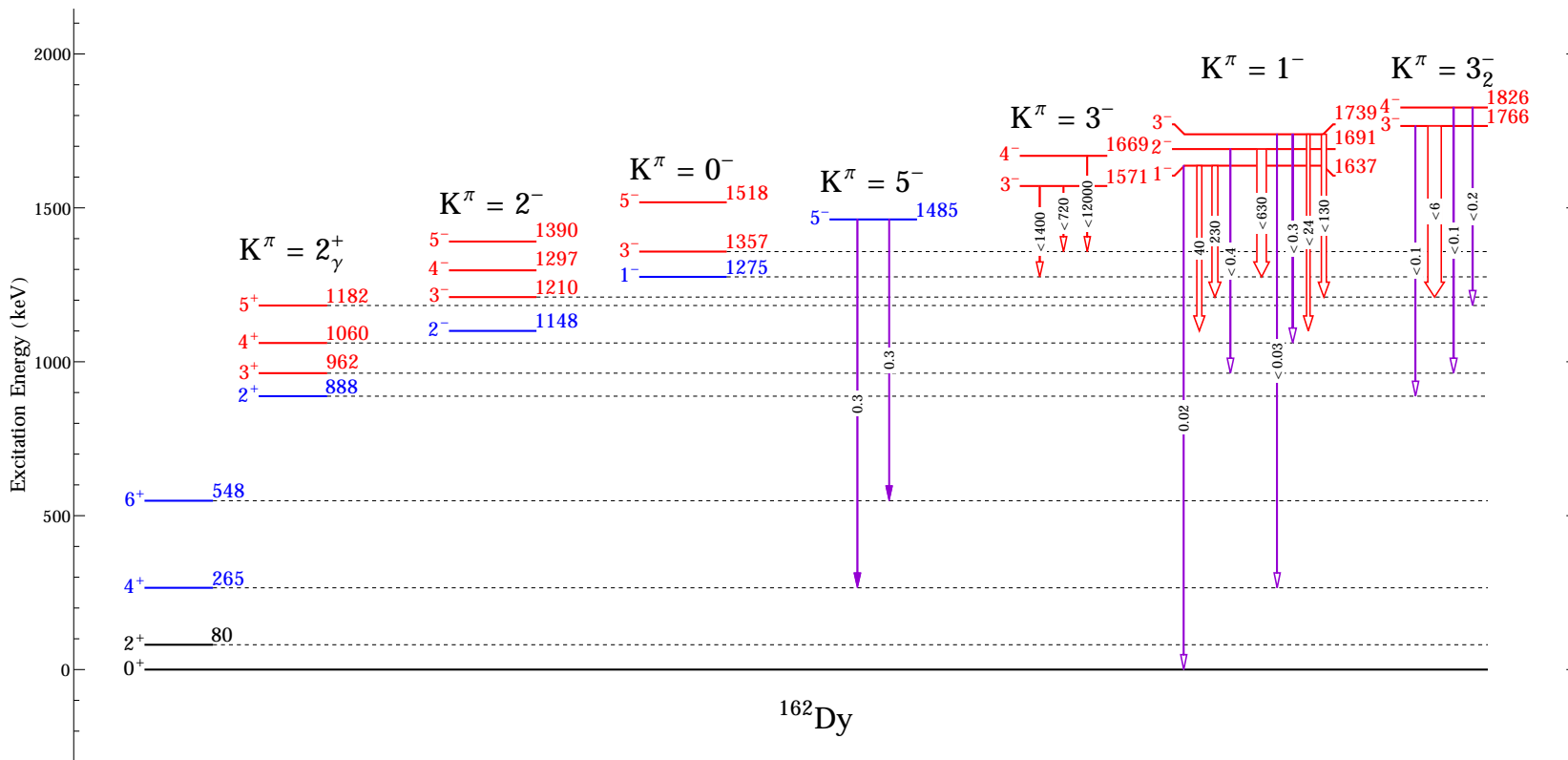


Figure 5.13. Observed γ -decays from higher lying $K^\pi=5^-$, 3^- , 1^- , 3_2^- bands in ^{162}Dy . Transition strengths are proportional in width, with E2 transitions in red and E1 transitions in violet (color online). Hollow (white with colored border) transition arrows indicate that the resulting transition probability is tentatively from an unreliable lifetime measurement.

5.2.6 $K\pi=1^+$ Band

In terms of rotational bands in ^{162}Dy , the discussion on results ends with the $K\pi=1^+$ band and the isovector M1 scissors mode. The latter excitations have been extensively studied with photon scattering experiments by [46, 54], and as mentioned before, offer a good calibration point or benchmark for our lifetime measurements, as the literature values fall within the sensitive range of what DSAM can measure.

At higher energies in this band, more channels are open to decay, which can be seen in Figure 5.14. While a fairly collective transition was measured to the γ -vibrational band, this should be taken as the exception to the rule, rather than implying that it is any collective behavior built on top of the existing quadrupole vibration. Oftentimes, a state can pick up a large two-quasiparticle amplitude from the ‘daughter’ state that would give rise to a nonzero $B(E2)$, however, this does not mean the state is collective in nature.

Overall, these transitions observed out of the 1^+ band are noncollective to any other excitation in ^{162}Dy , an assertion made very early by Soloviev [72], suggesting that the $K\pi=1^+$ band cannot stem from one or two-phonon coupling from the detailed quasiparticle-phonon nuclear model (QPNM) formalism outlined there.

5.2.7 States Above 2.2 MeV Excitation Energy

With the increasing level density and uncertainty in spin-parity assignments above 2.0 MeV, differentiation of negative parity bands (or *any* band structure) becomes difficult. Incidentally, levels above this energy threshold lie well above the pairing gap; recall that we are most likely to find the most collective excitations below this energy, however, above the pairing gap, we can expect to see mixing between multi-quasiparticle states and collective excitations. Since the nature and goal of $(n,n'\gamma)$ experiments at UKAL is *not* to identify new levels in the level scheme, but to confidently place existing γ -rays from the excitation functions, higher-lying states often

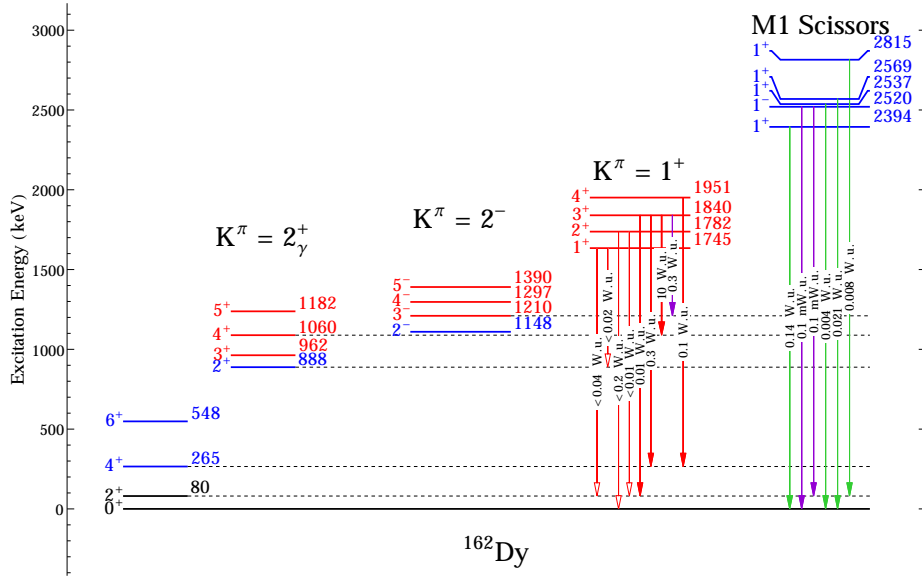


Figure 5.14. $K^\pi=1^+$ band and the 1^\pm -spin levels part of the isovector M1 scissors mode in ^{162}Dy . B(E1) in violet and in mW.u., B(M1) in green and W.u., and B(E2) in red in W.u.

cannot be confidently discussed in the scope of a vibrational phonon picture in this work. Of course, this does not imply that there is a lack of structure above this threshold, as we can observe multiphonon excitations at energies above the pairing gap [81, 84]. Reduced transition probabilities for transitions out of these states should not be given much weight, as a) the full E2 strength is reported for any potentially mixed multipolarity decays, and b) the $E_\gamma^{2\ell+1}$ factor for the calculation of reduced transition probabilities tends to dominate at this higher energy regime. Nevertheless, our measured lifetimes are presented and any observed branching ratios from multi-channel decays in the tables.

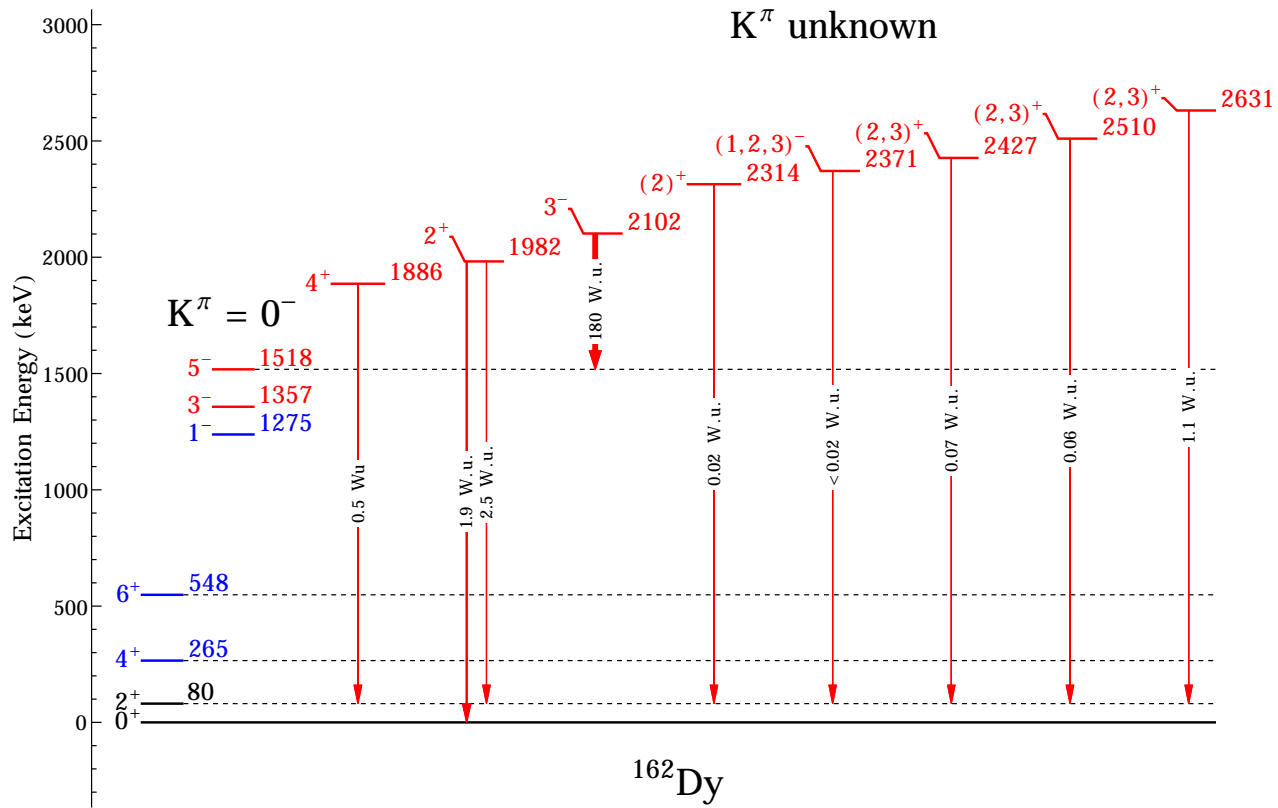


Figure 5.15. Levels in ^{162}Dy with no rotational band assignment above the pairing gap ($2\Delta n=1720$ keV & $2\Delta p=1914$ keV). $B(E2)$ strengths drawn in red and in W.u.

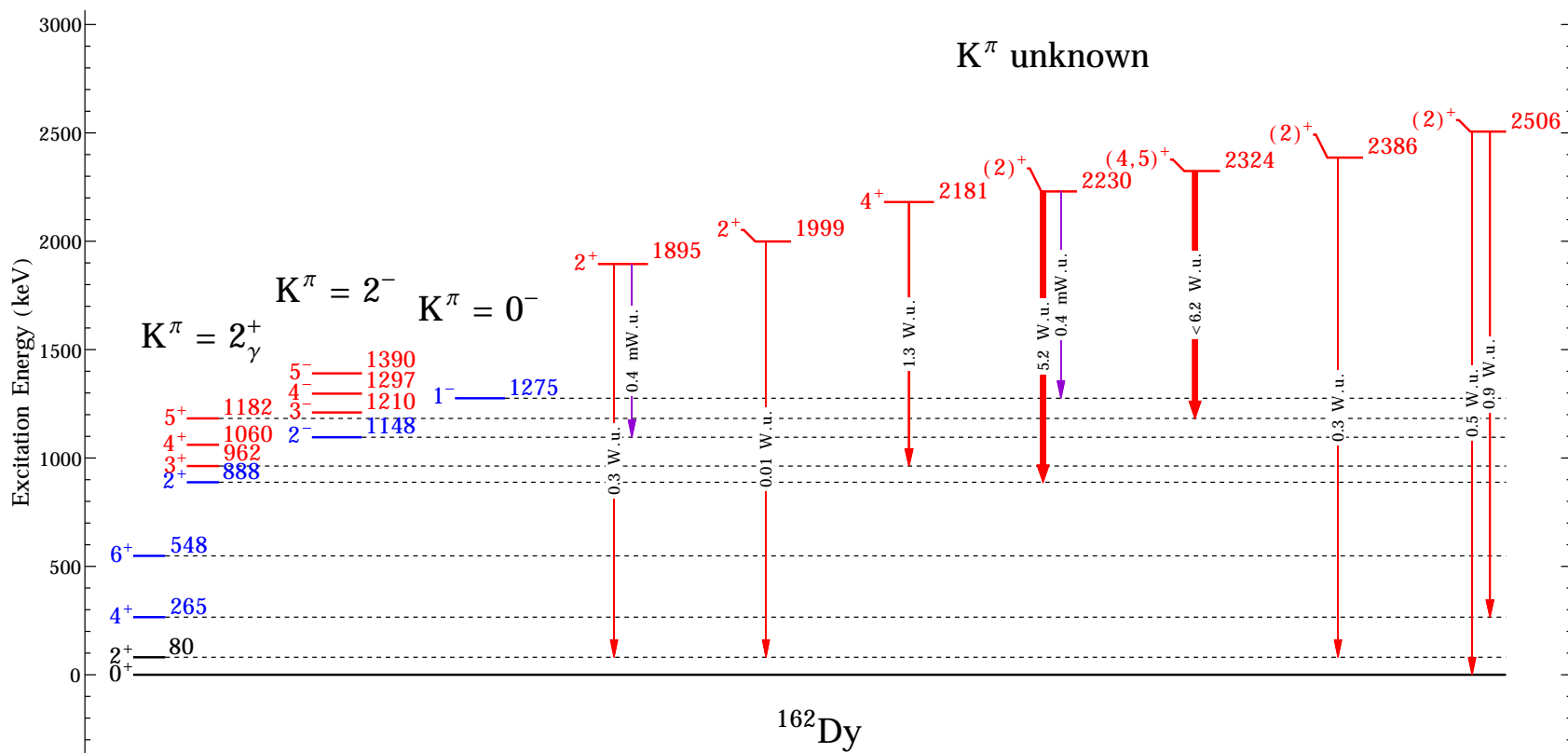


Figure 5.16. Levels in ^{162}Dy with no rotational band assignment above the pairing gap ($2\Delta n=1720$ keV & $2\Delta p=1914$ keV) (continued). B(E1) in violet and in mW.u., and B(E2) in red in W.u.

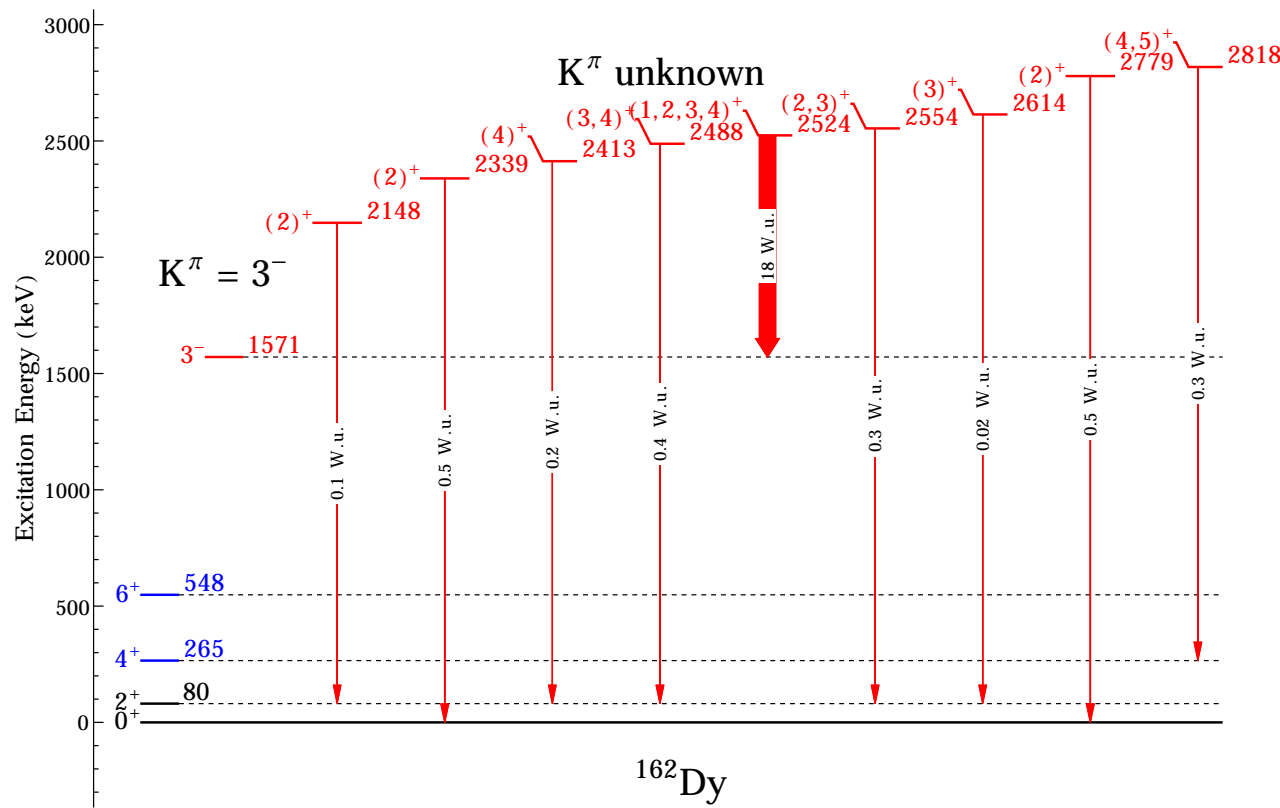


Figure 5.17. Levels in ^{162}Dy with no rotational band assignment above the pairing gap ($2\Delta n=1720$ keV & $2\Delta p=1914$ keV) (continued). B(E1) in violet and in mW.u., and B(E2) in red in W.u.

5.2.8 Implications and Further Discussion

Lifetime measurements for ^{162}Dy offer a remarkable survey of nuclear structure in this deformed nucleus. The definitive existence of single- and double-phonon quadrupole vibrations at the excitation energies $E_{K^\pi=2_\gamma^+}=888 \text{ keV}$, $E_{K^\pi=0_{\gamma\gamma}^+}=1400 \text{ keV}$, $E_{K^\pi=4_{1,\gamma\gamma}^+}=1535 \text{ keV}$, $E_{K^\pi=4_{2,\gamma\gamma}^+}=2181 \text{ keV}$ has set a new precedent for anharmonic quadrupole vibrations, as the majority of two-phonon cases in deformed rare-earth nuclei are at higher energies than a purely harmonic case. A new opening for a potential collective state built on-top of the γ -vibrational band has been proposed as a candidate for a $\beta\gamma$ -vibration, an excitation that has eluded experimentalists for years.

In a trend that continues throughout the rare-earth nuclei, lifetimes have been measured for only a few negative parity states that are surmised to be a part of the octupole vibrational states. The new decay patterns for the negative parity states in $2^- \rightarrow 2_\gamma^+$ transitions has been observed in our campaign of lifetime measurements, via strong E1 transitions to the γ -band. These measured $K^\pi=2^-$ bands seem to not be a part of the octupole vibration, but it cannot be solidified without precision B(E3) measurements in the interband cases; whether or not these states are a separate collective degree of freedom besides the traditional quadrupole/octupole vibration remains an open question.

CHAPTER 6

FINAL REMARKS AND FUTURE OUTLOOK

6.1 Impact of Presented Lifetime Measurements

Aside from the overall contribution of the lifetimes presented in this work in the global systematics of rare-earth structure, each isotope has local, isotopic significance and impetus for the measurement of nuclear lifetimes. The measurement of level lifetimes and corresponding reduced transition probabilities has been invaluable in understanding the structure of these nuclei in this geometric model, especially in terms of the new lifetimes of 0^+ excitations and new characterizations of vibrational states in deformed nuclei.

6.1.1 ^{160}Gd

Gadolinium-160 lies at the end of the road (figuratively) of decades long research on the structure of Gd isotopes; following the pioneering and continuing experimental works by Lesher, Aprahamian, de Haan, and others in $^{154-158}\text{Gd}$ [45, 51, 58], ^{160}Gd lifetimes act as a capstone to understanding nuclear structure at the edges of the valley of stability, as well as structure at the limits of stable prolate deformation. Careful examination of our data has narrowed the focus of the systematic and on-going study of 0^+ excitations in the region, as we ruled out two possible states and measured key lifetimes for the remaining two $K^\pi=0^+$ bands. Invaluable knowledge on the characteristics of low-lying negative parity bands and $K^\pi=4^+$ bands was also gathered from our data, which opened the possibility of observing octupole and hexadecapole

vibrations in deformed nuclei. Specifically, we observed a potential candidate for a collective β -vibration existing as the lowest 0^+ excitation at 1379 keV, and a well-defined two-phonon, $K^\pi=0^+$ $\gamma\gamma$ vibration for the other known 0^+ at 1558 keV. In contrast, we have not identified the $K^\pi=4^+$ branch of the $\gamma\gamma$ vibration in ^{160}Gd , but confirm the well-behaved $K^\pi=2_\gamma^+$ band as a γ -type vibration with characteristically collective decays to the ground state. We have also identified several negative parity bands surmised to be a part of the octupole vibration through our measurement of collective B(E1) transition probabilities in the $K^\pi=0^-$ and 1^- bands. Furthermore, we have observed collective decays from the $K^\pi=2^-$ band to the γ -vibrational band in an emerging trend in the rare-earth region [60].

6.1.2 ^{162}Dy

The fact that the 47 new ^{162}Dy lifetimes presented make is that these measurements account for a $\sim 0.2\%$ increase to the number of *all* known literature lifetimes across *all* 3000+ nuclei in existence. Putting this figure into even greater context, the 84 literature lifetimes for ^{168}Er were gathered from extremely high resolution and efficiency detector arrays and spread across decades of experiments around the globe. With a single detector and a modestly discriminating spin population ($J^\pi \leq 5^\pm$), we are able to provide a comparable number of lifetimes in ^{162}Dy , putting it near the top of the list of experimentally measured lifetimes of excited states, not only in the rare-earth region, but across the entire Chart of Nuclides. In addition, if the overall complexity of DSAM-INS experiments and data analysis at UKAL are compared to other lifetime measurements around the globe, it is clear that DSAM-INS is an *extremely* cost-efficient process and low barrier of entry to the experimentalist. The efficiency of cost stems from the single-detector setup with modest electronics required for signal processing, in comparison to the robust coincidence measurements needed elsewhere, and the straightforward analysis routines lend a veritable swiftness

to the time required to publish results. Overall, several vibrational phenomena have been identified in ^{162}Dy , with a $K^\pi=0^+$ $\gamma\gamma$ -vibration as the lowest-lying 0^+ band at 1400 keV, along with two $K^\pi=4^+$ $\gamma\gamma$ -vibrations at $E_x=1535$ and 2181 keV excitation energy, in a first-of-its-kind measurement of both flavors of two-phonon γ vibration. Much like the case for ^{160}Gd , octupole vibrational characteristics have been identified that compliment the literature B(E3) transition probabilities that exist in the $K^\pi=0^-$ band, as well as two $K^\pi=2^-\rightarrow 2_\gamma^+$ band decays; this trend of potential $2^+\otimes 3^-$ octupole-quadrupole vibration needs further study, but some key collective properties of these states has been uncovered.

6.2 What Lies Ahead for Rare-Earth Nuclei?

To reiterate the concerns of [41] on the nature of any possible quadrupole vibrations in deformed nuclei, the successful measurement of two-nucleon transfer reaction cross sections, absolute B(E2) values (which have been substantially augmented with this work), and the $\rho^2(E0)$ strengths is imperative. The spearheaded efforts by [58] and this work cover the first two criteria, with the most elusive and experimentally exhaustive work remaining to measure E0 transitions. Fortunately, measurement of these crucial internal conversion electrons is possible at the Nuclear Science Laboratory at the University of Notre Dame du Lac, with the Internal Conversion Electron BALL array (ICEBALL). Using coincidence measurements of multiple Germanium detectors and charged particle Lithium-drifted Silicon detectors (SiLi), conversion electron strengths can be measured through careful electronics gates. The preferred mode of excitation at the NSL is via a $(\alpha,2n)$ reaction for its preferential selection of positive parity, $L=0$ and $L=2$ states. The $(\alpha,2n)$ reaction also provides a secondary particle gate for proper event discrimination, with the implementation of triple-coincidence measurements being open (*e.g.* one can trigger on a Germanium detector, a SiLi detector, *and* a neutron detector, if desired).

In the specific case of ^{160}Gd , this α implantation reaction proves difficult, as the preferred target required must be stable, and no suitable candidates apply (^{158}Sm is unstable). The feasibility of using other reaction channels is discouraging from a cross-section standpoint; the (n,α) reaction cross section is well below a few micro-barns (μb) for MeV-range incident neutrons that would be extracted from the on-site Tandem accelerator at the NSL. Complicate this problem further with the current lack of neutron production capabilities at the NSL, and the successful measurement of E0 transitions begins to seem less realistic.

For ^{162}Dy , however, measurement of E0 transitions is readily possible at the NSL via the $(\alpha,2n)$ reaction; incidentally and ironically, the backed targets used in ICE-BALL experiments require a modest natural abundance of the particular isotope, in this case ironically, ^{160}Gd . Looking forward, E0 measurements could be a feasible experiment at Notre Dame in the very near future, and is worthwhile to carry out experiments of this type to continue research on the structurally rich ^{162}Dy .

To complete the picture of the evolution of nuclear structure in the rare-earth region, the measurement of absolute B(E2) transition probabilities for other nuclei would be ideal. This can be done for a modest number of the even-even Gd, Er, and Yb isotopes, yet distinct challenges arise in the feasibility of acquiring enough target material to perform DSAM measurements for other Dysprosium nuclei. A very large portion of the natural abundances of Dy nuclei is split between the odd-A isotopes; this poses a problem that would force either an (n,γ) reaction (not ideal because of the inherent neutron backgrounds) to be used, and that target production could become increasingly expensive. Piled on top of this, target purity greatly affects the reliability of lifetimes measured with DSAM, where we utilize very large quantities of >95% enriched oxide powders, but in lower quality targets, this enrichment would be severely impacted by the lack of natural abundances in certain isotopes.

As a supplement, refinement of lifetimes in the ^{160}Gd and ^{162}Dy is entirely pos-

sible and more than welcome in the cases where we can only measure lower limits for the lifetime. Luckily, methods to measure lifetimes in the super-picosecond range is achievable with the techniques mentioned in §2.1 such as GRID or Coulomb Excitation. Along the same lines in terms of the refinement of spectroscopy of the nuclei studied in this work, five (5) tentative and confirmed 0^+ excitations by [58] were not observed in our $(n,n'\gamma)$ experiments; these states could be probed further at the University of Notre Dame via $(\alpha, \alpha'\gamma)$ reactions with high-efficiency detectors in regular use in the lab (GEORGINA). Doing this removes certain, unfortunate, backgrounds (namely the (n,γ) humps that prevent the detection of the tentative 0^+ at 774.2 keV), and allows a much higher detection probability for much lower intensity γ rays. The precise coincidence measurements of γ rays stressed in §?? can also be done at the Nuclear Science Laboratory with multi-detector arrays like GEORGINA, further aiding the campaign to fully understand the nature of 0^+ excitations.

Since many rare-earth nuclei exist at the limits of a rotational, deformed shape, and that there is such a variation in the interpretation of the lowest-lying 0^+ states in the region, there may be latent trends hidden in the systematics of the states to further investigate. Figure 6.1 shows the energy of the 0_2^+ states in deformed rare-earth nuclei as a function of A (and N). Of note, we notice the sharp drop in energy for Samarium nuclei as deformation rapidly takes hold, with a somewhat local peak in energy around the $^{166,168}\text{Er}$ isotopes, followed by another downward trend for Ytterbium and Hafnium nuclei. Experimentally, the lifetimes of 0^+ bands in this local area are far from complete, as we only have concrete evidence for $\gamma\gamma$ -type vibrations existing in the Erbium nuclei (as the second and fifth 0^+). One question we want to ask is: does this local peaking of energy correlate to a different interpretation of the lowest-lying 0^+ state? There may *not* be a connection between the energy of the state and its makeup, however, without proper spectroscopy (including absolute B(E2) measurements), the question remains open, and perhaps this sparks a new

interest in some targeted areas of rare-earth nuclei. On the same subject, Figure 6.2 shows the current status of absolute $B(E2)$ measurements for the $0_2^+ \rightarrow 2_{gs}^+$ transitions as a function of A , which is not only a sparsely populated figure, but also scattered across orders of magnitude of $B(E2)$ strength.

Finally, the stage is set for more lifetime measurements to be made (especially for the excited 0^+ states found in [58]) for the vast set of rare-earth nuclei. The systematic pictures shown in §1.5 arise again, where we notice a complete paucity of lifetime information for these 0^+ excitations (namely $^{166,168}\text{Er}$ and $^{154,156}\text{Gd}$). These lifetimes have furthered the elucidation of single & double phonon vibrations in deformed nuclei, but “there is always work to do” in the rare-earth region of nuclei, as the mystery of many structure phenomena is far from clear or well understood.

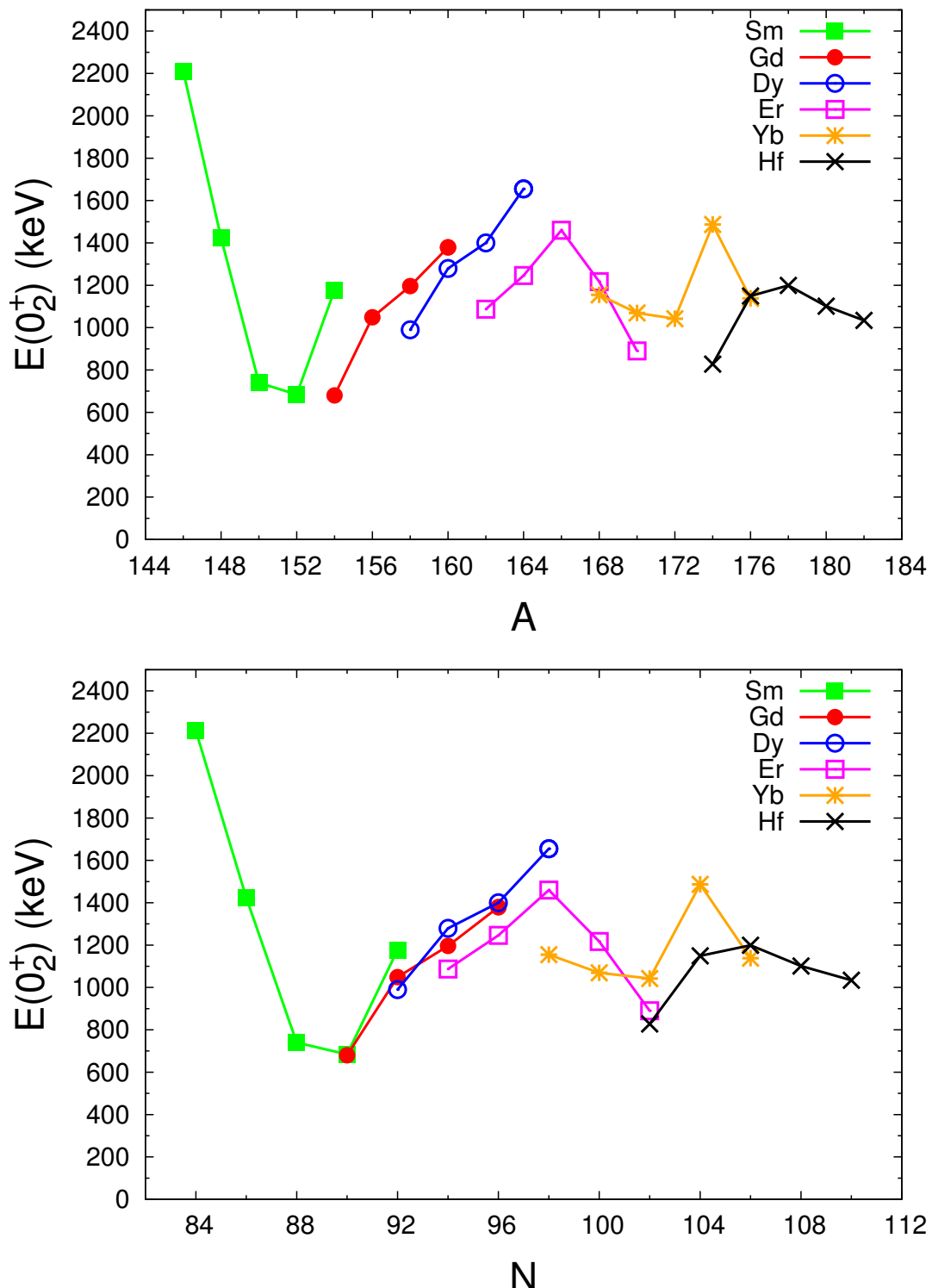


Figure 6.1. Energies of the lowest-lying 0^+ state as a function of A (top) and N (bottom) for rare earth Sm, Gd, Dy, Er, Yb and Hf isotopes.

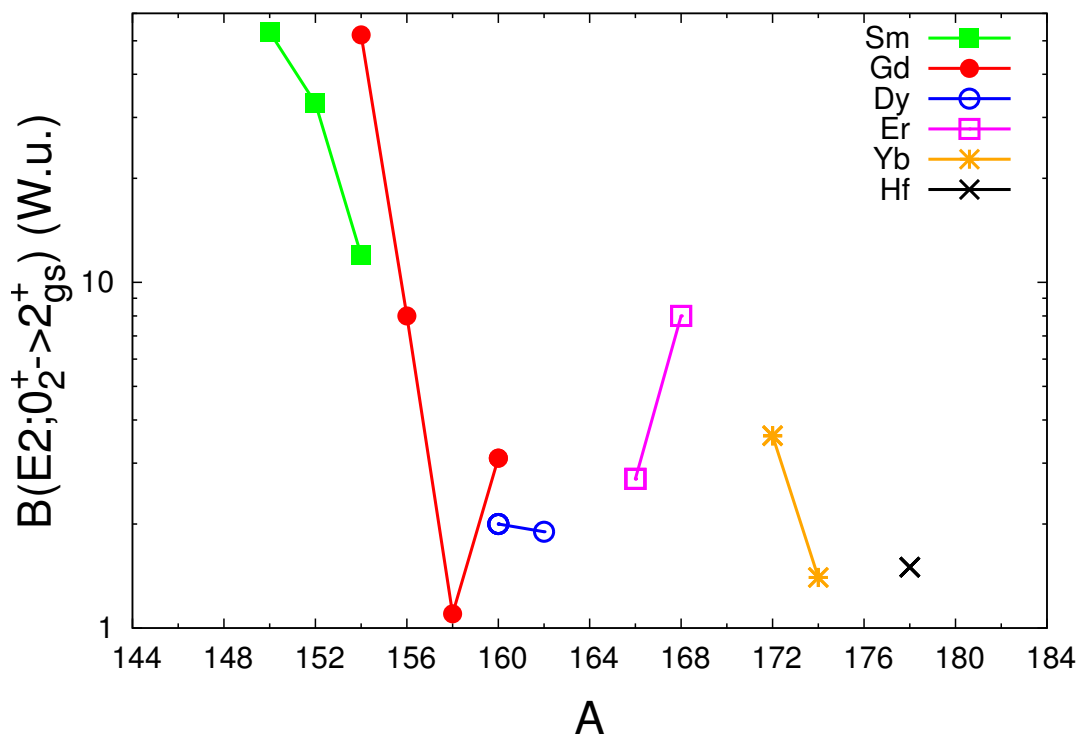


Figure 6.2. Known experimental $B(E2)$ strengths of the lowest-lying 0^+ state as a function of A for rare earth Sm, Gd, Dy, Er, Yb and Hf isotopes.

APPENDIX A

^{160}GD 0^+ STATES

Appendix A includes the formal submission to Phys. Rev. C (ref. [52]) of the paper authored by S.R. Lesher, A. Aprahamian, C. Casarella, *et. al* on the first set of results from the ^{160}Gd experiments, including the measurement of key lifetimes for $K^\pi=0^+$ bands.

Collectivity of 0^+ states in ^{160}Gd

S. R. Lesher,^{1,2,*} C. Casarella,² A. Aprahamian,² B. P. Crider,³ R. Ikeyama,¹ I. R. Marsh,¹ M. T. McEllistrem,³ E. E. Peters,⁴ F. M. Prados-Estévez,³ M. K. Smith,² Z. R. Tully,¹ J. R. Vanhoy,⁵ and S. W. Yates^{3,4}

¹Department of Physics, University of Wisconsin–La Crosse, La Crosse, Wisconsin 54601, USA

²Department of Physics, University of Notre Dame, Notre Dame, Indiana 46556, USA

³Department of Physics and Astronomy, University of Kentucky, Lexington, Kentucky 40506, USA

⁴Department of Chemistry, University of Kentucky, Lexington, Kentucky 40506, USA

⁵Department of Physics, United States Naval Academy, Annapolis, Maryland 21402, USA

(Received 14 October 2014; revised manuscript received 3 April 2015; published 18 May 2015)

Excited 0^+ states in ^{160}Gd have been examined with the $(n,n'\gamma)$ reaction at incident neutron energies up to 2.8 MeV. Gamma-ray excitation functions and angular distribution measurements allow the confirmation of the existence of 0^+ states at 1379.70 keV and 1558.30 keV, but we reject the assignments of additional previously suggested 0^+ candidates. Limits on the level lifetimes of the observed 0^+ states permit an evaluation of the collectivity of these states.

DOI: [10.1103/PhysRevC.91.054317](https://doi.org/10.1103/PhysRevC.91.054317)

PACS number(s): 21.10.Tg, 21.10.Re, 25.40.Fq, 27.70.+q

I. INTRODUCTION

The nature of excited 0^+ states remains an open challenge to our understanding in nuclear structure physics [1–6]. The review by Heyde and Wood [1] summarizes the difficulties that have emerged in understanding 0^+ states, both from experimental and theoretical viewpoints. The assertions in Ref. [1] are that a complete characterization of 0^+ states requires the measurements of transfer cross sections and $E0$ transition probabilities, in addition to the knowledge of level energies and absolute transition probabilities. Data on 0^+ states had been sparse until recent (p,t) studies established many excited $K^\pi = 0^+$ states in deformed nuclei [7–13]. Theoretical efforts [14–22] abound and continue to offer possible interpretations of these low-lying excitations in deformed nuclei.

In well-deformed regions of the nuclear landscape, excitations built on a deformed ground state have traditionally been described in terms of quadrupole excitations, leading to the decades-old classification of the first excited 0^+ bands as single-phonon β -vibrational bands. Newer interpretations include the possibility of phase changes at the onset of deformation (for example, at $N = 90$ and $Z = 64$) and the application of new symmetries to describe these nuclei [3,23–27]. Another explanation for the nature of 0^+ bands was given in terms of shape co-existence, where a competing shape is not the lowest favored shape but occurs low in excitation of a given nucleus. Other work [28] expanded on the original description of β vibrations and provided some guidelines to the clear identification of $K^\pi = 0^+$ bands as β vibrations if $B(E2; 2_\beta^+ \rightarrow 0_{\text{g.s.}}^+)$ values are in the range of 2.5–6 W.u., small two-neutron transfer strengths, and large $E0$ values connecting them to the ground state. In the IBM [29–31], the first excited 0^+ and 2^+ bands are members of the same representation in the SU(3) limit and they are only weakly (theoretically forbidden) connected to the ground-state band. Another recent development describes nuclei at or near the

onset of deformation within the Bohr Hamiltonian in the limit of rigid prolate axial symmetry with confined β -soft potentials [16,17,19]. These studies and others [32–34] on the nature of $K^\pi = 0^+$ bands in deformed nuclei show widely varying levels of collectivity for the first excited 0^+ states. Recent experiments have also shown enhanced collectivities in transitions connecting even higher excited states to the first excited 0^+ state [10,35–38].

The goal of this work is to investigate and characterize $K^\pi = 0^+$ bands in ^{160}Gd . In recent years, high-resolution (p,t) reactions on stable nuclei have been used to identify many 0^+ excitations in deformed nuclei; however, this reaction is not possible for ^{160}Gd as the required target nucleus, ^{162}Gd , is unstable ($T_{1/2} = 8.4$ min). The $^{158}\text{Gd}(t,p)^{160}\text{Gd}$ reaction has been performed [39] with the identification of a previously known 0^+ state at 1382 keV and a tentative candidate at 2236 keV. In the present work, we examine the known information on 0^+ states in ^{160}Gd and provide new limits on the collectivity of these excitations.

II. EXPERIMENT

We have measured γ -ray excitation functions and angular distributions using the $^{160}\text{Gd}(n,n'\gamma)$ reaction at the University of Kentucky Accelerator Laboratory (UKAL). Neutrons were produced by the $^3\text{H}(p,n)$ reaction. The scattering sample was 29.456 g of 98.12% enriched $^{160}\text{Gd}_2\text{O}_3$ contained in a thin-walled polyethylene cylinder 3.1 cm in height and 2.3 cm in diameter. The emitted γ rays were detected with a $\sim 50\%$ HPGe detector with time-of-flight gating for background reduction and an annular BGO shield for active Compton suppression [40]. A spectrum is shown in Fig. 1.

An excitation function measurement, performed from $E_n = 1.5$ to 2.8 MeV in 0.08- or 0.1-MeV steps, with the detector at 90° with respect to the incident beam, provided yields of γ rays as a function of neutron energy. This measurement allowed the placement of γ rays to levels based on thresholds. Gamma-ray angular distribution measurements were performed at incident neutron energies of 1.5, 2.0 and 2.8 MeV at ten angles over

*slesher@uwlax.edu

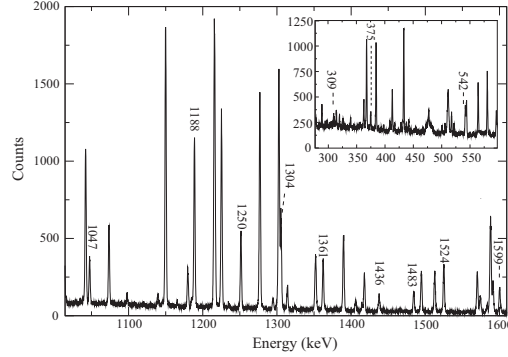


FIG. 1. Portion of the prompt γ -ray energy spectrum from the $^{160}\text{Gd}(n, n'\gamma)$ reaction with 2.0 MeV neutrons, recorded at 90° with respect to the beam axis. The γ -ray energies are given in keV and are located above the peak. The energies shown are for the γ rays associated with the 0^+ bands discussed in the text.

a range of 40° to 150°. The neutron energies were chosen to reduce feeding to the levels of interest to obtain the most accurate lifetimes. The yields of the γ rays, $W(\theta)$, were fitted with even-order Legendre polynomials,

$$W(\theta) = A_0[1 + a_2 P_2(\cos \theta_\gamma) + a_4 P_4(\cos \theta_\gamma)], \quad (1)$$

where a_2 and a_4 depend on the multipolarities and mixing amplitudes of the transition. These results may also be compared with statistical model calculations using CINDY [41] to determine or restrict spin possibilities. The angular

TABLE I. Energy levels, associated with $K^\pi = 0^+$ bands, observed in this work. E_L is the level energy found in this work with uncertainties; I_γ is the relative γ -ray intensity, normalized to 100 for the most intense transition from each level. Mean lifetimes, τ , shown here are the lower limits, therefore, the $B(E2)$ values are upper limits. All of the level lifetimes were obtained from the 2.0 MeV angular distribution data except for the 1379 keV level, in which the 1.5 MeV angular distribution data were used.

E_L (keV)	E_f (keV)	$J_i^\pi \rightarrow J_f^\pi$	E_γ (keV)	I_γ	$F(\tau)$ (fs)	τ (fs)	$B(E2)$ (W.u.)	$B(E1)$ $\times 10^3$ (W.u.)	Notes
$K^\pi = 0^+_2$									
1379.70(7)	75.25	$0^+_2 \rightarrow 2^+_g$	1304.46(5)	100	0.015 ± 0.014	>1350	<3.10		
1436.47(4)	248.64	$2^+ \rightarrow 4^+_g$	1187.81(5)	100(1)	0.062 ± 0.074	>340	<13.1		
	75.25	$2^+ \rightarrow 2^+_g$	1361.05(6)	36.4(4)	0.041 ± 0.068		<2.42		
	0.0	$2^+ \rightarrow 0^+_g$	1436.34(6)	13.5(2)	0.005 ± 0.070		<0.68		
1561.59(6)	515.10	$4^+ \rightarrow 6^+_g$	1046.67(6)	100(1)	0.051 ± 0.091	>320	<22		^a
	248.64	$4^+ \rightarrow 4^+_g$	1313.03(6)	74.8(3)	0.040 ± 0.072		<5.4		
$K^\pi = 0^+_3$									
1558.30(7)	75.25	$0^+_3 \rightarrow 2^+_g$	1483.06(6)	100	0.004 ± 0.069	>590	<3.74		
1599.00(4)	1290.01	$2^+ \rightarrow 3^-$	309.32(6)	8.9(4)	-0.132 ± 0.538	>300		<1.37	^b
	1224.33	$2^+ \rightarrow 1^-$	374.78(6)	14.8(3)	-0.205 ± 0.326			<1.3	^b
	1057.60	$2^+ \rightarrow 3^+$	541.53(6)	36.8(3)	0.161 ± 0.205		<174		^c
	75.25	$2^+ \rightarrow 2^+_g$	1523.59(6)	100(1)	0.056 ± 0.064		<2.68		
	0.00	$2^+ \rightarrow 0^+_g$	1598.85(6)	78.7(1)	0.055 ± 0.063		<1.66		

^aThis level may be assigned incorrectly, please see text.

^bThis transition was not used to calculate the level lifetime.

^cThis is a mixed $E2/M1$ transition, if a pure $M1$, the value is $B(M1) < 0.18\mu_N^2$.

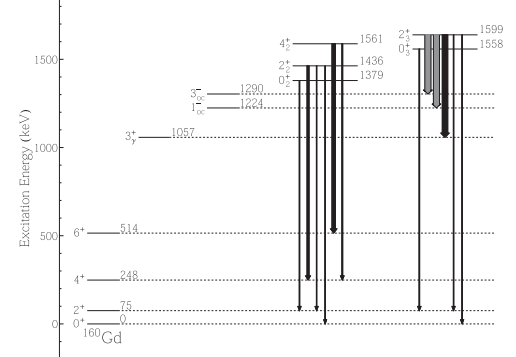


FIG. 2. Partial level scheme for the 0^+ bands discussed in this work. The solid black arrows are $E2$ transitions and the grey arrows are $E1$ transitions. The upper limits of the transition probabilities are given in Table I.

distribution measurements were also used to measure lifetimes of excited states shorter than 1 ps [42] via the Doppler-shift attenuation method (DSAM). The energies of the detected photons are

$$E_\gamma(\theta_\gamma) = E_{\gamma 0} \left[1 + \frac{v_0}{c} F(\tau) \cos \theta_\gamma \right], \quad (2)$$

where $E_{\gamma 0}$ is the unshifted γ -ray energy, v_0 is the recoil velocity of the center-of-mass frame, θ_γ is the angle of observation, and $F(\tau)$ is the experimental attenuation factor [42]. The average lifetime of a state, τ , is determined by

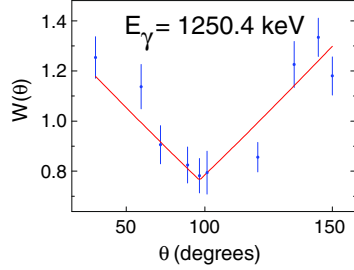


FIG. 3. (Color online) The γ -ray angular distributions for the 1250.4-keV γ ray, which is not isotropic and, therefore, is not from a 0^+ state.

examining the energy of the γ ray as a function of angle, extracting the $F(\tau)$ value, and comparing with the theoretical $F(\tau)$ curve calculated using the Winterbon formalism [43]. The lifetimes determined from each γ ray depopulating a level must match within experimental uncertainties, aiding in the assignment of γ rays to specific levels.

In all measurements, ^{226}Ra and ^{152}Eu standard sources were used out-of-beam for energy and efficiency calibrations. A ^{60}Co source placed near the detector during the angular distribution measurements was used as a continuous check for gain shifts. At higher neutron energies, an additional in-beam ^{24}Na source was employed for accurate energy identification. NaCl rings were irradiated off-line with neutrons from a ^{252}Cf source to produce ^{24}Na , which emits 1368.63- and 2754.03-keV γ rays. These methods and techniques are described in greater detail in other publications [40,44,45].

Lifetime and angular distribution measurements were compared with previous data. There are very few lifetimes known in the range of our measurements; however, we were able to compare our measured lifetime ($\tau = 21 \pm 2$ fs) of the 1^- level at 1224.28 keV with the evaluated value of $\tau = 22 \pm 6$ fs [46] which exhibits excellent agreement. The angular distribution were normalized to the known 0^+ γ -ray energy at 1304.46 keV.

III. RESULTS AND DISCUSSION

The results from these experiments are summarized for all of the 0^+ states in Table I. We confirm the 0^+ state at 1379.70 keV [39,47] and the former tentative assignment of a 0^+ state at 1558.30 keV [48]. We reject the former

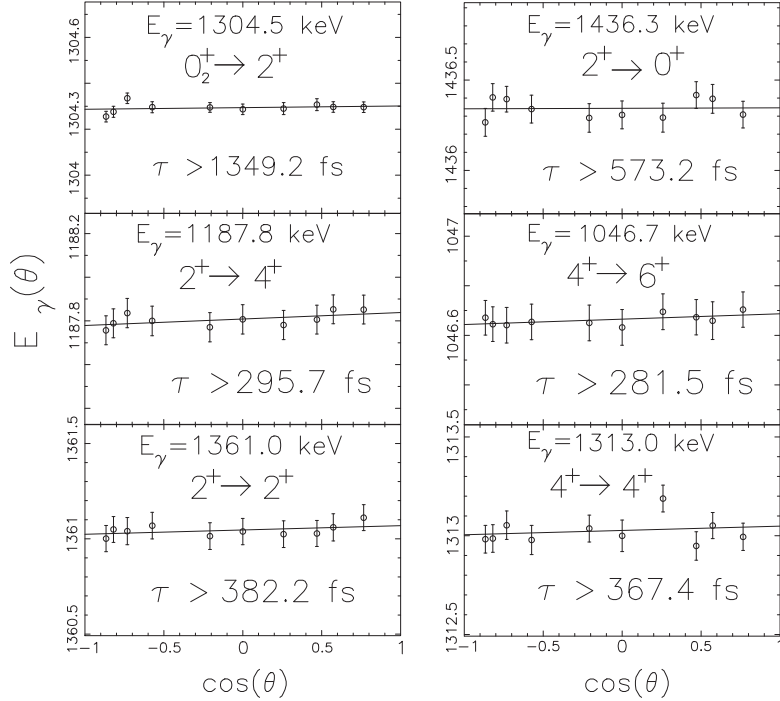


FIG. 4. $E_\gamma(\theta)$ (in keV) versus $\cos \theta$ for selected γ rays in ^{160}Gd . Each of the 0^+ , 2^+ , and 4^+ levels in the 0^+ bands are shown. The lifetime for each γ -ray transition is averaged (weighted for branching ratio) for the level lifetime. The γ rays exhibit small energy shifts and, therefore, only limits on the lifetimes are obtained.

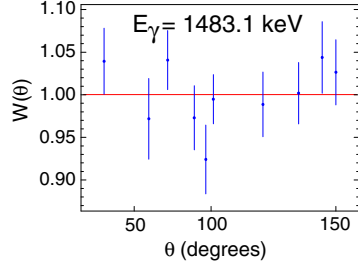


FIG. 5. (Color online) The γ -ray angular distribution of the 1483 keV γ ray from the 1558-keV 0^+ state, $a_2 = 0.053 \pm 0.038$.

tentative assignments of 0^+ for states at 1325.73 keV [49] and 2236 keV [39]. A partial level scheme is shown in Fig. 2 including the confirmed 0^+ bands. A detailed discussion of the measurements by level energies follows below.

In this experiment we did not attempt to assign new spin-0 states but to confirm the existing levels and obtain level lifetimes. The angular distributions and excitation functions aided the outcome in different ways. First, excitation functions supported the γ rays as depopulating a given level by their

appearance thresholds. This also led to the identification of any additional γ rays from the level by matching energy and excitation function thresholds.

In order to confirm the 0^+ assignment of a level, it is required that the γ -ray angular distributions from these 0^+ states be isotropic, i.e., $a_2 = 0$ in Eq. (1). The angular distribution data were also used to extract level lifetimes. A search for the in-band decays of the 2^+ members of the 0^+ bands was unsuccessful due to absorption in our thick sample and internal conversion, we are generally unable to observe <100 keV γ rays. Table I lists the 0^+ states of ^{160}Gd confirmed in this work and the spectroscopic information obtained in these experiments. As internal conversion electron data are not available, the $E0$ decays to the ground states are not taken into account. Specific details follow for each level.

A. 1325.73-keV level

The level at 1325.73 keV was formerly given a tentative 0^+ assignment based on energy considerations by Berzin *et al.* [49] in $(n,n'\gamma)$ measurement using reactor neutrons. Gover *et al.* [48] disagreed, stating that the transition is not isotropic and placing the $E_\gamma = 1250.42$ keV as a decay from a $J^\pi = 4^-$, 1498.87 keV level. From our measurement, the 1250.42 keV γ -ray transition is not isotropic (see Fig. 3). The

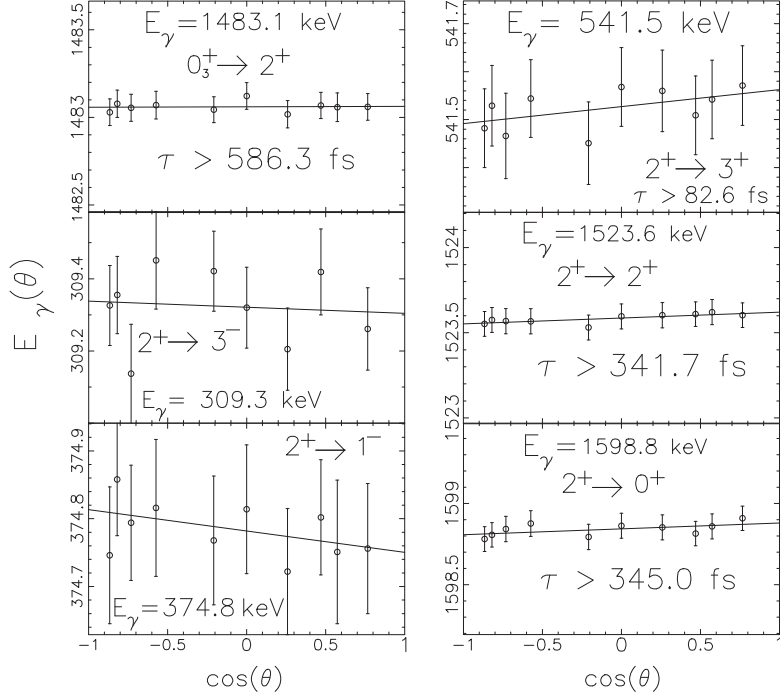


FIG. 6. $E_\gamma(\theta)$ (in keV) versus $\cos \theta$ of the 0_3^+ band in ^{160}Gd . Each of the 0^+ and 2^+ levels are shown. The lifetime for each γ -ray transition is averaged (weighted for branching ratio) for the level lifetime. The γ rays exhibit small energy shifts and, therefore, only limits on the lifetimes are obtained.

angular distribution has a nonzero a_2 value of 0.48 ± 0.10 , and therefore agree with Ref. [48] in excluding a spin and parity assignment of 0^+ at 1325.73 keV. The excitation function threshold of 1.5 MeV suggests two possible placements of this γ ray. One is the current placement at 1325 keV with decay to the 2_g^+ state; the second is at 1498 keV with decay to the 4_g^+ state. Since the threshold of the γ ray has a low intensity at $E_n = 1.5$ MeV, the placement at 1498 keV is favored. The CINDY calculations do not aid our ability to narrow down the spin possibilities. Our data, therefore, supports the placement of the 1250-keV γ ray at the 1498-keV level, but we cannot comment on the spin assignment made by Ref. [48], especially since the 441.51-keV γ ray was not observed.

B. $K = 0_2^+$ band

This band was observed in $^{158}\text{Gd}(t, p)$ reaction [39] and first assigned in early $(n, n'\gamma)$ work [47]. We have observed a single γ ray ($E_\gamma = 1304.46$ keV) from the 0_2^+ level at 1379.70 keV. The energy threshold of the excitation function supports this placement. We were able to extract a lifetime limit of > 1350 fs for this level, which was used to calculate a $B(E2; 0_2^+ \rightarrow 2_2^+)$ limit of < 3.10 W.u. as shown in Fig. 4.

Identified in Ref. [49] as part of the band structure, a 2^+ state at 1436 keV is included in Table I. Again, we were unable to observe the < 100 keV intraband transition. A level lifetime limit of > 340 fs was established and $B(E2)$ upper limits were calculated. The angular distribution data from the 2.0-MeV experiment was used for the lifetime measurements and branching ratios, because of the higher statistical quality than in the 1.5-MeV data.

Gover *et al.* [48] assigned a 4^+ state at 1561.48 keV as part of this band. Our γ ray intensities from this level agree within uncertainties with these in Ref. [48]. According to the Alaga rules, the $B(E2; 4^+ \rightarrow 2_g^+)$ should have approximately the same value as the $B(E2; 4^+ \rightarrow 4_g^+)$, however, the decay to the 2_g^+ is not observed. This is an indication that the 1561 keV level is not a member of this 0^+ band.

C. $K = 0_3^+$ band

A previous $(n, n'\gamma)$ experiment assigned $J^\pi = 0^+$ to the level at 1558.30 keV by the intensity and the nearly isotropic nature of the angular distribution of the 1483.06-keV γ ray [48]. The angular distribution data do not exclude the level as a spin-zero state, $a_2 = 0.053 \pm 0.038$ (Fig. 5). We were able to obtain a lower lifetime limit of 590 fs which corresponds to a $B(E2)$ upper limit of 3.74 W.u. The 2^+ member of the band at 1599.00 keV decays to many levels including the 3^+ level of the γ -vibrational band. The $B(E2)$ values are given

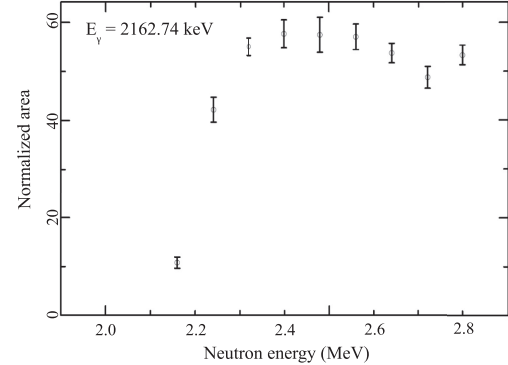


FIG. 7. Excitation function plot for the 2162.7-keV γ ray.

in Table I and the $F(\tau)$ plots are shown in Fig. 6. The lowest energy γ -ray decays have negligible shifts; these γ rays were not used in calculating the level lifetime.

D. 2236-keV level

One additional level was tentatively assigned as a spin-0 level in the (t, p) study [39]. We searched for γ rays from a possible level at this energy. A single γ ray, $E_\gamma = 2162.74$ keV, was observed, but it could not be assigned to this level, because the excitation function threshold of 2.16 MeV is too low (see Fig. 7) and the angular distribution is not isotropic.

IV. SUMMARY

We have studied the previously identified $K^\pi = 0^+$ states in ^{160}Gd with the $(n, n'\gamma)$ reaction. Gamma-ray excitation functions, angular distributions, and lifetime measurements were used to characterize the levels at 1325.73, 1379.70, 1558.30, and 2236 keV. Our results allow the confirmation of levels at 1379.70 keV and 1558.30 keV as 0^+ states and the measurements of level lifetimes for three and two states, respectively, built on these 0^+ states. Our angular distributions indicate that the levels at 1325.73 and the 2236 keV are not 0^+ states.

ACKNOWLEDGMENTS

We thank H. E. Baber for his help with accelerator maintenance and operation. This material is based upon work supported by the National Science Foundation under Grant Nos. PHY-1205412, PHY-1068192, and PHY-1305801.

-
- [1] K. Heyde and J. L. Wood, *Rev. Mod. Phys.* **83**, 1467 (2011).
[2] P. E. Garrett, W. D. Kulp, J. L. Wood, D. Bandyopadhyay, S. Choudry, D. Dashdorj, S. R. Lesher, M. T. McEllistrem, M. Mynk, J. N. Orce *et al.*, *Phys. Rev. Lett.* **103**, 062501 (2009).
[3] R. F. Casten and P. von Brentano, *Phys. Rev. C* **50**, R1280 (1994).
[4] A. Aprahamian, R. C. de Haan, S. R. Lesher, J. Döring, A. M. Bruce, H. G. Börner, M. Jentschel, and H. Lehmann, *J. Phys. G* **25**, 685 (1999).

- [5] X. Wu, A. Aprahamian, J. Castro-Ceron, and C. Baktash, *Phys. Lett. B* **316**, 235 (1993).
- [6] X. Wu, A. Aprahamian, S. M. Fischer, W. Reviol, G. Liu, and J. X. Saladin, *Phys. Rev. C* **49**, 1837 (1994).
- [7] S. R. Lesher, A. Aprahamian, L. Trache, A. Oros-Peusquens, S. Deyliz, A. Gollwitzer, R. Hertenberger, B. D. Vahlion, and G. Graw, *Phys. Rev. C* **66**, 051305(R) (2002).
- [8] D. A. Meyer, V. Wood, R. F. Casten, C. R. Fitzpatrick, G. Graw, D. Bucurescu, J. Jolie, P. von Brentano, R. Hertenberger, H.-F. Wirth *et al.*, *Phys. Rev. C* **74**, 044309 (2006).
- [9] D. Bucurescu, G. Graw, R. Hertenberger, H.-F. Wirth, N. Lo Iudice, A. V. Sushkov, N. Y. Shirikova, Y. Sun, T. Faestermann, R. Krücken *et al.*, *Phys. Rev. C* **73**, 064309 (2006).
- [10] S. R. Lesher, J. N. Orce, Z. Ammar, C. D. Hannant, M. Merrick, N. Warr, T. B. Brown, N. Boukharouba, C. Fransen, M. Scheck *et al.*, *Phys. Rev. C* **76**, 034318 (2007).
- [11] L. Bettermann, S. Heinze, J. Jolie, D. Mücher, O. Möller, C. Scholl, R. F. Casten, D. Meyer, G. Graw, R. Hertenberger *et al.*, *Phys. Rev. C* **80**, 044333 (2009).
- [12] C. Bernards, R. F. Casten, V. Werner, P. von Brentano, D. Bucurescu, G. Graw, S. Heinze, R. Hertenberger, J. Jolie, S. Lalkovski *et al.*, *Phys. Rev. C* **87**, 064321 (2013).
- [13] C. Bernards, R. F. Casten, V. Werner, P. von Brentano, D. Bucurescu, G. Graw, S. Heinze, R. Hertenberger, J. Jolie, S. Lalkovski *et al.*, *Phys. Rev. C* **87**, 024318 (2013).
- [14] N. V. Zamfir, J.-y. Zhang, and R. F. Casten, *Phys. Rev. C* **66**, 057303 (2002).
- [15] Y. Sun, A. Aprahamian, J.-y. Zhang, and C.-T. Lee, *Phys. Rev. C* **68**, 061301(R) (2003).
- [16] N. Pietralla and O. M. Gorbachenko, *Phys. Rev. C* **70**, 011304(R) (2004).
- [17] K. Dusling, N. Pietralla, G. Rainovski, T. Ahn, B. Bochev, A. Costin, T. Koike, T. C. Li, A. Linnemann, S. Pontillo *et al.*, *Phys. Rev. C* **73**, 014317 (2006).
- [18] R. Fossion, C. E. Alonso, J. M. Arias, L. Fortunato, and A. Vitturi, *Phys. Rev. C* **76**, 014316 (2007).
- [19] D. Bonatsos, E. A. McCutchan, R. F. Casten, R. J. Casperson, V. Werner, and E. Williams, *Phys. Rev. C* **80**, 034311 (2009).
- [20] R. M. Clark, R. F. Casten, L. Bettermann, and R. Winkler, *Phys. Rev. C* **80**, 011303(R) (2009).
- [21] N. Lo Iudice, V. Yu. Ponomarev, Ch. Stoyanov, A. V. Sushkov, and V. V. Voronov, *J. Phys. G: Nucl. Part. Phys.* **39**, 043101 (2012).
- [22] F.-Q. Chen, Y. Sun, and P. Ring, *Phys. Rev. C* **88**, 014315 (2013).
- [23] A. Arima and F. Iachello, *Ann. Phys. (NY)* **99**, 253 (1976).
- [24] R. F. Casten, P. von Brentano, and N. V. Zamfir, *Phys. Rev. C* **49**, 1940 (1994).
- [25] R. F. Casten and P. von Brentano, *Phys. Rev. C* **51**, 3528 (1995).
- [26] F. Iachello, N. V. Zamfir, and R. F. Casten, *Phys. Rev. Lett.* **81**, 1191 (1998).
- [27] V. Werner, E. Williams, R. J. Casperson, R. F. Casten, C. Scholl, and P. von Brentano, *Phys. Rev. C* **78**, 051303(R) (2008).
- [28] P. E. Garrett, *J. Phys. G: Nucl. Part. Phys.* **27**, R1 (2001).
- [29] D. D. Warner and R. F. Casten, *Phys. Rev. C* **25**, 2019 (1982).
- [30] D. D. Warner and R. F. Casten, *Phys. Rev. Lett.* **48**, 1385 (1982).
- [31] R. F. Casten and D. D. Warner, *Rev. Mod. Phys.* **60**, 389 (1988).
- [32] J. F. Sharpey-Schafer, T. E. Madiba, S. P. Bvumbi, E. A. Lawrie, J. J. Lawrie, A. Minkova, S. M. Mullins, P. Papka, D. G. Roux, and J. Timár, *Eur. Phys. J. A* **47**, 6 (2011).
- [33] J. F. Sharpey-Schafer, *AIP Conf. Proc.* **1377**, 205 (2011).
- [34] J. F. Sharpey-Schafer, S. M. Mullins, R. A. Bark, J. Kau, F. Komati, E. A. Lawrie, J. J. Lawrie, T. E. Madiba, P. Maine, A. Minkova *et al.*, *Eur. Phys. J. A* **47**, 5 (2011).
- [35] P. E. Garrett, M. Kadi, C. A. McGrath, V. Sorokin, M. Li, M. Yeh, and S. W. Yates, *Phys. Lett. B* **400**, 250 (1997).
- [36] R. C. de Haan, A. Aprahamian, H. G. Börner, C. Doll, M. Jentschel, A. M. Bruce, and S. R. Lesher, *J. Res. Natl. Inst. Stand. Technol.* **105**, 125 (2000).
- [37] A. Aprahamian, R. C. de Haan, H. G. Börner, H. Lehmann, C. Doll, M. Jentschel, A. M. Bruce, and R. Piepenbring, *Phys. Rev. C* **65**, 031301(R) (2002).
- [38] A. Aprahamian, *Phys. At. Nucl.* **67**, 1750 (2004).
- [39] G. Løvhøiden, T. F. Thorsteinsen, and D. G. Burke, *Phys. Scr.* **34**, 691 (1986).
- [40] P. E. Garrett, N. Warr, and S. W. Yates, *J. Res. Natl. Inst. Stand. Technol.* **105**, 141 (2000).
- [41] E. Shelton and V. C. Rodgers, *Comput. Phys. Commun.* **6**, 99 (1973).
- [42] T. Belya, G. Molnár, and S. W. Yates, *Nucl. Phys. A* **607**, 43 (1996).
- [43] K. B. Winterbon, *Nucl. Phys. A* **246**, 293 (1975).
- [44] P. E. Garrett, H. Lehmann, J. Jolie, C. A. McGrath, M. Yeh, W. Younes, and S. W. Yates, *Phys. Rev. C* **64**, 024316 (2001).
- [45] E. E. Peters, A. Chakraborty, B. P. Crider, B. H. Davis, M. K. Gnanamani, M. T. McEllistrem, F. M. Prados-Estévez, J. R. Vanhoy, and S. W. Yates, *Phys. Rev. C* **88**, 024317 (2013).
- [46] C. W. Reich, *Nucl. Data Sheets* **105**, 557 (2005).
- [47] S. A. Elbakr, I. J. van Heerden, D. R. Gill, N. Ahmed, W. J. McDonald, G. C. Neilson, and W. K. Dawson, *Phys. Rev. C* **10**, 1864 (1974).
- [48] L. I. Gover, A. M. Demidov, V. A. Kurkin, and I. V. Mikhailov, *Phys. Atomic Nuclei* **72**, 1799 (2009).
- [49] Ya. Ya. Berzin, E. P. Grigorév, T. V. Guseva, and Yu. Ya. Tamberg, *Bull. Acad. Sci. USSR, Phys. Ser.* **53**, 76 (1989).

APPENDIX B

^{160}Gd NEGATIVE PARITY STATES

Appendix B includes the final manuscript slated to be submitted to Phys. Rev. C in early 2017, authored by S.R. Lesher, A. Aprahamian, C. Casarella, *et. al* on the second set of results from the ^{160}Gd experiments, namely the measurement of key lifetimes of negative parity bands.

Lifetime measurements of low-spin negative-parity levels in ^{160}Gd

S.R. Lesher,^{1,2,*} C. Casarella,² A. Aprahamian,² L. M. Robledo,³ B. P. Crider,^{4,†} R. Ikeyama,¹ I. R. Marsh,¹ M. T. McEllistrem,⁴ E. E. Peters,⁵ F. M. Prados-Estévez,^{4,5} M. K. Smith,² Z. R. Tully,¹ J. R. Vanhoy,⁶ and S. W. Yates^{4,5}

¹*Department of Physics, University of Wisconsin – La Crosse, La Crosse, Wisconsin 54601-3742, USA*

²*Department of Physics, University of Notre Dame, Notre Dame, Indiana 46556, USA*

³*Dep. Física Teórica (Módulo 15), Universidad Autónoma de Madrid, E-28049 Madrid, Spain*

⁴*Department of Physics and Astronomy, University of Kentucky, Lexington, Kentucky 40506-0055, USA*

⁵*Department of Chemistry, University of Kentucky, Lexington, Kentucky 40506-0055, USA*

⁶*Department of Physics, United States Naval Academy, Annapolis, Maryland 21402, USA*

(Dated: November 29, 2016)

$^{160}\text{Gd}(n, n'\gamma)$ experiments were performed at the University of Kentucky Accelerator Laboratory with monoenergetic neutrons. Excitation functions at neutron energies from 1.5 to 2.8 MeV aided in the placement of γ rays in the level scheme and angular distributions at three neutron energies resulted in the determination of twenty eight excited-level lifetimes or limits in ^{160}Gd , including the lifetimes of several negative-parity levels attributed to octupole vibrations.

I. INTRODUCTION

The ^{160}Gd nucleus lies in the midst of the well-known rare-earth region of deformation between $N = 50$ and $N = 82$, and has an $R_{4/2} [\equiv E(4_{gs}^+)/E(2_{gs}^+)]$ ratio of 3.30, placing it close to the rotational limit of 3.33. An open question in nuclear structure is the viability of vibrational excitations in deformed nuclei. The lowest-lying excited vibrational modes include the quadrupole and octupole modes. Single-phonon quadrupole modes include γ and β vibrations. The γ vibration seems to be well characterized as the first $K^\pi = 2^+$ band and exhibits a systematic behavior across the region of deformed nuclei with typical $B(E2; 2_\gamma^+ \rightarrow 0_{gs}^+)$ values of a few Weisskopf units (W.u.). In contrast, the β vibration does not show these systematic characteristics as the $B(E2)$ values of transitions de-exciting the first excited $K^\pi = 0^+$ band vary greatly throughout the deformed region [1, 2]. The question regarding the viability of the β -vibration in deformed nuclei remains open to debate [3–8].

Octupole excitations in spherical nuclei are identified by large $B(E3; 0_{gs}^+ \rightarrow 3^-)$ [9] values, and a compilation of $B(E3)$ values of the lowest 3^- states can be found in Ref. [10]. In deformed nuclei, the octupole mode splits into $K^\pi = 0^-, 1^-, 2^-,$ and 3^- bands. The increasing level density with excitation energy and the proximity of the pairing gap complicate the identification of vibrations in deformed nuclei. Two-phonon octupole excitations have been observed in spherical nuclei of the rare-earth region – ^{144}Sm [11], ^{146}Sm [12], ^{146}Gd [13], ^{147}Gd [14], and ^{148}Gd [15, 16] – as has the combined two-phonon quadrupole-octupole vibrational mode ($2^+ \otimes 3^-$) in nearly spherical nuclei – e.g., ^{144}Sm [11], ^{146}Sm [17], and ^{148}Gd [12]. A few cases have been suggested as two-phonon double- γ vibrations ($K^\pi = 4^+$) in ^{164}Dy [18], ^{166}Er [19], ^{168}Er [20–22], and ($K^\pi = 0^+$) in ^{166}Er [23]. A two-phonon double- β vibration has also been proposed in ^{178}Hf [24].

The low-lying structure of ^{160}Gd has been extensively studied; there are numerous positive- and negative-parity bands identified in this nucleus, including an excited $K^\pi = 2^+$, and several excited $K^\pi = 0^+$ bands, as well as $K^\pi = 0^-$, 1^- , and 2^- bands. There is, however, a paucity of level lifetimes and transition probabilities to clearly identify the collectivity or lack of it for these excitations. Our recent paper reported on the lifetimes and characteristics of the $K^\pi = 0^+$ states [25] in this nucleus. This work reports mainly on the lifetime measurements of levels in low-lying $K^\pi = 0^-$, 1^- , and 2^- bands. Using the $(n, n'\gamma)$ reaction and Doppler-shift attenuation method, we have determined the lifetimes of twenty eight excited levels in ^{160}Gd , twenty of them for the first time.

II. EXPERIMENT

The low-lying states of ^{160}Gd were studied with the $(n, n'\gamma)$ reaction at the University of Kentucky Accelerator Laboratory (UKAL) with monoenergetic neutrons produced by the $^3\text{H}(p, n)^3\text{He}$ reaction. The scattering sample was

* Electronic address: slesher@uwlax.edu

† present address: National Superconducting Cyclotron Laboratory, Michigan State University, East Lansing, Michigan, 48824, USA

29.456 g of 98.12% enriched $^{160}\text{Gd}_2\text{O}_3$ contained in a thin-walled polyethylene cylinder 3.1 cm in height and 2.3 cm in diameter. The emitted γ rays were recorded with a Compton-suppressed HPGe detector with a relative efficiency of 50%. A bismuth germanate (BGO) active shield was used for Compton suppression. The HPGe detector was located at a distance of 119.3 cm from the scattering sample, and time-of-flight gating was used to suppress background radiation. Standard radioactive sources, ^{226}Ra and ^{152}Eu , were used for energy and efficiency calibration of the HPGe detector. In angular distribution measurements, a ^{60}Co source was placed near the detector as a continuous check on gain stability. At higher neutron energies, ^{24}Na was used as an additional in-beam source for accurate energy determination. Additional descriptions of the experimental setup and techniques are documented in Refs. [26–28].

The excitation function measurement provided yields of γ rays as a function of incident neutron energy (E_n), and spectra were measured for $E_n = 1.5$ to 2.8 MeV in 80- or 100-keV steps, with the detector at 90° with respect to the beam axis. Examples of the excitation functions obtained for γ rays from the same level are shown in Fig. 1. Excitation thresholds were used to place γ rays and establish levels. Angular-distribution spectra were recorded at neutron energies of 1.5, 2.0, and 2.8 MeV at ten angles over a range of 40° to 150° . To obtain the most accurate lifetimes, these neutron energies were chosen to reduce feeding to the levels of interest. The angular distributions of the γ -ray intensities, $W(\theta)$ were fitted with a function of even-order Legendre polynomials,

$$W(\theta) = A_o [1 + a_2 P_2(\cos \theta_\gamma) + a_4 P_4(\cos \theta_\gamma)], \quad (1)$$

where the parameters a_2 and a_4 depend on the multipolarities and mixing amplitudes of the transitions. The experimental values of these parameters were then compared to statistical model calculations from the code CINDY [29] to determine multipole mixing ratios (δ) of the transitions. If the intensity of the γ ray was small or if the statistical uncertainty was large, the a_2 and a_4 values were compared with those in Govor, *et al.* [30]. Provided the values matched within uncertainties, the values of Ref. [30] were used in relevant calculations and noted.

The angular distribution measurements were also used to extract lifetimes of excited states shorter than about 1 ps by the Doppler-shift attenuation method (DSAM) [31]. The energies of the γ rays have an angular dependence described by

$$E_\gamma(\theta_\gamma) = E_{\gamma 0} \left[1 + \frac{v_{cm}}{c} F(\tau) \cos \theta_\gamma \right] \quad (2)$$

where $E_{\gamma 0}$ is the unshifted γ -ray energy, v_{cm} is the recoil velocity of the center-of-mass, θ_γ is the angle of observation, and $F(\tau)$ is the attenuation factor, which depends on the stopping powers. By examining the energy of a γ ray as a function of angle, the $F(\tau)$ value can be extracted and compared with those calculated using the Winterbon stopping power formalism [32], and the lifetime of the state, τ , can be obtained. An extensive discussion on the DSAM can be found in Ref. [31].

III. RESULTS

We measured twenty eight excited level lifetimes in ^{160}Gd . The levels, depopulating transitions, multipole mixing ratios, and resulting $B(E\lambda)$ transition probabilities are listed in Table I. Energies listed for the γ rays were obtained from the angular distribution measurements at the lowest incident neutron energy for which the γ -ray yields were observed to have good statistics. This procedure allowed for accurate energies of peaks which may evolve into complex structures at higher incident neutron energies. The branching ratios and lifetimes were also obtained at the lowest feasible neutron energies. The level energies were determined by a weighted least-squares fit of all the γ rays to and from a level.

Since the last evaluation of ^{160}Gd [33], three papers have made additions to the ^{160}Gd level structure using the $(n, n'\gamma)$ reaction [25, 30, 34]. This information has been considered with the current results and is presented in Table I. Gamma rays from a level were only included if the excitation functions matched in shape and threshold for all γ rays. For weak branches, the threshold may not have been observed but the shape was consistent. The threshold energy was enough to determine if the γ ray did not belong to a level and an attempt was made to assign it to the correct level. For example, a γ -ray was observed before the level was populated with neutrons. There were also previously placed γ rays that were below our experimental observation threshold and these were not included in the level scheme [30].

In the following sections, we discuss levels which are germane to the $K^\pi = 2^+$ band and the negative-parity bands in ^{160}Gd . A partial level scheme is shown in Fig. 2.

A. $K^\pi = 2_7^+$ band

The 2_7^+ bandhead at 988.72 keV had a previously measured level lifetime of 1876(87) fs. This value is the weighted average of four Coulomb excitation experiments [35–38] as given in the latest nuclear data compilation of A=160 [33]. We observed three γ rays from this level, but only the 913.43- and 988.68-keV γ rays were used in extracting the level lifetime limit of > 1800 fs. This value is near the limit of our method, but is consistent with the accepted literature value. The 739.96 keV γ ray coincides with an experimental background line and, therefore, was not used in determining the level lifetime. In Table I, transition probabilities were calculated using this literature lifetime and the associated branching ratios from Ref. [30] to calculate the $B(E2)$ values presented, after ensuring the consistency of the observed branching ratios with our data.

The 4_7^+ member of the band at 1148.15 keV depopulates by 899.59 and 1072.85 keV transitions. Govor *et al.* [30] observed a doublet at a γ -ray energy of 632.89 keV, which they placed as decays from both the 1148.14- and 1621.44-keV levels. From the excitation function shape and threshold, we cannot support either placement nor were we able to obtain a lifetime.

The level at 1148.15 keV is assigned as $J^\pi = 4^+$ from polarized proton scattering measurements, and the authors concluded a hexadecapole component for this state [39]. Our work yields a level lifetime $\tau = 1080^{+730}_{-320}$ fs, leading to $B(E2; 4_7^+ \rightarrow 4_{gs}^+) = 16^{+5}_{-10}$ W.u. and $B(E2; 4_7^+ \rightarrow 2_{gs}^+) = 3.8^{+2.6}_{-1.1}$ W.u., consistent with the expected quadrupole collectivity of this level and the $K^\pi = 2^+$ γ bands in the rare-earth deformed region of nuclei.

The 1261.24-keV 5_7^+ level decays to the ground-state band, $B(E2; 5_7^+ \rightarrow 4_{gs}^+) = 35^{+8}_{-12}$ W.u. and $B(E2; 5_7^+ \rightarrow 6_{gs}^+) = 31^{+7}_{-10}$ W.u. The ratios of these transition probabilities are consistent, within error, with the Alaga rules.

B. $K^\pi = 0^-$ band

The 3_1^- level at 1289.90 keV depopulates by two γ rays, 1041.37 and 1214.79 keV. The 1214.79-keV γ ray is observed with an $a_2 = -0.276(33)$, which supports the assignment of an $E1$ transition. Ref. [30] assigns the 1214.79-keV γ ray as a doublet, but we see only a single γ ray in our measurements. A lifetime of $\tau = 74 \pm 20$ fs was reported from Coulomb excitation and Doppler-broadening measurements [38], but our value of $\tau = 34 \pm 3$ fs is not in agreement with this value. An advantage of the $(n, n'\gamma)$ reaction with accelerator-produced neutrons of variable energies is the ability to nonselectively populate levels up to the incident neutron energy. By determining the lifetime of the 1289.90-keV level at $E_n = 1.5$ MeV, the feeding of the level has been greatly reduced from levels with significantly longer lifetimes. If the neutron energy is increased to 2.0 MeV, increasing feeding from higher levels, the apparent lifetime is increased to $\tau = 60 \pm 10$ fs. The method of selecting the neutron energy for population of the level gives us confidence in our measured values. The $K^\pi = 0^-$ band with 1_1^- , 3_1^- , 5_1^- members at 1224.33, 1289.90, and 1427.40 keV, respectively, decay by $E1$ transitions to the ground-state band. $E1$ transitions to the γ band were not observed.

C. $K^\pi = 1^-$ band

The 1351.30-keV level is the bandhead of the $K^\pi = 1^-$ band and was introduced in Ref. [40] by the placement of 1351.0- and 1275.90-keV γ rays. We observe both of these γ rays, and our spectra are not complicated by the doublet at 1351.09 keV reported in Ref. [30]. We determine a level lifetime of $\tau = 180 \pm 20$ fs.

A level at 1388.64 keV was assigned by Berzin *et al.* [40] with five de-exciting γ rays, where those at 1388.7 and 1313.0 keV were the most intense. In later work [30], this level was rejected on the basis of a measured angular distribution and the 1388.56-keV γ ray was assigned to a new 3^- level at 1464.00 keV. This 1464.00-keV level was assigned as a $J^\pi = 3^-$ member of the 1^- band [30]. The 1388.75-keV γ ray has an excitation threshold of 1.5 MeV which favors the placement from the 1464.00-keV level with an a_2 value in agreement with Ref. [30]. Further evidence to support the removal of the 1388.7-keV level is obtained from the γ ray at 1313.03 keV. The excitation threshold is higher than for the 1388.64-keV γ ray and is consistent with the placement at the 1561.63-keV level. Our data do not support any other decays to or from the 1388.7- or the 1464.00-keV level. The 1388.64-keV level has been removed from the level scheme.

D. $K^\pi = 2^-$ band

A $K^\pi = 2^-$ band was proposed in Ref. [34] with levels at 1621.4 keV (2^-), 1691.4 keV (3^-), 1782.5 keV (4^-), and 1884.2 keV (5^-).

In Ref. [30], a doublet at 632.82 keV was reported and the γ rays were placed from the 1148.14-keV level (4_{γ}^{+}) and a 1621-keV level. The energy thresholds in our data do not support either placement. We have observed that the excitation functions of the 632.94- and 564.06-keV γ rays match; however, the threshold of the much more intense 632.94-keV γ ray is 1.6 MeV, which precludes the placement at 1621.4 keV. Although the 564.06-keV γ ray does not appear in the $E_n = 1.6$ -MeV spectrum, the intensity is one-fourth the intensity of the 632.94-keV γ ray. While the shapes of the excitation functions indicate that they are deexciting the same level, we are unable to place them.

The γ rays observed in this work from the 3^{-} level at 1691.68 keV agree with those proposed in Ref. [30]. We observe a level lifetime of $\tau = 230_{-100}^{+350}$ fs with a preferred decay to the γ band, $B(E1; 3_{\gamma}^{-} \rightarrow 4_{\gamma}^{+}) = 2_{-3}^{+1}$ mW.u., $B(E1; 3_{\gamma}^{-} \rightarrow 3_{\gamma}^{+}) = 2.1_{-3.2}^{+0.9}$ mW.u., and $B(E1; 3_{\gamma}^{-} \rightarrow 2_{\gamma}^{+}) = 1.5_{-2.3}^{+0.7}$ mW.u.

The 4^{-} level at 1782.67 keV was proposed in Ref. [34]. We confirm the placement of the 725.19 and 521.53 keV γ rays but are unable to calculate a lifetime due to low statistics.

Recent studies of quadrupole and octupole states in ^{168}Yb ($R_{4/2} = 3.27$) noted a pattern of strong decay from a $K^{\pi} = 2^{-}$ band into the γ -vibrational band when compared to the decay into the ground-state band [41]. This is consistent with the degree of K forbiddenness. Earlier work by Aprahamian [42] showed a difference of three orders of magnitude in $E1$ strength for transitions between states with the same K ($\Delta K = 0$) and for those with $\Delta K = 2$. The authors note [41] this interesting decay pattern has also been observed in the $J^{\pi} = 2^{-}$ states belonging to the $K^{\pi} = 2^{-}$ band in the nuclei from Gd ($Z = 64$) to W ($Z = 74$). The preferred decay ^{168}Yb is to the 3^{-} state to the $J^{\pi} = 4^{-}$ state. The enhanced $E1$ transitions indicate some overlap with the γ band but further study of the negative-parity states, including $E3$ strengths, are needed. The $J^{\pi} = 2^{-}$ state is not observed in ^{160}Gd ; however, the 3^{-} and 4^{-} levels preferentially decay to the γ band.

E. $K^{\pi} = 0^{+}$ bands

The 0^{+} states in ^{160}Gd were discussed in Ref. [25]. 0^{+} states at 1379.7 and 1558.3 keV were confirmed and assigned lifetime limits of > 1350 and > 590 fs, respectively, and states at 1325.73 and 2236 keV were rejected as possible 0^{+} states. The band structure of these levels was also explored and is included in Table I.

After evaluation of the full angular distribution data set at neutron energies of 1.5, 2.2, and 2.8 MeV, the $F(\tau)$ values were scrutinized. After careful evaluation of the full data set, only $F(\tau)$ value with uncertainties which overlapped the other values were used in the lifetime calculation. This process led to the recalculation of the lifetime of the 1599.05-keV level. The re-evaluated value of $\tau = 800_{-300}^{+730}$ fs is consistent with our formerly published limit of > 300 fs [25], albeit with a large uncertainty. The γ -ray decay from 1599.05 keV and 988.72 keV is located on a background line and was not observed in this set of experiments.

F. Discussion

We have studied levels in ^{160}Gd by $(n, n'\gamma)$ experiments. Excitation functions at neutron energies from 1.5 to 2.8 MeV aided in the placement of γ rays in the level scheme and angular distributions at three neutron energies resulted in the determination of level lifetimes for twenty-eight excited states and hence the depopulating $B(E2)$ and $B(E1)$ values for transitions from $K^{\pi} = 0^{+}, 2^{+}, 4^{+}, 0^{-}, 1^{-}$, and 2^{-} bands. In a previous paper [25], we identified excited $K^{\pi} = 0^{+}$ band heads at 1379 and 1558 keV and the excited levels built on them. The measured lifetimes for the first and second excited $K^{\pi} = 0^{+}$ band members were determined as limits. Nonetheless, the limits indicate potentially enhanced collective transitions from the 2^{+} and 4^{+} members of the band. In this work, we have measured the level lifetimes for several members of the negative-parity bands. Figure 3 shows the revised lifetime of the 2^{+} state of the $K^{\pi} = 0^{+}$ band at 1599 keV with an enhanced $B(E2)$ of 41_{-37}^{+16} W.u. connecting this state to the $K^{\pi} = 2^{+}$ band member, the 3^{+} state at 1057. This kind of enhanced $B(E2)$ transition probability could only be due to a collective excitation built on the $K^{\pi} = 2^{+}$ band. $B(E2)$ values to the g.s. band are 100 times weaker.

The lifetimes of the excited states in negative-parity bands are listed in Table I. A partial level scheme is shown for the depopulation of the negative-parity bands for $K^{\pi} = 0^{-}, 1^{-}$, and 2^{-} bands along with the $K^{\pi} = 2^{+}$ γ band. These transitions are $E1$ in nature and show $B(E1)$ values that are strongly enhanced for the $K=0^{-}$ band depopulating on the order of a few mW.u. These are three orders of magnitude more enhanced than typical $E1$ values in deformed nuclei [42, 43]. In comparison, the negative-parity bands with $K^{\pi} = 1^{-}$ and 2^{-} are one and two orders of magnitude weaker in $B(E1)$'s to the ground-state band while the $K^{\pi} = 2^{-}$ band member at 1692 shows enhanced $E1$ transitions connecting this level to the $K^{\pi} = 2^{+}$ band. The Alaga values for the ratio of $B(E1; 1_{K^{\pi}=0^{-}}^{-} \rightarrow 2_{gs}^{+})$ to $B(E1; 1_{K^{\pi}=0^{-}}^{-} \rightarrow 0_{gs}^{+}) = 2.0$ and the experimental ratio is 1.7.

Similarly, the $B(E1; 3_{K^\pi=0^-}^- \rightarrow 4_{gs}^+)$ to $B(E1; 3_{K^\pi=0^-}^- \rightarrow 2_{gs}^+) = 1.3$ and the experimental $B(E1)$ ratio is 0.9 in good agreement within errors. The ratio of $B(E1; 3_{K^\pi=2^-}^- \rightarrow 4_{K^\pi=2^+}^+)$ to $B(E1; 3_{K^\pi=2^-}^- \rightarrow 3_{K^\pi=2^+}^+)$ to $B(E1; 3_{K^\pi=2^-}^- \rightarrow 2_{K^\pi=2^+}^+)$ for the 1691.68 keV level to the $4^+, 3^+, 2^+$ members of the $K^\pi = 2^+$ γ band, should be 1.8:1.4:1.0 from the Alaga rules and the experimental equivalent is 1.3:1.4:1. This is also in good agreement within errors.

The agreement of the Alaga rules with the measured $B(E1)$ values at 1692 as the 3^- member of a $K^\pi = 2^-$ band is further evidence of the $K^\pi = 2^-$ assignment. If the 1692-keV level belongs to a $K^\pi = 3^-$ band, then the Alaga ratio would be 0.05:0.35:1, in complete disagreement with measured values.

The collective quadrupole and octupole degrees of freedom were analyzed in ^{160}Gd using the well-known Generator Coordinate Method (GCM) with the Gogny D1S energy density function. Mean-field Hartree-Fock-Bogoliubov (HFB) constrained calculations were carried out using the axially symmetric quadrupole and octupole mass moments in order to explore the shape of the potential energy surface (PES) and to check for the existence of octupole deformed minima. An in-depth discussion of this method can be found in Ref. [43–45]. The computed PES reveals a reflection symmetric (i.e., with zero octupole deformation) for the ground state but the PES along the octupole direction is rather soft indicating the need of a beyond-mean-field calculation using the GCM. Fig. 4 shows a deep minimum potential well that is quadrupole deformed. The lowest oblate minimum does not appear until 5 MeV. The first excited $K=0^-$ state appears at an excitation energy of 1.84 MeV with a $B(E1; 1_{K^\pi=0^-}^- \rightarrow 0_{gs}^+)$ value of 5.1 mW.u. The $B(E3; 3^- \rightarrow 0_{gs}^+) = 13.50$ W.u. The second excited 0^+ state is a one-phonon β vibration with an excitation energy of 3.36 MeV and the 2^+ member decays to the ground state with a $B(E2; 2^+ \rightarrow 0_{gs}^+) = 3.7$ W.u. and the $10^3\rho^2(E_0)$ transition strength of 230. The third excited 0^+ state in this calculation is a two-octupole phonon at 3.94 MeV with a $B(E2; 2^+ \rightarrow 0_{gs}^+) = 0.71$ W.u. and an $10^3\rho^2(E_0) = 9$. These calculated values are compared with the experimental values in Fig. 5. We have not measured any E3 transitions in this work, but the $B(E3)$ value used in comparison was established previously. Our experimental level scheme is compressed in comparison to the GCM calculations. There is, however, very good agreement between the calculated and experimental $B(E1; 1_{K^\pi=0^-}^- \rightarrow 0_{gs}^+)$ values. The prediction is for an excited $K^\pi = 0^+$ band at 3.9 MeV as a double octupole built on the $K^\pi = 0^-$ band at 1840 keV. Our work shows an excited $K^\pi = 0^+$ band at 1558 keV that is connected to the first excited $K^\pi = 2^+$ band. Our results indicate that the $K^\pi = 0^+$ band at 1558 keV is the double-phonon $\gamma\gamma$ vibrational band. The $K^\pi = 2^+$ γ band head is at 989 keV. The two-phonon $\gamma\gamma$ vibration in this case is 1.6 times the energy of the single γ -vibrational band. Negative anharmonicities similar to this have been observed in ^{232}Th [46] in the actinide region and ^{178}Hf [24] in the rare earths.

IV. SUMMARY

We report the level lifetimes of twenty five states in the low-lying excitation energy regime of ^{160}Gd . Transition probabilities were calculated from the level lifetimes and, where known, multipole mixing ratios are reported. The $B(E2)$ values from the $K^\pi = 2^+$ band indicate that this is indeed a quadrupole collective vibrational excitation. The level lifetimes of the 4^+ and 5^+ members of this band show transition rates consistent with other $K^\pi = 2^+$ γ -vibrational bands in this region of deformed nuclei. This work also allowed us to reassess our former measurement of the 2_4^+ level at 1599.05 keV. We had reported a limit in an earlier publication on the measurement of this level[25]. Our characterization of the same level with a revised multipole mixing ratio and the assignment or placement of the transitions to the γ band, would make the $B(E2; 2_4^+ \rightarrow 3_1^+) = 41^{+16}_{-37}$ W.u., potentially pointing to a two-phonon $\gamma\gamma$ -vibrational character for the $K^\pi = 0^+$ band at 1558.31 keV. The uncertainty on this $B(E2)$ value is large, but the observed collective strength, indicating a preferred decay to the $K^\pi = 2^+ \gamma$ band is difficult to ignore.

In deformed nuclei, low-lying negative-parity states are generally associated with octupole vibrations, and a simple pattern of $K^\pi = 0^-, 1^-, 2^-,$ and 3^- bands is frequently seen. In pioneering work, Neergård and Vogel [47] described the octupole states in deformed nuclei microscopically, and Barfield, Wood, and Barrett [48] treated the detailed spectra and $E3$ transition rates of nuclei in the rare earth region within the interacting boson model.

Experimentally, octupole bands are identified by enhanced $E3$ transitions between the $J^\pi = 3^-$ member of the band and the ground state in spherical nuclei. The compilation of experimental data by Spear [49] and the update by Kibédi and Spear [10] give the excitation energies of the 3^- states and reduced electric octupole transition probabilities, $B(E3; 0_1^+ \rightarrow 3_1^-)$, for the first 3^- states of even-even nuclides. Moreover, it is frequently found that known octupole states are populated strongly in single-nucleon transfer reactions, indicating that these states have a complex character with one or more large two-quasiparticle components. While a number of $E1$ transition rates from negative-parity states are reported in this work, the correlation between these $B(E1)$ s and octupole strength is less straightforward than that for the $B(E3)$ s. We note that for example, the 1224.33- and 1289.90-keV levels of the $K^\pi = 0^-$ band have de-exciting transitions of several mW.u. compared to the 1^- band where the $B(E1)$ s are less than 1 mW.u. Structural assignments based solely on $B(E1)$ values are cautioned in Ref. [50], therefore we note these values along

with the previous reported $B(E3; 3^- \rightarrow 0_{gs}^+) = 11.1(7)$ W.u. [38] indicates an octupole vibration. However, no new $B(E3)$ values are available from the current work, on the Also of note is a preferred $\Delta K = 0$ decay from the $K^\pi = 2^-$ band to the $K^\pi = 2^+$ γ band from the 3^- state at 1691.68 keV.

Although the energies of the calculated bands in the GCM are higher than the experimental results, what is striking is the agreement in the transition probabilities suggesting the population of a one-phonon β vibration and a two-octupole phonon state. Further work is underway to include two-quasiparticle excitations in the GCM. New measurements of extended $B(E2)$ and $B(E0)$ values in ^{160}Gd can further clarify the situation.

A. Acknowledgements

We thank H. E. Baber for his contributions to accelerator maintenance and operation. This material is based upon work supported by the National Science Foundation under Grant Nos. PHY-1606890, PHY-1419765, PHY-1205412, PHY-1507053, PHY-1068192, and PHY-1305801. L. M. Robledo has been supported in part by the Spanish MINECO grant No. FPA2012-34694. The enriched isotope used in this research was supplied by the United States Department of Energy Office of Science by the Isotope Program in the Office of Nuclear Physics.

TABLE I: Energy levels observed in the $^{160}\text{Gd}(n,n'\gamma)$ measurements. E_L is the level energy found in this work with uncertainties; I_γ is the relative γ -ray intensity. Lifetimes, τ , are mean lives in fs. Multipole mixing ratios, δ , are obtained in fits to measured angular distributions. When two values are given, they have similar χ^2 values. If one value is in brackets, the one with the smaller χ^2 value is given first and is the δ value adopted. Literature lifetime values (τ_{lit}) are taken from [33] unless otherwise noted and are shown under the measured lifetime. Parentheses denote tentative assignments or placements. For reference, $B(E1)_{mW.u.} = 0.190 e^2 b$ and $B(E2)_{W.u.} = 5.16 \times 10^{-7} e^2 b^2$.

	E_L (keV)	I_i^π, K	I_f^π, K	E_γ (keV)	I_γ	$F(\tau)$	τ (fs)	Mult.	δ	$B(E1)$ ($\times 10^{-3}$ W.u.)	$B(E2)$ (W.u.)	Notes
75.24(5)	$2_{gs}^+, 0$	$0_{gs}^+, 0$		75.26	100		$\tau_{lit} = 3.9 \times 10^6$					
248.55(6)	$4_{gs}^+, 0$	$2_{gs}^+, 0$		173.34(5)	100							
515.00(8)	$6_{gs}^+, 0$	$4_{gs}^+, 0$		266.52(5)	100							
988.72(6)	$2_\gamma^+, 2$	$4_{gs}^+, 0$		739.96(7)	—	0.008(14)	> 1800	E2				0.96(7) ^{1, 2, 3}
							$\tau_{lit} = 1876(87)$					
		$2_{gs}^+, 0$		913.43(5)	100(1)			E2/M1	$-0.45^{+0.04}_{-0.05}$			$1.2^{+0.22}_{-0.18}$
		$0_{gs}^+, 0$		988.68(5)	88.7(10)			E2	—			$4.1(2)^2$
1057.42(6)	$3_\gamma^+, 2$	$4_{gs}^+, 0$		809.06(5)	20.6(2)	0.011(13)	> 2200	E2/M1	0.11(3)			$< 0.04^2$
		$2_{gs}^+, 0$		982.28(5)	100(1)			E2/M1	47^{+18}_{-10}			$< 6.5^4$
1070.57(7)	$4_1^+, 4$	$6_{gs}^+, 0$		555.45(8)	1.6(1)							
		$4_{gs}^+, 0$		822.06(5)	100(2)							
		$2_{gs}^+, 0$		995.30(5)	64.2(13)							
1148.15(7)	$4_\gamma^+, 2$	$4_{gs}^+, 0$		899.59(5)	100(1)	0.037(15)	1080^{+730}_{-320}	E2/M1	21^{+21}_{-7}			16^{+5}_{-10} ⁴
		$2_{gs}^+, 0$		1072.85(5)	58.5(9)			E2	—			$3.8^{+2.6}_{-1.1}$
1224.33(6)	$1_1^-, 0$	$2_{gs}^+, 0$		1149.12(5)	100(1)	0.676(7)	20 ± 2	E1	—			6.5(6)
		$0_{gs}^+, 0$		1224.38(5)	67.5(8)			E1	—			3.6(4)
1261.24(9)	$5_\gamma^+, 2$	$6_{gs}^+, 0$		746.34(6)	19.6(9)	0.101(26)	350^{+120}_{-80}	E2/M1	8^{+13}_{-4}			31^{+7}_{-11}
		$4_{gs}^+, 0$		1012.65(5)	100(1)			E2/M1	$[0.24(10)]$			$1.7^{+1.4}_{-1.5}$
1289.90(7)	$3_1^-, 0$	$4_{gs}^+, 0$		1041.37(5)	54.6(7)	0.565(19)	34 ± 3	E1	15^{+17}_{-6}			35^{+8}_{-12} ⁵
		$2_{gs}^+, 0$		1214.79(5)	100(1)			E1	—			3.5(3)
1351.30(6)	$1_2^-, 1$	$2_{gs}^+, 0$		1276.06(5)	100(2)	0.184(8)	180 ± 20	E1	—			0.74(8)
		$0_{gs}^+, 0$		1351.30(5)	20.0(4)			E1	—			0.12(1)
1376.70(8)	$2_1^-, 1$	$3_\gamma^+, 2$		319.38(6)	1.8(1)	0.035(47)	> 550	E1	—			< 0.18 ^{2, 6}
		$2_{gs}^+, 0$		1301.46(5)	100(1)			E1	—			< 0.27
1379.71(10)	$0_1^+, 0$	$2_{gs}^+, 0$		1304.46(5)	100	0.015(14)	> 1350	E2	—			< 3.1 ⁷
1427.40(12)	$5_1^-, 0$	$4_{gs}^+, 0$		1178.85(6)	100	0.514(69)	50 ± 10	E1	—			4.0(8)
1436.34(7)	$2_2^+, 0$	$4_{gs}^+, 0$		1187.81(5)	100(1)	0.036(28)	> 340	E2	—			< 13 ⁷
		$2_{gs}^+, 0$		1361.05(6)	36.4(4)			E2/M1	$0.00(8)$			< 2.4
		$0_{gs}^+, 0$		1436.34(6)	13.5(2)			E2	$[2.4^{+0.6}_{-0.4}]$			< 2.0
1464.00(10)	$3_2^-, 1$	$2_{gs}^+, 0$		1388.75(5)	100	0.344(43)	50 ± 5	E1	—			< 0.70 ⁶

continued

TABLE I: *continued*

	E_L (keV)	I_i^{π}, K	I_f^{π}, K	E_{γ} (keV)	I_{γ}	$F(\tau)$	τ (fs)	Mult.	δ	$B(E1)$ ($\times 10^{-3}$ W.u.)	$B(E2)$ (W.u.)	Notes
1498.94(10)	$4_1^+, 1$	$4_{gs}^+, 0$	1250.39(5)	100	0.053(51)	> 400	$E1$	—	< 0.41	6		
1558.31(12)	$0_2^+, 0$	$2_{gs}^+, 0$	1483.06(6)	100	0.004(69)	> 590	$E2$	—		< 3.7	7	
1561.63(10)	$4_3^+, 0$	$6_{gs}^+, 0$	1046.67(6)	100(1)	0.049(53)	> 320	$E2$	—		< 22	7	
		$4_{gs}^+, 0$	1313.03(6)	74.8(3)			$E2/M1$	$0.28^{+0.34}_{-0.12}$		< 0.40		
1568.77(6)	$1_1^+, 1$	$1_2^-, 1$	217.51(6)	8.8(15)	0.044(28)	1000^{+1800}_{-400}	$E1$	—	$0.97^{+0.7}_{-1.8}$	2, 6		
		$2_{\gamma}^+, 0$	580.20(6)	89.2(16)			$E2/M1$	$0.28^{+0.25}_{-0.18}$		$5.2^{+6.7}_{-13}$		
		$2_{gs}^+, 0$	1493.40(6)	94.4(16)			$E2/M1$	$1.34^{+1.6}_{-0.6}$		$0.44^{+0.23}_{-0.88}$		
		$0_{gs}^+, 0$	1568.70(6)	100(2)			$M1$	—				
1586.61(12)	$2_3^+, 1$	$2_{gs}^+, 0$	1511.36(6)	100	0.044(39)	> 500	$E2/M1$	—		< 4.01	6	
1599.05(6)	$2_4^+, 0$	$3_1^-, 0$	309.32(6)	8.9(4)	0.056(26)	800^{+730}_{-300}	$E1$	—	$0.34^{+0.13}_{-0.31}$	8, 6		
		$1_1^-, 0$	374.78(6)	14.8(3)			$E1$	—	$0.32^{+0.12}_{-0.29}$			
		$3_{\gamma}^+, 2$	541.53(6)	36.8(3)			$E2/M1$	$-5.57^{+1.91}_{-5.00}$ $-0.01(9)$		41^{+16}_{-37} $0.004(77)$		
		$2_{gs}^+, 0$	1523.59(6)	100(1)			$E2/M1$	$-1.04^{+0.22}_{-2.10}$		$0.34^{+0.68}_{-0.32}$		
		$0_{gs}^+, 0$	1598.85(6)	78.7(1)			$E2$	—		$0.41^{+1.12}_{-0.77}$		
1648.06(12)	4_4^+	$2_{gs}^+, 0$	1572.81(6)	100	0.134(58)	300^{+260}_{-200}	$E2$	—		$5.5^{+2.8}_{-2.6}$	6	
1653.32(12)	$5_2^-, 1$	$6_1^+, 0$	(1138.51(6))	—	0.454(78)	60^{+20}_{-15}						2, 6
		$4_{gs}^+, 0$	1404.77(6)	100								
1661.75(9)		$4_{gs}^+, 0$	1413.16(7)	5.6(2)	0.050(32)	880^{+1600}_{-360}				9, 6		
		$2_{gs}^+, 0$	1586.52(6)	100(1)								
1691.68(7)	$3_4^-, 2$	$4_{\gamma}^+, 2$	543.45(6)	60.8(15)	0.170(95)	230^{+350}_{-100}	$E1$	—	2_{-3}^{+1}	10		
		$3_{\gamma}^+, 2$	634.56(6)	99.5(25)			$E1$	—	$2.1^{+3.9}_{-3.2}$			
		$2_{\gamma}^-, 2$	702.84(6)	100(2)			$E1$	—	$1.5^{+0.7}_{-2.3}$			
		$4_{gs}^+, 0$	1442.93(8)	8.6(6)			$E1$	—	$0.01^{+0.01}_{-0.02}$	9		
1782.67(10)	$4_2^-, 2$	$5_1^+, 2$	521.53(8)	23.6(6)								
		$3_{\gamma}^+, 2$	725.19(6)	100(2)								
1805.13(9)	2_5^+	$4_{\gamma}^+, 4$	734.50(6)	44.3(14)	0.055(96)	> 300	$E2$	—		< 76	6	
		$2_{\gamma}^+, 2$	816.46(6)	100(2)			$E2/M1$	$-0.76^{+0.10}_{-0.43}$ $[-3.90^{+0.97}_{-1.34}]$		< 37		
										< 94		
1931.96(7)	2_6^+	$3_{\gamma}^+, 2$	874.51(6)	43.4(21)	0.057(39)	760^{+1800}_{-330}	$E2/M1$	—		$8^{+3.5}_{-19}$	2, 6	
		$4_{gs}^+, 0$	1683.45(7)	45.4(20)			$E2$	—		$0.32^{+0.14}_{-0.72}$		
		$2_{gs}^+, 0$	1856.65(6)	100(3)			$E2/M1$	$0.92^{+0.41}_{-0.64}$ $[0.50^{+0.87}_{-0.24}]$		$0.20^{+0.47}_{-0.08}$ $0.08^{+0.08}_{-0.31}$		
		$0_{gs}^+, 0$	(1932.00(7))	31.5(17)			$E2$	—		$0.11^{+0.05}_{-0.26}$		
1966.66(10)	1_3^-	$2_{gs}^+, 0$	1891.33(6)	100(8)	0.606(48)	37^{+8}_{-7}	$E1$	—	$0.84^{+0.28}_{-0.21}$			
						$\tau_{lit} = 19(7)$						
		$0_{gs}^+, 0$	1966.97(13)	57.0(70)			$E1$	—	$0.43^{+0.16}_{-0.11}$	6		
2030.90(9)	(2 ⁺)	$4_{gs}^+, 0$	1782.14(6)	16.1(22)								
		$2_{gs}^+, 0$	1955.93(7)	100(3)								
2060.43(11)		$0_{gs}^+, 0$	2060.42(6)	100	0.187(44)	230^{+90}_{-50}						
2109.32(7)	1 ⁺	$3_{\gamma}^+, 2$	1051.87(6)	47.4(18)	0.138(34)	330^{+120}_{-70}	$E2$			6.2(1.7)	9, 6	
		$2_{\gamma}^+, 2$	1119.71(13)	57.9(29)			$E2/M1$	—		5.6(1.5)		
		$2_{gs}^+, 0$	2034.26(6)	100(2)			$E2/M1$	—		0.50(13)		
		$0_{gs}^+, 0$	2109.31(6)	73.3(21)			$M1$	—				
2135.76(13)		$0_{gs}^+, 0$	2135.74(7)	100	0.111(73)	420^{+880}_{-180}				6		

¹ This γ ray is mixed with an experimental background line, 739.42(5) keV from the $^{72}\text{Ge}(n, \gamma)$ reaction.² This γ ray was not used in the level lifetime determination.³ The branching ratios were taken from Ref. [30] and τ_{lit} were used for the transition probability calculations.⁴ The a_2 and a_4 values of this γ ray were within uncertainties of Ref. [30] and, therefore, the published δ value was used in this work.⁵ Level lifetime from Ref. [38]; see text for discussion.⁶ This level or spin assignment adopted from Ref. [30].⁷ Lifetime reported in Ref. [25].⁸ Lifetime modified from Ref. [25].⁹ This γ ray is not reliable for excitation function and/or lifetime determination due to its low intensity.¹⁰ This level or spin assignment adopted from Ref. [34].

-
- [1] A. Aprahamian, Phys. Atom. Nucl. **67**, 1750 (2004).
- [2] X. Wu, A. Aprahamian, S. M. Fischer, W. Reviol, G. Liu, and J. X. Saladin, Phys. Rev. C **49**, 1837 (1994).
- [3] P. E. Garrett, M. Kadi, C. A. McGrath, V. Sorokin, M. Li, M. Yeh, and S. W. Yates, Phys. Lett. B **400**, 250 (1997).
- [4] D. Bés, Nucl. Phys. **49**, 544 (1963).
- [5] W.-T. Chou, R. Casten, and P. von Brentano, Phys. Rev. C **45**, 9 (1992).
- [6] R. F. Casten and P. von Brentano, Phys. Rev. C **50**, R1280 (1994).
- [7] P. E. Garrett, J. Phys. G: Nucl. Part. Phys. **27**, R1 (2001).
- [8] J. Smallcombe, P. J. Davies, C. J. Barton, D. G. Jenkins, L. L. Andersson, P. A. Butler, D. M. Cox, R. D. Herzberg, A. Mistry, E. Parr, et al., Phys. Lett. B **732**, 161 (2014).
- [9] P. D. Cottle, M. A. Kennedy, and K. A. Stuckey, Phys. Rev. C **42**, 2005 (1990).
- [10] T. Kibédi and R. H. Spear, Atom. Data Nucl. Data **80**, 35 (2002).
- [11] R. A. Gatenby, J. R. Vanhoy, E. M. Baum, E. L. Johnson, S. W. Yates, T. Belgia, B. Fazekas, A. Veres, and G. Molnár, Phys. Rev. C **41**, R414 (1990).
- [12] L. Bargiono, P. G. Bizzeti, A. M. Bizzeti-Dona, D. Bazzacco, S. Lunardi, P. Pavan, C. Rossi-Alvarez, G. de Angelis, G. Maron, and J. Rico, Phys. Rev. C **51**, R1057 (1995).
- [13] L. Caballero, B. Rubio, P. Kleinheinz, S. W. Yates, A. Algora, A. Dewald, A. Fitzler, A. Gadea, J. Jolie, R. Julin, et al., Phys. Rev. C **81**, 031301(R) (2010).
- [14] P. Kleinheinz, J. Styczen, M. Piiparinens, J. Blomqvist, and M. Kortelahti, Phys. Rev. Lett. **48**, 1457 (1982).
- [15] S. Lunardi, P. Kleinheinz, M. Piiparinens, M. Ogawa, M. Lach, and J. Blomqvist, Phys. Rev. Lett. **53**, 1531 (1984).
- [16] M. Piiparinens, P. Kleinheinz, J. Blomqvist, A. Virtanen, A. Atac, D. Muller, J. Nyberg, T. Ramsøy, and G. Sletten, Phys. Rev. Lett. **70**, 150 (1993).
- [17] C. Küppersbusch, S. Pascu, P. von Brentano, D. Buscurescu, Gh. Căta-Danil, D. Deleanu, J. Endres, M. Elvers, D. Filipescu, C. Frießner, et al., Eur. Phys. J. A **48**, 1 (2012).
- [18] F. Corminboeuf, J. Jolie, H. Lehmann, K. Föhl, F. Hoyler, H. G. Börner, C. Doll, and P. E. Garrett, Phys. Rev. C **56**, R1201 (1997).
- [19] C. Fahlander, A. Axelsson, M. Heinebrodt, T. Härtlein, and D. Schwalm, Phys. Lett. B **388**, 475 (1996).
- [20] H. G. Börner, J. Jolie, F. Hoyler, S. J. Robinson, B. Krusche, R. Piepenbring, R. F. Casten, A. Aprahamian, and J. P. Draayer, Phys. Rev. Lett. **66**, 691 (1991).
- [21] M. Oshima, T. Morikawa, Y. Hatsukawa, S. Ichikawa, N. Shinohara, M. Matsuo, H. Kusakari, N. Kobayashi, M. Sugawara, and T. Inamura, Phys. Rev. C **52**, 3492 (1995).
- [22] T. Härtlein, M. Heinebrodt, D. Schwalm, and C. Fahlander, Eur. Phys. J. A **2**, 253 (1998).
- [23] P. E. Garrett, M. Kadi, Min. Li, C. A. McGrath, V. Sorokin, M. Yeh, and S. W. Yates, Phys. Rev. Lett. **78**, 4545 (1997).
- [24] A. Aprahamian, R. C. de Haan, S. R. Lesher, J. Döring, A. M. Bruce, H. G. Börner, M. Jentschel, and H. Lehmann, J. Phys. **G25**, 685 (1999).
- [25] S. R. Lesher, C. Casarella, A. Aprahamian, B. P. Crider, R. Ikeyama, I. R. Marsh, M. T. McEllistrem, E. E. Peters, F. M. Prados-Estévez, M. K. Smith, et al., Phys. Rev. C **91**, 054317 (2015).
- [26] P. E. Garrett, N. Warr, and S. W. Yates, J. Res. Natl. Inst. Stand. Technol. **105**, 141 (2000).
- [27] P. E. Garrett, H. Lehmann, J. Jolie, C. A. McGrath, M. Yeh, W. Younes, and S. W. Yates, Phys. Rev. C **64**, 024316 (2001).
- [28] E. E. Peters, A. Chakraborty, B. P. Crider, B. H. Davis, M. K. Gnanamani, M. T. McEllistrem, F. M. Prados-Estévez, J. R. Vanhoy, and S. W. Yates, Phys. Rev. C **88**, 024317 (2013).
- [29] E. Shelton and V. C. Rodgers, Comput. Phys. Commun. **6**, 99 (1973).
- [30] L. I. Govor, A. M. Demidov, V. A. Kurkin, and I. V. Mikhailov, Yad. Fiz. **72**, 1799 (2009).
- [31] T. Belgia, G. Molnár, and S. W. Yates, Nucl. Phys. A **607**, 43 (1996).
- [32] K. B. Winterbon, Nucl. Phys. **A246**, 293 (1975).
- [33] C. W. Reich, Nucl. Data Sheets **105**, 557 (2005).
- [34] E. P. Grigoriev, Phys. Atom. Nucl. **75**, 1427 (2012).
- [35] Y. Yoshizawa, B. Elbek, B. Herskind, and M. C. Olesen, Nucl. Phys. **73**, 273 (1965).
- [36] C. Baktash, J. X. Saladin, J. O'Brien, I. Y. Lee, and J. E. Holder, Phys. Rev. C **10**, 2265 (1974).
- [37] R. Ronningen, J. Hamilton, A.V.Ramayya, L. Varnell, G. Garcia-Bermudez, J. Lange, W. Lourens, L. Riedinger, R. Robinson, P. Stelson, et al., Phys. Rev. C **15**, 1671 (1977).
- [38] F. K. McGowan and W. T. Milner, Phys. Rev. C **23**, 1926 (1981).
- [39] T. Ichihara, H. Sakaguchi, M. Nakamura, M. Yosoi, M. Ieiri, Y. Takeuchi, H. Togawa, T. Tsutsumi, and S. Kobayashi, Phys. Rev. C **36**, 1754 (1987).
- [40] Y. Y. Berzin, E. P. Grigorév, and T. V. Guseva, Bull. Acad. Sci. USSR, Phys. Ser. **53**, 76 (1989).
- [41] S. Pascu, D. Buscurescu, G. Căta-Danil, V. Derya, M. Elvers, D. Filipescu, D. G. Ghită, T. Glodariu, A. Hennig, C. Mihai, et al., Phys. Rev. C **91**, 034321 (2015).
- [42] A. Aprahamian, Phys. Rev. C **46**, 2093 (1992).
- [43] L. M. Robledo and G. F. Bertsch, Phys. Rev. C **84**, 054302 (2011).
- [44] L. M. Robledo and G. F. Bertsch, Phys. Rev. C **86**, 054306 (2012).
- [45] K. Nomura, R. Rodríguez-Guzmán, and L. M. Robledo, Phys. Rev. C **92**, 014312 (2015).

- [46] W. Korten, P. Brocking, H. Hubel, W. Pohler, U. van Severen, P. Willsau, T. Haertlein, C. Ender, P. Reiter, D. Schwalm, et al., Z. Phys. **A351**, 143 (1995).
- [47] K. Neergård and P. Vogel, Nucl. Phys. A **145** (1970).
- [48] A. F. Barfield, J. L. Wood, and B. R. Barrett, Phys. Rev. C **34**, 2001 (1986).
- [49] R. H. Spear, Atom. Data Nucl. Data **42**, 55 (1989).
- [50] D. P. DiPrete, E. L. Johnson, E. M. Baum, C. A. McGrath, D. Wang, M. F. Villani, S. W. Yates, T. Belgya, B. Fazekas, and G. Molnár, Phys. Rev. C **52**, R2831 (1995).

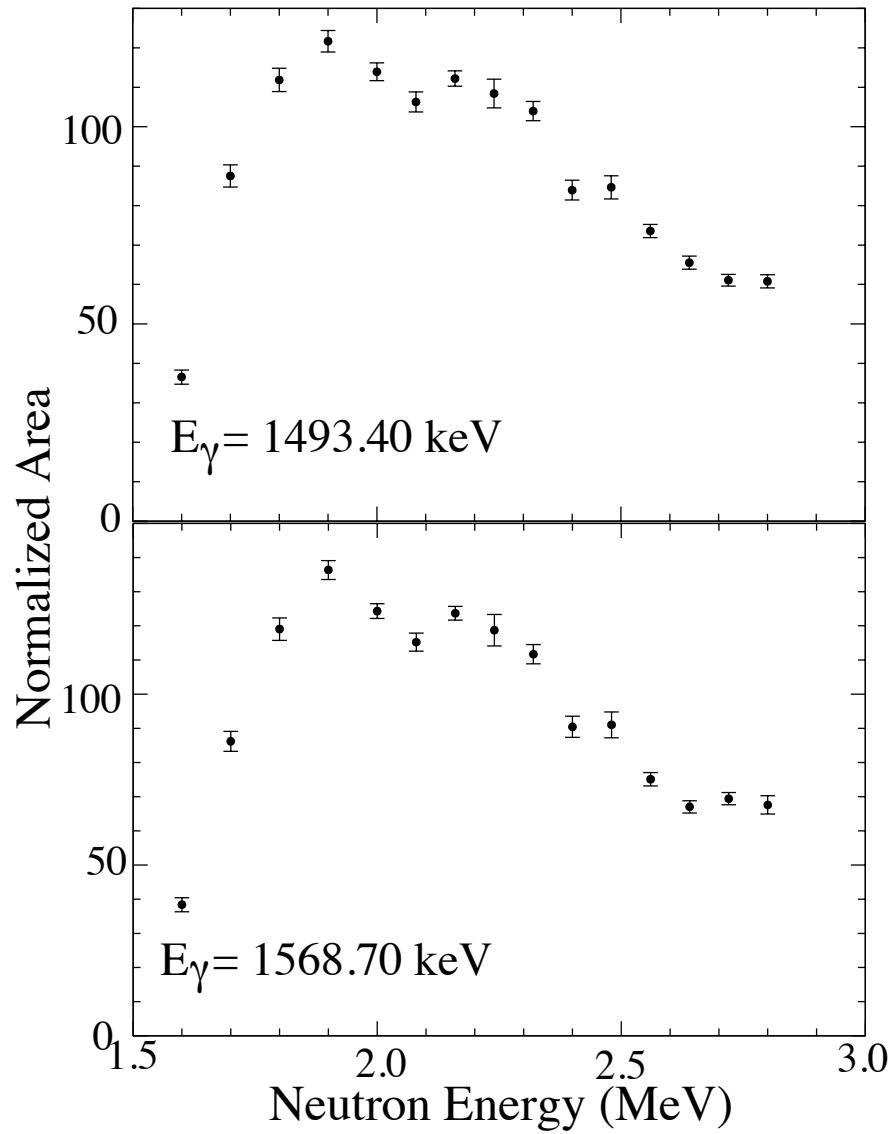


FIG. 1: Excitation functions for the 1493.40- and 1568.70-keV γ rays originating from the 1568.77-keV level. Both exhibit the same excitation energy threshold and overall shape.

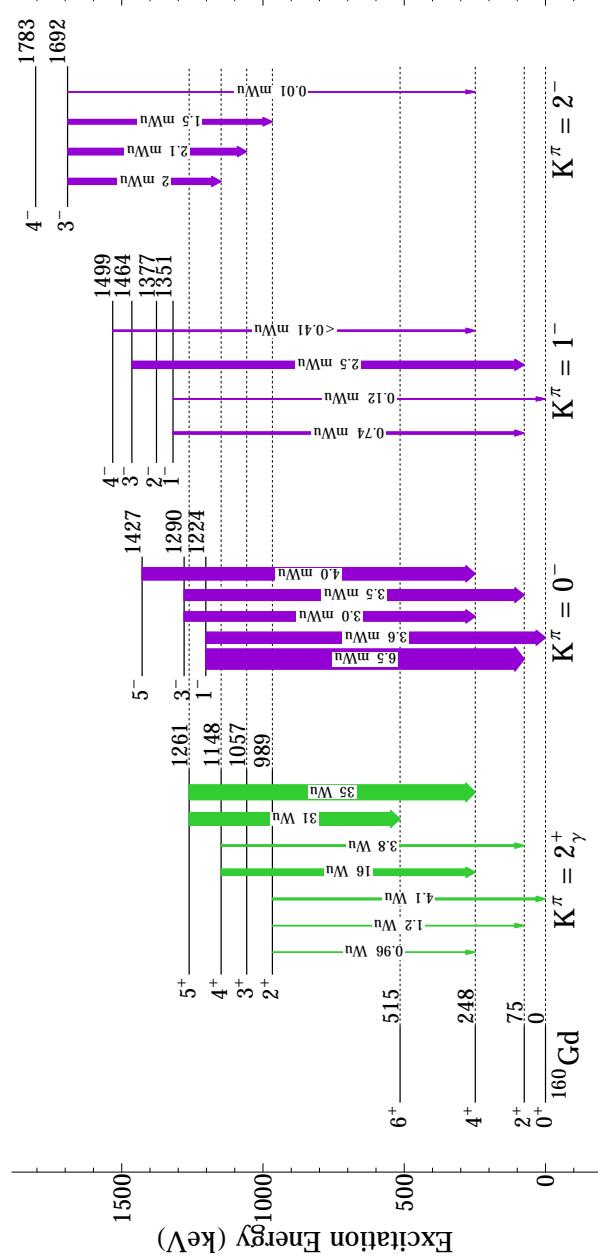


FIG. 2: (color online) A partial level scheme of ^{160}Gd highlighting the $K^\pi = 2^+$ γ and negative-parity bands. The $B(E2)$ values in W.u. are shown in green and $B(E1)$ values in mW.u. in purple and scaled separately. All values are also listed in Table I.

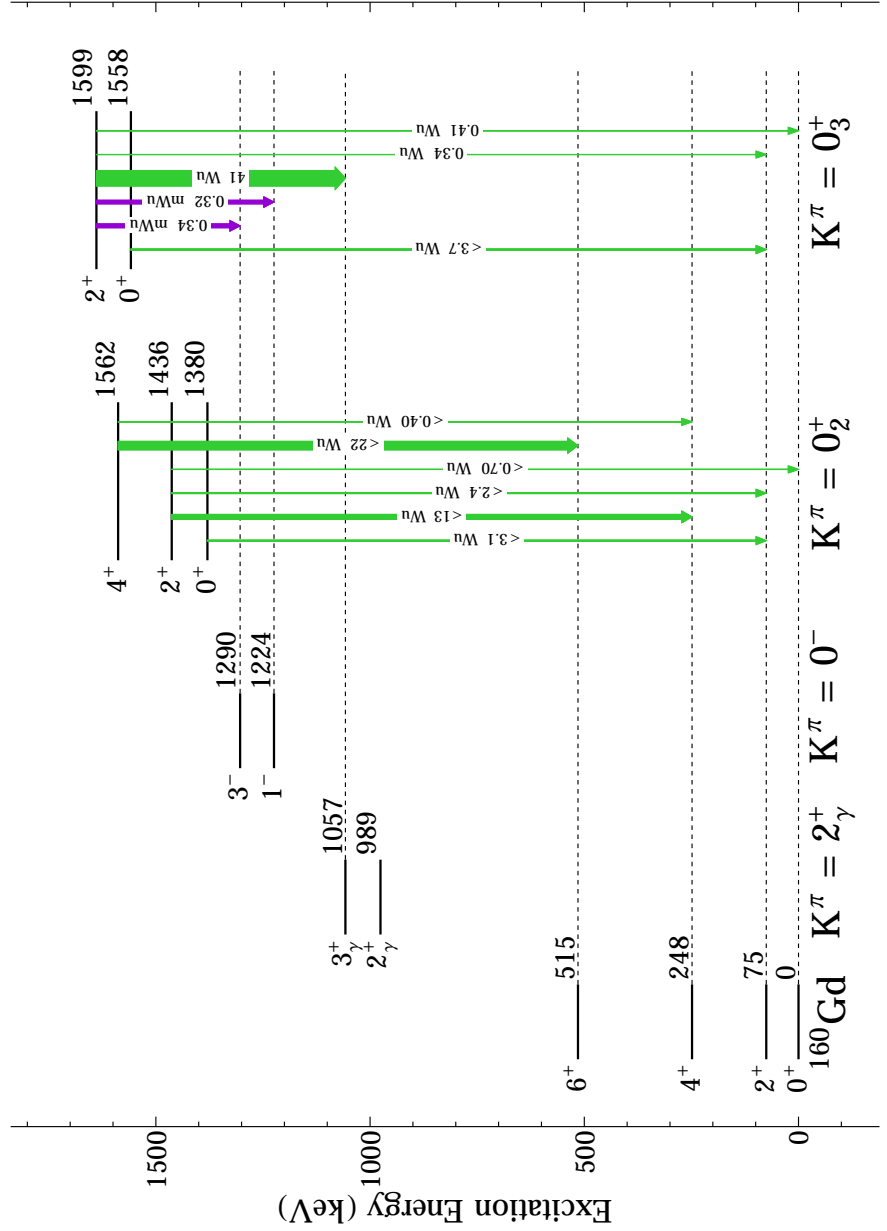


FIG. 3: A level scheme of ^{160}Gd highlighting the $K^\pi = 0^+$ bands. The $B(E2)$ values in W.u. are shown in green and $B(E1)$ values in mW.u. in purple and are scaled separately. All values are also listed in Table I.

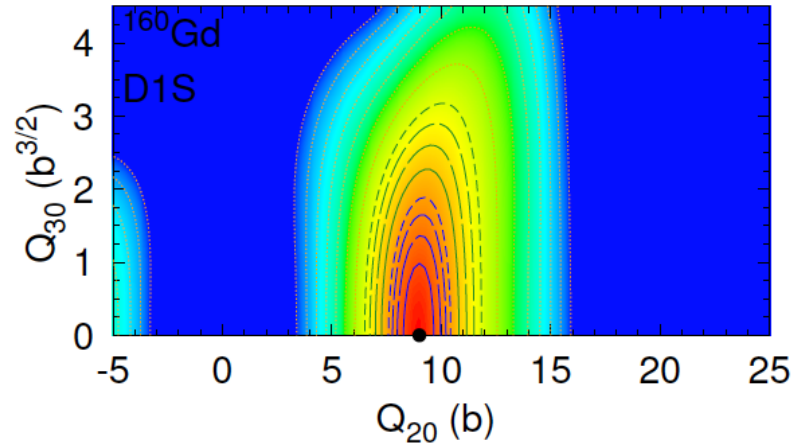


FIG. 4: (color online) Potential energy surface as a function of the quadrupole and octupole degrees of freedom for ^{160}Gd . The dot is located at the ground-state minimum.

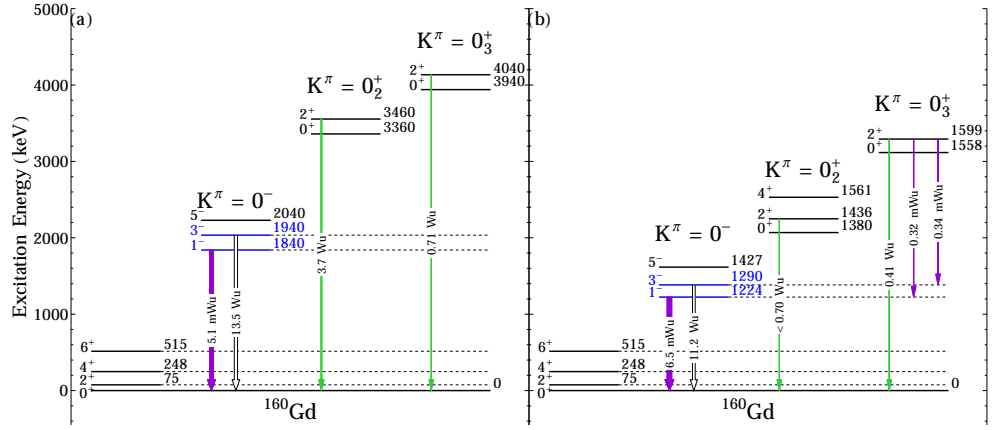


FIG. 5: (color online) Partial level schemes for ^{160}Gd . The $B(E2)$ values in W.u. are shown in green, $B(E1)$ values in mW.u. in purple, and $B(E3)$ values in W.u. in white outlined in black. The two level schemes are scaled separately. a) GCM calculations using the Gogny D1S energy density functional is shown along with calculated transition probabilities. In this calculation, the first excited $K^\pi = 0^-$ state appears at an excitation energy of 1.84 MeV and a $B(E1; 1_K^\pi=0^- \rightarrow 0_{gs}^+)$ value of 5.1 mW.u. The $B(E3; 3^- \rightarrow 0_{gs}^+)$ = 13.50 W.u. The second excited state is a one-phonon β vibration with an excitation energy of 3.36 MeV and the 2^+ member decays to the ground state with a $B(E2; 2^+ \rightarrow 0_{gs}^+)$ = 3.7 W.u. The third excited zero is a two-octupole phonon at 3.94 MeV, and $B(E2; 2^+ \rightarrow 0_{gs}^+)$ = 0.71 W.u. The GCM calculation predicts a double-octupole excited $K^\pi = 0^+$ band at 3.9 MeV built on the $K^\pi = 0^-$ band at 1840 keV. b) The experimental partial level scheme with experimental transition probabilities. The $B(E3; 3^- \rightarrow 0_{gs}^+)$ for the 1289-keV level is taken from Ref. [38].

APPENDIX C

^{162}DY QUADRUPOLE EXCITATIONS

Appendix C includes a near-final draft of the first of two papers on the lifetimes presented in this dissertation to be submitted to Physical Review C in 2017.

Lifetime Measurements of Single- and Multi-phonon Vibrations in ^{162}Dy

C. Casarella¹, S.R. Lesher^{1,2}, A. Aprahamian¹, B.P. Crider³, M. Lowe², E.E.
Peters³, F.M. Prados-Estévez³, T.J. Ross³, Z. Tully², and S.W. Yates³

¹*University of Notre Dame, Notre Dame, IN 46556*

²*University of Wisconsin-La Crosse, La Crosse, WI, 54601 and*

³*University of Kentucky, Lexington, KY, 40506*

(Dated: February 16, 2017)

Abstract

The nature of excited 0^+ bands in nuclei continues to be an outstanding challenge in nuclear structure physics, such as their potential interpretation as quadrupole vibrations on top of a pre-existing deformed ground state. Lifetimes of nuclear excited states in ^{162}Dy were measured using inelastic scattering of neutrons at the University of Kentucky Van de Graaff accelerator facility. Successful measurement of six new lifetimes of 0^+ states below $E_x=3.1$ MeV are reported and will be discussed. Our measurement of weakly collective transitions to the ground state band imply an overall lack of any β -vibrational characteristic, but ^{162}Dy has both flavors of $\gamma\gamma$ -vibrations, in a first of its kind observation with one $K^\pi=0^+$ and two $K^\pi=4^+$ bands in the same nucleus, as well as discussion for a potential candidate for a $\beta\gamma$ -vibration at $E_x=2230$ keV.

I. INTRODUCTION & MOTIVATION

One of the most highly debated issues in nuclear structure over the past several decades involves the nature of low-lying 0^+ bands in deformed nuclei [1–4]. The characterization of lowest-order (quadrupole) surface vibrations built on top of a deformed ground state remains a mystery, and countless experimental and theoretical efforts have been implemented to answer this age-old query [5–10]. The predominant phonon picture of a $K^\pi=2^+$ axial symmetry-breaking ‘ γ ’ vibration is extremely ‘well-behaved’ and documented [11, 12], while the aligned $K^\pi=0^+$ ‘ β ’ vibration lacks uniformity in overall behavior in the rare-earth region of nuclei [4, 8, 13, 14], most notably at the onset of strong deformation (traditionally observed when the energy ratio of the ground state 4^+ and 2^+ is greater than 3). The existence of a β -vibrational degree of freedom has been questioned in the rare earth region, with order of magnitude variance in $B(E2)$ strengths from $K^\pi=0^+$ bands [4, 15]. Further murkiness on the exact nature of 0^+ excitations is encountered with the existence of strongly collective, higher-lying, anti-aligned two-phonon vibrations, as a ‘ $\gamma\gamma$ ’-type, the ‘ $\beta\beta$ ’-type, and the single ‘ β ’-type all share the same angular momentum projection onto the symmetry axis, $K^\pi=0^+$ [16–18]. While these multiphonon configurations have been experimentally observed, they are far from common across the region of deformation between $150 < A < 180$. Successful development and refinement of theories to describe the feasibility of this phonon structure all hinge on the measurement of absolute transition probabilities between nuclear excitations; in terms of experimentally measurable quantities, this equates to the crucial measurement of nuclear lifetimes in the rare-earth region.

In particular, the ^{162}Dy nucleus remains one of the best studied nuclei on the Chart of Nuclides [19], yet lifetime measurements of many excited states (most notably 0^+ excitations) are scarce. Additional interest can be placed on the exhaustive measurement of lifetimes because ^{162}Dy contains an outstanding number of 0^+ excitations in the region (see Figure 1). The comprehensive (p,t) reaction study by Meyer [20] established several new $L=0$ excitations in ^{162}Dy , and has spearheaded new interest in these states in the rare-earth region of nuclei. Many of these 0^+ states fall below the neutron and proton pairing gaps, where we would expect to find the strongest collective, macroscopic vibrations of the nucleus.

Upon examination of literature lifetimes for these lowest-lying $K=0,2$ modes of excitation, we are presented with an alarming lack of lifetimes for 0^+ states across the entire chain

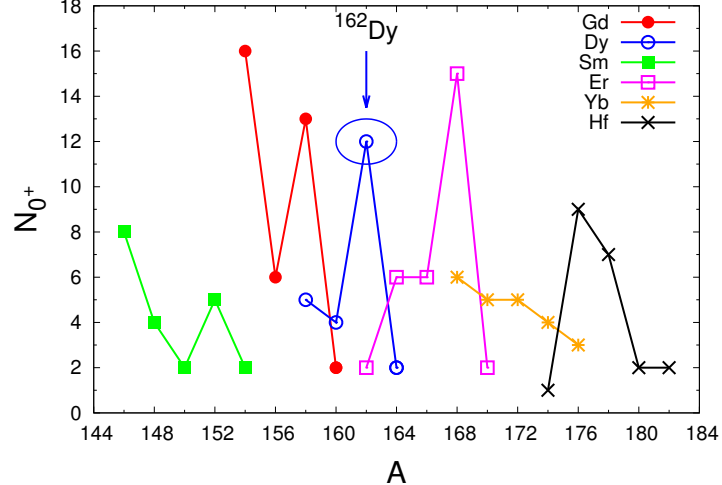


FIG. 1. Schematic showing the total number of confirmed and tentative 0^+ excitations (color online) among several deformed rare-earth nuclei (Sm, Gd, Dy, Er, Yb & Hf).

of Dysprosium isotopes. Figure 2 shows the current state of known experimental B(E2) measurements (equivalent to level lifetimes) leaving known 0^+ states and the lowest 2^+ band for even- A Dy nuclei juxtaposed with the proton and neutron pairing gaps, $2\Delta_\pi$ & $2\Delta_\nu$, respectively (calculated from [21]).

Motivation and impetus for the lifetime measurements presented in this work is evident; full elucidation of the nature of this common type of low-lying excitation ($K^\pi=0^+$) is contingent on the measurement of transition probabilities between nuclear states [5], and ^{162}Dy provides an excellent avenue to do this, with its abundance of 0^+ excitations [20] and complimentary wealth of knowledge about the nuclear structure already available [19]. With this work, we hope to provide crucial information about the collectivity of states in the nucleus as they pertain to the vibrational characteristics and structure of a deformed nucleus.

II. EXPERIMENT

Lifetimes of excited states were measured with the Doppler Shift Attenuation Method via Inelastic Neutron Scattering (DSAM-INS) at the University of Kentucky Accelerator

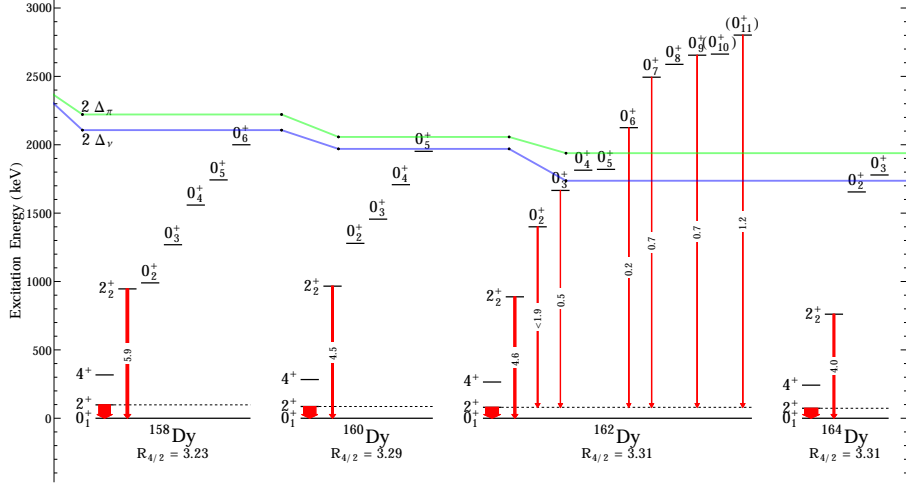


FIG. 2. Systematics for the energies of excited 0^+ states, the first excited 2^+ bandhead, and low-lying ground state band members for a few even-even Dysprosium nuclei. New transition probabilities are presented in ^{162}Dy , with the widths of all transitions proportional to known literature $B(\text{E}2)$ values (in W.u); also shown are the proton and neutron pairing gap ($2\Delta_\pi$ and $2\Delta_\nu$, respectively) for each isotope.

Laboratory [22–24]. Quasi-monoenergetic neutrons from a primary $^3\text{H}(\text{p},\text{n})$ reaction scatter off a vial of 98.12% enriched ^{162}Dy oxide powder to populate excited states for study. Lifetimes are extracted from the angular distributions of γ rays taken at various angles between 40 and 150 degrees with respect to the beam direction and at three bombarding neutron energies ($E_n=1.6, 2.2, 3.1$ MeV) to populate states up to 3.1 MeV excitation energy. Decay radiation can be assigned to distinct levels populated via the complimentary measurement of excitation functions for all observed decays. In ideal cases, specific levels can be populated by placing the neutron energy just above the threshold energy of the level; this ‘dialing-in’ of levels will eliminate (or minimize) lifetime inflation from higher level-feeding. Confirmation of 0^+ states can be made from the observation of isotropic angular distributions, and confident placement of γ rays in the level scheme is achieved with complimentary excitation

function measurements.

Lifetimes from DSAM are extracted according to the Winterbon formalism that provides a lifetime-dependent attenuation to the Doppler shifted energies of γ rays [25], related linearly with $\cos(\theta)$, seen in Equation 1. Examples of energy shifted γ rays and corresponding isotropic angular distributions from 0^+ states are seen in Figures 3 & 4, respectively. Angular distributions of γ rays are normalized to the well-established ($0_2^+ \rightarrow 2_{g.s.}^+$) transition to ensure decays from other 0^+ states are isotropic where the nucleus is left in an unaligned state (this same normalization justification is used in numerous (n,n'γ) works [26, 27]). Anisotropy in the angular distributions can be seen where a_2 is not consistent with zero in the Legendre polynomial expansion shown in Equation 2, and absolute intensities can be measured via extraction of the A_0 coefficient in the same Equation 2. Multipolarity information (namely multipole mixing fractions, δ_{mixing}) for mixed-multipolarity transitions is also extracted from the angular distribution coefficients, another added benefit to performing DSAM measurements at the University of Kentucky.

$$E_\gamma(\theta_{lab}) = E_{\gamma,o}[1 + \beta F(\tau) \cos(\theta_{lab})] \quad (1)$$

$$W(\theta) \approx A_0[1 + a_2 P_2(\cos \theta_{lab}) + a_4 P_4(\cos \theta_{lab})] \quad (2)$$

III. RESULTS

Lifetimes for six (6) of the eleven (11) confirmed and tentative excited 0^+ states [20] were measured in the campaign of experiments (shown in Table I). We have also measured lifetimes (including lower limits) of the five lowest-lying rotational members of the $K^\pi=2^+$ band, the bandhead of the lowest $K^\pi=4^+$ band, and a total of 52 other states in ^{162}Dy . All of the measured lifetimes can be seen in Figure 5, where the lifetime in femtoseconds is plotted as a function of excitation energy in keV. Also shown in Figure 5 are the bombarding neutron energies used to extract each lifetime; these are chosen so that $F(\tau)$ is at least 1σ deviant from 0 for the lowest bombarding neutron energy threshold. The absolute intensities of decays discussed in this work were extracted from the angular distributions and are shown in Table IV, with unobserved transition intensities taken from literature [19, 28, 29] to provide pertinent discussion later in this manuscript.

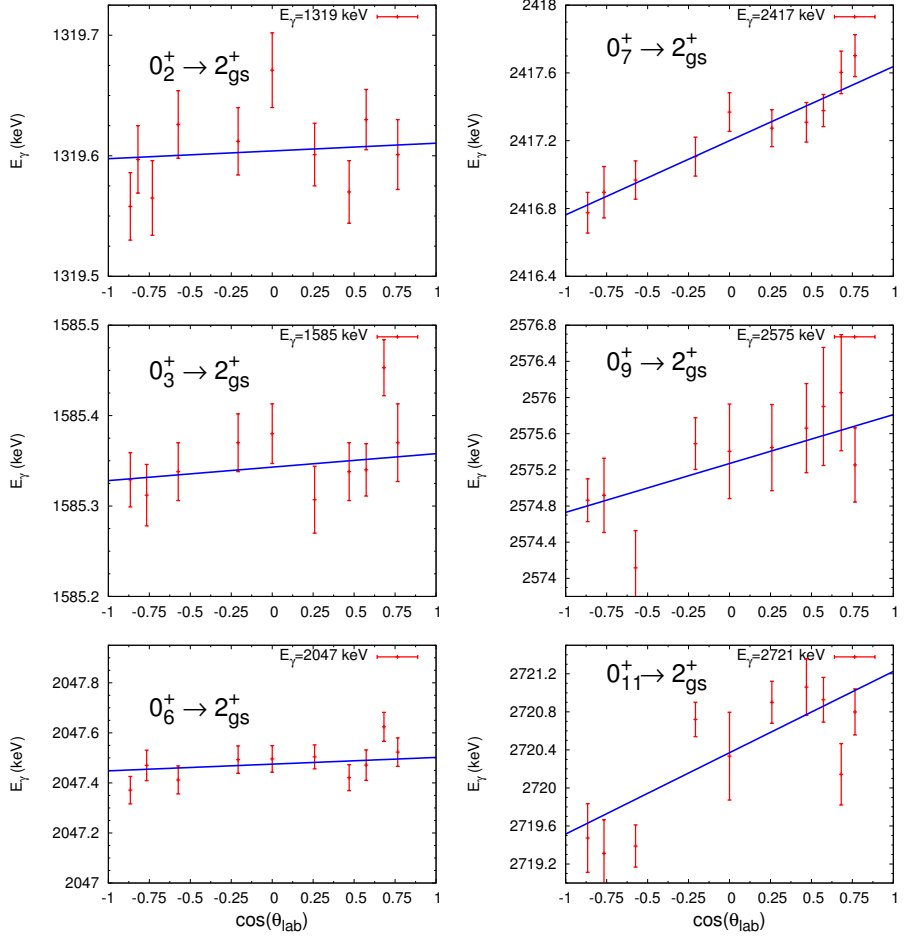


FIG. 3. Doppler energy shifts of $0_i^+ \rightarrow 2_{g.s.}^+$ γ -rays (color online).

The full tabulation of γ decays observed for the de-excitation of $K^\pi=0^+$ bands is shown in Table II, which includes experimentally measured lifetimes in femtoseconds, branching ratios, and γ -ray energies in keV. Mixed multipolarity de-excitations are assigned a multipole mixing fraction (δ_{mixing}) from comparison of our gathered angular distributions to a statistical model calculation, performed with CINDY [30]. A level scheme outlining all observed decays from 0^+ bands to the ground state band is also shown in Figure 7.

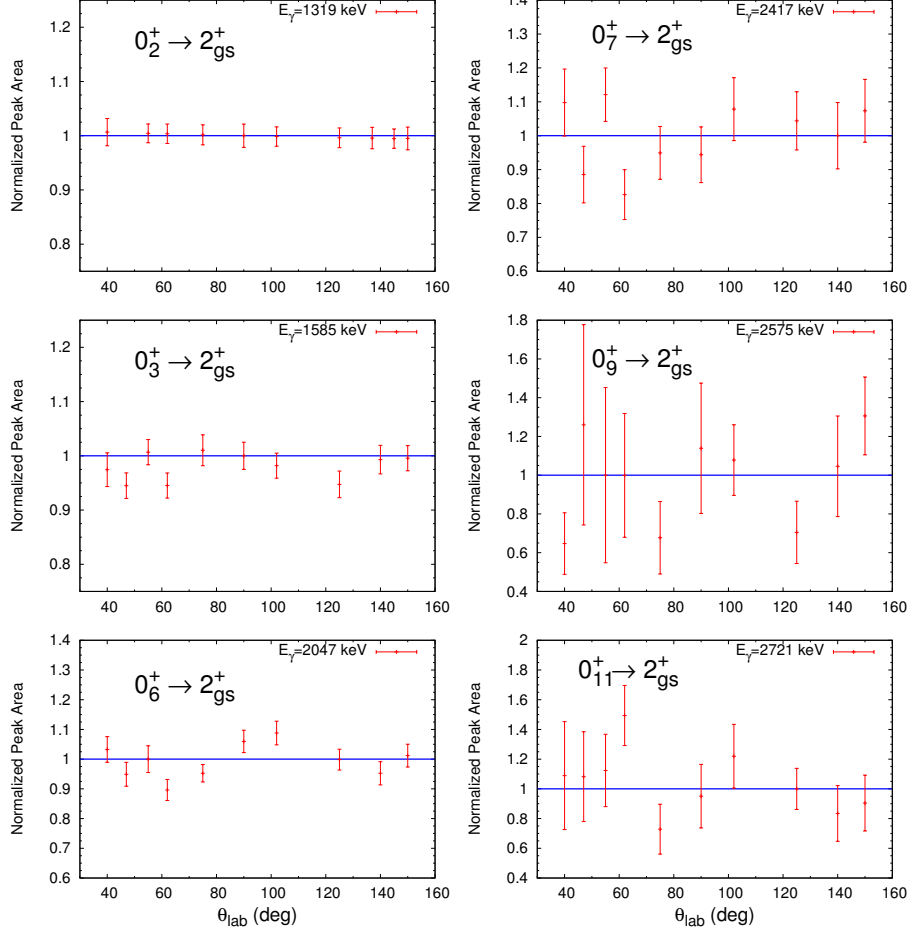


FIG. 4. Angular distributions of $0_i^+ \rightarrow 2_{g.s.}^+$ γ -rays, highlighting their isotropic nature (color online).

Lifetimes for the three lowest-lying rotational members of the 0_2^+ band were measured; the single, most intense γ ray at 1319 keV was used to measure (a shallow) $F(\tau)$ to extract the lifetime from the $E_n=1.6$ MeV dataset. The weighted average of $F(\tau)$ from both the 1187 & 1372 keV γ ray is used to measure the lifetime of the 2^+ state. Only the 1308 keV de-excitation contributes to the lifetime of the 4^+ state at $E_x=1574$ keV, as the 1025 keV

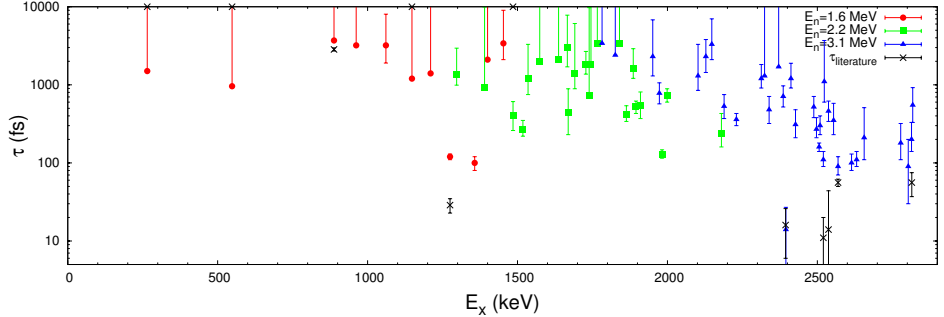


FIG. 5. All measured lifetimes in ^{162}Dy (in femtoseconds) plotted as a function of excitation energy in keV. Data points in red are extracted from the $E_n=1.6$ MeV angular distributions, points in green correspond to lifetimes extracted from the 2.2 MeV angular distributions, and blue points are lifetimes from the 3.1 MeV dataset. (color online)

transition exhibits a negative $F(\tau)$ value.

We have measured the lifetime of the bandhead and 2^+ member of the 0_3^+ band at $E_x=1666$ keV, with good lifetime resolution extracted from the $E_n=2.2$ MeV dataset. The single 1585 keV transition from the bandhead to the ground state yields a 3000^{+4800}_{-1300} fs lifetime, while only the 1647 and 1728 keV γ rays offer contributions to the 2^+ lifetime of 1800^{+880}_{-430} fs, as the decay at 1462 keV is coincident with a background line, making that particular $F(\tau)$ unreliable.

We adopt the placement [31] of the (2^+) state at 2189 keV as the 2^+ rotational band member of the 0_6^+ band at $E_x=2128$ keV, and have measured lifetimes for these two states from the single-channel decays of 2109 & 2047 keV, respectively. The lifetime of the bandhead was found to be 2300^{+1500}_{-860} fs, and 530^{+220}_{-160} fs for the 2^+ member.

The seventh and ninth 0^+ states decay via full energy de-excitations to the ground state at $E_\gamma=2417$ & 2575 keV, respectively. These corresponding lifetimes extracted from the $E_n=3.1$ MeV dataset are 270^{+110}_{-60} fs for the 0^+ state at 2497 keV, and 210^{+300}_{-100} fs at 2655 keV.

Due to the isotropic radiation observed for the 2721 keV γ -ray that depopulates the (0_{11}^+) state at 2802 keV, we support the assignment of this state as a 0^+ excitation, where further mentions of this state are considered as a confirmed 0^+ state. The Doppler shift from this 2721 keV decay gives us our shortest 0^+ lifetime of 90^{+110}_{-60} fs.

TABLE I: Observed 0^+ states in our $(n,n'\gamma)$ experiments compared with (p,t) experiments from [20], with $[\dagger]$ as the labeled ‘contaminant’ at $E_x=774.2$ keV.

0_i^+	E_x	Observed?
$[\dagger]$	774.2 (3)	$[\dagger]$
0_2^+	1398.3 (3)	✓
0_3^+	1666.3 (4)	✓
0_4^+	1814.6 (5)	
0_5^+	1820.3 (5)	
0_6^+	2126.5 (6)	✓
0_7^+	2496.7 (7)	✓
0_8^+	2588.8 (7)	
0_9^+	2655.3 (7)	✓
(0_{10}^+)	2663.0 (7)	
(0_{11}^+)	2802.9 (7)	✓

A. 0^+ Excitations Not Observed in $(n,n'\gamma)$

We did not observe γ rays for every excited 0^+ state seen in (p,t) experiments by [20] in ^{162}Dy , namely the excitations at 1814.6, 1820.3, 2588, and 2663 keV (Table I). Figure 6 shows cuts of our γ -singles spectra above the level energy thresholds where we would expect to see the full energy ($0_i^+ \rightarrow 2_{gs}^+$ transitions at the drawn vertical lines) de-excitations of the aforementioned states. Locally, there are no obvious peaks above our background, with the exception of the expected γ -ray leaving the 2588 keV state; if this peak exists, it would be a doublet with a γ at 2506 keV, belonging to a state of the same energy, making its energy shift unreliable and thus difficult to extract a lifetime with DSAM.

The tentative 0^+ assigned in [20] as a probable contaminant at $E_x=774.2$ keV was not observed in our experiment. The only decay channel available to such a state was not observed at $E_\gamma \approx 693.5$ keV ($(0_{774.2}^+) \rightarrow 2_{g.s.}^+$), due to the prominent $\text{Ge}(n,\gamma)$ detector background at the expected peak location. We can place a generous upper limit to the intensity of any peak on top of this background of 3% of the intensity of the strong 807 keV γ ray that de-excites the γ -band bandhead. This upper limit is well below half of the intensity of the lowest intensity γ rays observed in this $(n,n'\gamma)$ study, and as such, we are unable to measure

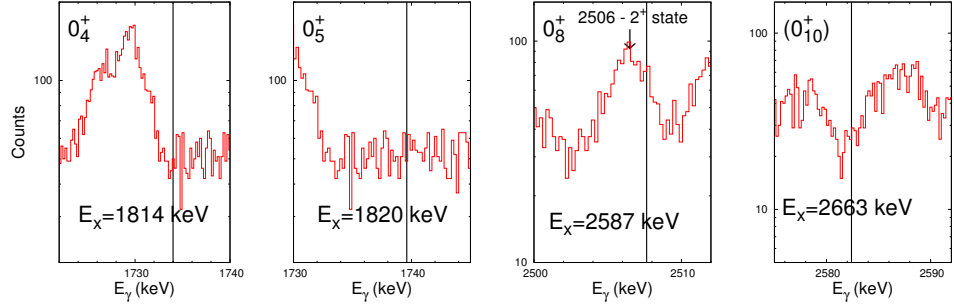


FIG. 6. Singles spectra cuts where remaining 0^+ excitations should be observed. Spectra for $0_{4,5}^+$ placements are from the $E_n=1.925$ MeV excitation function measurements, with $0_{8,10}^+$ from the $E_n=2.9$ MeV dataset.

a lifetime for this state using the Doppler Shift Attenuation Method. Govorin [32] observes an unplaced γ ray at 694.19 keV (well within the detector resolution to consider this γ ray as a candidate) at a lower intensity than our upper limit discussed above; it is entirely possible that this state exists, but the experiments so far have lacked the sensitivity to detect the de-excitation at ~ 693.5 keV. The ‘contaminant’ state at 774.2 keV is not observed in any other ^{162}Dy studies ($(\alpha,2n)$, (n,γ) , $(n,n'\gamma)$, etc [19]), further justifying its lack of detection in this campaign of experiments. We emphasize the use of other reactions such as $(\alpha,\alpha'\gamma)$ to remove the (n,γ) background in hopes of finding this state at 774.2 keV.

IV. DISCUSSION

A. A Lack of Strong β Vibrations in ^{162}Dy

As it stands from our measurement of the lifetimes, the generally weakly-collective ($B(E2)<2$ W.u.) transitions to the ground state band point away from a single-phonon β -vibration assignment for *any* observed 0^+ state in ^{162}Dy , shown in Table II. Common allegations on the collectivity of a β -vibration are that the $B(E2;0_i^+ \rightarrow 2_{g.s.}^+) \sim 12-33$ W.u. [4], with decays from higher-lying members of the band falling around 6-10 W.u. in strength, when in reality, this behavior is far from common across the deformed nuclear landscape. While the E0 strengths are not available for the states in the 0^+ bands of ^{162}Dy , and the two

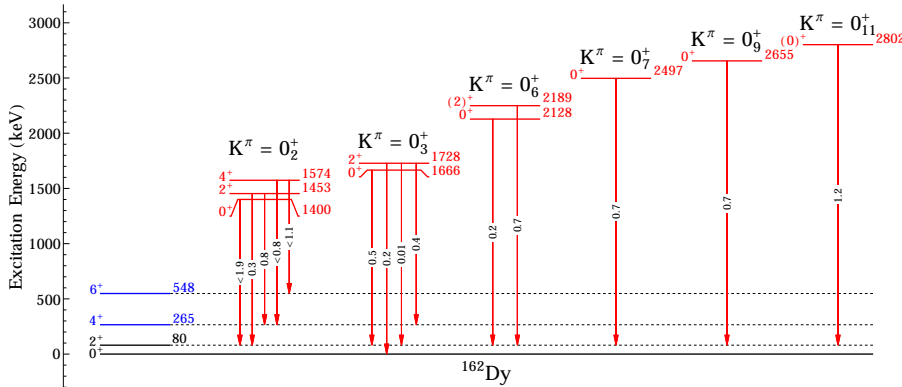


FIG. 7. Level scheme outlining all measured lifetimes for $K^\pi=0^+$ bands in ^{162}Dy . New lifetime measurements are shown in red (color online), and new $B(E2;0_i^+ \rightarrow \text{g.s.})$ calculations are expressed in Weisskopf units (W.u.).

nucleon transfer reaction cross sections to all but one 0^+ excitation are small (<10.6% of the ground state cross section [20]), order of magnitude differences in the above assertions on B(E2) strength, and the low absolute value of our B(E2) measurements do not lend credence to this β -vibration picture. In addition, our evaluation of upper limits to the B(E2) strength in a few cases is not conclusive enough to confirm any band as a β -vibration, even in the face of a potentially collective transition to the ground state at 1.9 Weisskopf units. Traditionally, the lowest lying K=0,2 bands were tenaciously defended as quadrupole vibrations, but this paradigm has evolved as the experimental data trickles in, and as we notice the unclear nature of 0^+ excitations in deformed nuclei [13, 33]. The search for higher-lying collective 0^+ excitations in ^{162}Dy has merit, as both ^{166}Er and ^{158}Gd show signs of strong (>2 W.u.) collectivity in states above the first excited 0^+ band [16, 34], but again, our findings fail to reveal any concrete signature of a strongly collective β -vibration at *any* excitation energy in ^{162}Dy . Our most likely candidate and correspondingly most collective B(E2) ($1.2_{-0.6}^{+2.3}$ W.u.) to the ground state lies in the 0_{11}^+ state at 2802 keV excitation energy. *If* this state is the true β vibration in ^{162}Dy and the state at 774.2 keV is *not* the lowest 0^+ , it follows the empirical

behavior of well-deformed rare-earth nuclei, where the β mode of quadrupole vibration does not exist as the lowest-lying $K^\pi=0^+$ band. The curious lack of an observed collective β vibration in our data is alarming, but we must not forget the unobserved excitations below the pairing gap(s) at 774, 1814, & 1820 keV, as any one of these states *could* be the collective β -vibration in ^{162}Dy .

B. On the Two-Phonon Characteristics

With the experimental evidence of two-phonon quadrupole vibrations in nearby rare-earth nuclei (^{178}Hf), we are given impetus to further examine any multiphonon configurations in the 0^+ states in ^{162}Dy .

1. 2_γ^+ band

The axial symmetry-breaking γ vibration has stood up as one of the benchmarks and cornerstones of quadrupole surface vibrations in the geometric model. While not as enigmatic in behavior as their $K^\pi=0^+$ counterparts (the proposed β vibration), the lowest $K^\pi=2^+$ band provides the basis of understanding nuclear collective motion in deformed nuclei. Lifetimes of the $K^\pi=2^+$ band up to $J=5$ were measured and are shown in Table III and Figure 9. In the eight decays from the 2^+ band, two of the γ rays (the 697 keV and 634 keV de-excitations) are not used in the calculation of the level lifetime, as they have Doppler shifts that correspond to an $F(\tau)<0$. Lower limits for the lifetime are measured in several cases due to the inherent limitations of sensitive lifetimes DSAM can measure (up to a few picoseconds). Systematics for the γ -vibrational band decays to the ground state across the even Dysprosium nuclei show inflated levels of collectivity on the order of ~ 5 W.u. in strength [11, 12], where we observe similarly collective (~ 4 W.u.) transitions in our $(n,n'\gamma)$ experiments; this gives a reasonable, unambiguous assignment as the $K^\pi=2^+$ γ -vibration in ^{162}Dy , and provides the foundation for the multiphonon configurations in the nucleus. Since our deduced $B(E2)$ does not offer refinement beyond the previously measured transition probabilities from Coulomb Excitation, we report our measured value, but adopt the literature values in discussion.

2. 0_2^+ band $\gamma\gamma$ -vibration

Considerable theoretical and experimental focus [20, 28, 31, 35] has been placed into the assessment of the 0_2^+ band as a $\gamma\gamma$ -vibration, and its confirmation is contingent on the measurement of level lifetimes and the $0^+ \rightarrow \gamma$ -vibration interband transitions: a weak $E_\gamma=565$ keV line decaying from the 2^+ member of the band, a $E_\gamma=686$ keV line leaving the 4^+ member, and the elusive $E_\gamma=512$ keV line from the 0^+ bandhead, to name a few. The broad annihilation peak in our spectra prevents detection of this latter γ ray in our γ -singles-based experiments, and the low literature intensities of the other two make detection less than straightforward. We can, however, calculate the transition probabilities using our measured lifetimes, the literature values for the intensities [19, 28], and with assumption that no multipolarity mixing is present. The existence of this double-phonon characterization in the 0_2^+ seems fairly evident as a $\gamma\gamma$ -vibration from our lifetime measurements (with lower limits of lifetimes in a few cases), with calculated $B(E2;2^+ \rightarrow 4_\gamma^+) = 2.7$, $B(E2;4^+ \rightarrow 4_\gamma^+) < 3.7$, and $B(E2;0^+ \rightarrow 2_\gamma^+) < 16$ W.u. Clearly, the $B(E2)$ probabilities greater than 1 are plausible in the interband cases for decays of the 2^+ member, and the upper limit of a 16 Weisskopf unit $B(E2)$ for the 512 keV γ ray is difficult to ignore, which points toward some collective behavior built on top of the γ -vibrational band. However, the overall $B(E2)$ strength observed is not blatantly conclusive, so we emphasize a *tentative* two-phonon ($\gamma\gamma$) vibration characterization of the $K^\pi=0_2^+$ band. That being said, the relative inflation and enhancement of transition probabilities to the γ -vibrational band is evident in Table VI, where we see more than a factor of 2 increase in $B(E2)$ for like-spin changing transitions ($2^+ \rightarrow 2_\gamma^+$ versus $2^+ \rightarrow 2_{gs}^+$, for example), strengthening our argument for this $\gamma\gamma$ assignment in ^{162}Dy . Comparison of our deduced transition probabilities out of the 0_2^+ band to the Alaga rules (Table ??) yield some mixed results; for decays to the ground state, we observe good agreement, but the decays to the γ -vibrational band are in stark disagreement. The disagreement cannot be explained due to multipole mixing in any case (recall that our reported $B(E2)$ s to the γ -band assume no mixing and are practically upper limits). An inset level scheme for the 0_2^+ band is shown in Figure 9, showing our measured decays and the interband decays (with literature intensities). These interband transition strengths are also seen in Table II, marked by a $[\dagger]$ symbol in the column for the branching ratio, corresponding to literature branching ratios taken from [19]. The measurement and confirmation of $\gamma\gamma$ collectivity in

this 0_2^+ band also implies certain degrees of anharmonicity at work in the two-phonon vibration, as the 0_2^+ band lies 375 keV below the expected excitation energy for a harmonic $\gamma\gamma$ -vibration (at 1.6 times the energy of the single γ -vibrational phonon case). Anharmonic double-phonon vibrations are not completely unprecedented in the literature (^{178}Hf [18] & ^{232}Th [36]), but this is one of the lowest-lying $\gamma\gamma$ vibrations in well-deformed rare-earth nuclei at $E_x=1400$ keV. On top of this, the nuclei in the actinides (Th and Os) that exhibit two-phonon vibrations have energy ratios very close to the expected value of 2, with ^{232}Th less than 2, yet ^{162}Dy is contrasted with the intriguing evidence of other rare-earth two-phonon vibrations that have a $\frac{E_{\gamma\gamma}}{E_\gamma}$ ratio >2 [37].

3. $K^\pi=4_{1,2}^+$ bands at 1535, 2181 keV as $\gamma\gamma$ -vibrations

In the case of an aligned $K^\pi=4^+$ $\gamma\gamma$ -vibration, strong B(E2) transition probabilities are expected between the 4^+ band and the existing γ -vibration. In our experiments, we do not observe full-energy de-excitations of the $K^\pi=4^+$ band to the ground state due to K-forbiddenness, but instead with transitions to the previously mentioned γ -vibrational band (shown in Figure 9). The lifetime of the bandhead 4^+ state at 1535 keV is extracted from the Doppler shift of the 572 keV γ ray, as the 475 keV decay lies on top of a background, and as such, the Doppler shift is unreliable; the 647 keV line exhibits a negative $F(\tau)$ value, and is not used in the lifetime calculation. Evidence for the existence of a background contaminant can be seen in the branching ratios for the decays, as they are not consistent with literature intensities. In Table III, deduced B(E2) values from our experiments are reported alongside calculations using the literature intensities from [19] in parentheses. The level of collectivity in these interband transitions (in either our deduced B(E2) strengths or the ones calculated with literature intensities) is striking and extremely hard to ignore! Due to the preferential decays observed and the collective transitions to the $2^+\gamma$ -band, it seems definitive that this lowest-lying $K^\pi=4^+$ band is the second $\gamma\gamma$ -vibration in ^{162}Dy , at a slightly anharmonic energy ($R_{\frac{E_{\gamma\gamma}}{2E_\gamma}} \approx 0.86$).

Wu characterizes the $\gamma\gamma$ vibration in ^{162}Dy as a highly fragmented excitation, with significant collective strength lying in the two 4^+ states at 1535 & 2181 keV [29]. We have measured the lifetime of this second 4^+ state at 2181 keV, via a 1217 keV γ ray to the 3^+ member of the γ band, but we have not observed the 1294 keV decay to the bandhead (this

line would also be coincident with an inherent $^{115}\text{In}(n,n'\gamma)$ background). The $\tau=240_{-80}^{+190}$ fs lifetime and mostly M1 radiation observed from the 1217 keV decay translates to a deduced B(E2) of 1.3 W.u.; this deduced value from our experiments does not account for the $\sim 50\%$ branch of the 1294 keV decay, where in reality, this B(E2) is cut in half by using literature intensities [29, 31]. Using the literature intensities from [29], we do observe a distinctly collective E2 transition from this higher-lying 4^+ state to the bandhead of 8.5 W.u., however, this degree of collectivity is contrasted with the lower-lying 4^+ state that we assign as a $\gamma\gamma$ -vibration, where the authors in [29] imply that there is a significant component of a two-phonon vibration in this state at 2181 keV. Instead, we observe an overwhelming portion of collectivity in the lower-lying 4^+ state, with the calculated transition strengths leaving this higher-lying state in Table III. This is not to imply complete disagreement with [29], as we still observe a highly fragmented and collective $\gamma\gamma$ -vibration in these two states at 1535 and 2181 keV. Falling in line with other 4^+ $\gamma\gamma$ -vibrations in rare-earth nuclei, this two-phonon vibration is anharmonic, with a $R_{E_{\gamma\gamma}/E_{\gamma}}=2.5$ [REFS].

4. $(2,3,4)^+$ state at 2230 keV

Our comprehensive lifetime measurements of $J\leq 5$ states below 3.1 MeV has yielded an interestingly strong transition from a state at 2230 keV excitation energy to the γ -vibrational band. From our measurement of a mixed E2/M1 multipolarity γ -ray ($\sim 89\%$ E2 if the state is a 2^+) at $E_{\gamma}=1342$ keV that decays to the bandhead of the γ -band, we can place a tentative $(2,3,4)^+$ spin assignment on this level. Aprahamian observed a similar energy γ -ray, but places an E1 multipolarity assignment, where our angular distribution is consistent with a $\Delta L=2$ transition (Figure 8) [19]. Given any of the tentative positive parity, low-spin assignments, our measured B(E2) is distinctly collective, at 5.2 W.u. in strength; this behavior of distinct collectivity is completely expected for a two-phonon $\beta\gamma$ -vibration in structure, and would be one of the first experimental evidences of this mode of multiphonon configuration. These are, of course, large assumptions to make about the rotational band assignment of this state, but provide an interesting avenue to continue research into the structure of this nucleus.

This begs the question, once again: where is the single-phonon β vibration in ^{162}Dy ? If we take this state at 2230 keV as part of the $\beta\gamma$ -vibration and with close to harmonic

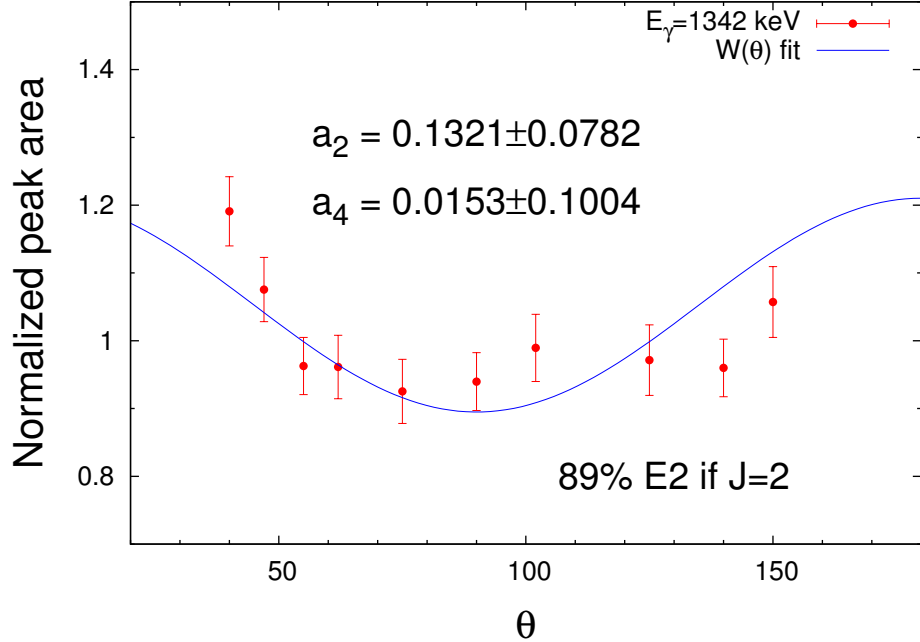


FIG. 8. Measured angular distribution of 1342 keV γ ray leaving the 2230 keV level, $W(\theta)$ fit is shown with a_2 and a_4 coefficients from the $E_n=3.1$ MeV angular distribution.

vibrations, the β vibration *should* be around $E_x \approx 1350$ keV; this is clearly not the case based on our lifetime measurements of the 0_2^+ band and its characterization as the $K=0$ $\gamma\gamma$ -vibration. That being said, it is entirely possible that a strong β -vibration exists at either of the 0^+ excitations at 1814 or 1820 keV (or at the unobserved and elusive state at 774 keV). In the case of a β vibration at ~ 1800 keV, it would imply that the $\beta\gamma$ is fairly anharmonic, clocking in at $\sim 80\%$ of the expected two-phonon energy, which is reasonable, considering that the $K^\pi=0^+$ $\gamma\gamma$ -vibration in ^{162}Dy is $\sim 79\%$ harmonic ($R_{\frac{E_{\gamma\gamma}}{2E_\gamma}} \approx 0.79$), and the $K^\pi=4^+$ $\gamma\gamma$ -vibration is similarly anharmonic at $R_{\frac{E_{\gamma\gamma}}{2E_\gamma}} \approx 0.86$. We strongly emphasize further study on the 0^+ states in ^{162}Dy to find the collective β -vibration at 774, 1814, or 1820 keV (if the β -vibration even exists in this nucleus).

E_{lev} (keV)	$ E_\gamma$ (keV)	$ L_{\gamma,abs}$ (n,n'γ)	$ L_\gamma$ (lit.)	$ \delta_{mixing} $
888.18(22)	807.54(50)	976.596(9.252)		$ -0.45^{+0.05}_{-0.06} $

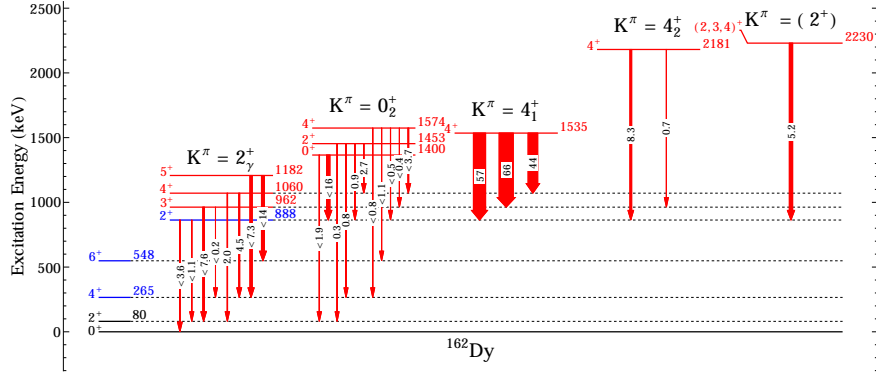


FIG. 9. Level scheme showing all observed transitions from the lowest-lying 2_{γ}^{+} , 0_{2}^{+} , and 4_{1}^{+} band with all interband ($K^{\pi}=J_i^{+} \rightarrow K^{\pi}=2_{\gamma}^{+}$) decays. Intensities for transitions to the γ -band are taken from [19]. Also shown is a tentative (2^{+}) state at 2230 keV with a strong decay to the 2_{γ}^{+} band.

E_{lev} (keV)	E_{γ} (keV)	$I_{\gamma,abs}$ (n,n'γ)	I_{γ} (lit.)	δ_{mixing}
	888.18(50)	887.460(7.953)		
962.96(27)	697.30(50) \otimes	166.366(2.981)		$0.20^{+0.06}_{-0.06}$
	882.31(50)	877.632(9.095)		<-21
1061.05(29)	795.35(50)	213.256(1.374)		$-0.92^{+0.04}_{-0.05}$
	980.36(51)	121.782(1.166)		
1182.88(26)	634.24(61)	67.548(1.514)		<-7
	917.18(51)	214.971(2.635)		<-21
1400.29(36)	512.0(2)	[†] 11(5)* [28]		
	1319.60(51)	163.971(1.238) 133(3)* [28]		
1453.50(30)	395.49 (10)	[†] 0.18(2) [19]		
	565.32 (12)	[†] 0.37(6) [19]		
	1187.81(51)	125.506(1.610) 12.7(3) [19]		
	1372.80(51)	169.820(1.989) 18.1(8) [19]		$1.3^{+0.2}_{-0.2}$
1535.97(23)	475.27(54) \otimes	53.276(3.388) 4.5(3) [19]		$-0.89^{+0.32}_{-0.80}$
	572.96(50)	90.678(1.588) 21.8(9) [19]		<-21
	647.61(50) \otimes	141.966(2.084) 50.1(8) [19]		
1574.34(29)	513.31 (2)	[†] 0.51(3) [19]		
	611.23 (5)	[†] 0.12(2) [19]		
	686.15 (6)	[†] 0.29(8) [19]		
	1025.84(58) \otimes	25.251(0.916) 5.0(2) [19]		
	1308.65(51)	135.879(1.997) 24(2) [19]		$0.93^{+0.14}_{-0.15}$
1666.01(33)	1585.35(51)	131.018(1.476)		
1728.31(20)	1462.70(51) \otimes	110.002(1.779) 0.81(6) [32]		
	1647.64(51)	133.790(2.206) 1.21(7) [32]		$-0.22^{+0.08}_{-0.08}$

E_{lev} (keV)	E_γ (keV)	$ I_{\gamma,abs} (n,n'\gamma)$	$ I_\gamma $ (lit.)	$ \delta_{mixing} $
	1728.29(53)	85.273(1.611)	0.66(6) [32]	
2128.02(33)	2047.34(61)	286.080(6.065)		
2180.69(53)	1217.73(58)	300.230(5.134)	1.13(24) [29]	$0.24^{+0.07}_{-0.06}$
	1292.51(58) ^[⊗]	319.833(9.558)	1.00 [29]	
2189.65(52)	2109.10(50)	140.677(3.860)		$2.7^{+1.8}_{-0.9}$
2231.06(38)	1342.57(50)	239.620(6.282)		$3.1^{+2.1}_{-1.0}$
2497.77(52)	2417.22(50)	116.520(4.933)		
2655.83(33)	2575.28(53)	59.373(5.424)		
2802.04(61)	2721.48(55)	50.490(15.032)		

TABLE IV: Absolute intensities ($I_{\gamma,abs}$) and multipole mixing

fractions (δ_{mixing} where applicable) for γ -decays observed in $(n,n'\gamma)$ experiments. $[\dagger]$: γ ray not observed, reporting literature intensity ([19, 32] gives absolute intensities, while [28, 29] report relative intensities).

V. CONCLUSION

The assertion that *any* of the observed 0^+ bands in ^{162}Dy is a coherent ‘ β ’ vibration is tenuous at best, based on our measurement of weakly collective (<2 W.u.) B(E2)s to the ground state band in contrast to the convention that a β vibration should show substantial B(E2) transition strength of several Weisskopf units [4]. However, with the measurement of lifetimes for the 0_2^+ band, we observe collective transitions to the well-behaved 2_γ^+ band that signify a definitive, somewhat anharmonic and anti-aligned $\gamma\gamma$ -vibrational characteristic. Furthermore, preferential, strong decays from the lowest 4^+ band to the γ -band suggest the second $\gamma\gamma$ -vibration with $K^\pi=4^+$, as well as a distinctly collective E2 from the higher-lying 4^+ state at 2181 keV, as a second branch of the $\gamma\gamma$ -vibration. A ‘ $\beta\beta$ ’ type vibration must exhibit strong, collective transitions to a pre-existing β -band; we do not observe any transitions of this type (nor do we observe collective $0_i^+ \rightarrow \text{g.s.}$ transitions) in our data. Here, we mirror and expand upon similar assertions made by countless works in the field, in that careful, well-gated, low-background measurements must be made to observe the potential 0^+ state at 774 keV and the other, unobserved excitations mentioned in Table I in hopes of finding any signatures of a β -vibration in ^{162}Dy .

VI. ACKNOWLEDGEMENTS

This work is funded by the National Science Foundation (NSF) under grant numbers PHY-1068192, PHY-1205412, and PHY-0956310. Special thanks to R. Casten for invaluable physics insight and discussions.

- [1] X. Wu, A. Aprahamian, S. M. Fischer, W. Reviol, G. Liu, and J. X. Saladin, Phys. Rev. C **49**, 1837 (1994).
- [2] A. Aprahamian, Nuclear Physics A **731**, 291 (2004).
- [3] H. G. Börner, M. Jentschel, N. V. Zamfir, R. F. Casten, M. Krticka, and W. Andrejtscheff, Phys. Rev. C **59**, 2432 (1999).
- [4] P. Garrett, Journal of Physics G: Nuclear and Particle Physics **27**, R1 (2001).
- [5] Heyde, Kris and Wood, John L., Rev. Mod. Phys. **83**, 1467 (2011).
- [6] Bonatsos, Dennis and E. A. McCutchan and Casten, R. F. Casperson, R. J. and Werner, V. and Williams, E., Phys. Rev. C **80**, 034311 (2009).
- [7] R. Clark, R. Casten, L. Bettermann, and R. Winkler, Phys. Rev. C **80**, 011303 (2009).
- [8] N. Pietralla and O. M. Gorbachenko, Phys. Rev. C **70**, 011304 (2004).
- [9] N. V. Zamfir, J.-y. Zhang, and R. F. Casten, Phys. Rev. C **66**, 057303 (2002).
- [10] Y. Sun, A. Aprahamian, J.-y. Zhang, and C.-T. Lee, Phys. Rev. C **68**, 061301 (2003).
- [11] F. K. McGowan and W. T. Milner, Phys. Rev. C **23**, 1926 (1981).
- [12] T. Grotdal, K. Nyb, T. Thorsteinsen, and B. Elbek, Nuclear Physics A **110**, 385 (1968).
- [13] Sharpey-Schafer, J.F., Mullins, S.M., Bark, R.A., Kau, J., Komati, F., Lawrie, E.A., Lawrie, J.J., Madiba, T.E., Maine, P., Minkova, A., Murray, S.H.T., Ncapayi, N.J., and Vymers, P.A., Eur. Phys. J. A **47**, 5 (2011).
- [14] V. G. Soloviev, A. V. Sushkov, and N. Y. Shirikova, Fiz.Elem.Chastits At.Yadra **27**, 1643 (1996).
- [15] J. P. Delaroche, M. Girod, J. Libert, H. Goutte, S. Hilaire, S. Péru, N. Pillet, and G. F. Bertsch, Phys. Rev. C **81**, 014303 (2010).
- [16] P. E. Garrett, M. Kadi, M. Li, C. A. McGrath, V. Sorokin, M. Yeh, and S. W. Yates, Phys. Rev. Lett. **78**, 4545 (1997).

- [17] H. Lehmann, J. Jolie, F. Corminboeuf, H. G. Börner, C. Doll, M. Jentschel, R. F. Casten, and N. V. Zamfir, Phys. Rev. C **57**, 569 (1998).
- [18] A. Aprahamian, R. C. de Haan, H. G. Börner, H. Lehmann, C. Doll, M. Jentschel, A. M. Bruce, and R. Piepenbring, Phys. Rev. C **65**, 031301 (2002).
- [19] A. Aprahamian, X. Wu, S. Lesher, D. Warner, W. Gelletly, H. Börner, F. Hoyler, K. Schreckenbach, R. Casten, Z. Shi, D. Kusnezov, M. Ibrahim, A. Macchiavelli, M. Brinkman, and J. Becker, Nuclear Physics A **764**, 42 (2006).
- [20] D. A. Meyer, V. Wood, R. F. Casten, C. R. Fitzpatrick, G. Graw, D. Bucurescu, J. Jolie, P. v. Brentano, R. Hertenberger, H.-F. Wirth, N. Braun, T. Faestermann, S. Heinze, J. L. Jerke, R. Krücken, M. Mahgoub, O. Möller, D. Mücher, and C. Scholl, Phys. Rev. C **74**, 044309 (2006).
- [21] M. Jammari and R. Piepenbring, Nuclear Physics A **487**, 77 (1988).
- [22] P. Garrett, N. Warr, and S. Yates, J. Res. Natl. Inst. Stand. Technol. **105**, 141 (2000).
- [23] T. Belgia, G. Molnar, and S. W. Yates, Nuclear Physics A **607**, 43 (1996).
- [24] S. R. Lesher, C. J. McKay, M. Mynk, D. Bandyopadhyay, N. Boukharouba, C. Fransen, J. N. Orce, M. T. McEllistrem, and S. W. Yates, Phys. Rev. C **75**, 034318 (2007).
- [25] K. Winterbon, Nuclear Physics A **246**, 293 (1975).
- [26] S. R. Lesher, C. Casarella, A. Aprahamian, B. P. Crider, R. Ikeyama, I. R. Marsh, M. T. McEllistrem, E. E. Peters, F. M. Prados-Estevez, M. K. Smith, Z. R. Tully, J. R. Vanhoy, and S. W. Yates, Phys. Rev. C **91**, 054317 (2015).
- [27] E. E. Peters, A. Chakraborty, B. P. Crider, B. H. Davis, M. K. Gnanamani, M. T. McEllistrem, F. M. Prados-Estevez, J. R. Vanhoy, and S. W. Yates, Physical Review C **88**, 024316 (2013).
- [28] N. V. Zamfir, R. F. Casten, B. Liu, D. S. Brenner, C. J. Barton, R. Krücken, C. W. Beausang, J. R. Novak, J. R. Cooper, G. Cata-Danil, R. L. Gill, and D. D. Warner, Phys. Rev. C **60**, 054319 (1999).
- [29] C. Y. Wu, D. Cline, M. W. Simon, G. A. Davis, R. Teng, A. O. Macchiavelli, and K. Vetter, Phys. Rev. C **64**, 064317 (2001).
- [30] E. Sheldon and V. Rogers, Computer Physics Communications **6**, 99 (1973).
- [31] J. Berzins, P. Prokofjevs, R. Georgii, R. Hucke, T. von Egidy, G. Hlawatsch, J. Klora, H. Lindner, U. Mayerhofer, H. Schmidt, A. Walter, V. Soloviev, N. Shirikova, and A. Sushkov, Nuclear Physics A **584**, 413 (1995).

- [32] L. I. Govor, A. M. Demidov, and V. A. Kurkin, Physics of Atomic Nuclei **65**, 785 (2002).
- [33] P. E. Garrett, Journal of Physics G: Nuclear and Particle Physics **27**, R1 (2001).
- [34] S. R. Lesher, J. N. Orce, Z. Ammar, C. D. Hannant, M. Merrick, N. Warr, T. B. Brown, N. Boukharouba, C. Fransen, M. Scheck, M. T. McEllistrem, and S. W. Yates, Phys. Rev. C **76**, 034318 (2007).
- [35] C. Günther, S. Boehmsdorff, K. Freitag, J. Manns, and U. Müller, Phys. Rev. C **54**, 679 (1996).
- [36] W. Korten, T. Hrtlein, J. Gerl, D. Habs, and D. Schwalm, Physics Letters B **317**, 19 (1993).
- [37] W. Younes, D. E. Archer, J. A. Becker, L. A. Bernstein, P. E. Garrett, N. Warr, M. Kadi, A. Martin, S. W. Yates, G. D. Johns, R. O. Nelson, and W. S. Wilburn, AIP Conference Proceedings **481**, 464 (1999).

TABLE II: Lifetimes of excited 0^+ bands in ^{162}Dy , with calculated $B(E2)$ in W.u., from our measured multipole mixing fractions, branching ratios, γ -ray energies, and lifetimes, all extracted from the angular distributions. $B(E2)$ strengths in parentheses are calculated using literature intensities.

K^π	E_{level} (keV)	E_γ (keV)	$J_{K_i}^\pi$	$J_{K_f}^\pi$	$F(\tau)_{av}$	τ (fs)	BR	$\pi\ell$	$B(\pi\ell)$ (W.u.)
$K^\pi=0_2^+:$	1400.29(36)	512.0(2)	$0_{0_2^+}^+$	$2_{2_1^+}^+$	$0.031 \pm 0.038 > 2100^{[\vartheta]}$		[†]	E2	(<16)
	1319.60(51)		$0_{0_2^+}^+$	$2_{0_1^+}^+$		1.000	E2		<1.9
	1453.50(30)	395.49 (10)	$2_{0_2^+}^+$	$4_{2_1^+}^+$	$0.042 \pm 0.026 \quad 3400^{+5600}_{-1300} [\vartheta]$	[†]	E2		$(2.7^{+1.7}_{-1.7})$
	565.32 (12)		$2_{0_2^+}^+$	$2_{2_1^+}^+$		[†]	E2[‡]		$(0.9^{+0.6}_{-0.6})$
	1187.81(51)		$2_{0_2^+}^+$	$4_{0_1^+}^+$		0.425(4)	E2		$0.8^{+0.5}_{-0.5}$
	1372.80(51)		$2_{0_2^+}^+$	$2_{0_1^+}^+$		0.575(4)	E2/M1 ^[a,s]		$0.3^{+0.2}_{-0.2}$
	1574.34(29)	513.31 (2)	$4_{0_2^+}^+$	$4_{2_1^+}^+$	$0.043 \pm 0.031 > 2000^{[s]}$	[†]	E2[‡]		(<3.7)
	611.23 (5)		$4_{0_2^+}^+$	$3_{2_1^+}^+$		[†]	E2[‡]		(<0.4)
	686.15 (6)		$4_{0_2^+}^+$	$2_{2_1^+}^+$		[†]	E2		(<0.5)
	1025.84(58) ^[\oslash]		$4_{0_2^+}^+$	$6_{0_1^+}^+$		0.157(5)	E2		<1.1
	1308.65(51)		$4_{0_2^+}^+$	$4_{0_1^+}^+$		0.843(5)	E2/M1 ^[b,s]		<0.8
$K^\pi=0_3^+:$	1666.01(33)	1585.35(51)	$0_{0_3^+}^+$	$2_{0_1^+}^+$	$0.051 \pm 0.033 \quad 3000^{+4800}_{-1300} [s]$	1.000	E2		$0.5^{+0.4}_{-0.3}$
	1728.31(20)	1462.70(51) ^[\otimes]	$2_{0_3^+}^+$	$4_{0_1^+}^+$	$0.081 \pm 0.023 \quad 1800^{+880}_{-430} [s]$	0.334(5) ^[*]	E2		$0.4^{+0.1}_{-0.1} (0.5^{+0.1}_{-0.1})$
	1647.64(51)		$2_{0_3^+}^+$	$2_{0_1^+}^+$		0.407(5)	E2/M1 ^[c,s]		$0.01^{+0.01}_{-0.01} (0.02^{+0.01}_{-0.02})$
	1728.29(53)		$2_{0_3^+}^+$	$0_{0_1^+}^+$		0.259(4)	E2		$0.2^{+0.1}_{-0.1} (0.2^{+0.1}_{-0.1})$
$K^\pi=0_6^+:$	2128.02(33)	2047.34(61)	$0_{0_6^+}^+$	$2_{0_1^+}^+$	$0.071 \pm 0.031 \quad 2300^{+1500}_{-860} [\varpi]$	1.000	E2		$0.2^{+0.1}_{-0.1}$
	2189.65(52)	2109.10(50)	$(2)_{0_6^+}^+$	$2_{0_1^+}^+$	$0.267 \pm 0.058 \quad 530^{+220}_{-160} [\varpi]$	1.000	(E2/M1) ^[d,\varpi]		$0.7^{+0.3}_{-0.2}$
$K^\pi=0_7^+:$	2497.77(52)	2417.22(50)	$0_{0_7^+}^+$	$2_{0_1^+}^+$	$0.376 \pm 0.055 \quad 270^{+110}_{-60} [\varpi]$	1.000	E2		$0.7^{+0.2}_{-0.2}$
$K^\pi=0_9^+:$	2655.83(33)	2575.28(53)	$0_{0_9^+}^+$	$2_{0_1^+}^+$	$0.436 \pm 0.164 \quad 210^{+300}_{-100} [\varpi]$	1.000	E2		$0.7^{+0.6}_{-0.4}$
$K^\pi=0_{11}^+:$	2802.04(61)	2721.48(55)	$0_{0_{11}^+}^+$	$2_{0_1^+}^+$	$0.653 \pm 0.200 \quad 90^{+110}_{-60} [\varpi]$	1.000	E2		$1.2^{+2.3}_{-0.6}$

[†]: Intensity information taken from [19, 28] (γ -ray not seen in this work), [‡]: Mixing information not available, full E2 strength reported, $[\oslash]$: γ ray not used in $F(\tau)$ calculation ($F(\tau)<0$).

$[\vartheta]$: $F(\tau)$ or δ_{mixing} extracted from $E_n=1.6$ MeV angular distributions, $[s]$: $F(\tau)$ or δ_{mixing} extracted from $E_n=2.2$ MeV angular distributions, $[\varpi]$: $F(\tau)$ or δ_{mixing} extracted from $E_n=3.1$ MeV angular distributions, $[\otimes]$: γ ray coincident with background, not used in calculation of $\frac{B(E2)}{B(E1)}$.

TABLE III: Lifetimes of excited 2^+ band, both 4^+ bands, and tentative 2^+ state at 2230 keV in ^{162}Dy , with calculated $B(E2)$ in W.u., from our measured multipole mixing fractions, branching ratios, γ -ray energies, and lifetimes, all extracted from the angular distributions. $B(E2)$ strengths in parentheses are calculated using literature intensities.

K^π	E_{level} (keV)	E_γ (keV)	$J_{K_i}^\pi$	$J_{K_f}^\pi$	$F(\tau)_{av}$	τ (fs)	BR	$\pi\ell$	$B(\pi\ell)$ (W.u.)
$K^\pi=2_2^+:$	888.18(22)	807.54(50)	$2_{2\gamma}^+$	$2_{0_1^+}^+$	$0.022 \pm 0.018 > 3700$ [θ]	0.524(3)	E2/M1 ^[a,θ]	<1.1	
		888.18(50)	$2_{2\gamma}^+$	$0_{0_1^+}^+$		0.476(3)	E2	<3.6	
	962.96(27)	697.30(50) ^[∅]	$3_{2\gamma}^+$	$4_{0_1^+}^+$	$0.021 \pm 0.025 > 3200$ [θ]	0.159(3)	E2/M1 ^[b,θ]	<0.2	
		882.31(50)	$3_{2\gamma}^+$	$2_{0_1^+}^+$		0.841(3)	E2/M1 ^[c,θ]	<7.6	
	1061.05(29)	795.35(50)	$4_{2\gamma}^+$	$4_{0_1^+}^+$	$0.047 \pm 0.030 \quad 3200^{+4800}_{-1300}$ [θ]	0.637(3)	E2/M1 ^[d,θ]	$4.5^{+2.7}_{-3.1}$	
		980.36(51)	$4_{2\gamma}^+$	$2_{0_1^+}^+$		0.363(3)	E2	$2.0^{+1.3}_{-1.2}$	
	1182.88(26)	634.24(61)	$5_{2\gamma}^+$	$6_{0_1^+}^+$	$0.034 \pm 0.030 > 2500$ [s]	0.239(5)	E2/M1 ^[e,θ]	<14	
		917.18(51)	$5_{2\gamma}^+$	$4_{0_1^+}^+$		0.761(5)	E2/M1 ^[f,θ]	<7.3	
$K^\pi=4_1^+:$	1535.97(23)	475.27(54) ^[⊗]	$4_{4_1^+}^+$	$4_{2\gamma}^+$	$0.124 \pm 0.077 \quad 1200^{+2100}_{-450}$ [s]	0.186(10) ^[★]	E2/M1 ^[g,s]	$44^{+34}_{-40} (23^{+18}_{-21})$	
		572.96(50)	$4_{4_1^+}^+$	$3_{2\gamma}^+$		0.317(6)	E2/M1 ^[h,s]	$66^{+42}_{-40} (98^{+63}_{-59})$	
		647.61(50) ^[∅]	$4_{4_1^+}^+$	$2_{2\gamma}^+$		0.497(7)	E2	$57^{+34}_{-36} (120^{+74})$	
$K^\pi=4_2^+:$	2180.69(53)	1217.73(58)	$4_{4_2^+}^+$	$3_{2\gamma}^+$	$0.383 \pm 0.095 \quad 240^{+190}_{-80}$ [s]	1.000 (113(24) ^[†])	E2/M1 ^[i,s]	$1.3^{+1.0}_{-0.9} (0.7^{+0.6}_{-0.5})$	
		1292.51(58) ^[†]	$4_{4_2^+}^+$	$3_{2\gamma}^+$		(100 ^[†])	E2	$(8.3^{+4.2}_{-3.7})$	
$K^\pi=(2^+):$	2231.06(38)	1342.57(50)	$(2,3,4)_T^+$	$2_{2\gamma}^+$	$0.333 \pm 0.031 \quad 360^{+70}_{-60}$ [ω]	0.577(9)	E2/M1 ^[j,ω]	$5.2^{+0.9}_{-1.2}$	

[∅]: γ ray not used in $F(\tau)$ calculation ($F(\tau)<0$), [⊗]: γ ray not used in $F(\tau)$ calculation (doublet

with background line), [★]: Measured branching ratio unreliable (γ -ray on top of background)

[θ]: $F(\tau)$ or δ_{mixing} extracted from $E_n=1.6$ MeV angular distributions, [s]: $F(\tau)$ or δ_{mixing}

extracted from $E_n=2.2$ MeV angular distributions, [ω]: $F(\tau)$ or δ_{mixing} extracted from

$E_n=3.1$ MeV angular distributions

[Υ]: No K^π band assignment for this level, [†]: Intensity information taken from Ref. [29] (γ -ray

not seen in this work)

TABLE V: Alaga rule comparisons of measured $B(E2)$ strengths for the $K^\pi=2^+_1$, 0^+_2 , and 4^+_1 band in ^{162}Dy . [★]: Alaga comparison shown in parentheses uses literature intensities to

calculate $B(E2)$ strengths.			
K^π	$\frac{J_{K_i} \rightarrow J'_{K_f}}{J_{K_i} \rightarrow J''_{K_f}}$	Exp	Th
$K_i^\pi = 2^+_1:$	$\frac{4^+ \rightarrow 4^+}{4^+ \rightarrow 2^+}$	2.3	2.9
$K_i^\pi = 0^+_2:$	$\frac{2^+ \rightarrow 4^+}{2^+ \rightarrow 2^+}$	1.5	1.8
	$\frac{4^+ \rightarrow 6^+}{4^+ \rightarrow 4^+}$	1.4	1.7
	$\frac{2^+ \rightarrow 4^+_\gamma}{2^+ \rightarrow 2^+_\gamma}$	3.1	0.8
	$\frac{4^+ \rightarrow 4^+_\gamma}{4^+ \rightarrow 2^+_\gamma}$	10	44
	$\frac{4^+ \rightarrow 4^+_\gamma}{4^+ \rightarrow 3^+_\gamma}$	9.3	3.2
	$\frac{4^+ \rightarrow 3^+_\gamma}{4^+ \rightarrow 2^+_\gamma}$	0.8	14
$K_i^\pi = 4^+_1:$	$\frac{4^+ \rightarrow 4^+}{4^+ \rightarrow 3^+}$	0.5[★] (0.2)	0.4
	$\frac{4^+ \rightarrow 4^+}{4^+ \rightarrow 2^+}$	0.8[★] (0.2)	0.2

TABLE VI: Ratios of $B(E2)$ probabilities of the transitions to the γ -band over the ground

state band transitions.		
K	$\frac{J_i \rightarrow J_f}{J_i \rightarrow J_f}$	$\frac{B(E2 \rightarrow \gamma)}{B(E2 \rightarrow g.s.)}$
$K^\pi = 0^+_2:$	$\frac{0^+ \rightarrow 2^+_\gamma}{0^+ \rightarrow 2^+_{g.s.}}$	8.4
	$\frac{2^+ \rightarrow 2^+_\gamma}{2^+ \rightarrow 2^+_{g.s.}}$	3.0
	$\frac{2^+ \rightarrow 4^+_\gamma}{2^+ \rightarrow 4^+_{g.s.}}$	3.4
	$\frac{4^+ \rightarrow 4^+_\gamma}{4^+ \rightarrow 4^+_{g.s.}}$	4.6

APPENDIX D

^{162}DY NEGATIVE PARITY STATES

Appendix D includes a near-final draft of the second of two papers on the lifetimes presented in this dissertation to be submitted to Physical Review C in 2017.

On the Lifetime Measurements of Negative Parity Bands in ^{162}Dy

C. Casarella¹, S.R. Lesher^{1,2}, A. Aprahamian¹, B.P. Crider³, M. Lowe², E.E. Peters³, F.M. Prados-Estévez³, T.J. Ross³, Z. Tully², and S.W. Yates³

¹*University of Notre Dame, Notre Dame, IN 46556*

²*University of Wisconsin-La Crosse, La Crosse, WI, 54601 and*

³*University of Kentucky, Lexington, KY, 40506*

(Dated: February 16, 2017)

Abstract

The negative parity states that manifest from the fragmentation of $\lambda=3$ surface deformations in rare-earth nuclei present a unique problem in nuclear structure. Traditionally, these states are not well-studied across the region of nuclear deformation, as lifetime measurements for all four lowest-lying negative parity states is unprecedented. Any interpretation of octupole correlations hinges on the measurement of $B(E3)$ strengths, yet the measurement of lifetimes, and subsequently, absolute $B(E1)$ transition strengths can provide key insight into the collectivity of states. Lifetimes of nuclear excited states, angular distributions of γ -rays, and reduced transition probabilities of de-excitations from 3 negative parity bands ($K^\pi=2^-, 0^- & 2^-_2$) in ^{162}Dy were measured using inelastic scattering of neutrons at the University of Kentucky Van de Graaff accelerator facility.

INTRODUCTION & MOTIVATION

Low-lying excitations in deformed nuclei have been the focus of great experimental and theoretical efforts [12? ? ? ? ?], with the various vibrational degrees of freedom manifesting in various forms in well-deformed nuclei. The earliest geometric considerations place the dynamic octupole vibration as a fragmented quartet of states with K^π projections 0^- , 1^- , 2^- , and 3^- [1]. Strong octupole shape correlations have been experimentally observed in spherical/transitional nuclei (and in extremely neutron rich ^{144}Ba) [2, 3] by the observation of strong $B(E3)$ transitions to the ground state, and corresponds to the early microscopic formulation by Neergard [4]. In well-deformed nuclei (where the ratio to the ground state 4^+ to 2^+ energies approaches and exceeds 3), the splitting and fragmentation of the octupole modes has presented distinct challenges, with the ordering inversion of negative parity bands with increasing A , and a preferential decay pattern to the ground state of the $K^\pi=0^-$ band over the $K^\pi=1^-$ band [5]. This degree of K -forbiddenness is extended in the quartet of negative parity states, with experimentally measured hindrances of transition probabilities for $\Delta K>1$ [3], but the full systematic evolution of any octupole strength across the range of fragmented negative parity states is yet to be established. To complicate matters further, the coupling of octupole and quadrupole vibrations has been observed in strong $K^\pi=2^- \rightarrow K^\pi=2_\gamma^+$ transitions (in the form of a $2^+ \otimes 3^-$ phonon coupling) in several nearby cases [6, 7], which mirrors and expands upon the feasibility of multi-phonon quadrupole states in deformed nuclei [8, 9]. However, this decay pattern is new and distinctly contrasted with the historical notion of octupole collectivity being built on top of the ground state. The existence of strong E1 transitions in this interband case is not without its own set of challenges, in that modern theoretical descriptions do not correctly predict this behavior (globally or locally), and that this behavior is *sui generis* in the deformed rare-earth region of nuclei, and works stress that this should not be applied systematically across the region, even with the observed cases of nearby and nearly spherical/transitional ^{152}Sm and ^{150}Nd [10]. Even with recent advancements of the *spdf* IBM, octupole correlations remain cloudy in the rare-earth region, implying some extraneous interpretation or origin of octupole and electric dipole strength with regards to the inclusion of the p and f bosons [11].

In γ -singles experiments with modest detection efficiency, higher-order multipolarity radiation is exponentially diminishing in intensity, making observation of the direct electric

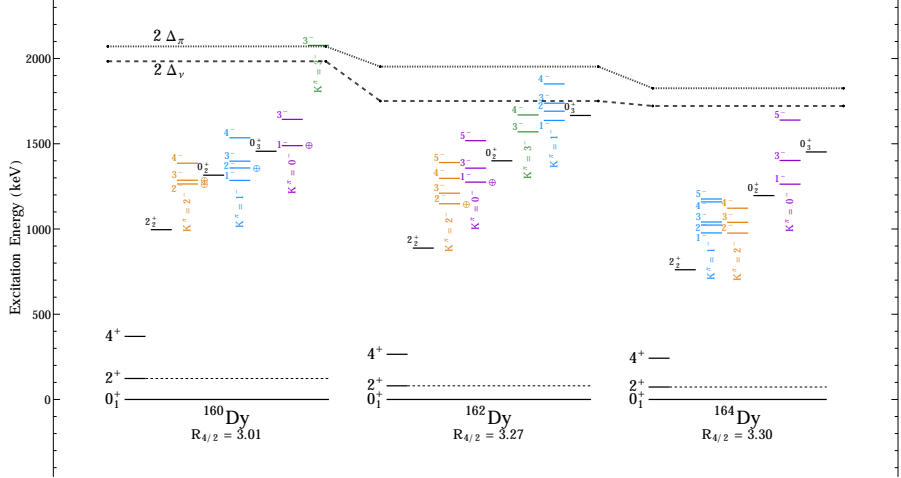


FIG. 1. Negative parity bands below the proton and neutron pairing gaps ($2\Delta_\pi$ & $2\Delta_\nu$, respectively) in $^{160-164}\text{Dy}$ nuclei (color online). Levels with an associated literature lifetime are marked with a “⊕” on the right of each level. (We dispute the two literature lifetime values for ^{162}Dy in this work.)

octupole (E3) radiation difficult. Although the direct correlation of octupole strength is not governed by E1 transitions directly, the E1 transition strengths are an indication of reflection-asymmetry, making it useful to discern the standard $\lambda=3$ dynamic deformation in form. Measurement of absolute strong E1 transitions are not the ‘smoking gun’ of octupole deformation, but are still indicative and critical in the determination of any single and/or double phonon octupole characteristics in deformed nuclei, as other modes of collective excitations may arise via the electric dipole strengths between nuclear states [12]. Calculation of these reduced transition probabilities is achieved via the measurement of nuclear lifetimes, branching ratios, and γ -ray energies.

Energetics for the lowest-lying negative parity states in Dysprosium nuclei can be seen in Figure 1, where the energy inversion and variation of the lowest-lying negative K^π bands can immediately be seen. At the risk of redundancy by mirroring the assertions made by

the numerous preceding works with regards to quadrupole excitations in deformed nuclei, consistent measurement of nuclear lifetimes will allow the full elucidation of the negative parity states in the rare earth region of nuclei (whether they are quasiparticle excitations, stable octupole deformations, octupole degrees of freedom on top of quadrupole modes, or something completely different). No rare-earth nucleus contains lifetime information for all four negative parity bands (0^- , 1^- , 2^- , & 3^-) surmised to be a part of the octupole vibration, and ^{162}Dy is no exception to this rule. Furthermore, we can motivate the measurement of lifetimes in ^{162}Dy by the clear lack of lifetime information for the vast majority of negative parity states in Dysprosium nuclei (6 literature lifetimes exist in the $^{160-164}\text{Dy}$ chain - seen in Figure 1) and the seemingly enigmatic nature and systematics of octupole correlations in the rare-earth region.

EXPERIMENT

Lifetimes of excited states were measured with the Doppler Shift Attenuation Method via Inelastic Neutron Scattering (DSAM-INS), a technique that exploits the fact that any emitted radiation from a recoiling nucleus will be energy shifted with respect to the laboratory angle of observation. De-exciting γ -rays will be Doppler shifted linearly as a function of $\cos(\theta_{lab})$, the unshifted γ -ray energy $E_{\gamma,o}$, the recoil velocity of the decaying nucleus β , and a lifetime-dependent attenuation factor $F(\tau)$, all shown in Equation 1.

$$E_\gamma(\theta_{lab}) = E_{\gamma,o}[1 + \beta F(\tau) \cos(\theta_{lab})] \quad (1)$$

Population of excited states (and subsequent nuclear recoil) is achieved with a $^{162}\text{Dy}(n,n'\gamma)$ reaction at the University of Kentucky Accelerator Laboratory (UKAL). Pulsed, bunched protons are accelerated by the 7 MV Van De Graaff accelerator on site, where they impinge on a pressurized ^3H gas cell at the end of the beamline to create neutrons according to the $^3\text{H}(p,n)$ reaction. Neutrons then scatter inelastically off a polyethylene vial containing enriched ^{162}Dy oxide powder. De-exciting γ -rays are observed in γ -singles mode by the single Ortec HPGe detector equipped with both passive and active shielding [13, 14]. A schematic drawing of the experimental setup at UKAL is shown in Figure 2.

Two experiments are performed with this setup, excitation function and angular distribution measurements; the excitation functions serve to confirm population thresholds of

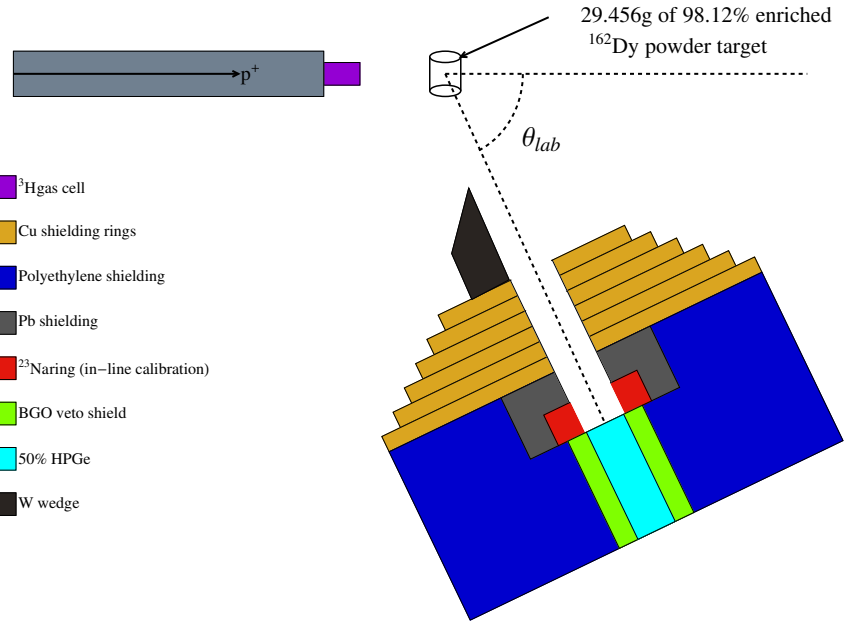


FIG. 2. Not-to-scale cartoon of experimental setup (color online) at UKAL for γ -singles measurements (Made in M. Caprio's SciDraw software for Mathematica [REF])

γ -rays to confidently place them in the level scheme. The gross population rate of states as a function of neutron energy can also be inferred from the excitation functions, and act as a guide in choosing optimal neutron energies to perform angular distribution measurements. Excitation function measurements also aid in the selection of appropriate bombarding neutron energies, as any contaminants or γ rays of a similar energy can be used to populate states in ^{162}Dy . The inelastic scattering reaction used to populate states in ^{162}Dy serves multiple beneficial experimental facets: the use of neutrons as a probe forgoes any need to overcome the Coulomb barrier of the nucleus, is generally non-selective on the type of excitations populated (single particle, collective excitations, etc. are all populated), and will realistically only populate $J^\pi \leq 5^\pm$ excitations.

The $\sim 50\%$ HPGe detector sits 125 cm away from the suspended sample of Dy powder, and can be moved on a circular track to observe γ -rays at various lab angles to populate the

angular distribution measurements needed to measure the lifetimes of states.

Angular distributions were collected at angles between 40 and 150 degrees with respect to the beam direction over the course of the experimental campaign. Measurement of the angular distributions offers several distinct assets for nuclear structure studies; absolute intensities of γ -rays, inferred multipolarities (and multipole mixing fractions) of γ -rays, and most importantly, the extraction of $F(\tau)$ are all achieved in the angular distribution experiments at UKAL. Confirmation of dipole, E1 radiation (shown in Figure 3) can be made by examination of the relative sign/magnitude of the a_2 and a_4 coefficients in Equation 2 ($a_2 \neq 0$ for E1/M1 radiation); absolute intensities of γ -rays can also be extracted from the A_0 parameter.

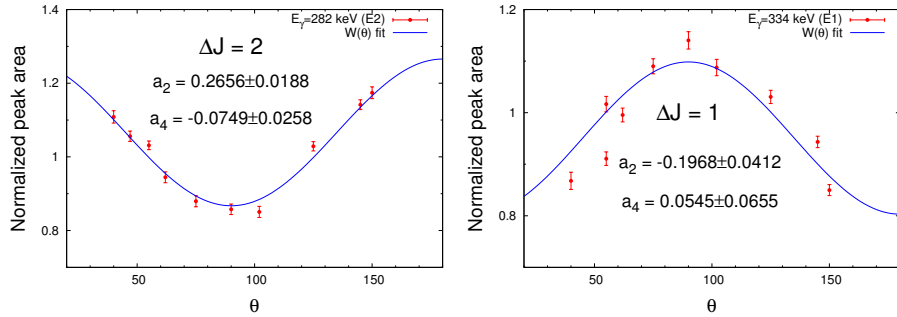


FIG. 3. Angular distributions from two multipolarity γ -rays, highlighting the distinct radiation pattern for varying multipolarities.

$$W(\theta) \approx A_0[1 + a_2 P_2(\cos \theta_{lab}) + a_4 P_4(\cos \theta_{lab})] \quad (2)$$

To extract the lifetime of a state from the angular distribution, energy shifts of γ -rays are observed as a function of angle, and are fit linearly according to Equation 1, where the slope is $F(\tau)$. The experimental $F(\tau)$ factors for a particular γ -ray are compared with theoretical calculations of this lifetime-dependent attenuation according to the Winterbon formalism outlined in [15]. The sensitivity and applicability of DSAM-INS lifetimes is dependent on both the nuclear and electronic stopping powers of the target, which places an effective range of $\sim 10\text{-}2000$ fs on the lifetimes measurable with this method. Lifetimes outside of this range

will exhibit very small energy-shifts over the range of angles used in the measurement, and will be reported as lower limits for the lifetime.

Spectra from angular distributions are TOF gated for active background subtraction, have a 5th-order polynomial ADC nonlinearity applied, and are efficiency calibrated using an offline ²²⁶Ra source.

RESULTS & DISCUSSION

We have measured a wealth of lifetimes for $J^\pi \leq 5^\pm$ states in ¹⁶²Dy, shown in Figure 4. Of these 68 lifetimes, we have observed decays from this lowest-lying quartet of negative parity states (Figure 5), however, the measured $F(\tau)$ values for the 1⁻ and 3⁻ bands are either consistent with zero within 1 σ or outright negative in value. This acts as a flag to tell us that these 1⁻ and 3⁻ band lifetimes are not reliable; as such, they are not discussed in this work and need refinement with other lifetime measurement techniques. To further indicate unreliable lifetime measurement of the 1⁻ and 3⁻ bands, comparison of the calculated transition probabilities to the Alaga rules yield a vast discrepancy. This disagreement with Alaga *may* indicate that these bands are indeed not part of the octupole vibration coupled to the rotational ground state, but instead could be the product of mixing (another 3⁻ band appears at 1766 keV).

A total of 10 well-convergent level lifetimes were measured (8 of which are new) for three negative parity bands in ¹⁶²Dy. All observed transitions from negative parity bands can be seen in Figure 8, with corresponding transition strengths from Table I. Absolute intensities of γ -decays reported in this work can be seen in Table IV. The traditional picture of octupole collectivity in well-deformed nuclei exists with the initial, lowest-lying and fragmented quartet of states of $K^\pi=0^-, 1^-, 2^-, \& 3^-$. However, the current ordering of negative parity bands in ¹⁶²Dy is difficult (read: impossible) to predict with modern models [11]. We have measured lifetimes for two bands of this lowest-lying set of states in ¹⁶²Dy, where we provide individual discussion on our measurements.

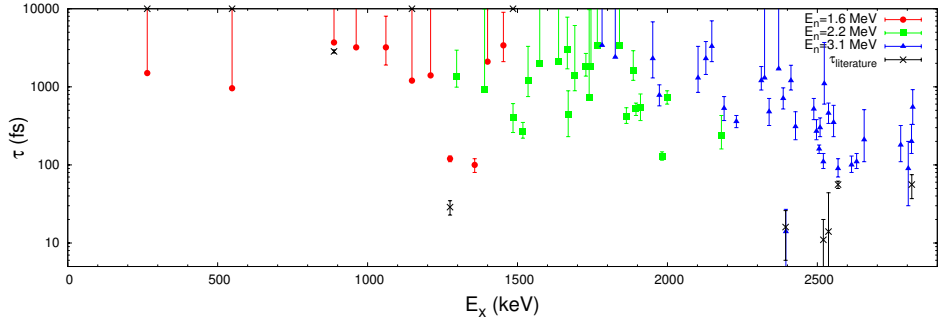


FIG. 4. All measured lifetimes in ^{162}Dy (in femtoseconds) plotted as a function of excitation energy in keV. Data points in red are extracted from the $E_n=1.6$ MeV angular distributions, points in green correspond to lifetimes extracted from the 2.2 MeV angular distributions, and blue points are lifetimes from the 3.1 MeV dataset. (color online)

K^π=2⁻ Band at 1148 keV

We are immediately presented with some of the limitations of DSAM with our measurement of the lifetime of the bandhead of the $K^\pi=2^-$ band. Firstly, γ -ray energies can be heavily attenuated in the physical size of the near-molar-weight target; while we correct for this γ absorption in the peak area/intensity, lifetimes from the Doppler shift of γ -rays sub-500 keV are difficult to extract, as $F(\tau)$ can be within 1 or 2σ of 0. Normally, DSAM measurements are taken at the lowest possible bombarding neutron energy, but due to this attenuation of low-energy γ rays, a more precise measurement of the lifetimes in this band are taken from the 2.2 MeV bombarding neutron dataset. While we expect a natural inflation of the lifetimes because of this choice of neutron energy, the vast majority of observed transitions displayed negative (or consistent with zero within 1σ uncertainty) $F(\tau)$ values. This justification is supported by Figure 6, which shows all excitation functions for γ rays that both de-excite this band and contribute to the lifetime; take note that the gain in statistics by a factor of ~ 2 by increasing the neutron energy, where we are exempt from higher-lying decays acting as a contaminant (see the trajectories as the neutron energy increases to 3.1 MeV). Extraction of the lifetime for the bandhead at 2100_{-950}^{+7200} fs involves the measurement of a 260 keV γ ray, shown in Figure 6, and does not agree with the literature

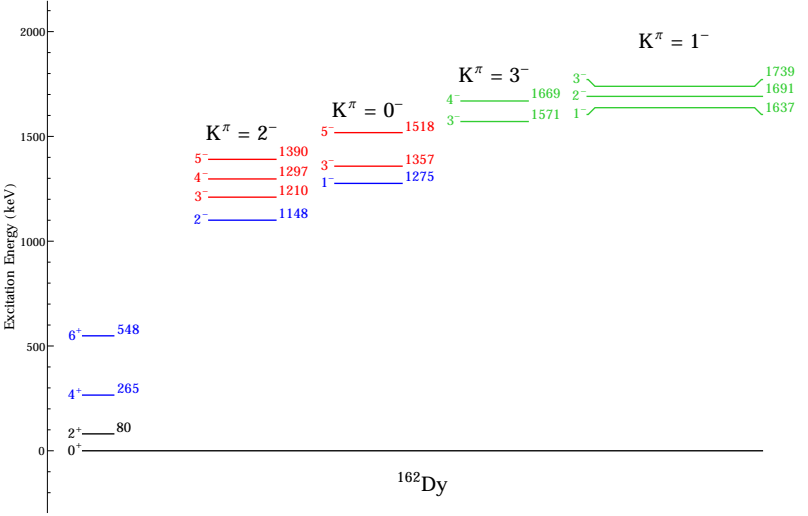


FIG. 5. Lowest-lying negative parity bands in ^{162}Dy with reliable lifetimes measured in our experiments in red, existing literature values in blue, and unreliable lifetimes measured in green (color online).

value of 303 ps [16], as the shallow $F(\tau)$ is just over 1σ away from 0, making this lifetime partially unreliable. We do not observe the other decay channel to the 3^+ member of the γ -band, as that decay energy is 185 keV, directly on top of our strongest line in our spectra, the ground state $4^+ \rightarrow 2^+$ transition. With no higher energy decays observed to the ground state, we report this measurement of the bandhead's lifetime, but it should be taken as a tentative, cautious measurement, given the very large discrepancy from literature. However, we regain good lifetime resolution on the measurement of the 3^- and 4^- bandmembers; the former state's lifetime of 3100^{+3700}_{-1200} fs comes from the 944 keV γ ray, where the other exit channels have either a negative $F(\tau)$ value.

Modestly collective transitions to the known γ -vibrational states are observed leaving the 2^- band at 1148 keV. This highly-favored trend of γ -rays to the $K^\pi=2^+$ band is dif-

ficult to ignore in the face of notably strong (\sim 2-5 mWu), absolute B(E1) measurements between these two modes of excitations. Pascu [6] stresses the importance of this preferential $K^\pi=2^-\rightarrow K^\pi=2^+$ decay in nearby nuclei via the measurement of direct E3 radiation as a potential octupole-quadrupole coupling, however, this decay pattern could be a product of K-forbiddenness, as any decays to the ground state involve $\Delta K=2$ versus the $\Delta K=0$ transitions to the γ -band. We also mirror these same concerns on the continued study of interband decay radiation in the rare-earth region to fully understand this band; B(E3; $5^- \leftrightarrow 2_\gamma^+$) strengths would be remarkably useful in this aspect. ^{162}Dy offers some distinct challenges in terms of the detection of radiation for low-lying excitations; for example, measurement of the interband $2^-\rightarrow 3_\gamma^+$ transition lies at 185 keV, placing it directly on top of our most strongly populated $4_{g.s.}^+ \rightarrow 2_{g.s.}^+$ transition. This experimental challenge is out of the scope of the γ -singles-based experiments performed in this work at UKAL, and would require much more discriminating coincidence measurements to observe the γ -decays.

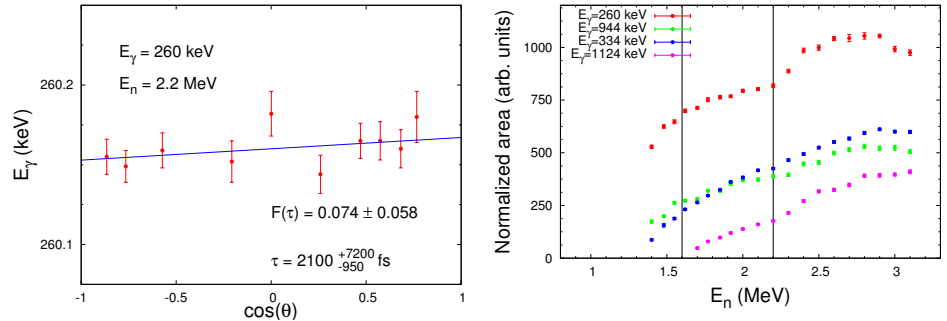


FIG. 6. $E_\gamma=260$ keV γ ray (from the $E_x=1148$ keV level) Doppler shift and excitation functions for decays from the first 2^- band (color online).

$K^\pi=0^-$ Band at 1275 keV

We have measured lifetimes for the 3 lowest-lying members of the 0^- band, currently assigned as the single octupole vibration in ^{162}Dy from the clearly collective literature B(E3; $3^- \rightarrow 0_{gs}^+$) measurements ranging from 1.4-4.7 W.u. [17, 18]. The deduced lifetime from the direct B(E1) \uparrow measurement in [19] of the bandhead of the $K^\pi=0^-$ band has been

called into question by the NDS evaluator, with the distinct comment that the γ -branches of E1 radiation depopulating the state differs drastically from the adopted values. We are confident in our lifetime measurement from the extremely well-defined Doppler energy-shifts of the two de-excitations from this $E_x=1275$ keV level (shown in Figure 7). The 5^- state at 1518 keV is below the threshold to be populated by $E_n=1.6$ MeV neutrons, the de-excitations are not observed until the $E_n=2.2$ MeV dataset; this implies that the resulting lifetime will be inflated, as $F(\tau)$ is directly related to the bombarding neutron energy.

Overall in the $K^\pi=0^-$ band, we observe inflated, clearly collective B(E1) transition probabilities to the ground state (Table I), with excellent agreement to Alaga predictions (Table II). Although these B(E1)s are weaker overall than other confirmed single-phonon octupole vibrations in the region (^{168}Er [20]), the transition probabilities are well above the threshold for what is considered generally non-collective in the mass region ($\sim 10^{-5}$ mWu strengths). Furthermore, our measured $B(\text{E1}; 1_{K^\pi=0^-}^- \rightarrow 0_{g.s.}^+)$ of $0.002\text{e}^2\text{fm}^2$ compares very nicely with the systematic behavior of E1 strengths leaving the bandhead of $K^\pi=0^-$ bands in deformed rare-earth nuclei ($B(\text{E1}) \sim 0.002\text{-}0.004 \text{ e}^2\text{fm}^2$) [21]. From these measured collective E1 strengths, this suggests some significant reflection asymmetry in this $K^\pi=0^-$ band, which is especially and notably consistent with the picture of well-behaved octupole collectivity.

$K^\pi=2_2^-$ Band at 1863 keV

The final set of lifetime measurements of negative parity states is the second $K^\pi=2^-$ band. Two γ -ray placements from [11] are made into the bandhead of this 2^- band, the 900 and 975 keV transitions, both showing a well-behaved Doppler shift to yield a level lifetime of 420^{+120}_{-80} fs. We have also placed two γ -ray transitions from the $E_x=1974$ keV 4^- state [22], a 912 keV and a 1010 keV decay to the γ -vibrational band. Confirmation of the placement of these de-excitations is made with the measurement of the excitation functions, shown in Figure 9; these γ -rays were also observed in [11], but were unplaced in their level scheme. Our absolute intensities are in reasonable agreement with the literature values in [11, 22], further justifying their correct placement in the level scheme.

Much like the lower 2^- band, our measurement of mildly inflated B(E1) transition probabilities to the γ -band is striking, and supports the arguments in numerous works of new, emerging decay patterns [6, 10, 12] of enhanced E1 transitions to the 2^+ band as a differing

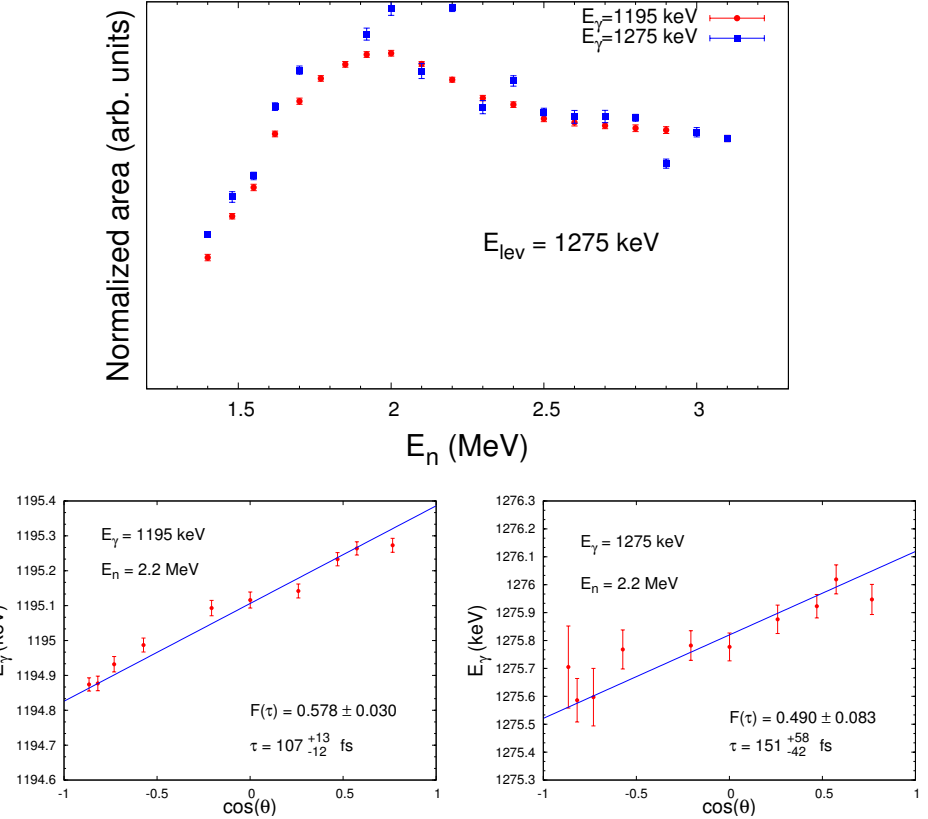


FIG. 7. $E_{\gamma}=1195$ & 1275 keV (de-excitations from the $E_x=1275$ keV level) Doppler shifts and excitation functions (color online). The excitation function (in blue) for the 1275 keV γ ray is scaled by a factor of 1.53 .

form of collective dipole excitation built on top of the γ -vibration. Along the same lines, assertions from IBM considerations with the inclusion of p and f bosons imply that the structure of the lowest-lying negative parity bands *may not* be of purely collective nature [11, 23], which supports our experimental findings. Deduced B(E1)s behave well when compared to Alaga considerations (Table II), giving us confidence of correct lifetime measurements. Of particular note, however, is the lower relative B(E1) strength than its lower-energy cousins in the first 2^- band, however, the decays from this band are still above the threshold for what

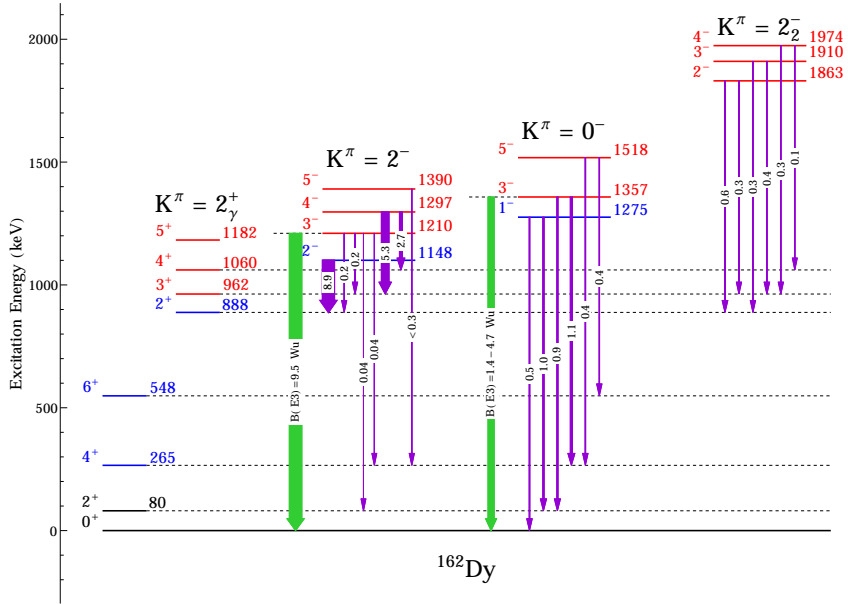


FIG. 8. Observed γ -decays from negative parity, $K^\pi=2^-, 0^-, 2_2^-$ bands in ^{162}Dy . Transition strengths are drawn proportional in width to their deduced $B(E1)$, with E1 transitions ($B(E1)$ in milli-Weisskopf units) in violet (color online).

would be considered non-collective. Once again, the interband B(E3) strengths to/from these negative parity bands would be invaluable in the further discussion and feasability of this pattern.

CONCLUSIONS

While we cannot place definite octupole characteristics to some of the negative parity states in ^{162}Dy from the observed E1 transitions, we *can* point future experiments in the right direction to fully ascertain any E3 decays among excited states, based on our measurement

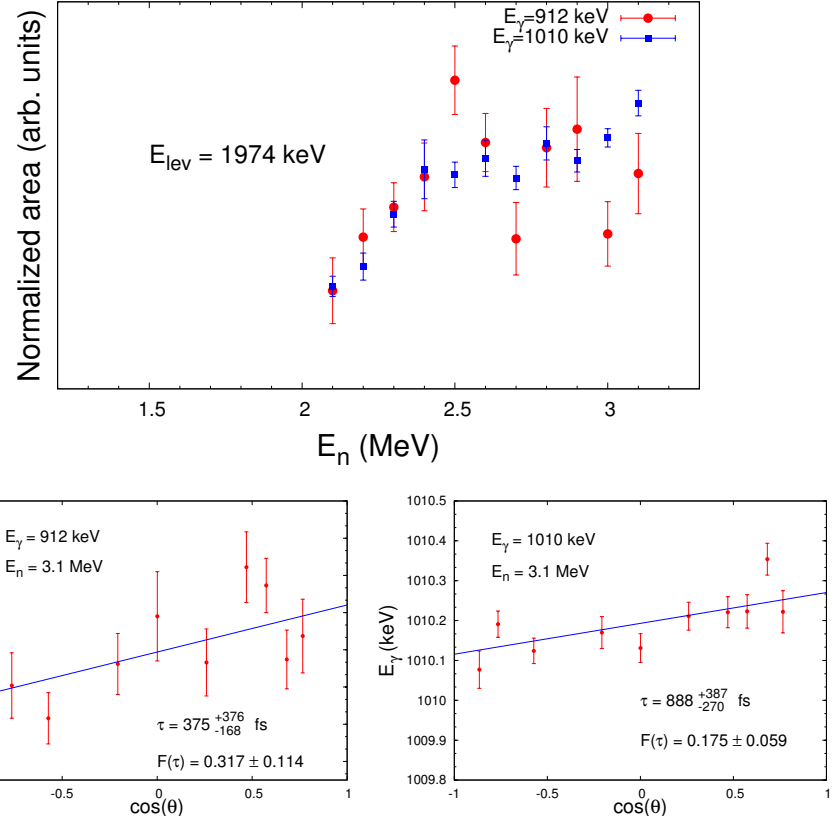


FIG. 9. $E_\gamma=912$ & 1010 keV (de-excitations from the $E_x=1974$ keV level) Doppler shifts and excitation functions (color online). The excitation function (in blue) for the 1010 keV γ ray is scaled by a factor of 0.33.

of lifetimes and absolute electric dipole reduced transition probabilities. Overall, the story of well-defined, single-phonon octupole correlations in a fragmented quartet of states below the pairing gap in ^{162}Dy seems indefinite from our incomplete measurement of lifetimes of the negative parity bands. The generally weak, yet still collective $B(E1)$ transition probabilities from the low-lying negative parity bands to the ground state could even imply that octupole correlations are weak in ^{162}Dy . We have opened a few avenues to study multiphonon effects in regards to octupole-quadrupole coupling in well-deformed nuclei with this data, and hope

to see continued study in this area.

ACKNOWLEDGEMENTS

This work is funded by the National Science Foundation (NSF) under grant numbers PHY-1068192, PHY-1205412, and PHY-0956310. Special thanks to R. Casten for invaluable physics insight and discussions.

- [1] A. Bohr and B. R. Mottelson, *Nuclear Structure*, First ed., Vol. II (World Scientific Publishing Co., 1975).
- [2] B. Bucher, S. Zhu, C. Y. Wu, R. V. F. Janssens, D. Cline, A. B. Hayes, M. Albers, A. D. Ayangeakaa, P. A. Butler, C. M. Campbell, M. P. Carpenter, C. J. Chiara, J. A. Clark, H. L. Crawford, M. Cromaz, H. M. David, C. Dickerson, E. T. Gregor, J. Harker, C. R. Hoffman, B. P. Kay, F. G. Kondev, A. Korichi, T. Lauritsen, A. O. Macchiavelli, R. C. Pardo, A. Richard, M. A. Riley, G. Savard, M. Scheck, D. Seweryniak, M. K. Smith, R. Vondrasek, and A. Wiens, Phys. Rev. Lett. **116**, 112503 (2016).
- [3] Garrett, P. E. and Kulp, W. D. and Wood, J. L. and Bandyopadhyay, D. and Choudry, S. and Dashdorj, D. and Lesher, S. R. and McEllistrem, M. T. and Mynk, M. and Orce, J. N. and Yates, S. W., Phys. Rev. Lett. **103**, 062501 (2009).
- [4] K. Neergard and P. Vogel, Nuclear Physics A **145**, 33 (1970).
- [5] R. F. Casten, *Nuclear Structure from a Simple Perspective*, Second ed. (Oxford University Press, 1990).
- [6] S. Pascu, D. Bucurescu, *et al.*, Phys. Rev. C **91**, 034321 (2015).
- [7] H. Maser, S. Lindenstruth, I. Bauske, O. Beck, P. von Brentano, T. Eckert, H. Friedrichs, R. D. Heil, R.-D. Herzberg, A. Jung, U. Kneissl, J. Margraf, N. Pietralla, H. H. Pitz, C. Wesselborg, and A. Zilges, Phys. Rev. C **53**, 2749 (1996).
- [8] A. Aprahamian, Nuclear Physics A **731**, 291 (2004).
- [9] X. Wu, A. Aprahamian, S. M. Fischer, W. Reviol, G. Liu, and J. X. Saladin, Phys. Rev. C **49**, 1837 (1994).

- [10] A. Chakraborty, F. M. Prados-Estévez, S. Choudry, B. Crider, P. Garrett, W. D. Kulp, A. Kumar, M. T. McEllistrem, S. Mukhopadhyay, M. Mynk, J. Orce, E. E. Peters, J. L. Wood, and S. W. Yates, Phys. Rev. C **86**, 064314 (2012).
- [11] A. Aprahamian, X. Wu, S. Lesher, D. Warner, W. Gelletly, H. Börner, F. Hoyler, K. Schreckenbach, R. Casten, Z. Shi, D. Kusnezov, M. Ibrahim, A. Macchiavelli, M. Brinkman, and J. Becker, Nuclear Physics A **764**, 42 (2006).
- [12] M. Spieker, S. Pascu, A. Zilges, and F. Iachello, Phys. Rev. Lett. **114**, 192504 (2015).
- [13] P. Garrett, N. Warr, and S. Yates, J. Res. Natl. Inst. Stand. Technol. **105**, 141 (2000).
- [14] T. Belgya, G. Molnar, and S. W. Yates, Nuclear Physics A **607**, 43 (1996).
- [15] K. Winterbon, Nuclear Physics A **246**, 293 (1975).
- [16] B. Sethi and S. K. Mukherjee, Phys. Rev. **166**, 1227 (1968).
- [17] W. Korten, T. Hrtlein, J. Gerl, D. Habs, and D. Schwalm, Physics Letters B **317**, 19 (1993).
- [18] R. Oehlberg, L. Riedinger, A. Rainis, A. Schmidt, E. Funk, and J. Mihelich, Nuclear Physics A **219**, 543 (1974).
- [19] A. Zilges, P. von Brentano, H. Friedrichs, R. Heil, U. Kneissl, S. Lindestruth, H. Pitz, and C. Wesselborg, Z Phys. A - Hadrons and Nuclei **340**, 155 (1991).
- [20] F. McGowan, W. Milner, R. Robinson, P. Stelson, and Z. Grabowski, Nuclear Physics A **297**, 51 (1978).
- [21] H. G. Börner, M. Jentschel, N. V. Zamfir, R. F. Casten, M. Krticka, and W. Andrejtscheff, Phys. Rev. C **59**, 2432 (1999).
- [22] J. Berzins, P. Prokofjevs, R. Georgii, R. Hucke, T. von Egidy, G. Hlawatsch, J. Klora, H. Lindner, U. Mayerhofer, H. Schmidt, A. Walter, V. Soloviev, N. Shirikova, and A. Sushkov, Nuclear Physics A **584**, 413 (1995).
- [23] F. Iachello and A. Arima, *The Interacting Boson Model* (Cambridge University Press, Cambridge, 1987).
- [24] F. K. McGowan and W. T. Milner, Phys. Rev. C **23**, 1926 (1981).

TABLE I: Lifetimes of negative parity bands (2^- , 0^- , 2^-_2) in ^{162}Dy , with experimentally deduced $B(E1)$ in mW.u.

E_{level} (keV)	E_γ (keV)	$J^\pi_{K_i}$	$J^\pi_{K_f}$	$F(\tau)_{av}$	τ (fs)	BR	$B(E1)$ (mW.u.)
1148.20(20)	260.16(50)	$2^-_{2^-_1}$	$2^+_{2^+_1}$	0.074 ± 0.058	2100^{+7200}_{-950} [s]	1.000	$8.9^{+7.3}_{-6.9}$
1210.05(18)	247.27(55) $[\emptyset]$	$3^-_{2^-_1}$	$3^+_{2^+_1}$	0.052 ± 0.030	3100^{+3700}_{-1200} [s]	0.056(2)	$0.2^{+0.2}_{-0.1}$
	322.05(51) $[\emptyset]$	$3^-_{2^-_1}$	$2^+_{2^+_1}$			0.083(2)	$0.2^{+0.1}_{-0.1}$
	944.48(50)	$3^-_{2^-_1}$	$4^+_{0^+_1}$			0.310(4)	$0.04^{+0.03}_{-0.02}$
	1129.46(50) $[\emptyset]$	$3^-_{2^-_1}$	$2^+_{0^+_1}$			0.552(4)	$0.04^{+0.03}_{-0.02}$
1297.06(27)	236.09(60) $[\emptyset]$	$4^-_{2^-_1}$	$4^+_{2^+_1}$	0.103 ± 0.049	1400^{+1500}_{-350} [s]	0.150(5)	$2.7^{+0.9}_{-1.4}$
	334.15(50)	$4^-_{2^-_1}$	$3^+_{2^+_1}$			0.850(5)	$5.3^{+1.8}_{-2.8}$
1390.52(35)	1124.88(88)	$5^-_{2^-_1}$	$4^+_{0^+_1}$	0.090 ± 0.082	>920 [s]	1.000	<0.3
1275.81(24)	1195.10(50)	$1^-_{0^-_1}$	$2^+_{0^+_1}$	0.568 ± 0.028	120^{+10}_{-10} [ϑ]	0.605(6)	$1.0^{+0.1}_{-0.1}$
	1275.82(53)	$1^-_{0^-_1}$	$0^+_{0^+_1}$			0.395(6)	$0.5^{+0.1}_{-0.1}$
1358.00(30)	1092.27(71)	$3^-_{0^-_1}$	$4^+_{0^+_1}$	0.612 ± 0.043	100^{+20}_{-20} [ϑ]	0.429(9)	$1.1^{+0.3}_{-0.2}$
	1277.33(58)	$3^-_{0^-_1}$	$2^+_{0^+_1}$			0.571(9)	$0.9^{+0.2}_{-0.2}$
1518.47(29)	970.01(55)	$5^-_{0^-_1}$	$6^+_{0^+_1}$	0.372 ± 0.041	270^{+80}_{-50} [s]	0.294(7)	$0.4^{+0.1}_{-0.1}$
	1252.74(51)	$5^-_{0^-_1}$	$4^+_{0^+_1}$			0.706(7)	$0.4^{+0.1}_{-0.1}$
1863.85(26)	900.90(55)	$2^-_{2^-_2}$	$3^+_{2^+_1}$	0.297 ± 0.035	420^{+120}_{-80} [s]	0.251(5)	$0.3^{+0.1}_{-0.1}$
	975.65(50)	$2^-_{2^-_2}$	$2^+_{2^+_1}$			0.749(5)	$0.6^{+0.1}_{-0.1}$
1910.50(26)	947.51(56)	$3^-_{2^-_2}$	$3^+_{2^+_1}$	0.250 ± 0.063	550^{+260}_{-180} [s]	0.552(8)	$0.4^{+0.2}_{-0.1}$
	1022.33(53)	$3^-_{2^-_2}$	$2^+_{2^+_1}$			0.448(8)	$0.3^{+0.1}_{-0.1}$
1972.99(66)	912.09(50)	$4^-_{2^-_2}$	$4^+_{2^+_1}$	0.205 ± 0.053	780^{+280}_{-210} [ϖ]	0.246(13)	$0.1^{+0.1}_{-0.1}$
	1010.19(50)	$4^-_{2^-_2}$	$3^+_{2^+_1}$			0.754(13)	$0.3^{+0.1}_{-0.1}$

$[\emptyset]$: γ ray not used in $F(\tau)$ calculation ($F(\tau) < 0$).

$[\vartheta]$: $F(\tau)$ extracted from $E_n=1.6$ MeV angular distributions, $[\varsigma]$: $F(\tau)$ extracted from $E_n=2.2$ MeV

angular distributions, $[\varpi]$: $F(\tau)$ extracted from $E_n=3.1$ MeV angular distributions

$[\dagger]$: Lifetime not reliable ($F(\tau)$ consistent with zero within 1σ)

TABLE II: Comparison of E1 transition probabilities from the $K^\pi=2^-, 0^-, & 2^-$ bands

K^π	with the Alaga rules.		
	$\frac{J_{K_i} \rightarrow J'_{K_f}}{J_{K_i} \rightarrow J''_{K_f}}$	Exp	Th
$K_i^\pi = 2^-:$	$\frac{3^- \rightarrow 3_\gamma^+}{3^- \rightarrow 2_\gamma^+}$	1.0	1.4
	$\frac{4^- \rightarrow 4^+}{4^- \rightarrow 3^+}$	0.5	0.6
	$\frac{1^- \rightarrow 2^+}{1^- \rightarrow 0^+}$	2.0	2.0
$K_i^\pi = 0^-:$	$\frac{3^- \rightarrow 4^+}{3^- \rightarrow 2^+}$	1.2	1.3
	$\frac{5^- \rightarrow 6^+}{5^- \rightarrow 4^+}$	1.0	1.2
	$\frac{2^- \rightarrow 3^+}{2^- \rightarrow 2^+}$	0.5	0.5
$K_i^\pi = 2_2^-:$	$\frac{3^- \rightarrow 3^+}{3^- \rightarrow 2^+}$	1.6	1.4
	$\frac{4^- \rightarrow 4^+}{4^- \rightarrow 3^+}$	0.3	0.6

 TABLE III: Known experimentally determined B(E3) probabilities (in W.u.) from $[\dagger, \ddagger]$ ([18, 24], respectively) in the Dysprosium nuclei.

A	E_x (keV)	K_i^π	$B(E3; 3^- \rightarrow 0_{gs}^+)$ (W.u.)
160	1286.711	2^-	16
160	1398.964	1^-	6.0
160	1643.26	0^-	6.1
162	1210	2^-	9.5 $[\dagger]$
162	1357	0^-	1.4-4.7 $[\dagger-\ddagger]$
164	1039.3	2^-	7.8

TABLE IV: Absolute intensities for γ -decays observed in (n,n'γ) experiments.

E_{lev} (keV)	E_γ (keV)	$I_{\gamma,abs}$ (n,n'γ)
1148.20(20)	260.16(50)	658.762(7.577)
1210.05(18)	247.27(55)	38.973(1.420)
	322.05(51)	57.699(1.240)
	944.48(50)	216.160(3.227)
	1129.46(50)	384.769(5.182)
1297.06(27)	236.09(60)	43.374(1.380)
	334.15(50)	245.585(4.666)
1390.52(35)	1124.88(88)	94.848(2.193)
1275.81(24)	1195.10(50)	429.944(4.249)
	1275.82(53)	280.443(6.356)
1358.00(30)	1092.27(71)	134.371(1.271)
	1277.33(58)	178.995(6.684)
1518.47(29)	970.01(55)	32.453(0.775)
	1252.74(51)	78.039(1.893)
1863.85(26)	900.90(55)	47.527(1.219)
	975.65(50)	141.639(1.587)
1910.50(26)	947.51(56)	48.580(0.955)
	1022.33(53)	39.474(0.978)
1972.99(66)	912.09(50)	82.148(3.125)
	1010.19(50)	251.922(15.219)

BIBLIOGRAPHY

1. A. Aprahamian. From ripples to tidal waves: Low lying vibrational motion in nuclei. *Nuclear Physics A*, 731:291 – 298, 2004.
2. A. Aprahamian, R. C. de Haan, H. G. Börner, H. Lehmann, C. Doll, M. Jentschel, A. M. Bruce, and R. Piepenbring. Lifetime measurements of excited $K^\pi = 0^+$ bands in ^{178}Hf . *Phys. Rev. C*, 65:031301, Feb 2002.
3. A. Aprahamian, X. Wu, S. Lesher, D. Warner, W. Gelletly, H. Börner, F. Hoyler, K. Schreckenbach, R. Casten, Z. Shi, D. Kusnezov, M. Ibrahim, A. Macchiavelli, M. Brinkman, and J. Becker. Complete spectroscopy of the ^{162}Dy nucleus. *Nuclear Physics A*, 764:42 – 78, 2006. ISSN 0375-9474.
4. Aprahamian, A. and Brenner, D. S. and Casten, R. F. and Gill, R. L. and Piotrowski, A. First observation of a near-harmonic vibrational nucleus. *Phys. Rev. Lett.*, 59:535–538, Aug 1987.
5. T. Belgya, G. Molnar, and S. W. Yates. Analysis of Doppler-shift attenuation measurements performed with accelerator-produced monoenergetic neutrons. *Nuclear Physics A*, 607:43 – 61, 1996.
6. M. Bender, K. Rutz, P. G. Reinhard, and J. A. Maruhn. Pairing Gaps from Nuclear Mean-Field Models. *EPJ manuscript CHECK*, 731:291 – 298, 2004.
7. Y. Y. Berzin, E. P. Grigorev, T. V. Guseva, and Y. Y. Tamberg. The Levels of ^{160}Gd Nucleus. *Izv. Akad. Nauk, SSSR: Ser. Fiz.* 53, 901, 1989.
8. J. Berzins, P. Prokofjevs, R. Georgii, R. Hucke, T. von Egidy, G. Hlawatsch, J. Klora, H. Lindner, U. Mayerhofer, H. Schmidt, A. Walter, V. Soloviev, N. Shirikova, and A. Sushkov. ^{162}Dy studied with (n, γ) , $(n, n'\gamma)$, (d, p) and (d, t) reactions. *Nuclear Physics A*, 584(3):413 – 448, 1995.
9. P. R. Bevington and D. K. Robinson. *Data Reduction and Error Analysis for the Physical Sciences*. McGraw-Hill, 2003.
10. J. Blatt and V. Weisskopf. *Theoretical Nuclear Physics*. Wiley, London, 1952.
11. A. Blaugrund. Notes on Doppler-shift lifetime measurements. *Nuclear Physics*, 88(3):501 – 512, 1966.

12. A. Bohr and B. R. Mottelson. *Nuclear Structure*, volume II. World Scientific Publishing Co., Singapore, First edition, 1975.
13. Bohr, A. and B. R. Mottelson and D. Pines. Possible Analogy between the Excitation Spectra of Nuclei and Those of the Superconducting Metallic State. *Physical Review*, 110:936–938, May 1958.
14. Bonatsos, Dennis and E. A. McCutchan and Casten, R. F. Casperson, R. J. and Werner, V. and Williams, E. Regularities and symmetries of subsets of collective 0^+ states. *Phys. Rev. C*, 80:034311, Sep 2009.
15. J. Boring. *Gamma-ray ABSorption Correction (ABSCOR)*. PhD thesis, University of Kentucky, 1960.
16. H. G. Börner, M. Jentschel, N. V. Zamfir, R. F. Casten, M. Krticka, and W. Andrejtscheff. Ultrahigh resolution study of collective modes in ^{158}Gd . *Phys. Rev. C*, 59:2432–2439, May 1999.
17. B. Bucher, S. Zhu, C. Y. Wu, R. V. F. Janssens, D. Cline, A. B. Hayes, M. Albers, A. D. Ayangeakaa, P. A. Butler, C. M. Campbell, M. P. Carpenter, C. J. Chiara, J. A. Clark, H. L. Crawford, M. Cromaz, H. M. David, C. Dickerson, E. T. Gregor, J. Harker, C. R. Hoffman, B. P. Kay, F. G. Kondev, A. Korichi, T. Lauritsen, A. O. Macchiavelli, R. C. Pardo, A. Richard, M. A. Riley, G. Savard, M. Scheck, D. Seweryniak, M. K. Smith, R. Vondrasek, and A. Wiens. Direct evidence of octupole deformation in neutron-rich ^{144}Ba . *Phys. Rev. Lett.*, 116:112503, Mar 2016.
18. D. Burke. Hexadecapole-Phonon versus Double- γ -Phonon Interpretation for $K^\pi=4^+$ Bands in Deformed Even-Even Nuclei. *Phys. Rev. Lett.*, 73, Oct 1994.
19. M. Caprio. Levelscheme: A level scheme drawing and scientific figure preparation system for mathematica. *Computer Physics Communications*, 171(2):107 – 118, 2005.
20. R. F. Casten. *Nuclear Structure from a Simple Perspective*. Oxford University Press, Second edition, 1990.
21. Casten, R. F. and Hasegawa, M. and Mizusaki, T. Jing-ye, Zhang and E. A. McCutchan and N. V. Zamfir and Krücken, R. Anomalous behavior of the first excited 0^+ state in $N \approx Z$ nuclei. *Phys. Rev. C*, 71:014319, Jan 2005.
22. A. Chakraborty, F. M. Prados-Estévez, S. Choudry, B. Crider, P. Garrett, W. D. Kulp, A. Kumar, M. T. McEllistrem, S. Mukhopadhyay, M. Mynk, J. Orce, E. E. Peters, J. L. Wood, and S. W. Yates. New decay pattern of negative-parity states at $N = 90$. *Phys. Rev. C*, 86:064314, Dec 2012.
23. A. Charvet, R. Chry, R. Duffait, M. Morgue, and J. Sau. Lifetimes and structures of some levels above 1.5 mev in ^{168}yb , ^{164}er and $^{158,160,162}\text{dy}$. *Nuclear Physics A*, 213(1):117 – 124, 1973.

24. R. Clark, R. Casten, L. Bettermann, and R. Winkler. Unified framework for understanding pair transfer between collective states in atomic nuclei. *Phys. Rev. C*, 80:011303, Jul 2009.
25. Crider, B. P. and Peters, E. E. and Allmond, J. M. and McEllistrem, M. T. and Prados-Estévez, F. M. and Ross, T. J. and Vanhoy, J. R. and Yates, S. W. Inelastic neutron scattering cross sections for ^{76}Ge relevant to background in neutrinoless double- β decay experiments. *Phys. Rev. C*, 92:034310, Sep 2015.
26. D. J. Rowe and J. L. Wood. *Fundamentals of NucleSar Models: Foundational Models*. World Scientific Publishing Co. Pte. Ltd., First edition, 2010.
27. C. Engelbrecht. Multiple scattering correction for inelastic scattering from cylindrical targets. *Nuclear Instruments and Methods*, 80(2):187 – 191, 1970.
28. G. Løvhøiden and T. F. Thorsteinsen and D. G. Burke. States in $^{160,162}\text{Gd}$ Studied with the (t, p) Reaction. *Physica Scripta*, 34(6A):691, 1986.
29. Gabriela Ilie and Richard F. Casten. $E0$ transitions in deformed nuclei. *Phys. Rev. C*, 84:064320, Dec 2011.
30. P. Garrett. Characterization of the β vibration and 0_2^+ states in deformed nuclei. *Journal of Physics G: Nuclear and Particle Physics*, 27(1):R1, 2001.
31. P. E. Garrett. Characterization of the β vibration and 0_2^+ states in deformed nuclei. *Journal of Physics G: Nuclear and Particle Physics*, 27(1):R1, 2001.
32. P. E. Garrett, M. Kadi, M. Li, C. A. McGrath, V. Sorokin, M. Yeh, and S. W. Yates. $K^\pi = 0^+$ and 4^+ Two-Phonon γ -Vibrational States in ^{166}Er . *Phys. Rev. Lett.*, 78:4545–4548, Jun 1997.
33. Garrett, P. E. and Kulp, W. D. and Wood, J. L. and Bandyopadhyay, D. and Choudry, S. and Dashdorj, D. and Lesher, S. R. and McEllistrem, M. T. and Mynk, M. and Orce, J. N. and Yates, S. W. New Features of Shape Coexistence in ^{152}Sm . *Phys. Rev. Lett.*, 103:062501, Aug 2009.
34. L. I. Govor, A. M. Demidov, and V. A. Kurkin. Multipole mixtures in γ transitions accompanying the (n, n' γ) reaction on ^{162}Dy . *Physics of Atomic Nuclei*, 65 (5):785–794, 2002.
35. L. I. Govor, A. M. Demidov, V. A. Kurkin, and I. V. Mikhailov. Multipole mixtures in gamma transitions in the (n, n' γ) reaction on ^{160}Gd . *Physics of Atomic Nuclei*, 72(11):1799–1811, 2009.
36. W. Greiner and J. A. Maruhn. *Nuclear Models*. Springer, Berlin, 1 edition, 1996.
37. E. P. Grigoriev. Structure of levels of the ^{160}Gd nucleus. *Physics of Atomic Nuclei*, 75(12):1427–1431, 2012.

38. T. Grotdal, K. Nyb, T. Thorsteinsen, and B. Elbek. Collective vibrational states in even dysprosium nuclei. *Nuclear Physics A*, 110(2):385 – 399, 1968.
39. Günther, C. and Boehmsdorff, S. and Freitag, K. and Manns, J. and Müller, U. Is there experimental evidence for an interpretation of the lowest $K = 0$ collective excitation of deformed nuclei as a phonon excitation of the γ band? *Phys. Rev. C*, 54:679–683, Aug 1996.
40. K. Heyde. *Basic Ideas and Concepts in Nuclear Physics*. Institute of Physics Publishing, Second edition, 1999.
41. Heyde, Kris and Wood, John L. Shape coexistence in atomic nuclei. *Rev. Mod. Phys.*, 83:1467–1521, Nov 2011.
42. V. Hönig. Messung von Halbertszeiten K-berbotener Übergänge in gg-Kernen der Seltener Erden. *Z. Physik*, 225:327 – 335, 1969.
43. F. Iachello and A. Arima. *The Interacting Boson Model*. Cambridge University Press, Cambridge, 1987.
44. M. Jammari and R. Piepenbring. Anharmonicities of γ -vibrations in deformed nuclei. *Nuclear Physics A*, 487(1):77 – 91, 1988.
45. M. Jentschel, L. Sengele, D. Curien, J. Dudek, and F. Haas. The negative parity bands in ^{156}Gd . *Physica Scripta*, 89(5):054017, 2014. URL <http://stacks.iop.org/1402-4896/89/i=5/a=054017>.
46. E. L. Johnson, E. M. Baum, D. P. DiPrete, R. A. Gatenby, T. Belgia, D. Wang, J. R. Vanhoy, M. T. McEllistrem, and S. W. Yates. Lifetime measurements of scissors mode excitations in $^{162,164}\text{Dy}$. *Phys. Rev. C*, 52:2382–2386, Nov 1995.
47. G. F. Knoll. *Radiation Detection and Measurement*. John Wiley & Sons, Third edition, 2000.
48. W. Korten, T. Hrtlein, J. Gerl, D. Habs, and D. Schwalm. Observation of a harmonic two-phonon vibration in a deformed nucleus. *Physics Letters B*, 317(1):19 – 24, 1993.
49. H. Lehmann, J. Jolie, F. Corminboeuf, H. G. Börner, C. Doll, M. Jentschel, R. F. Casten, and N. V. Zamfir. Lifetimes of the lowest $2_{K\pi=0^+}^+$ levels in ^{168}Er and ^{164}Dy . *Phys. Rev. C*, 57:569–576, Feb 1998.
50. S. R. Lesher, A. Aprahamian, L. Trache, A. Oros-Peusquens, S. Deyliz, A. Gollwitzer, R. Hertenberger, and B. D. New 0^+ excitations in ^{158}Gd . *Phys. Rev. C*, 66:051305, Nov 2002.
51. S. R. Lesher, J. N. Orce, Z. Ammar, C. D. Hannant, M. Merrick, N. Warr, T. B. Brown, N. Boukharouba, C. Fransen, M. Scheck, M. T. McEllistrem, and S. W. Yates. Study of 0^+ excitations in ^{158}Gd with the $(n, n'\gamma)$ reaction. *Phys. Rev. C*, 76:034318, Sep 2007.

52. S. R. Lesher, C. Casarella, A. Aprahamian, B. P. Crider, R. Ikeyama, I. R. Marsh, M. T. McEllistrem, E. E. Peters, F. M. Prados-Estévez, M. K. Smith, Z. R. Tully, J. R. Vanhoy, and S. W. Yates. Collectivity of 0^+ states in ^{160}Gd . *Phys. Rev. C*, 91:054317, May 2015.
53. H. Mang, J. Poggenburg, and J. Rasmussen. Nuclear structure and pairing correlations for the heavy elements. *Nuclear Physics*, 64(3):353 – 378, 1965.
54. J. Margraf, T. Eckert, M. Rittner, I. Bauske, O. Beck, U. Kneissl, H. Maser, H. H. Pitz, A. Schiller, P. v. Brentano, R. Fischer, R.-D. Herzberg, N. Pietralla, A. Zilges, and H. Friedrichs. Systematics of low-lying dipole strengths in odd and even Dy and Gd isotopes. *Phys. Rev. C*, 52:2429–2443, Nov 1995.
55. F. McGowan, W. Milner, R. Robinson, P. Stelson, and Z. Grabowski. Coulomb excitation of vibrational-like states in ^{166}Er . *Nuclear Physics A*, 297(1):51 – 60, 1978.
56. F. K. McGowan and W. T. Milner. Reduced $M1$, $E1$, $E2$, and $E3$ transition probabilities for transitions in $^{156-160}\text{Gd}$ and $^{160-164}\text{Dy}$. *Phys. Rev. C*, 23:1926–1937, May 1981.
57. D. Meyer. *Nuclear Structure Studies in the Rare Earth and Trans-lead Regions*. PhD thesis, Yale University, 2006.
58. D. A. Meyer, V. Wood, R. F. Casten, C. R. Fitzpatrick, G. Graw, D. Bucurescu, J. Jolie, P. v. Brentano, R. Hertenberger, H.-F. Wirth, N. Braun, T. Faestermann, S. Heinze, J. L. Jerke, R. Krücken, M. Mahgoub, O. Möller, D. Mücher, and C. Scholl. Extensive investigation of 0^+ states in rare earth region nuclei. *Phys. Rev. C*, 74:044309, Oct 2006.
59. R. Oehlberg, L. Riedinger, A. Rainis, A. Schmidt, E. Funk, and J. Mihelich. Coulomb excitation studies of ^{160}dy , ^{162}dy and ^{164}dy . *Nuclear Physics A*, 219(3):543 – 562, 1974.
60. S. Pascu, D. Bucurescu, et al. Detailed spectroscopy of quadrupole and octupole states in ^{168}Yb . *Phys. Rev. C*, 91:034321, Mar 2015.
61. P.E. Garrett and others. Octupole and hexadecapole bands in ^{152}Sm . *Journal of Physics G: Nuclear and Particle Physics*, 31(10):S1855, 2005.
62. D. Pelte and D. Schwalm. *Heavy Ion Collisions*, volume 3.
63. E. E. Peters, A. Chakraborty, B. P. Crider, B. H. Davis, M. K. Gnanamani, M. T. McEllistrem, F. M. Prados-Estevez, J. R. Vanhoy, and S. W. Yates. Level lifetimes in the stable Zr nuclei: Effects of chemical properties in Doppler-shift measurements. *Physical Review C*, 88:024316, Aug 2013.
64. Peters, E.E. and others. E0 transitions in ^{106}Pd : Implications for shape coexistence. *The European Physical Journal A*, 52(4):1–5, 2016.

65. N. Pietralla and O. M. Gorbachenko. Evolution of the “ β excitation” in axially symmetric transitional nuclei. *Phys. Rev. C*, 70:011304, Jul 2004.
66. D. N. Poenaru and W. Greiner. *Experimental Techniques in Nuclear Physics*. Walter de Gruyter, Boston, 1997.
67. S. D. Conte and C. de Boor. *Elementary Numerical Methods of Analysis: An Algorithmic Approach*.
68. B. Sethi and S. K. Mukherjee. Half-lives of the excited states of ^{46}Ti , ^{84}Rb , ^{99}Tc , ^{162}Dy , ^{164}Er , and ^{196}Au . *Phys. Rev.*, 166:1227–1233, Feb 1968.
69. J. F. Sharpey-Schafer, T. E. Madiba, S. P. Bvumbi, E. A. Lawrie, J. J. Lawrie, A. Minkova, S. M. Mullins, P. Papka, D. G. Roux, and J. Timár. Blocking of coupling to the 0_2^+ excitation in ^{154}Gd by the [505]11/2- neutron in ^{155}Gd . *The European Physical Journal A*, 47(1):1–4, 2011.
70. Sharpey-Schafer, J.F., Mullins, S.M., Bark, R.A., Kau, J., Komati, F., Lawrie, E.A., Lawrie, J.J., Madiba, T.E., Maine, P., Minkova, A., Murray, S.H.T., Ncaayi, N.J., and Vymers, P.A. Congruent band structures in ^{154}Gd : Configuration-dependent pairing, a double vacuum and lack of β -vibrations. *Eur. Phys. J. A*, 47(1):5, Jan 2011.
71. E. Sheldon and V. Rogers. Computation of total and differential cross section for compound nuclear reactions of the type (a,a), (a,a'), (a,b), (a, γ), (a, $\gamma\gamma$), (a,b γ) and (a,b $\gamma\gamma$). *Computer Physics Communications*, 6(3):99 – 131, 1973.
72. V. G. Soloviev, A. V. Sushkov, and N. Y. Shirikova. Low-lying nonrotational states in strongly deformed even-even nuclei of the rare-earth region. *Fiz. Elem. Chastits At. Yadra*, 27:1643, 1996.
73. M. Spieker, S. Pascu, A. Zilges, and F. Iachello. Origin of Low-Lying Enhanced $E1$ Strength in Rare-Earth Nuclei. *Phys. Rev. Lett.*, 114:192504, May 2015.
74. Y. Sun, A. Aprahamian, J.-y. Zhang, and C.-T. Lee. Nature of excited 0^+ states in ^{158}Gd described by the projected shell model. *Phys. Rev. C*, 68:061301, Dec 2003.
75. University of Fribourg Nuclear Structure Group, Fribourg, Switzerland. FiTPiC spectra fitting program, version 5.1-8, (1996).
76. V. G. Soloviev. Quadrupole and Hexadecapole Vibrational Excitations in Deformed Nuclei. *International Journal of Modern Physics E, Nuclear Physics*, 06: 437–473, 1997.
77. C. Wesselborg, P. V. Brentano, K. Zell, R. Heil, H. Pitz, U. Berg, U. Kneissl, S. Lindenstruth, U. Seemann, and R. Stock. Photoexcitation of dipole modes in $^{160,162,164}\text{Dy}$. *Physics Letters B*, 207(1):22 – 26, 1988.

78. K. Winterbon. An analytic theory of Doppler-shift attenuation. *Nuclear Physics A*, 246(2):293 – 316, 1975.
79. S. S. Wong. *Introductory Nuclear Physics*. Wiley-VCH, Second edition, 1998.
80. C. Y. Wu, D. Cline, M. W. Simon, G. A. Davis, R. Teng, A. O. Macchiavelli, and K. Vetter. Electromagnetic properties of the rotationally aligned band in ^{162}Dy . *Phys. Rev. C*, 64:064317, Nov 2001.
81. X. Wu, A. Aprahamian, S. M. Fischer, W. Reviol, G. Liu, and J. X. Saladin. Multiphonon vibrational states in deformed nuclei. *Phys. Rev. C*, 49:1837–1844, Apr 1994.
82. W. Younes, D. E. Archer, J. A. Becker, L. A. Bernstein, P. E. Garrett, N. Warr, M. Kadi, A. Martin, S. W. Yates, G. D. Johns, R. O. Nelson, and W. S. Wilburn. Two-phonon excitations in ^{170}Er . *AIP Conference Proceedings*, 481(1):464–472, 1999. doi: <http://dx.doi.org/10.1063/1.59530>. URL <http://scitation.aip.org/content/aip/proceeding/aipcp/10.1063/1.59530>.
83. N. V. Zamfir, R. F. Casten, B. Liu, D. S. Brenner, C. J. Barton, R. Krücken, C. W. Beausang, J. R. Novak, J. R. Cooper, G. Cata-Danil, R. L. Gill, and D. D. Warner. Status of the $K^\pi = 0_2^+$ band in ^{162}Dy . *Phys. Rev. C*, 60:054319, Oct 1999.
84. N. V. Zamfir, J.-y. Zhang, and R. F. Casten. Interpreting recent measurements of 0^+ states in ^{158}Gd . *Phys. Rev. C*, 66:057303, Nov 2002.
85. A. Zilges, P. von Brentano, H. Friedrichs, R. Heil, U. Kneissl, S. Lindestruth, H. Pitz, and C. Wesselborg. A survey of $\Delta K=0$ dipole transitions from low lying $J=1$ states in rare earth nuclei. *Z Phys. A - Hadrons and Nuclei*, 340:155 – 158, Apr 1991.

This document was prepared & typeset with pdfL^AT_EX, and formatted with NDDiss2 _{ε} classfile (v3.2013[2013/04/16]) provided by Sameer Vijay and updated by Megan Patnott.